PRESSURE PULSATIONS

IN SIEVE-TRAY COLUMNS

by

Geoffrey Hugh Priestman, B.Sc. Tech.

A thesis submitted for

consideration for the degree of

Doctor of Philosophy under Ordinance 3(c).

Department of Chemical Engineering and Fuel Technology,
The University of Sheffield,
Mappin Street,
Sheffield S1 3JD.

April, 1979.

PRESSURE PULSATIONS IN SIEVE-TRAY COLUMNS

by G.H. PRIESTMAN.

SUMMARY

Destructive vibrations occur in industrial sieve-tray columns under certain flow conditions. The vibrations result from regular pulsations of the gas flow and pressure in the column. These pulsations have been studied with a 3 m. high perspex model sieve-tray column having a single active test-tray using air and water as process fluids.

The effects on the amplitude and frequency of the pressure pulsations of gas velocity, tray liquid head, liquid crossflow and tray and column geometry were determined using pressure transducers with real time signal analysis. Pulsations were produced with fifteen tray geometries, including five hole diameters between 4.76 mm and 15.87 mm. Most of the pulsations were produced at gas velocities below 12 m/s and liquid heads below 200 N/m^2. The pulsation fundamental frequency varied between 12 Hz. and 40 Hz., with an r.m.s. amplitude of up to 60 N/m^2.

The gas-liquid behaviour on the sieve-tray was studied using high speed cine-photography and electrical conductivity probes. This showed conclusively that, during the occurrence of pulsations, the gas-liquid interaction was highly regular and synchronised with the pressure pulsations. Detailed measurements were obtained of the degree of synchronisation and of the liquid motion on the tray. Several modes of gas-liquid interaction were identified. During pulsation production, the pulsating jet and the imperfect bubble were most common. Calculated fluctuations in the gas flow rate through the test-tray based on measured pressures agreed well with the results of the film analysis.

A model of the synchronisation process is proposed based upon control by the pulsating jet. The model explains the measured limits of pulsation

occurrence and permits some prediction of these limits for systems other than air-water. A simplified system flow analysis accounts for effects of gas density and column geometry on the pulsation frequency. The form of the empirical correlation of frequency with experimental variables is consistent with a physical description of the pulsating jet.

ACKNOWLEDGEMENTS

I thank:

Dr. D.J. Brown* for his considerable enthusiasm, guidance and criticism throughout this work;

Dr. H.K. Kohler** for his suggestions and assistance;

I.C.I. Ltd., Agricultural Division, Teesside, for their financial aid and assistance, in particular Mr. J.B. Erskine;

Dr. A. Wraith+ for his assistance and for the permission to use his film analysis equipment;

Mr. M. Wilde* (photographer) for his valuable assistance in the cine-photography and for the photographic reduction of certain figures;

Mr. A. Sanby* (glass technician) for his assistance in the preparation of the drilled glass tray inserts;

The technical staff* and other members of the department* for their assistance.

*Department of Chemical Engineering and Fuel Technology, University of Sheffield.

**Department of Mechanical Engineering, University of Sheffield.

+Department of Metallurgy, University of Newcastle.

CONTENTS

LIST OF TABLES

LIST OF FIGURES

NOTATION

a	Tray hole free area ratio.	
a_h	Tray hole free area.	m^2
A	Amplitude of pressure pulsation fundamental beneath test-tray.	N/m^2
A_c	Column cross sectional area.	m^2
b	Column tray spacing.	m
c	Velocity of sound in air.	m/s
C	Inverse chamber capacitance.	$kg/m^4.s^2$
d	Hole diameter.	mm
d'	Equivalent hole diameter.	mm
f	Pressure pulsation fundamental frequency.	Hz. (s^{-1})
F	Superficial hole gas flow 'F' factor.	$kg^{\frac{1}{2}}/m^{\frac{1}{2}}.s.$
F_{max}	Maximum 'F' value for pulsation production.	$kg^{\frac{1}{2}}/m^{\frac{1}{2}}.s.$
g	Acceleration due to gravity.	m/s^2
G	Column mean gas volumetric flowrate.	$m^3/s.$
G_o	Gas volumetric flowrate through bottom tray.	$m^3/s.$
G_1	Gas volumetric flowrate through test-tray.	$m^3/s.$
h	Tray liquid head.	mm.of water
H	Equivalent height of clear liquid on tray.	m
I	Tray pressure loss due to gas inertial changes.	N/m^2
k_1, k_2	Constants: Cervenka and Kolar (52).	
K	Dry tray apparent loss coefficient.	
K_B	Bottom tray loss coefficient (v. basis).	
K_{BC}	Bottom tray loss coefficient (u. basis).	
K_C	Modified tray loss coefficient: Cervenka and Kolar (52).	
K_h	Modified tray loss coefficient: Davy and Haselden (51).	
K_T	Test-tray total loss coefficient.	
ℓ	Tray liquid crossflow velocity.	mm/s.
L	Water flowrate.	$m^3/hr.$
ΔM	Gas momentum head.	N/m^2
n	Number of holes in the tray.	
p	Hole pitch (equilateral triangular).	mm.
P_1	Pressure beneath test-tray.	N/m^2
P_2	Pressure at upper surface of tray.	N/m^2
P_3	Pressure above test-tray.	N/m^2
ΔP_d	Dry tray pressure drop.	N/m^2
ΔP_i	Hole event initiation pressure drop.	N/m^2
ΔP_I	Inertial pressure loss.	N/m^2

ΔP_m	Pressure drop across gas-liquid mixture on tray.	N/m^2
ΔP_{min}	Minimum tray pressure drop during pulsation cycle.	N/m^2
ΔP_r	Residual pressure drop.	N/m^2
ΔP_t	Total tray pressure drop.	N/m^2
ΔP_w	Active tray hole pressure drop.	N/m^2
q	Individual hole gas volumetric flowrate.	$m^3/s.$
Q	Chamber volume.	m^3
Q_e	Equivalent chamber volume.	m^3
s	Hole event liquid radial spread diameter.	mm
S_1	Constant: Appendix X.	
S_2	Hole closure rate due to liquid inflow.	m/s
s_{max}	Maximum event liquid radial spread diameter.	mm
t	Tray thickness.	mm
t_f	$t_t - t_{max}$	ms.
t_m	Time for hole event momentum transfer.	ms.
t_{max}	Time to reach maximum liquid radial spread.	ms.
t_t	Total hole event duration.	ms.
t_w	Hole event waiting period.	ms.
u	Superficial column gas velocity.	m/s
v	Superficial hole gas velocity (gas velocity).	m/s
v_{max}	Maximum value of v for pulsation production.	m/s.
v_{min}	Gas velocity at weep point: Eduljee (34).	m/s
Z	'Bubbling factor' : Davy and Haselden (51).	
β_m	Bulk modulus.	$kg/m.s^2$
ρ	Gas density.	kg/m^3
ρ_ℓ	Liquid density.	kg/m^3
σ	Liquid surface tension.	N/m
θ	Hole blockage parameter: Cervenka and Kolar (52).	
ϕ	Percentage tray free area.	
μ	Liquid viscosity.	kg/m.s.

Chapter 1.

INTRODUCTION

Introduction

In recent years there have been several reports of the rapid deterioration and failure of the 'internals' of industrial absorption and distillation columns. The damage has been characterised by fatigue cracking of the trays and tray support systems and the loosening of retaining bolts. (At least one case is known of total internal collapse (1)). Damage has been found to occur in large diameter columns following a period of column operation with reduced gas or vapour loading, and has coincided with or been associated with high levels of low frequency column vibration.

An understanding is needed of when this type of damage occurs and how it is produced, so that column damage can be avoided.

The damage has been found to occur with both sieve-trays and valve trays. However, because valve-trays are less commonly used than sieve-trays, in this investigation of the damage mechanism only a study of sieve-tray columns has been made.

Several examples of damage in sieve-tray columns are given later. To provide a background to these examples and to the subsequent experimental work on sieve-tray columns, an outline is given of sieve-tray column design and operation. The outline also describes the limits of column operability and gives the ranges of industrial column dimensions.

Following the examples given of column damage, features common to each example are identified, and factors which may have contributed to the column damage are discussed.

A preliminary investigation of the problem has been carried out by Waddington (2,3,4,5). The investigation identified column vibration as the major factor responsible for the column damage. Such vibrations were produced in a model column and were found to result from regular pulsations of the gas flow in the column. A short review of this work is given at

the end of the Chapter with a more detailed review being given in Chapter 3 and Appendix V.

1.1 OUTLINE OF SIEVE-TRAY COLUMN DESIGN AND OPERATION.

The purpose of a distillation or absorption column is to provide efficient mass transfer between a gas (or vapour) and a liquid. This requires a high interfacial contact area and turbulent mixing of the two phases.

The sieve-tray is a simply constructed and widely used device for contacting a gas with a liquid. It is basically a flat sheet of metal in which is drilled, or punched, a symmetrical pattern of small round holes. A sieve-tray column may contain over one hundred of these horizontal trays. Figure 1.1 shows a diagrammatic arrangement of operation in a typical sieve-tray column.

Liquid flows down the column downcomers and across the sieve-trays. The gas or vapour flows up the column, passing through the holes due to a pressure differential across the tray. This results in extensive gas and liquid mixing on the tray.

1.1.1 Two-phase flow regimes.

The nature of the gas and liquid mixture on the tray (the two-phase flow regime) is largely dependent upon the fluid flow rates. The two-phase flow regimes encountered in sieve-tray operation are discussed more fully in Chapter 2. Ho, Muller and Prince (6) defined four main regimes, as shown in Figure 1.2. These are, in order of increasing gas flow rate:

a) Bubble flow;
b) Cellular foam;
c) Froth;
d) Spray.

The transitions between regimes are not sharp and two regimes may co-exist. In the first three regimes liquid is the continuous phase; in the fully developed spray regime gas is the continuous phase.

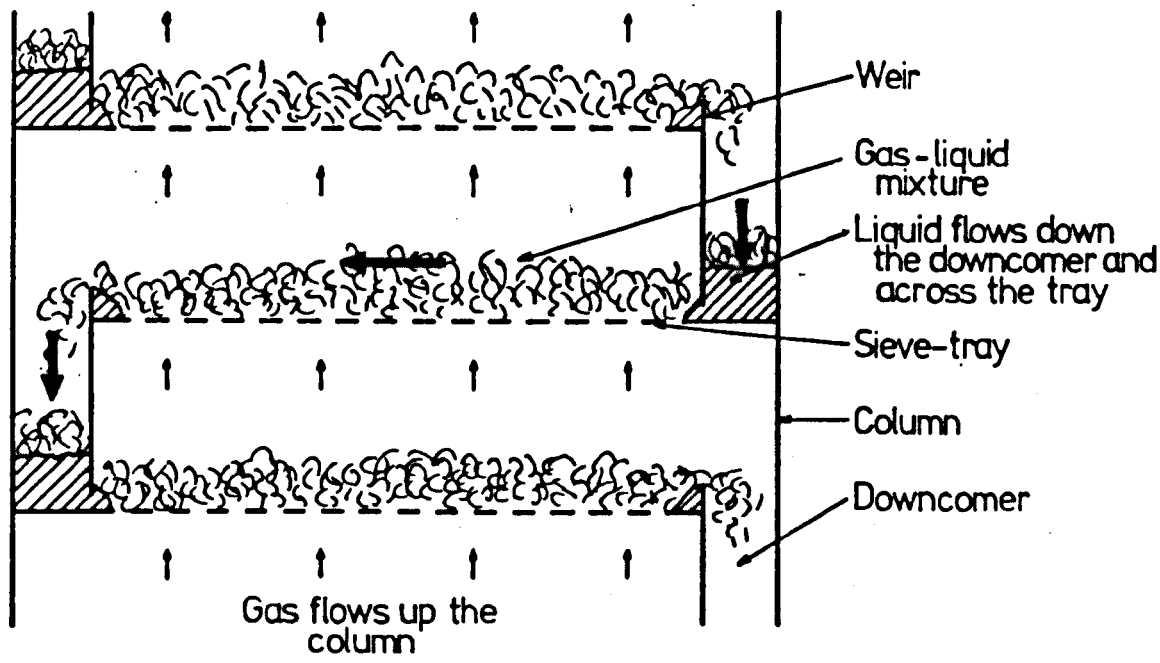

Fig.1.1 SECTION OF AN OPERATING SIEVE-TRAY COLUMN SHOWING TYPICAL FLOW

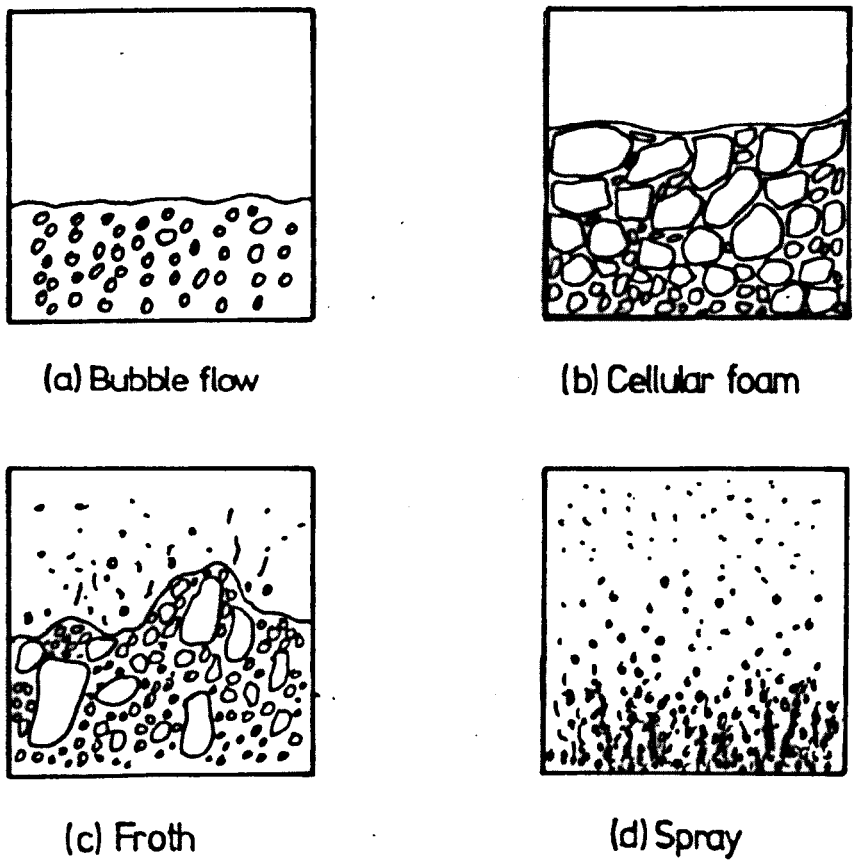

Fig.1.2 TWO-PHASE FLOW REGIMES

The amount of liquid on the tray also affects the two-phase regime. The smaller the head of liquid on the tray, the greater is the tendency toward the spraying regime.

1.1.2 Limits of column operability.

The gas flow through the tray tends to prevent liquid leakage down through the holes. Such leakage is known as weeping and the gas flow rate at which weeping begins is called the weep point. As the gas flowrate is decreased below the weep point the proportion of liquid weeping increases. Eventually the gas flowrate is reduced to a point at which liquid stops flowing over the weir and down the downcomer, this being defined as the seal point (7). The range of gas flow between the weep point and the seal point is called the weeping range.

Columns are sometimes operated in the weeping range, and normally the seal point is taken as the minimum operating gas flowrate.

The upper limit of gas flowrate in column operation is usually determined by the onset of column 'flooding'. This is a severe restriction of liquid downflow, with liquid passing upward from tray to tray. This may result from either substantial liquid entrainment or from the tray froth rising in the space between the trays, or in the downcomer, to a level such that it reaches the tray above. Severe oscillations of the two-phase mixture may also result in liquid passing up the column (8).

It is not possible to define in general terms the values of fluid flowrates corresponding to the maximum and minimum operating limits, because they depend upon column design and fluid properties. However, superficial hole gas velocities as high as 40 m/s may be used. The superficial hole gas velocity (or simply gas velocity) of a sieve-tray is defined as the total volumetric gas flowrate in the column divided by the total hole area of the tray.

1.1.3 Dimensions of Industrial Columns.

The dimensions of industrial sieve-tray columns vary greatly, depending upon the process requirements. The tendency, of recent years, to increase plant throughput has resulted in larger diameter columns, usually with larger hole sizes.

Table 1.1 gives the range of industrial column dimensions as extracted from the literature.

Table 1.1 Industrial Sieve-tray Column Dimensions.

Column Variable	Range of dimensions.
Column diameter	0.3 m. to 9 m.
Tray spacing	0.3 m. to 4.5 m.
Number of trays	10 to 100
Tray hole diameter	1.5 mm. to 25 mm., commonly 4 mm. to 16 mm.
Hole pitch/diameter ratio	2 to 5
Percentage tray free area	5% to 20%
Tray thickness	1.5 mm to 6.5 mm.
Outlet Weir height	0 mm to 100 mm.

1.2 EXAMPLES OF SIEVE-TRAY COLUMN DAMAGE.

This section gives examples of sieve-tray columns which have suffered rapid deterioration of the column internals, thought to result from column vibrations. The examples give the basic column dimensions, the extent and type of the damage and the operating conditions thought to be responsible, with details of any associated column vibrations.

Case 1. Sieve-tray absorption plant (3)

The absorption plant consisted of four sieve-tray columns linked in series.

Column dimensions.

Column diameter	=	4.4 m.
Column height	=	43 m.
Tray spacings - variable.		
Column I	=	1.5 m. to 2.2 m.
Column II	=	2.2 m. to 2.9 m.
Column III	=	3.3 m. and 3.7 m.
Column IV	=	4.02 m.
Tray thickness	=	3.0 mm.
Hole diameter	=	4.5 mm.
Hole pitch	=	17 mm triangular, equilateral.

The trays were of stainless steel.

There was extensive and widespread fatigue cracking of several trays and support beams in columns III and IV. The damage resulted from several hours of operation at gas flow rates below normal operating values.

Detailed measurements of the beam dynamic stress and column shell noise and vibration led to the following conclusions:-

i) Maximum beam stress and most pronounced tuning of shell noise occurred at reduced gas flow rates. The frequencies of stress and noise matched closely;

ii) At maximum beam stress conditions, shell noise had fundamental frequencies at 43 Hz and 53 Hz. (There were higher frequency components in the ratio 1:2:3 etc., a series considered typical of systems with acoustic resonances). The noise predominated in columns III and IV;

iii) At conditions resulting in slightly lower levels of beam stress, shell noise from columns II, III and IV had fundamental frequencies in the range 60 Hz to 64 Hz, again with a harmonic series, but weaker than the 43 Hz and 53 Hz series;

iv) The calculated acoustic resonant frequencies for the inter-tray chambers in columns III and IV were in the range 40 Hz to 70 Hz.

Case 2. A sieve-tray stripping column (9)

Column dimensions.

Column diameter	=	2.9 m.
Tray spacing	=	0.46 m.
Tray thickness	=	3.175 mm.
Hole diameter	=	12.7 mm.
Hole pitch	=	38.1 mm. equilateral triangular.

The upper trays were of stainless steel and the lower ones of titanium. Halide ions were present in the operating fluids.

There was cracking of the upper steel trays at points of high internal stress but no weld damage. There were loose retaining bolts in the other steel trays.

The damage followed operation for one year at variable fluid flow rates.

Measurements showed high levels of tray vibration in the frequency range 30 Hz to 60 Hz.

Other Cases (2).

A 2.3/2.6 m. diameter sieve-tray column, with 12.7 mm. diameter holes, suffered extensive fatigue cracking of the trays and tray supports throughout the column. The damage resulted from six hours of operation at about half the normal vapour rates. Severe vibrations of the column shell were observed at the low flow conditions.

A 4.7 m. diameter sieve-tray column with 12.7 mm. diameter holes, showed extensive fatigue damage to the trays at the top of the column. Measurements showed that at specific column flow rates there were high shell vibration levels in the frequency range 17 Hz to 50 Hz.

A 2.45 m. diameter sieve-tray column suffered two collapses of column internals following operation at low vapour rates.

1.3 FEATURES COMMON TO EXAMPLES OF COLUMN DAMAGE AND POSSIBLE FACTORS CONTRIBUTING TO THE DAMAGE.

The examples of column damage given have the following main features in common:

i) Damage is associated with abnormally high levels of column vibration, typically in the frequency range 17 Hz to 60 Hz;

ii) Damage follows column operation at reduced gas flow rates;

iii) Damage is characterised by fatigue cracking of the column trays and tray supports, sometimes accompanied by loosening of bolts;

iv) Damage occurs in columns of relatively large diameter, in the range 2 m. to 5 m.

It is clear that the fundamental cause of the column damage is flow induced column vibrations occurring predominantly at low gas or vapour flow rates.

The following factors may influence the extent of damage resulting from vibration.

1.3.1 Acoustic or mechanical resonance.

If the frequency of vibration produced by a specific gas flow rate is close to the acoustic resonant frequency of a column chamber, or to the natural frequency of part of the column structure, the magnitude of the column vibrations may be increased, resulting in greater damage.

In Case 1 the measured column vibrations were in the same frequency range as the calculated acoustic resonant frequencies for the inter-tray chambers in Columns III and IV. Furthermore, the vibrations had higher frequency components in the ratio 1:2:3 etc., a series considered typical of systems with acoustic resonances.

The calculated acoustic resonant frequencies for columns I and II, which had smaller chambers of a variety of sizes, were higher than those for columns III and IV.

Damage was almost entirely limited to columns III and IV.

The natural frequency of the column shells and of the tray/support system, was not thought to be in the vibration frequency range.

In this case it is possible that acoustic resonance, at the vibration fundamental frequency, in columns III and IV led to an increase in the level of column vibration, resulting in greater damage.

1.3.2 Stress Corrosion Cracking.

Stress corrosion cracking is a particularly severe type of corrosion. The consequence of a stress corrosion crack in a high strength steel can be the initiation of a catastrophic brittle fracture or of rapid fatigue crack propagation, (10).

Stress corrosion cracking in stainless steels depends critically upon several factors, including applied stress and environmental contaminants, such as halide ions (floride ion concentrations as low as 2 p.p.m. can be sufficient). In all cases, rise in stress intensity leads to a rapid (sometimes exponential) rise in crack growth rate.

Stress corrosion cracking is more likely at points of a structure with high levels of internal stress.

If a column environment is conducive to stress corrosion cracking, then the presence of vibrations, leading to higher stress levels, is likely to accelerate this type of attack.

Case 2 has conditions conducive to stress corrosion cracking; i.e. tray vibrations likely to raise stress levels, and the presence of halide ions. The damage in this case was identified as being that typical of stress corrosion cracking (11).

1.3.3 Poor column design or fabrication.

Although poor column design or fabrication will tend to increase column damage, this is not thought to be a major factor.

In several cases, columns with tray design the same throughout the column, only show evidence of localised damage. Also, separate columns of similar design may only exhibit damage in certain cases.

The occurrence of unexpected column vibrations may lead to stress levels above those designed for. Trays of relatively thin 'exotic' metals have proved to be particularly susceptible to damage (2).

1.4 INVESTIGATION BY WADDINGTON.

An experimental investigation of the flow induced vibration phenomenon was carried out by Waddington (2,5). A model column was used which was 2.75 m. high and contained three active sieve-trays with a tray spacing of 0.73 m. Each tray had 391, 6.35 mm. diameter holes on a 19.05 mm. equilateral triangular pitch.

It was shown that at critical low air and water flowrates, within the weeping range, there was a significant increase in column vibration level. The vibrations were found to result from the occurrence of regular gas pulsations of the column gas flow at a specific frequency. The frequency and level of the gas pressure pulsations were found to be sensitive to both the gas and the liquid flowrates.

The results of Waddington are discussed more fully in section 3.2 and Appendix V, with typical results being shown on Figure 3.1. The gas pulsations measured were in the frequency range 20 Hz. to 40 Hz. which corresponds to the range of vibration frequencies associated with the tray damage.

Waddington correlated his frequency results with the maximum bubbling frequencies for single hole trays as reported by Davidson and Amick (12) and Hughes, Handlos, Evans and Maycock (13).

The empirical correlation produced is examined in section 3.2 and found to be inadequate. The data for single hole work used is shown to be unapplicable to the Waddington system, and the correlation is found to predict only a few of Waddington's measured pulsation frequencies.

No investigation was made of the possible effects of tray geometry, tray spacing, fluid physical properties or column acoustics, on the production of the gas pulsations.

The mechanism of pulsation production was thought to be due to bubbling at the tray holes synchronising over part of the tray. However, no direct evidence of synchronous behaviour, or any association of the pulsations with the bubbling mechanism, was obtained.

1.5 SUMMARY.

The examples of sieve-tray column damage clearly show the existence of destructive flow-induced column vibrations occurring at low gas or vapour flow rates. In at least one case there is evidence that column acoustic resonance, at the vibration fundamental frequency, resulted in increased damage. In another case evidence suggests that the high stress levels induced by the vibrations led to accelerated attack by stress corrosion cracking.

In order to avoid column damage it is necessary to know when, how and why the damaging vibrations will occur. This requires the determination of how various parameters affect the vibrations and the phenomena responsible for their production.

An experimental investigation with this objective was carried out by Waddington (2). Using a large model sieve-tray column it showed the existence of high levels of column vibration at critical low air and water flowrates. The vibrations were shown to result from regular pulsations in the column gas flow, the frequency and level of the pulsations being sensitive to both gas and liquid flow rates. However, this investigation

did not include the effect of other important parameters on the pulsations and no direct evidence was obtained of how the pulsations are produced.

Clearly, further investigation of the production of the regular gas pulsations is required. They occur because of gas-liquid interaction on the tray, about which a considerable amount is known. As a basis for further work, both single-hole and multi-hole tray operation are reviewed in Chapter 2. The types of gas pulsations which can occur in sieve-tray systems, including a consideration of the static and dynamic pressures, are reviewed in Chapter 3.

Chapter 2.

OPERATING CHARACTERISTICS OF SIEVE-TRAY COLUMNS.

Introduction.

Figure 1.1 of Chapter 1 shows four main regimes of sieve-tray operation. This chapter describes these regimes in more detail and determines how they are affected by system parameters.

The mechanisms of gas-liquid interaction at the tray holes likely to be associated with these regimes are then examined in a review of single hole tray operation.

2.1 REGIMES OF SIEVE-TRAY OPERATION.

The regimes of bubble flow, cellular foam, froth and spray are examined in turn.

2.1.1 Bubble Flow.

This regime consists of a suspension of individual gas bubbles formed at the tray holes, rising in a continuous liquid. Ho, Muller and Prince (6) assumed this regime to have a gas hold-up of 0.5 (the gas hold-up is the volume fraction of gas in the gas-liquid mixture), and predicted that it could only be formed at superficial hole gas velocities below 1.0 m/s for an air-water system. Cervenka and Kolar (14), using air and water on a sieve-tray without liquid crossflow, found the maximum (superficial hole) gas velocity for bubble flow to be in the range 3 m/s to 5 m/s, the regime occurring at tray liquid heads between 10 mm. of water and 30 mm. of water. (1 mm. of water $\equiv$ 9.81 N/m^2). Hole diameter was varied between 2.5 mm. and 10 mm., and tray free area between 5% and 20%. It was found that the larger hole diameter trays did not always form this regime because of serious liquid drainage through the holes. Wallis (15) reported that smaller diameter holes were more likely to produce bubble flow, the higher surface tension resistance to flow preventing serious liquid drainage.

It is apparent that the bubble flow regime occurs at gas flow rates well below those used in industrial columns.

2.1.2 Cellular foam.

As the gas flow rate is increased, the bubbles produced at the tray holes interact to form a cellular foam. Ho et al. (6) found the foam to consist of four, five or six-sided polyhedral cells. Cervenka et al. (14) showed the cell size to increase with increasing height above the tray, the foam floating upon a layer of clear liquid next to the tray. Gas hold-up in this regime is about 0.8.

Cervenka et al. (14) found the maximum gas velocity at which a cellular foam was formed to be in the range 5 m/s to 7 m/s, for air and water in the absence of liquid crossflow.

Rennie and Evans (16) found that foams were more likely to be formed on trays with closely spaced small diameter holes. These workers found that a hole gas Reynolds Number of 2100 was the maximum at which foams could be formed. This is equivalent to a gas velocity of 5.0 m/s for air passing through 6.35 mm. diameter holes.

Fane, Lindsey and Sawistowski (17) stated that cellular foams could not be formed by surface tension negative systems (i.e. surface tension increases with increasing concentration of the more volatile component).

Calderbank (18) stated that cellular foams are not characteristic of industrial column operation, being confined to small diameter holes and low gas and liquid flow rates.

It is apparent that columns are only likely to operate in the cellular foam regime at fluid loadings below those normally used.

2.1.3 Froth.

Turbulence induced by increased gas or liquid flow rates causes the cellular foam to break down to form a froth consisting of a wide size range of smaller bubbles. The gas hold-up decreases to lie in the range 0.6 to 0.8. Calderbank and Burgess (19) showed the gas hold-up to increase with increasing height above the tray.

In this regime bubbles are still formed at the tray holes. Ashley and Haselden (20) showed the existence of two distinct types of bubbles. Firstly there was a continuous phase of small, almost spherical, bubbles, with diameters of between 5 mm.and 10 mm.; and secondly, formed within this continuous phase, there were much larger bubbles (termed vapour voids) with diameters between 40 mm. and 80 mm. It was claimed that vapour voids accounted for a substantial part of the gas flow for operation at gas velocities in the range 9 m/s to 18 m/s.

At high fluid loadings the froth becomes very turbulent with many liquid drops forming above the surface with liquid entrainment.

Under certain conditions bulk movement of the froth, or gas-liquid mixture, in an oscillatory manner, has been observed.

2.1.4 Oscillations of the gas-liquid mixture.

McAllister and Plank (21) and Barker and Self (22) reported oscillations of the froth across the tray with a frequency of between 1.0 Hz. and 1.5 Hz. Biddulph and Stephens (8), using a 0.69 m. diameter column with air and water, identified two distinct types of oscillations, full-wave oscillations and half-wave oscillations, as shown in Figure 2.1. With full-wave oscillations, the gas-liquid mixture moves simultaneously from the column walls to meet at the centre of the tray. Then the motion reverses and the mixture moves outwards, perpendicular to the direction of liquid flow, to strike the column walls. The frequency is about 1.2 Hz. and the liquid entrainment can increase by up to 40%. Half wave oscillations were found to occur on increasing the gas flow. For this type of oscillation the gas-liquid mixture moves violently from side to side, perpendicular to the direction of liquid flow, with a frequency of between 2 Hz. and 3 Hz.. Increases in entrainment of up to 70% were found.

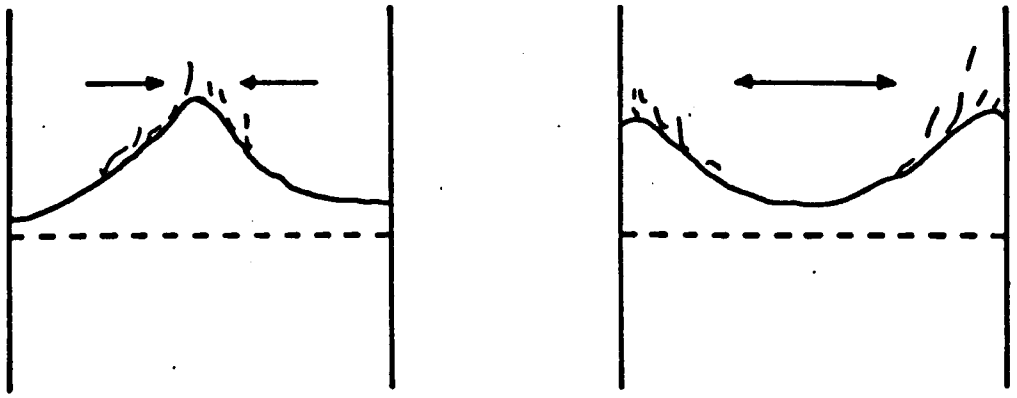

(a) Full-wave oscillations

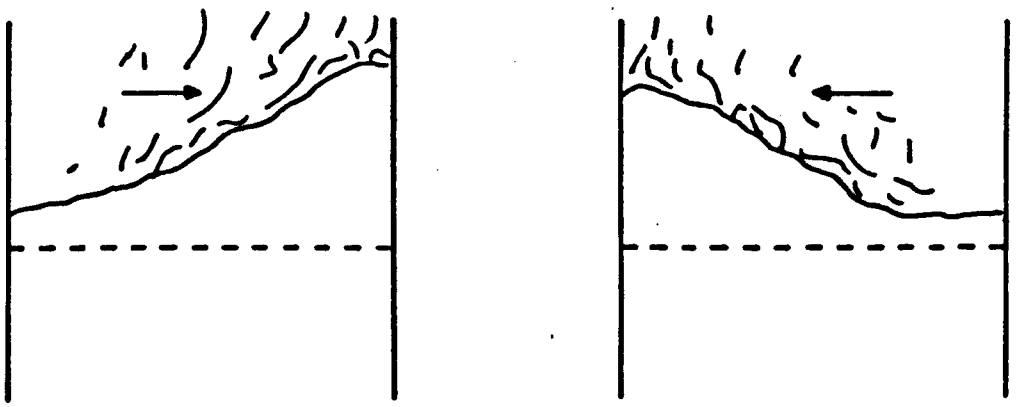

(b) Half-wave oscillations

(Liquid flowing across the tray into the paper)

Fig. 2.1. GAS-LIQUID OSCILLATIONS (BIDDULPH AND STEPHENS)

Using as a basis the theory of Hinze (23), Biddulph and Stephens (8) formulated a dimensionless group having critical values corresponding to the onset of full-wave oscillations and of half-wave oscillations. For an air-water froth on a 0.69 m. diameter tray containing 6.35 mm. diameter holes with 10% free area, full-wave oscillations were found to be produced above a gas velocity of about 15 m/s, these changing to half wave as the gas velocity went above about 20 m/s.

Biddulph (24) found that the dimensionless group was valid for a range of gas densities and it was also shown that full-wave oscillations could increase weeping by up to 150%.

Pinczewski and Fell (25) said that the onset of half-wave oscillations corresponded to the transition point from the froth regime to the spray regime, and that the difference in the nature of these two regimes meant that Biddulph's dimensionless number was not strictly applicable.

They claimed that the occurrence of half-wave oscillations in the spray regime depended upon the ratio of the height of the gas-liquid mixture to the effective tray width, and that in industrial size columns this ratio is too low for half-wave oscillations to occur. Biddulph and Stephens (8) suggested that full-wave oscillations were unlikely to occur in columns of diameter greater than 1.0 m. operating at atmospheric pressure or above. It can therefore be concluded that bulk oscillations of the two-phase mixture are unlikely to be an important operating regime in large diameter columns.

2.1.5 Spray.

Increasing the gas flow rate results in a gradual change from the froth regime, in which liquid is the continuous medium, to the spray regime, in which gas is the continuous medium.

Ho et al. (6) described the spray regime as a fluidised bed of drops of various sizes and velocities; however, other workers (26,27) have shown this description to be inadequate. Fane and Sawistowski (27) found this regime to consist of a clear liquid layer, next to the tray, from which liquid drops were produced by gas-liquid interaction at the holes to form a droplet dispersion. The drops followed free trajectories through the gaseous medium which were dependent upon their initial projection velocity. Pinczewski and Fell (26) agreed with this description, and divided the droplet dispersion into two vertical zones; one,closest to the tray, associated with droplet formation, and the other in which the droplets appear to follow free trajectories.

They found that the liquid hold-up (the volume fraction of liquid in the gas-liquid mixture) in the spray regime was not greatly influenced by the gas or liquid loadings, depending more upon the hole diameter and the tray free area. Large holes and low free areas favoured high liquid hold-up. In the droplet dispersion above the liquid layer, liquid hold-up is usually less than 0.2.

The mechanism of gas-liquid interaction at the tray holes in the three previous regimes is accepted as being primarily of a bubbling nature. Pinczewski and Fell (26,28) claimed that in the spray regime the mechanism is one of jetting, although Fane, Lindsey and Sawistowski (17,29) observed a form of bubbling to occur within the spray regime.

Because the mechanism of gas-liquid interaction in the froth regime and in the spray regime, is different, the factors affecting the transition between these regimes are likely to have an important affect on the gas-liquid behaviour at the tray holes.

2.1.6 Froth to Spray transition.

The transition from the froth regime to the spray regime (termed 'phase inversion') is not very sharp. Various techniques have been used to measure the transition point.

Pinczewski and Fell (28) studied the transition using an electrical conductivity probe to monitor gas-liquid behaviour at tray holes. The probe was located centrally in a hole and gave a pulse when a liquid bridge was formed across the hole. In the froth regime the pulse rate was found to be between 17 and 25 pulses/second. As the gas velocity was increased, it was found that at a certain velocity the pulse rate decreased rapidly, passed through a local maximum and then decreased again, more slowly, to a rate below 5 pulses/second. The local increase in pulse rate was taken to be the transition point, this being in agreement with visual observation of the gas-liquid mixture. Using air and water the transition point was determined for a range of tray geometries, the results being shown in Figure 2.2.

Superficial hole gas velocity and tray liquid head were found to be the major fluid flow parameters affecting transition, the head at transition increasing with increasing gas velocity. It was also found that spraying was favoured by large hole diameter and that gas velocity at transition was increased slightly with increasing liquid crossflow, particularly at liquid flows below 60 m^3/hr. m. weir length. Varying weir height between 25 mm. and 76 mm. had little affect on transition.

Porter and Wong (30) used a light transmission technique to determine the transition. With no liquid crossflow, tray liquid head was increased at constant gas velocity, until a sharp increase in measured light transmission occurred; this was taken as the transition point from spray to froth. Figure 2.2 shows results obtained for an air water system; the hole pitch/diameter ratio was 4:1 in each case (≈ 5% free area).

Again gas velocity and tray liquid head were identified as the major fluid flow parameters, with large hole diameter favouring spraying. The effect of fluid properties was also investigated. Liquid hold-up at

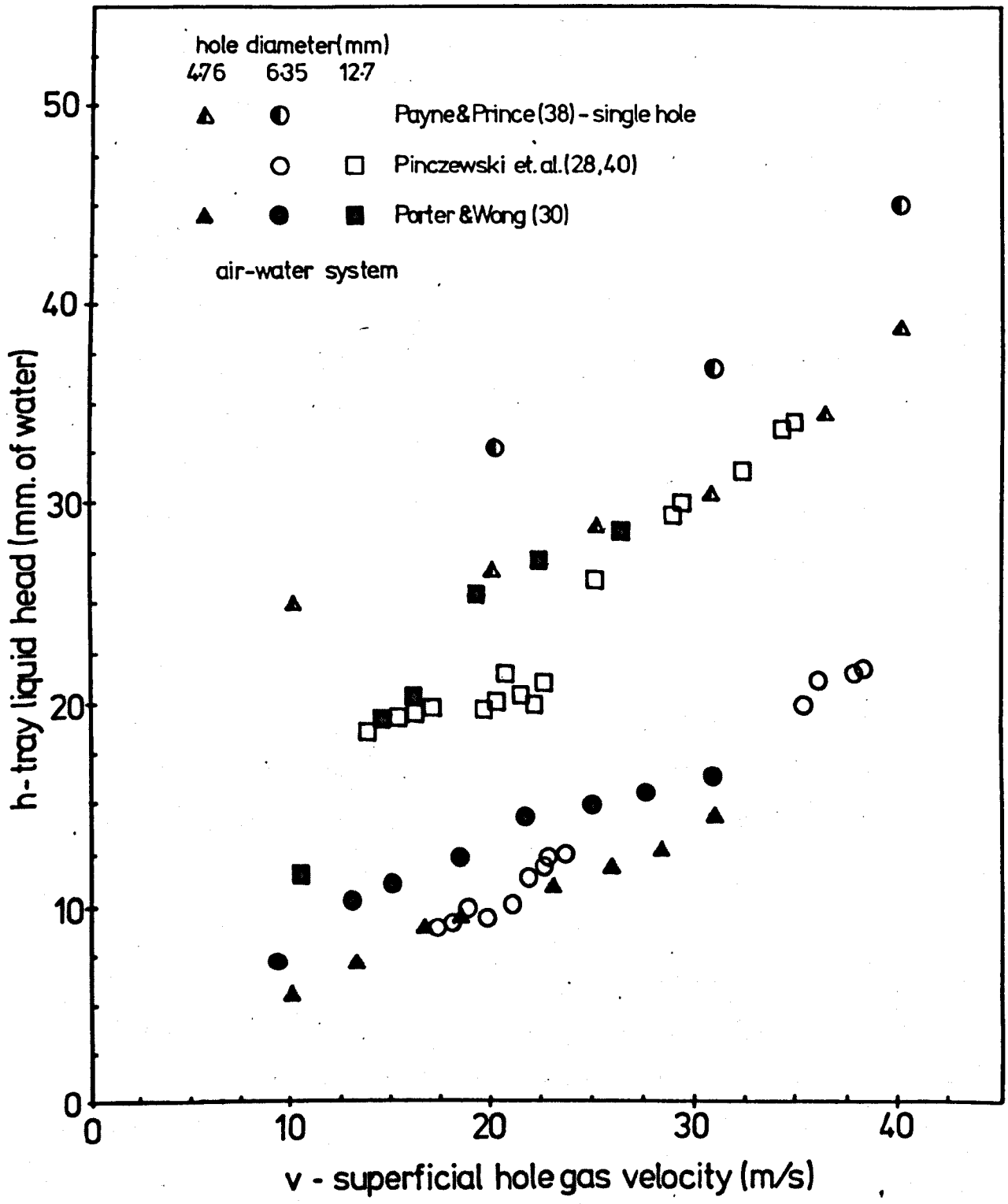

Fig.2:2 FROTH-SPRAY TRANSITION POINTS

transition was found to increase with increasing gas density, to decrease with increasing liquid density and to be independent of liquid viscosity.

Burgess and Robinson (31) extended the work of Porter and Wong (30) to include the effect of liquid cross flow. They found good agreement for 12.7 mm diameter holes. Results for 4.76 mm. diameter holes showed disagreement, attributed to maldistribution of fluid flow on the tray of Burgess and Robinson.

Comparison of the results obtained by Pinczewski and Fell (28) and by Porter and Wong (30), (Figure 2.2) show the transition heads of the latter workers to be slightly higher. However, considering that Pinczewski and Fell measured both the transition point and the tray liquid head by a different method to Porter and Wong, and that Porter and Wong's results were in the absence of liquid crossflow, the agreement between the results is good.

Payne and Prince (32) determined the froth to spray transition point using electrical conductivity probes, light transmission and residual pressure drop measurements (the concept of residual pressure drop is discussed in sections 2.2.1 and 3.1.2). The results obtained were in general agreement with the findings of other workers (28,29,30), there again being some disagreement with the results of Burgess and Robinson (32). Payne and Prince reported liquid crossflow to have little or no effect on the froth to spray transition liquid head. However, the spray to froth transition was found to be unstable under crossflow conditions resulting in a hysteresis of the transition point. No hysteresis was observed in the absence of liquid crossflow.

The above groups of workers studied transition in the absence of mass transfer. However, Jeronimo and Sawistowski (33) claimed that the effect of mass transfer on the transition point was not very strong except for strongly

negative systems, in which the transition velocity is about 25% lower than for other systems.

It can be concluded that the main factors affecting transition from froth to spray are, tray liquid head, gas velocity, hole diameter, gas density and liquid density, with liquid crossflow being of minor importance.

2.1.7 Summary of sieve-tray operating regimes.

It has been found that the superficial hole gas velocity and the tray liquid head are the primary fluid flow parameters which determine the regime of tray operation. Figure 2.3 indicates how the various gas-liquid regimes depend upon these two factors for an air-water mixture on a sieve-tray containing 6.35 mm. diameter holes without liquid crossflow. The boundary lines shown are only approximate indications of the areas of regime transition. The weep point is also indicated. This is based upon the correlation of Eduljee (34):

$$\left[\frac{v_{min} \cdot \rho^{\frac{1}{2}}}{1.22} - 5.5\right] = \left[\frac{d}{3.63} + 0.25\right]\left[\frac{h}{249.1} + 1.1\right] \quad - \quad (2.1)$$

It is clear that the froth and spray regimes are those most likely to be formed in industrial columns, with cellular foams occurring at low gas flows. Full or halfwave oscillations of the gas-liquid mixture are unlikely to be found in columns with a diameter greater than 1.0 m. The effect of liquid crossflow on the froth to spray transition was found to be small. However, turbulence induced by high liquid flow is likely to inhibit cellular foam formation.

Hole diameter has been found to have a primary effect on the type of regime obtained, with hole pitch (or tray free area) having a smaller effect.

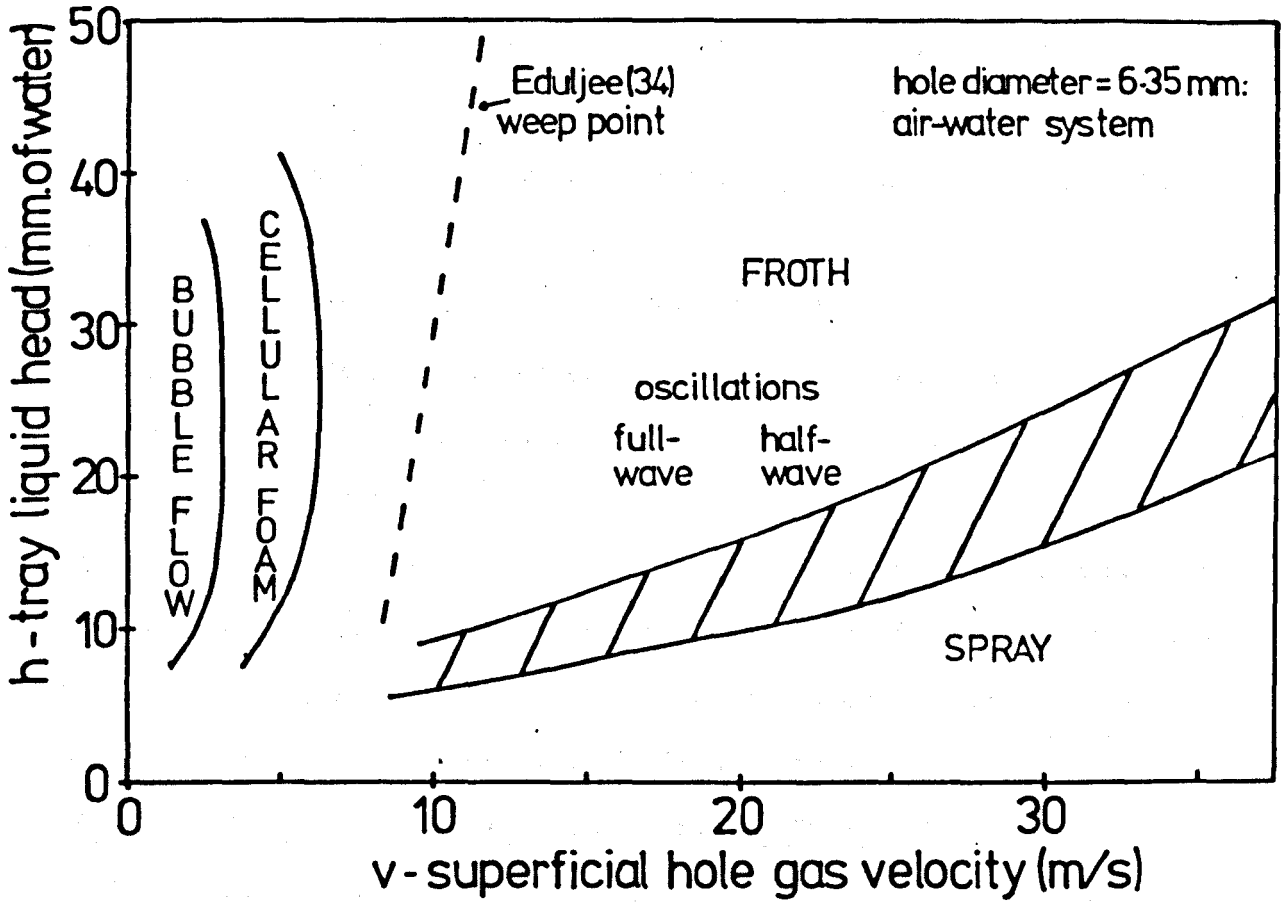

Fig. 2.3 REGIMES OF SIEVE-TRAY OPERATION

Bubble flow and cellular foam formation is more likely with small hole diameters and low free area; spray formation is more likely with large hole diameters.

Gas and liquid density have been found to be the primary fluid physical properties affecting the type of regime. Some workers incorporate gas density in their measure of gas flow by using a superficial hole gas 'F' factor; $F = v. \rho^{\frac{1}{2}}$.

Comparison of Figures 3.1 and 2.3 shows that the regular gas pulsations measured by Waddington (2) occurred in the froth regime near the weep point and in the cellular foam regime. (Few, if any, measurements were made in the spray regime.)

The mechanism of gas-liquid interaction at the tray holes is a primary factor affecting the tray operating regime. To determine more closely the gas-liquid behaviour at the holes a brief review is carried out of the regimes of gas-liquid behaviour on a single hole tray.

2.2 REGIMES OF GAS-LIQUID BEHAVIOUR ON A SINGLE HOLE TRAY.

Valentin (35) identified eighteen principal factors affecting the gas-liquid behaviour at a single hole. The factors related to fluid flow rates, fluid physical properties, hole geometry and the gas chamber volume beneath the tray.

For multi-hole tray, the main factors affecting the regime of operation were the gas velocity and the tray liquid head. Hayes, Hardy and Holland (36) and Davidson and Amick (12), showed that liquid depth had no effect on the gas-liquid interaction at a single hole for values of depth greater than twice the diameter of the bubbles formed at the hole.

However, Muller and Prince (37) showed the depth of liquid to be a major controlling factor of the gas-liquid interaction for values below 100 mm. of water. Taking the gas velocity as the other major controlling

factor, six regimes of gas-liquid behaviour were defined, as shown in Figure 2.4. The regimes indicated are for an air-water system and a 6.35 mm. diameter hole.

The regimes are defined as follows:

i) Perfect bubble, i.e. discrete bubbles of approximately spherical shape;

ii) Deformed bubble, i.e. bubbles become distorted due to flow induced turbulence with possible interference between successive bubbles;

iii) Imperfect bubble, i.e. bubbles break the surface before they are fully formed;

iv) Pulsating jet, i.e. continuous gas flow with liquid entrainment, regular liquid oscillations at the hole inducing gas flow pulsations;

v) Steady jet, i.e. continuous gas flow with liquid entrainment and no liquid oscillations;

vi) Meniscus, i.e. continuous gas flow with no liquid entrainment.

2.2.1 Jetting to bubbling transition.

On Figure 2.4, the transition lines 1 and 2 were determined by measuring liquid entrainment at a hole with a very small gas chamber volume beneath it. Lines 3 and 4 were determined from dynamic pressure measurements in the gas chamber beneath the hole (volume = 0.0056 m^3). The dependence of the frequency of pressure fluctuations on the liquid depth was found to be different for the jetting and bubbling regimes (see also section 3.3.1).

Payne and Prince (38) carried out a further study of the transition between jetting and bubbling, their transition lines being shown on Figure 2.4. The lines were determined from measurements of the hole residual pressure drop (see section 3.1.2). At a constant gas velocity, increasing the liquid depth produced a rise in residual pressure drop which

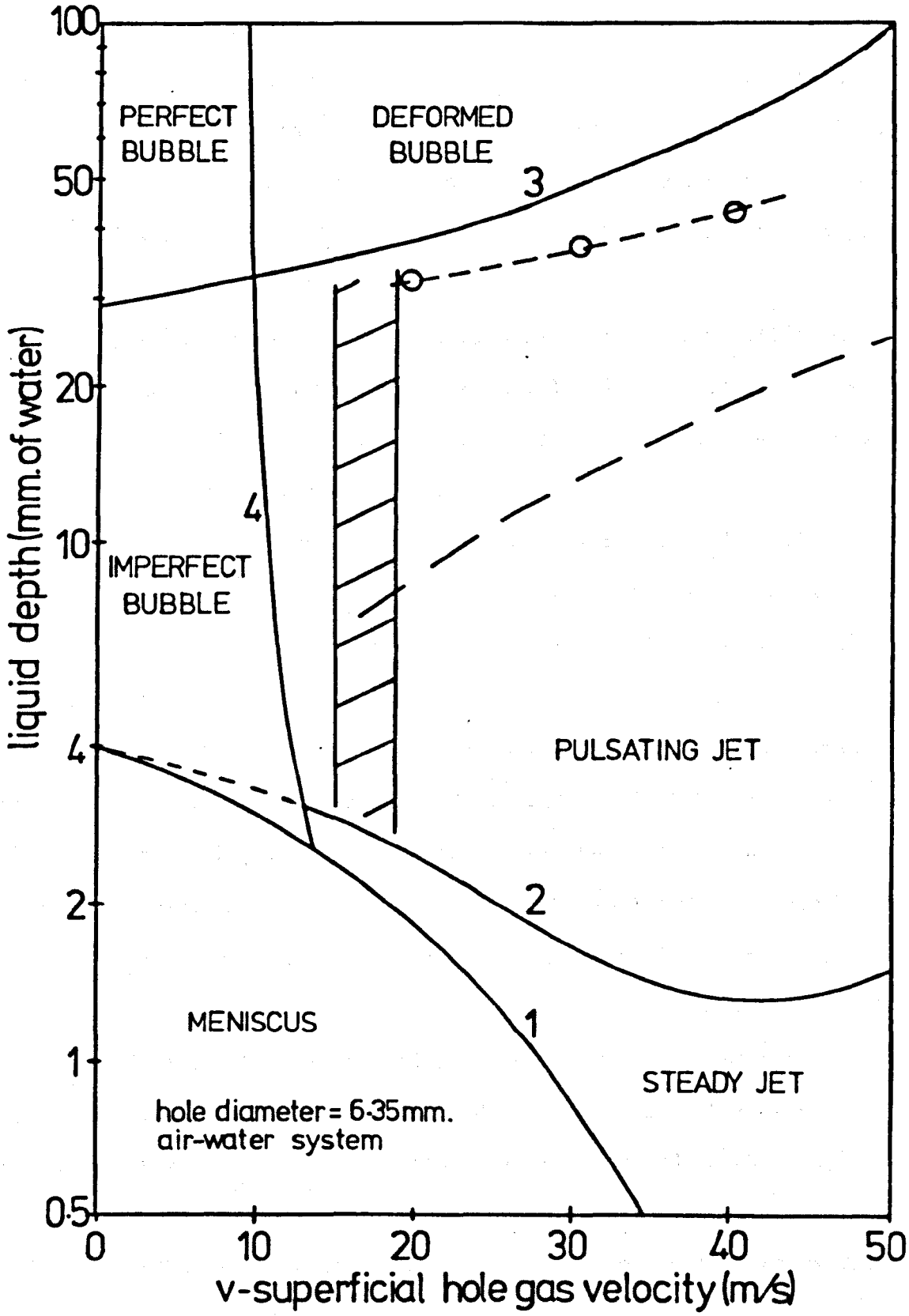

Fig. 2.4 SINGLE HOLE OPERATING REGIMES, MULLER AND PRINCE (37)

reached a peak at a specific depth. For gas velocities below 20 m/s, a further increase in liquid depth produced only a gradual fall in residual pressure drop; in such cases the peak was taken to represent the transition from imperfect bubbling to bubbling. For gas velocities over 20 m/s, an increase in liquid depth beyond the peak value produced a steep decrease in residual pressure drop. In these cases the peak was taken to represent the transition from jetting to bubbling.

The changes in residual pressure drop were claimed to result from variations of the gas momentum transfer to the liquid. Pressure increase resulting from pulsating gas flow was claimed to account for a maximum of only 25% of the residual pressure drop.

Payne and Prince (32) found that the residual pressure drop also indicated the froth/spray transition on sieve-trays of low free area, and that this transition point corresponded to the measured bubble to jetting transition point.

Good agreement was found between the residual pressure drop transition points and those determined by Banerjee, Roy and Rao (39) by measuring entrainment rates. Figure 2.4 shows good agreement between the jetting to bubbling transition lines of Muller and Prince (37) and Payne and Prince (38), although the later workers report imperfect bubbling to occur at higher gas velocities.

Fane, Lindsey and Sawistowski (17) and Lindsey (29), observed imperfect bubbling at a gas velocity of 40 m/s. Considerable drop formation (and therefore, momentum transfer) was observed in this regime, and it is therefore possible that transition between imperfect bubbling and jetting based upon entrainment measurements or residual pressure drop fluctuations, may be unreliable.

Payne and Prince (38) identified the following effects on the liquid depth at transition from jetting to bubbling;

i) Critical depth is independent of chamber volume for volumes greater than 0.002 m^3; below this value, depth increases slightly, reaches a maximum and then falls;

ii) Critical depth increases with increasing hole diameter;

iii) Density is the only significant liquid property affecting transition, critical depth decreasing with increasing density;

iy) Critical depth increases with increasing gas density.

The last three findings are the same as those reported for the critical tray liquid head at froth to spray transition.

Figure 2.2 shows the jetting to bubbling transition depths of Payne and Prince (38) to be higher than the liquid head for froth/spray transition reported by Pinczewski et al. (40) and Porter and Wong (30). Payne and Prince claimed that the transition heads were lower because Pinczewski et al. (40) had taken the transition point to be represented by 100% continuous gas flow through the tray holes; Payne and Prince (38) claimed that transition was equivalent to continuous gas flow for only about 70% of the time.

Yeo (41) monitored gas-liquid behaviour at a single hole tray using an electrical conductivity probe. He indicated that the transition line used by Payne and Prince (38) does not correspond to continuous gas flow and postulated that a regime of 'chain' bubbling should be included between the regimes of pulsating jet (100% continuous flow) and deformed bubbling (about 70% flow). This postulated transition line is shown in Figure 2.4; it agrees quite closely with the froth/spray transition lines.

It is therefore apparent that the mechanism of gas-liquid behaviour at the holes changes gradually from one of continuous gas 'jetting' to one of bubbling (deformed, perfect or imperfect) as the gas velocity is decreased, or the tray liquid head increased. The transition from spray

to froth corresponds to this change, its exact location being dependent upon the definition of transition.

2.2.2 Bubbling on single hole trays.

For operation at high tray liquid depths, bubbling (deformed or perfect) is the primary mechanism of gas-liquid interaction at the hole. Extensive study of bubbling at holes has been carried out, most of this work using high liquid depths (> 100 mm. of water) and low gas velocities.

Hughes, Handlos, Evans and Maycock (13) and Davidson and Amick (12) showed the volume of the gas chamber beneath the hole to have a significant effect on bubble formation.

The chamber volume is defined as, that volume beneath the tray which is between the hole and a point in the gas stream where the resistance is large. For a constant gas supply rate two extreme effects of the chamber volume on gas flow can be identified:

i) Constant flow. With zero chamber volume; the fluctuations of the forces opposing gas flow associated with the bubble formation have a negligible effect on the gas flow, and the gas flow rate through the hole can be considered constant.

ii) Constant Pressure. With an infinite chamber volume; the fluctuating resistance to gas flow induces a corresponding fluctuation in the gas flow rate through the hole, but the chamber pressure remains constant.

In practice the chamber volume has a finite value and the induced fluctuations in gas flow rate result in fluctuations in the chamber pressure. Because the pressure drop across the hole is a main factor controlling the gas flow rate, the pressure fluctuations below the tray affects the gas flow rate through the hole. The gas flow rate, and hence the rate of bubble growth, is therefore affected not only by the forces associated

with the gas-liquid interaction at the hole, but also by the chamber volume.

The chamber volume can be regarded as a capacitance for gas flow; McCann and Prince (42) defined a quantity of inverse capacitance, C,

$$C = \frac{c^2 \cdot \rho}{Q} \qquad - \qquad (2.2)$$

McCann and Prince (43) classified bubbling regimes in terms of the gas velocity and the chamber inverse capacitance, at a constant liquid depth of 152 mm. of water. Six regimes were identified:

i) Single bubbling;

ii) Double bubbling;

iii) Pairing;

iv) Double pairing;

v) Single bubbling with delayed release;

vi) Double bubbling with delayed release.

The regimes were defined as follows:

i) Single bubbling. The bubble maintains a spherical shape during formation and rises due to buoyancy. When the bottom of the bubble becomes level with the tray, detachment occurs if the liquid pressure behind the bubble at the hole is greater than the bubble pressure. Weeping is possible after bubble detachment if the liquid pressure is greater than the chamber pressure.

ii) Double bubbling. Decreasing the chamber volume increases the frequency of bubbling. At high bubble frequencies, the wake of the preceding bubble affects the formation of the second bubble and double bubbling occurs when the second bubble is sucked into the proceeding one. The phenomenon of double bubbling occurs closer and closer to the hole as the bubbling frequency increases.

iii + iv) Pairing. This occurs at large chamber volumes. If, at detachment, the chamber pressure exceeds the pressure in the wake of a bubble, then a second bubble forms rapidly and attaches to the preceeding bubble. The original bubble is then joined to the hole by a bubble 'tail' and continues to grow until the tail detaches from the hole. Pairing can take place with double bubbling, in which case bubble 'pairs' coalesce.

v + vi) Delayed release. As the chamber volume is reduced, the gas flow into the expanding bubble can reduce the pressure in the chamber to a level below that required to maintain the flow necessary for continued bubble growth. This results in a delay of the bubble growth whilst the chamber pressure is increased by a net inflow of gas. In this case, the chamber pressure exhibits two pressure cycles per bubble.

Although the regimes described were for a single hole tray operating at a liquid depth above those likely to be found in industrial columns, they clearly show the chamber volume to have an important effect on bubble formation. The work also indicates that at gas velocities over about 6 m/s, the phenomenon of double bubbling becomes important, suggesting that this might be important in the froth regime.

This analysis does not indicate how the 'vapour voids', observed by Ashley and Haselden (20) on an operating tray, could occur.

2.2.3 Summary of gas-liquid behaviour at a single hole.

The various mechanisms of gas-liquid interaction on single hole trays are summarised in Figure 2.4.

The transition from froth to spray corresponds to a gradual change in the interaction mechanism from one of pulsating jetting in the spray regime, to one of bubbling (deformed, perfect or imperfect) in the froth regime.

The factors affecting the change in mechanism are found to be the same as those affecting froth-spray transition, the effects being the same in each case. Liquid depth and gas velocity are the main factors affecting orifice mechanism, with chamber capacitance being of importance in the bubbling regimes.

2.3 CONCLUSIONS.

The various regimes of gas-liquid behaviour on sieve-trays have been identified and the mechanism of gas-liquid interaction at the tray holes, corresponding to those regimes, established.

The main system variables which have been found to affect the operating regimes and interaction mechanism are:

i) Superficial hole gas velocity;

ii) Tray liquid head;

iii) Tray liquid crossflow rate;

iv) Hole diameter;

v) Tray hole free area (equivalent to hole pitch);

vi) The volume of the gas chamber beneath the tray;

vii) Gas and liquid density.

It is now necessary to establish the types of gas pulsations which can be produced by sieve-tray operation. A review of the relevant literature is carried out in Chapter 3.

Chapter 3.

GAS PULSATIONS IN SIEVE-TRAY SYSTEMS

Introduction

Fluctuations of the gas flow in the column will result from fluctuations of the resistance of the tray to gas flow. Tray resistance is usually measured in terms of a pressure drop. Static sieve-tray pressure drops are reviewed; firstly, to determine the various components of the total pressure drop across an operating sieve tray; secondly, to find what correlations are available for the prediction of these pressure drops; and thirdly, to find any component pressure drop which could exhibit dynamic fluctuations likely to result in the reported gas flow pulsations.

Reported measurements of gas pressure fluctuations in sieve-tray columns are reviewed to determine the types of gas pulsations that can occur. The system factors affecting the pulsations are determined and the effects identified. The mechanisms of gas-liquid interaction at the tray holes likely to produce gas pulsations are investigated in a review of measurements made on single hole trays.

3.1 STATIC PRESSURE DROPS IN SIEVE-TRAY OPERATION.

The total static pressure drop across an operating sieve-tray can be expressed as the sum of a number of terms representing additive resistance to gas flow. The total pressure drop, ΔP_t, is normally taken to be the sum of the pressure drop across the tray holes in the presence of a gas-liquid mixture on the tray, ΔP_w, and the pressure drop across the gas-liquid mixture, ΔP_m:

$$\Delta P_t = \Delta P_w + \Delta P_m \qquad (3.1)$$

3.1.1 Static pressure drop across the gas-liquid mixture, ΔP_m.

Various workers (44,45,46) have shown that ΔP_m can be expressed in terms of an equivalent clear liquid head on the tray,

$$\Delta P_m = H \cdot \rho_l \cdot g \qquad - \qquad (3.2)$$

where H equals the height of the clear liquid layer that would exist on the sieve-tray if the gas were removed from the gas-liquid mixture.

3.1.2 Static pressure drop across the tray holes in the presence of a gas-liquid mixture on the tray, ΔP_w.

Kolodzie and van Winkle (47) showed that the pressure drop across a dry sieve-tray, ΔP_d, can be well correlated by a classical orifice equation:

$$\Delta P_d = K \cdot \frac{\rho \cdot v^2}{2} \qquad - \qquad (3.3)$$

where K is an apparent coefficient of resistance or an apparent loss coefficient, (for trays having equal upstream and downstream column flow cross-sectional areas, the apparent loss coefficient is the same as the total loss coefficient). The value of K was shown to depend upon hole diameter, hole pitch and tray thickness, and also upon the hole Reynolds number, Re, for 2000>Re>20,000.

McAllister, McGinnes and Plank (48) and Durgaprasada and Venkata (49) showed that frictional resistance to gas flow through the holes was only important for trays with a thickness to hole diameter (t/d) ratio greater than 2.0. Industrial sieve-trays normally have a t/d ratio less than 1.0 and so frictional resistance can be ignored; such trays are termed 'thin trays'.

Cervenka and Kolar (50) developed an expression for K for thin sieve-trays. Reynolds number was taken to have no effect on K. Analysis of data for 78 trays gave the expression:

$$K = \frac{0.94\ (1 - a^2)}{a^{0.2}\ (t/d)^{0.2}} \qquad - \qquad (3.4)$$

valid over the ranges, $0.1 < t/d < 0.8$, $0.015 < a < 0.2$, for triangular hole pitch.

However, it has been found that when a gas-liquid mixture is present on the sieve-tray, the pressure drop across the holes is greater than that for a dry tray. This extra pressure drop can be accounted for by introducing a 'residual pressure drop' term, ΔP_r;

$$\Delta P_r = \Delta P_t - \Delta P_d - \Delta P_m \qquad - \qquad (3.5)$$

Burgess and Robinson (31) and Davies and Porter (44) found ΔP_r to have a constant value of about 100 N/m^2. Hunt, Hanson, and Wilke (46) found ΔP_r to be dependent upon tray geometry. For a given tray its value was constant and for different trays values between 50 N/m^2 and 200 N/m^2 were found.

The residual pressure drop is explained as being due to the gas-liquid mixture on the tray affecting the gas flow through the holes.

Davy and Haselden (51) proposed several ways in which this could occur:

i) Not all the holes have an equal instantaneous vapour rate. Owing to the irregular movement of liquid across the tray, some holes, or groups of holes, may be discharging rapidly at a given instant, while others may be temporarily inactive;

ii) Liquid may penetrate into the holes, effectively reducing the area available to vapour flow;

iii) The rate of flow through an individual hole is oscillatory, as bubbles grow and then detach;

iv) There is a venturi effect produced by the core of liquid around the gas stream at the outlet of each hole which will tend to decrease the pressure drop and could give rise to pressure recovery. This is likely to be most noticeable at high velocities when gas emerges from the holes nearly continuously rather than as distinct bubbles.

To account for these factors, Davy and Haselden (51) modified the dry tray apparent resistance coefficient by introducing a 'bubbling factor', Z:

$$K_h = \frac{K}{Z} \qquad - \qquad (3.6)$$

where K_h is the modified coefficient. An empirical equation was developed for Z:

$$Z = 1 - \exp\ [-0.0265\ (u/100.a)\ \rho/(\rho\ell-\rho)]^{\frac{1}{2}} \qquad - \qquad (3.7)$$

This method predicted the tray pressure drop well for low gas flows in the froth regime, but underestimated the pressure drop at higher gas flows.

Cervenka and Kolar (52) accounted for the modification to gas flow by using the concept of a hypothetical tray (containing the same number of holes on the same pitch as the original tray) on which the free area was reduced by a factor θ, to a value of '$\theta.a$ ', to allow for hole blockage. A further coefficient, k_1, was introduced to represent possible non-uniform configuration of the openings available to gas flow. Using equation 3.4 an expression for a modified apparent resistance coefficient, K_c, was obtained:

$$K_c = \frac{0.94.k_1\ .\ (1 - \theta^2 a^2)}{\theta^{.2}\ .\ a^{.2}.\ (t/d)^{.2}} \qquad - \qquad (3.8)$$

An expression for θ was developed from an analysis of the forces acting at the hole, with the introduction of a further coefficient, k_2

$$\theta = 1 - (k_2 \cdot \sigma/d)/(P_1 - P_2) \quad - \quad (3.9)$$

Coefficients k_1 and k_2 were determined from experimental values of total tray pressure drop for 14 trays. Values obtained were $k_1 = 1.10$ and $k_2 = 2.35$, applicable for air/water systems with trays having 2.5 mm < d < 10 mm, and 0.05 < a < 0.2.

No account of tray liquid head was taken in determining k_1 and k_2 because, in equation 3.9, $(P_1 - P_2)$ was expressed theoretically in terms of θ, and not measured directly. Coefficients were not determined for systems other than air/water, and Davy and Haselden (51) found the reported values to be inadequate for organic systems.

Muller and Prince (37) and Payne and Prince (38), studying a single hole, found that the residual pressure drop varied as the mechanism of gas-liquid behaviour at the hole changed from jetting to bubbling, reaching a peak value at transition. Payne and Prince (32) observed similar behaviour at the froth to spray transition on low free area sieve-trays. These workers explained the variation by claiming that the residual pressure drop was due mainly to momentum transfer from the gas to the liquid, the rate of transfer for bubbling being different to that for jetting.

The correlations of Davy and Haselden (51) and Cervenka and Kolar (52) do not account for these observed variations in residual pressure drop.

3.1.3 Measurement of the static tray pressure drops and the effect of gas momentum.

Three tray static pressures are usually measured. These are:

(i) The pressure in the gas chamber beneath the sieve-tray, P_1;

(ii) The pressure at the top surface of the sieve-tray, as measured by pressure tappings mounted in the tray, P_2;

(iii) The pressure in the gas chamber above the sieve-tray and gas-liquid mixture, P_3.

Davies and Porter (44) showed that the pressure difference (P_2-P_3) was equal to the pressure drop across the gas-liquid mixture, ΔP_w, minus a gas momentum head term, ΔM.

$$P_2 - P_3 = H \cdot \rho_\ell \cdot g - \Delta M \qquad - \qquad (3.10)$$

where ΔM corresponds to the pressure recovery due to the gas slowing down from its velocity in the holes to its velocity in the column. It was expressed assuming superficial values of these velocities:

$$\Delta M = (v-u) \cdot u \cdot \rho \qquad (3.11)$$

Cervenka and Kolar (52) performed a force and momentum balance on the tray system and developed an identical expression for ΔM. Using this expression the pressure differences (P_1-P_2) and (P_2-P_3) can be written as follows:

$$P_1-P_2 = \Delta P_w + u^2 \cdot \rho \cdot (1/a-1) \qquad - \qquad (3.12)$$

$$P_2-P_3 = H.\rho\ell. g - u^2.\rho. (1/a-1) \qquad - \qquad (3.13)$$

Cervenka and Kolar (52) modified these equations by changing a to θa, in order to account for the effect of hole blockage (resulting from the presence of a gas-liquid mixture on the tray) on the gas velocity.

Equations 3.12 and 3.13 relate the measured static pressure drops to the pressure drop across the holes and the tray liquid head respectively.

3.1.4 Summary of sieve-tray static pressure drops.

It has been found that the total resistance of an operating sieve-tray to gas flow is made up of two main additive resistances:

i) The resistance due to the head of liquid on the tray;

ii) The resistance of the sieve-tray in the presence of a gas-liquid mixture on the tray.

The tray resistance can be considered to be equivalent to the dry tray resistance, modified to account for an extra 'residual' pressure drop.

The dry tray resistance is found to be well correlated by a classical orifice equation. The residual pressure drop has been accounted for by either using a simple constant additive resistance term or by modifying the orifice equation resistance coefficient. Neither method adequately predicts observed behaviour of the residual pressure drop. The magnitude of the residual pressure drop is dependent upon the mechanism of gas-liquid interaction at the holes.

By using a gas momentum head term it is possible to determine the tray liquid head and hole static pressure drop, from measured static pressure drops, by using equations 3.12 and 3.13.

Of the various resistances to gas flow, those due to the tray liquid head and the 'residual' pressure drop could have dynamic characteristics which could result in regular pulsations of the gas flow.

3.2 GAS PRESSURE FLUCTUATIONS IN MULTI-HOLE TRAY SYSTEMS.

As reported in Chapter 1, Waddington (2) showed column vibrations to be caused by regular pulsations in the column gas flow induced, under certain conditions, by the gas-liquid interaction on the tray. Such pulsations were produced in a model sieve-tray column and found to have frequencies in the same range as the vibrations associated with industrial column damage.

The column contained three sieve-trays operating with air and water. Simultaneous gas pressure pulsations were detected within the gas-liquid mixture and in the gas chambers above and below the centre tray, over a limited range of fluid flow rates. The pulsations were in the frequency range 25 Hz. to 40 Hz. and occurred at gas velocities between 5 m/s and 12 m/s., the frequency increasing with increasing gas velocity.

Figure 3.1 shows the frequency and amplitude of gas pulsations measured in the gas chamber beneath the centre tray. The tray regimes were determined from visual observation, and compare well with those shown in Figure 2.3. The pulsations of highest amplitude are seen to occur in a regime of stable froth.

Comparison of results obtained at weir heights of 12.7 mm.,25.4 mm. and 76.2 mm. showed no significant change in the pulsations. However, the comparison was not strictly valid as a different water flowrate was used for each weir height. From the effects he found of liquid flow rate on the pulsations, Waddington concluded that they could not be produced at tray liquid cross-flow velocities greater than 0.03 m/s (calculated from the flow rate per unit of weir length divided by the weir height and equivalent to a liquid flow rate of 2.72 m^3/hr. m. weir length at a weir height of 25.4 mm.).

The occurrence of gas pulsations was not reported in terms of tray liquid head, which has been found to be a primary liquid flow parameter controlling tray operation. Waddington also failed to investigate possible affects of the other main system parameters found to affect tray operation: hole diameter, hole pitch, gas chamber volume, fluid densities and liquid surface tension.

Although it was shown that the pulsation frequency was apparently not dependent on the tray mechanical response, no experimental investigation of the possible affects of acoustic resonance on the pulsations was performed.

It was noted that the experimental pulsation frequencies were in the same range as the maximum bubbling frequencies measured for single hole trays, as reported by Davidson and Amick (12) and Hughes et al. (13). Waddington (2,5) correlated his results with these frequencies and produced the empirical correlation:

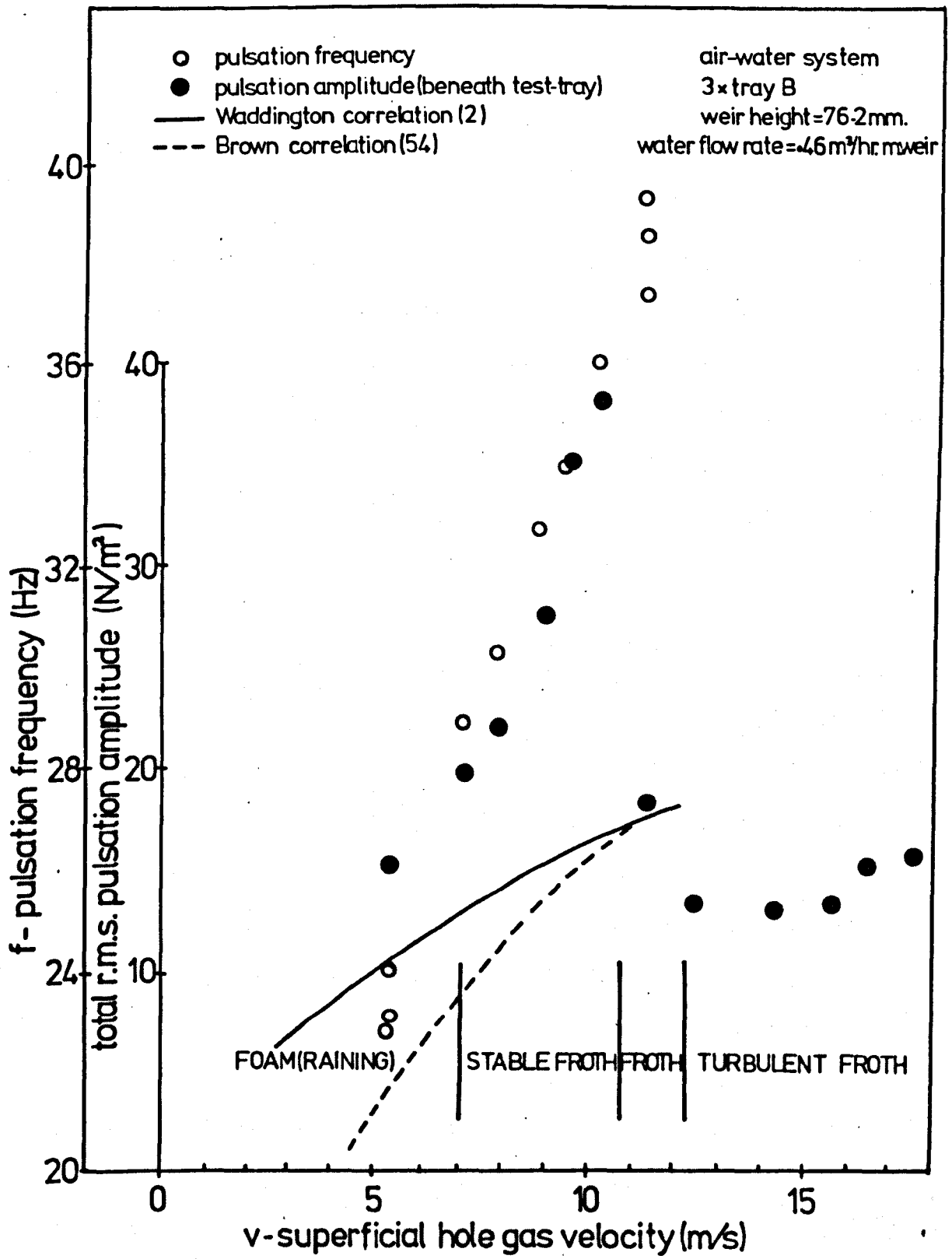

Fig.3.1. TYPICAL RESULTS OF WADDINGTON (2)

$$n_m = 11.6 \cdot \frac{V_h^{0.13}}{r^{0.27}} \qquad - \qquad (3.14)$$

where; n_m = single hole maximum bubbling frequency, Hz.

V_h = superficial hole gas velocity ft/sec.

r = hole radius inches.

The correlation is plotted on Figure 3.1., and is seen to be of limited value in predicting the pulsation frequencies of Waddington.

It is later shown (section 3.3) that the bubbling frequencies reported by Davidson and Amick (12) and Hughes et al. (13), were obtained under conditions approximating to constant flow, and that such frequencies are not applicable to systems with large chamber volumes which exhibit flow fluctuations through the tray holes.

Frequencies for conditions of fluctuating flow, (i.e. comparable to the conditions in Waddington's model column), were measured for single holes by McCann and Prince (42), Kupferberg and Jameson (53) and Muller and Prince (37), and found to be much lower than those frequencies found under constant flow conditions. These frequencies were not included in the data used in obtaining Waddington's correlation.

Waddington's correlation cannot account for any possible dependency of frequency on tray liquid head, hole pitch, fluid density, number of holes or chamber volume, which are all factors later shown to affect the frequency of pulsations measured on multi-hole or single hole trays.

Brown (54) measured the frequency and amplitude of pressure fluctuations produced under single sieve-trays, containing a small number of holes, without liquid crossflow. For each set of conditions a four second sample of the pressure fluctuations was analysed. A definite frequency of gas pulsations was identified in most cases. The amplitude of the fluctuations of a given sample was found to vary greatly, in an apparently random manner.

A few results were obtained for trays containing 29, 41 and 49 holes of 6.35 mm. diameter. These are shown on Figure 3.2, which also gives further details of the operating conditions. Of the two sets of 49 hole data, one was obtained with a baffle placed around the holes, but it is not specified which set. The frequencies found are in a similar range to those of Waddington (2) and occur over the same range of gas velocities, frequency increasing with increasing velocity.

Most of the results obtained by Brown (54) were for trays containing only three holes. These results had lower frequencies, all below 15 Hz. However, the following trends were identified for the three hole trays:

i) Frequency is practically independent of hole diameter (d = 6.35, 9.53, 12.7 mm.) but increases as the hole pitch increases (19.05 mm < p < 50.8 mm);

ii) The only significant liquid property affecting frequency is density, frequency increasing with decreasing density;

iii) Gas properties have a slight affect on frequency, but no definite dependence was identified;

iv) Tray liquid head has no recognisable affect on frequency (25.4 mm. of water < h < 100 mm. of water).

For trays containing three holes and seven holes it was found that:

i) Increasing the volume of the gas chamber below the tray decreased the frequency, ($0.0015\ m^3 < Q < 0.0043\ m^3$);

ii) Increasing the number of holes increased the frequency.

These two effects were found to be well correlated by using a volume per hole criterion. This ratio was also found to be roughly applicable to the data for the tray with 29 holes.

The frequency data for all the trays was correlated to produce the empirical equation:

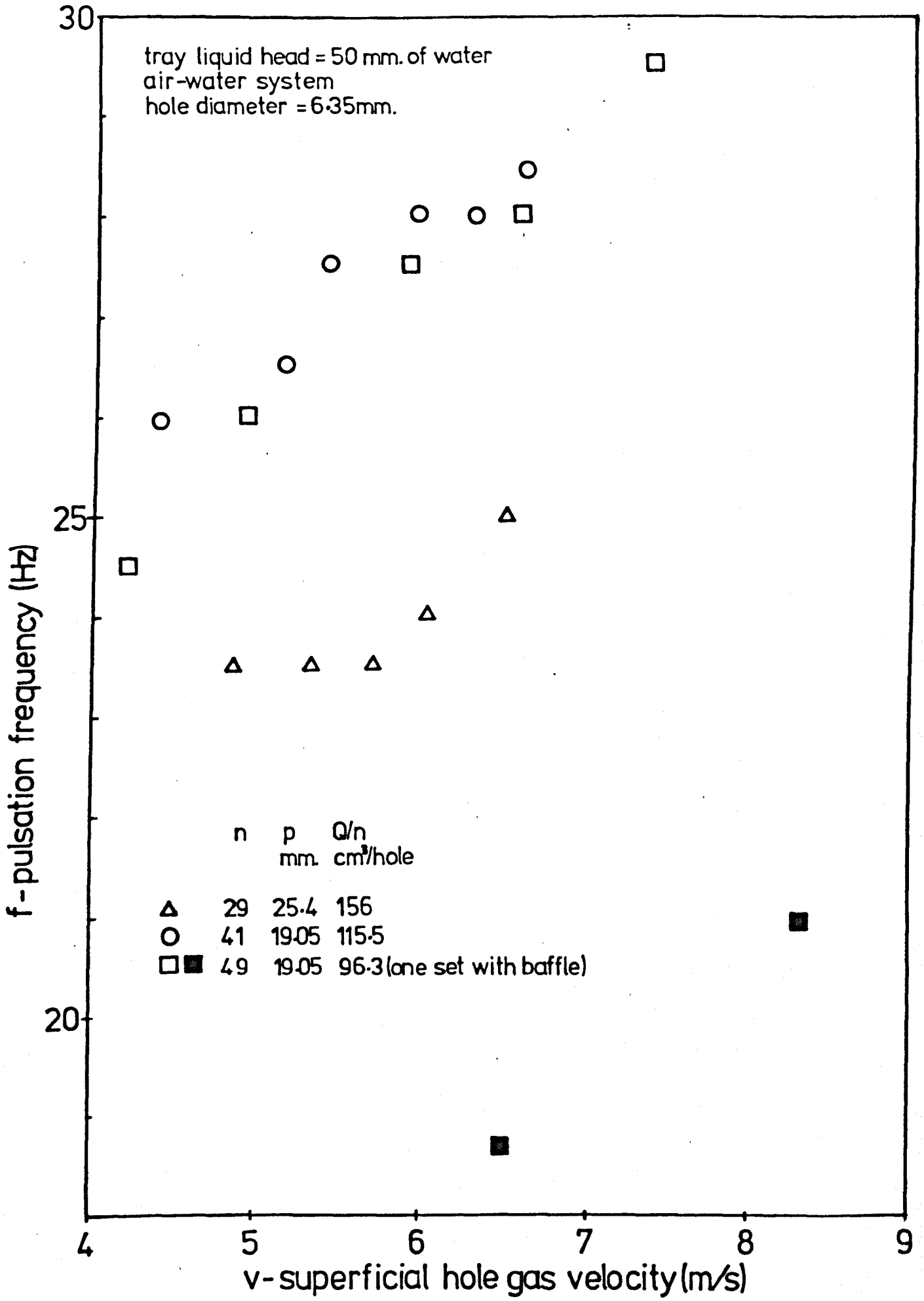

Fig.3.2 BROWN(54): PULSATION FREQUENCIES FOR MULTI-HOLE TRAYS

$$p.f/v = 46{,}700\ (n.p^3/Q)^{0.46}\ (d.v.\rho/\mu)^{-0.69}\ (\rho/\rho_\ell)^{0.84}\ (p/d)^{-0.54}$$

The equation fitted the data with a standard deviation of 10%.

Although the correlation was based, to a certain extent, on bubbling action at a single hole, it was stated that the measured pressure pulsation frequencies were not necessarily the same as the bubbling frequencies.

Most of the correlated data was obtained for a tray with only three holes and is not necessarily applicable to a normal sieve-tray, particularly with respect to the effect of hole pitch. (In the correlation $f \propto p^{-0.16}$, which disagrees with the observed increase in frequency with increasing pitch).

The equation, as applied to Waddington's conditions, is plotted on Figure 3.1; the frequencies predicted are seen to be below those found by Waddington, suggesting that the correlation cannot be applied to trays containing more than a few holes.

Brown was not able to correlate the amplitude data due to its apparently random fluctuations. For three hole trays he did identify the following trends:

i) The pulsation pressure amplitude tended to increase with decreasing frequency;

ii) The pulsation pressure amplitude tended to increase with increasing gas velocity.

Kupferberg and Jameson (55) measured the dynamic pressure fluctuations beneath a tray containing up to seven 6.35 mm. diameter holes, and up to nineteen 3.175 mm. diameter holes. However, the gas velocities used were all below 1.0 m/s and therefore the results are not likely to be applicable to sieve-tray operation. Regular gas pulsations were detected with frequencies below 7 Hz. and with amplitudes up to 200 N/m^2. The following trends were identified:

i) The pulsation frequency was lower than the bubble frequency;

ii) Frequency increased with increasing gas velocity;

iii) Frequency was independent of hole diameter;

iv) The number of holes had little affect on the frequency.

Trends ii) and iii) are seen to be in agreement with Brown's work.

Davies and Porter (44) measured fluctuations in tray pressure drops, the space above the tray being open to atmosphere.

Pressure variations were found across the tray holes, (P_1-P_2), and across the froth, (P_2-P_3), but no variations of the total tray pressure drop were found. The froth pressure drop variations were thought to result from local variations of the height or density of the air-water mixture on the tray. No frequencies over 15 Hz. were detected.

Chan and Prince (7,56) postulated that weeping on a sieve-tray resulted from variations of the gas pressure at the individual holes on the tray. A theoretical equation was developed to predict the frequency of pressure variations at an individual hole. The instantaneous pressure at a hole was assumed to be due to additive pressure drops of capacitance, resistance, inertia and other factors.

The resistance term included the effect of gas friction loss (which is applicable only to 'thick' trays), and assumed no dynamic variation of tray liquid head. The capacitance was based upon the total gas chamber volume below the tray, and did not include the number of holes in the tray. Hole pitch was not considered in the equation.

Chan and Prince (56) detected pressure fluctuations of frequency 2 Hz. to 4 Hz. below a sieve-tray containing 12.7 mm. diameter holes operating at a gas velocity of 3 m/s with air and water. The amplitude of fluctuation varied between 50 N/m^2 and 100 N/m^2. The frequency predicted by them using their equation was 6.8 Hz.

The pressure fluctuations reported by Chan and Prince (56) are in a similar frequency range to the bulk oscillations of the gas-liquid mixture reported earlier, in section 2.1.4.

McAllister and Plank (21) claimed that these oscillations resulted from resonance in the column system of a fundamentally acoustic nature. Biddulph and Stephens (8) disagreed with this, claiming that it could not account for the observed occurrence of oscillations in an open tank system. It was also claimed that the oscillations were unlikely to result from pressure fluctuations below the tray, but to be due to turbulence of the gas-liquid mixture. Hinze (23) showed by theoretical analysis that certain conditions in the turbulent froth regime could result in amplified oscillations of the gas-liquid mixture.

Garland and Davidson (57) pointed out that once oscillations of the gas-liquid mixture are established, the resulting variations in tray liquid head will cause local fluctuations of the gas flow through the tray. These fluctuations could be expected to result in fluctuations of the column gas pressure.

Cermak (58) measured pressure fluctuations beneath an operating sieve-tray with 6 mm. diameter holes, using air and water without liquid crossflow. Regular pressure pulsations were detected whilst the tray was operating in the oscillating froth regime. The frequency of pulsation was about 2.5 Hz., and corresponded to the frequency of oscillations. Under all regimes of operation, Cermak detected peaks in the pressure frequency spectrum of between 4 Hz. and 5 Hz. These were thought to result from standing waves in the gas-liquid mixture. For operations in the bubble flow regime at a gas velocity of 1.0 m/s, peaks at 10.5 Hz. and 21.0 Hz. were present, and for operation in the cellular foam regime at a gas velocity of 2.3 m/s, a peak at 21.0 Hz. was present.

These higher frequency components were thought to result from bubble formation at the tray holes.

3.2.1 Summary of gas pressure fluctuations in multi-hole tray systems.

Two distinct types of pressure fluctuation have been identified:

i) Pulsations in the frequency range 1 Hz. to 3 Hz., which result from bulk oscillations of the gas-liquid mixture on the tray;

ii) Pulsations in the frequency range 10 Hz. to 40 Hz., thought to be associated with the gas-liquid behaviour at the tray holes.

The first type of pulsation is of a frequency well below the range associated with the damaging tray vibrations. Furthermore, it has been reported that such oscillations are unlikely to occur in columns of diameter greater than 1.0 m. at operating pressures of atmospheric and above. These gas pulsations have been shown to result from the fluctuations in tray liquid head caused by the oscillations. Chan and Prince (7) assumed the tray liquid head had no dynamic characteristics, and therefore their equation cannot be applied to this type of pressure fluctuation.

The second type of pressure pulsation is that reported by Waddington (2, 5) and Brown (54) and it is thought to be responsible for the column damage.

The frequency of pulsation has been shown to increase with increasing gas hole velocity, and the following factors have also been found to affect the pulsations:

i) Number of holes;
ii) Hole pitch;
iii) Volume of the gas chamber beneath the sieve-tray;
iv) Liquid density;
v) Gas density;
vi) Liquid flow rate.

The correlations of Brown and Waddington fail to predict adequately the measured frequencies on sieve-trays containing a substantial number of holes. No correlation is available for prediction of the pulsation amplitudes.

3.3 GAS PRESSURE FLUCTUATIONS IN SINGLE-HOLE TRAY SYSTEMS.

The superficial hole gas velocity, the tray liquid depth and the volume of the gas chamber beneath the tray, have been identified as three major factors affecting single hole operation.

Muller and Prince (37) measured the gas pulsations in a gas chamber of constant volume (0.0056 m^3) whilst varying the gas velocity and the liquid depth. The frequencies of the gas pulsations measured for a 6.35 mm. diameter hole operating with air and water, are shown in Figure 3.3. The line taken by these workers to indicate the transition from pulsating jet to bubbling is also indicated.

In all cases the frequency is seen to increase with increasing gas velocity, the rate of increase being higher for the lower liquid depths, and becoming almost linear at a depth of 10 mm.

In the pulsating jet regime the frequency is seen to decrease with increasing liquid depth, but becomes independent of depth in the bubbling regime.

The amplitude of pulsation was found to increase with increasing liquid depth in the pulsating jet regime, reaching a maximum value of between 150 N/m^2 and 250 N/m^2 at transition to the bubbling regime, and then decreasing with further increase in liquid depth. (This decrease was not found for operation at a gas velocity of 5 m/s.). The variation of amplitude with liquid depth corresponds to that found for the magnitude of the residual pressure drop.

The frequencies found by Muller and Prince (37) are lower than those found by Waddington (2) and Brown (54) (for 29, 41 and 49 hole trays), for a given gas velocity.

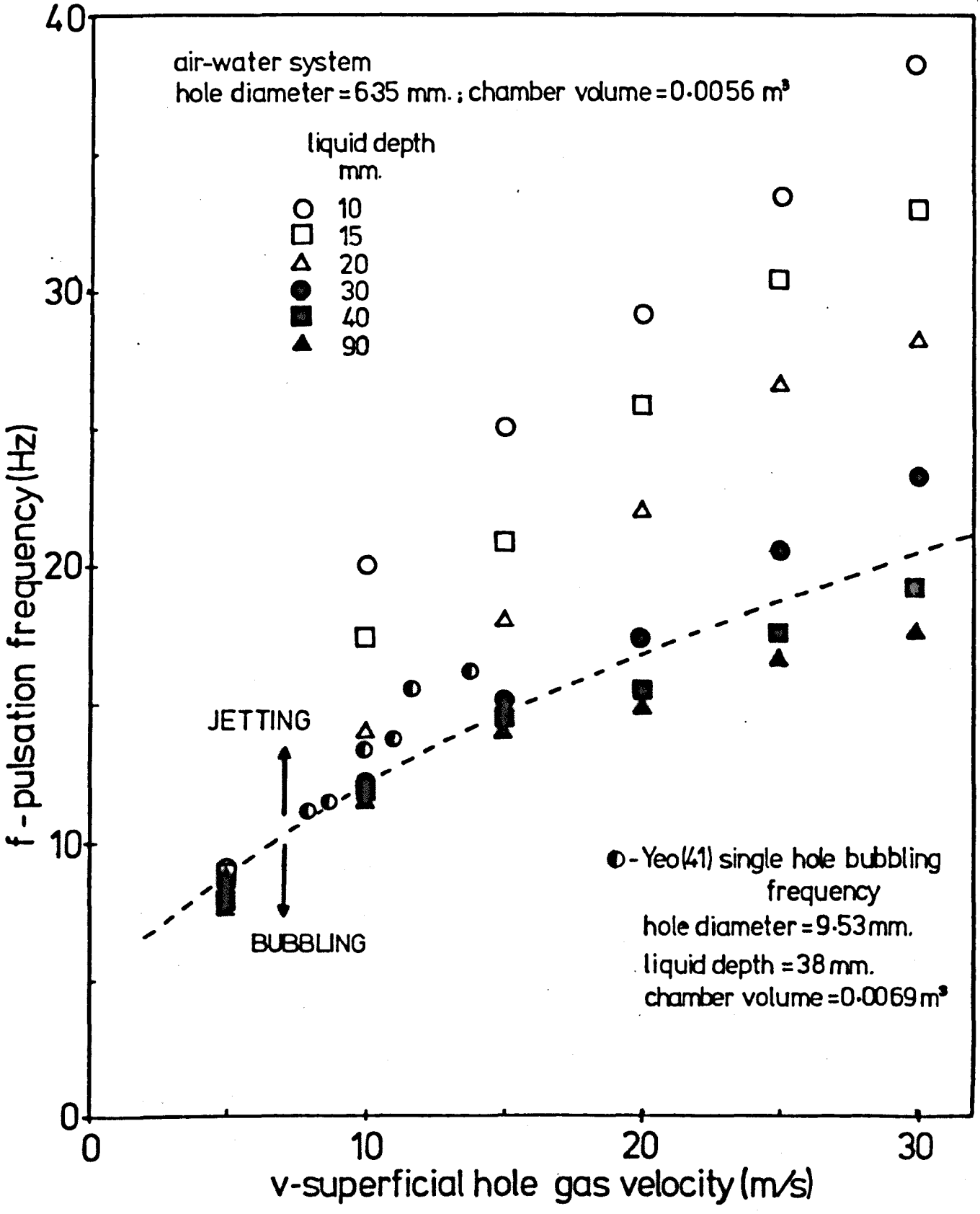

Fig.3.3 MULLER & PRINCE(37); PULSATION FREQUENCIES FOR SINGLE-HOLE TRAY

The frequency of pulsations in the bubbling regime is dependent upon the frequency and mode of bubbling.

McCann and Prince (42) measured pressure pulsations in the chamber below a single hole tray operating in the bubbling regime. Using air and water, and hole diameters of 4.76, 6.35 and 9.53 mm., measurements were taken over a range of gas velocities (<12 m/s.) and chamber volumes (0.00225 $m.^3$ to 0.0288 $m.^3$), for a constant liquid depth of 152 mm.

Results for a hole diameter of 6.35 mm. are shown in figure 3.4. The work indicated the following points:

i) Frequencies are lower than 12 Hz. ;

ii) Frequency increases with increasing gas velocity up to a velocity of about 6 m/s or 7 m/s, after which it is fairly independent of velocity.

iii) Increasing the chamber volume decreases the frequency;

iv) Varying the hole diameter has little affect on frequency.

Kupferberg and Jameson (53) measured pulsation frequencies under similar conditions to McCann and Prince (42), but used lower gas velocities (<7 m/s) and smaller chamber volumes (0.0005 $m.^3$ to 0.005 $m.^3$). Some of the frequencies found for a 6.35 mm. diameter hole are shown in Figure 3.4. These show good agreement with the results of McCann and Prince, but demonstrate that the frequency can be considerably raised by reducing the chamber volume.

McCann and Prince (43) give a sample trace of the pressure pulsations produced by bubbling at a 6.35 mm. diameter hole at a gas velocity of 4.6 m/s. and a chamber volume of 0.00017 $m.^3$, under which conditions the bubbling mechanism is complex, with double bubbling and delayed release. The pressure trace indicates about 32 pressure pulses per second.

Titomanlio, Rizzo and Acierno (59), using trays containing one or two holes, claimed that for low gas flow rates and high liquid depth, the

volume of bubbles coming out from a single hole approximates that of simultaneous bubbles growing from a chamber which has double the capacitance and is fed by double the gas flow rate. This finding is in agreement with Brown (54), who showed the chamber volume per hole to be the relevant factor determining bubble behaviour.

Yeo (41) used an electrical conductivity probe to monitor the frequency of gas-liquid interaction at a single hole. Using air and water, with hole diameters of 9.53, 12.7 and 15.87 mm., he varied the gas velocity (<50 m/s.), the liquid depth (38, 76, 114 and 152 mm.) and the chamber volume (0.0069 $m.^3$ to 0.0414 $m.^3$).

Some of the results obtained for the 9.53 mm. diameter hole are shown in Figure 3.4 and are seen to be in good agreement with those of McCann and Prince (42) whose frequencies for a 9.53 mm. diameter hole were very similar to those for the 6.35 mm. diameter hole.

For gas velocities higher than about 15 m/s., the conductivity probe did not produce regularly spaced pulses, which indicates either that the gas-liquid behaviour at the hole was no longer regular, or that the probe was not monitoring the behaviour accurately.

The measured frequencies were found to be higher for operation at a liquid depth of 38 mm. than for the other depths used, the frequency being independent of liquid depth for the higher depths. At a depth of 38 mm. the frequency increased with increasing gas velocity. It was also found that increasing the chamber volume decreased the frequency, and that the frequency was largely independent of hole diameter. These findings are in agreement with those reported by the other workers.

La Nauze and Harris (60), working with a 32.2 mm. diameter hole, low gas flow and high liquid depth, found that increasing the system gas pressure, and therefore the gas density, increased the frequency of bubbling.

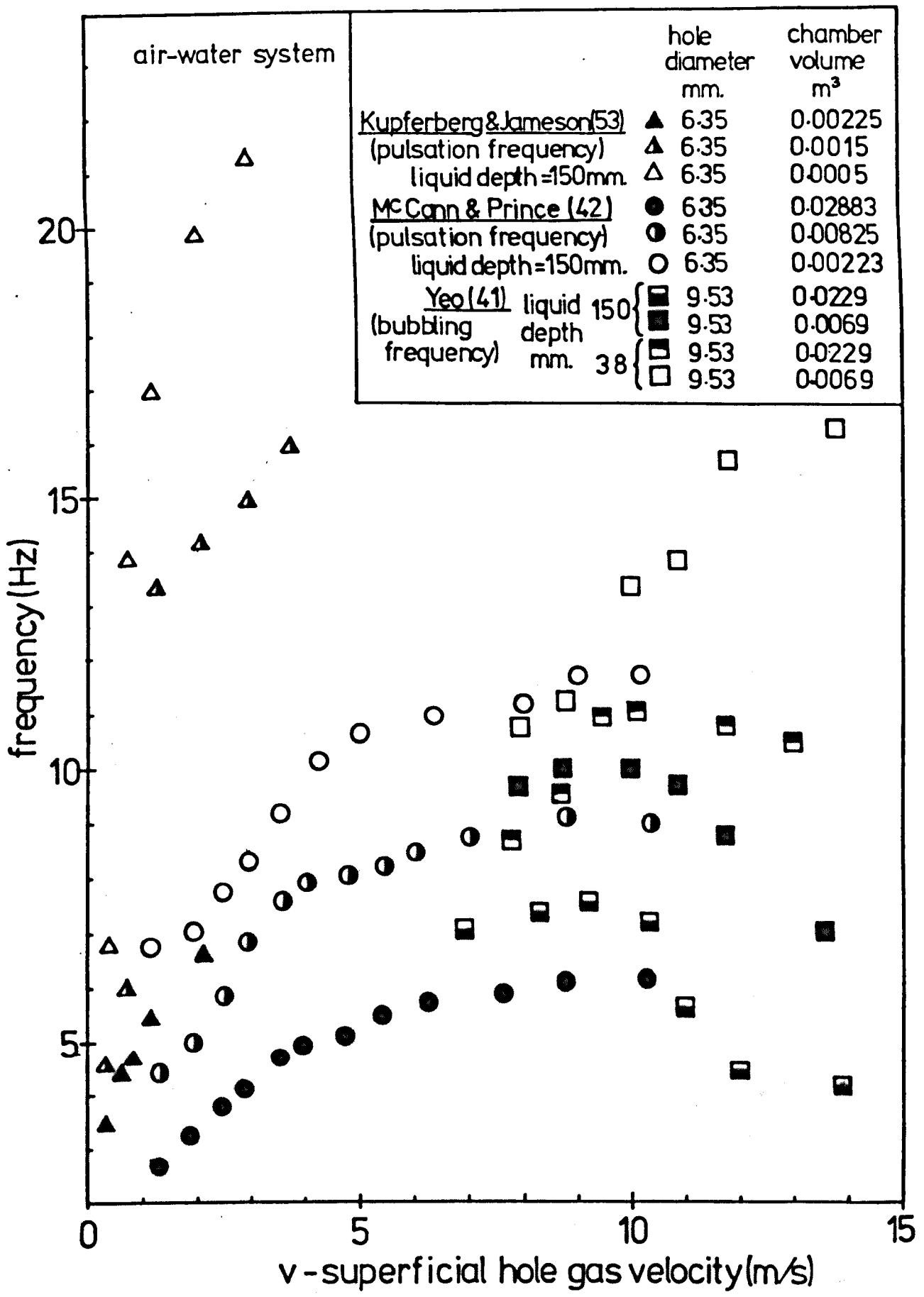

Fig.3.4. BUBBLING AND PULSATION FREQUENCIES FOR SINGLE-HOLE TRAYS

The frequencies found by McCann and Prince (42) and Kupferberg and Jameson (53), at low gas flow rates and high liquid depth, were shown to be well correlated by using the potential flow theory to describe bubble growth. The theory is applied assuming the bubble to remain spherical during formation and the depth of liquid to be large compared with the bubble diameter. McCann and Prince (43) stated that it was not possible to apply the theory to operation at higher gas flows when bubble formation became complex, and the various forms of double bubbling predominated. These workers showed double bubbling to result from high bubble frequencies, suggesting that at the frequencies measured by Waddington (2), (which are much higher than those found for single holes), double bubbling could be favoured.

It has been shown that for operation below liquid depths of 40 mm. of water, the frequency becomes depth dependent. Potential flow theory does not predict this dependency, suggesting that the second main assumption made (liquid deep with respect to bubble diameter), is not valid below depths of 40 mm.

Davidson and Amick (12) and Hughes et al. (13), showed that the bubbling frequency no longer increases with decreasing chamber volume, when the chamber volume becomes sufficiently small; the frequency then being independent of chamber volume. Davidson and Amick (12) found that this change took place at a chamber volume of about 0.00002 $m.^3$, for a 3.2 mm. diameter hole operating with air and water at a superficial hole gas velocity of 5.5 m/s. The condition of operation of a system with such a small chamber volume is taken to approximate to that of constant flow, (as defined in section 2.2.2), which is not representative of the operating conditions within sieve-tray systems, which contain relatively large gas chambers.

The maximum bubbling frequencies (12,13) used by Waddington (2) in obtaining his correlation, were mainly obtained for gas chambers sufficiently small as to have no effect on the frequency, that is for operation close to constant flow. These bubbling frequencies, which were much higher than those reported by other workers (37,42,53), are therefore not applicable to sieve-tray systems.

3.3.1 Summary of gas pressure fluctuations in single hole tray systems.

The frequencies of gas pressure fluctuations produced by single hole tray operation are, in general, much lower than those found for multi-hole trays by Waddington (2) and Brown (54) (29, 41 and 49 hole trays) under similar conditions.

The superficial hole gas velocity is the primary parameter affecting the pulsation frequency. Tray liquid depth becomes an important factor when it is below 40 mm. of water, (corresponding to operation in the pulsating jet regime), the frequency then increasing with decreasing liquid depth. Frequency is essentially independent of liquid depth in the bubbling regime (>40 mm. of water).

Most of the reported work has been carried out using high liquid depths (>40 mm. of water) and gas velocities corresponding to operation in the bubbling regimes. The gas pulsations are then directly related to the frequency and mode of bubbling. For such conditions the chamber volume is an important parameter affecting frequency; the frequency increasing with decreasing chamber volume. For small chamber volumes ($\simeq 0.0002$ m.^{3}), the mechanisms of delayed release and double bubbling may occur, resulting in an increased gas pulsation frequency. When the chamber becomes sufficiently small ($\simeq 0.00002$ m.^{3}) the hole operates in a manner approximating to constant flow, and the bubbling frequency is independent of chamber volume. This type of bubbling is not applicable to sieve-tray systems containing relatively large chamber volumes.

For simple bubbling at high liquid depths the bubble growth is described well using potential flow theory, but when double bubbling occurs or when the liquid depth falls below 40 mm. of water, this description is inadequate.

Increasing the gas density increases the bubbling frequency under certain conditions.

There is apparently no information available about the dependence of the pulsation frequency on the chamber volume for operation at low liquid depths in the pulsating jet regime (<40 mm. of water).

3.4 CONCLUSIONS.

Two types of gas pulsations have been found to occur in sieve-tray columns.

One type results from regular fluctuations of the tray liquid head and shows frequencies well below the range of damaging column vibrations.

The other type is in the 'correct' frequency range and is associated with the mechanism of gas-liquid interaction at the tray holes. However, the frequency of comparable gas-liquid behaviour on single hole trays is found to be at a lower frequency than the reported pulsations.

There is no adequate correlation available for predicting the frequency or amplitude of the damaging pulsations. There is little information available on how the pulsations are affected by various system parameters and it is not certain how they are produced. A further experimental investigation of these problems is therefore justified.

3.5 EXPERIMENTAL WORK REQUIRED.

It has been shown that the reported behaviour on single hole trays cannot account for the gas pulsations produced by a multi-hole tray. It is therefore necessary to investigate the production of gas pulsations using a multi-hole tray system.

The main parameters which affect the gas-liquid behaviour on a sieve-tray, and the fluid behaviour at the tray holes, have been identified as follows:

i) Superficial hole gas velocity;

ii) Tray liquid head;

iii) Liquid cross-flow rate;

iv) Hole diameter;

v) Hole pitch;

vi) Number of holes;

vii) Chamber capacitance;

viii) Liquid density;

ix) Gas density.

It is therefore necessary to determine the effects of all of these parameters, if possible, on the frequency and amplitude of the gas pressure fluctuations.

The column acoustics and vibrational response are also important factors affecting column damage, and should be investigated.

Furthermore, it is necessary to determine how and why the regular gas pulsations are produced. This requires observation of the gas-liquid behaviour at the tray holes during pulsation production, and the determination of how this behaviour results in the measured pulsations.

The experimental apparatus and measurement techniques required to achieve these objectives are described in the next chapter.

Chapter 4.

EXPERIMENTAL APPARATUS AND MEASUREMENT TECHNIQUES.

Introduction.

This chapter contains details of the experimental apparatus and measurement techniques used to study the effects of the important system parameters, as identified by Chapters 2 and 3, on the production of regular gas pulsations in sieve-tray systems.

A model sieve-tray column was used, which was sufficiently large as to be representative of an industrial column. It was a modification of that column used by Waddington (2). Details of its design and construction are given at the beginning of the chapter.

Tray geometry has been found to be an important factor governing gas-liquid behaviour. Various sieve-trays were used, with geometries typical of those used in industry. Appendix I contains details of the trays used.

Gas and liquid density have been found to affect gas-liquid behaviour; however, air and water were the only fluids used in this research. Details are given of the air and water system and the methods of flow measurement used.

Static and dynamic pressure measurements were made to determine the static gas resistances across the operating sieve-tray, including the tray liquid head, and to determine the frequency and amplitude of system gas pressure fluctuations. The tray and column mechanical vibration levels were also measured.

It was concluded in Chapter 3 that the mechanism of gas-liquid interaction at individual holes on the tray should be studied. Two main techniques were used. These were: electrical conductivity probes, similar to those used by other workers, and direct high speed cine photography.

4.1 MODEL SIEVE-TRAY COLUMN.

The overall arrangement of the experimental rig is shown in Figure 4.1. It can be divided into three sections: the model sieve-tray column; the

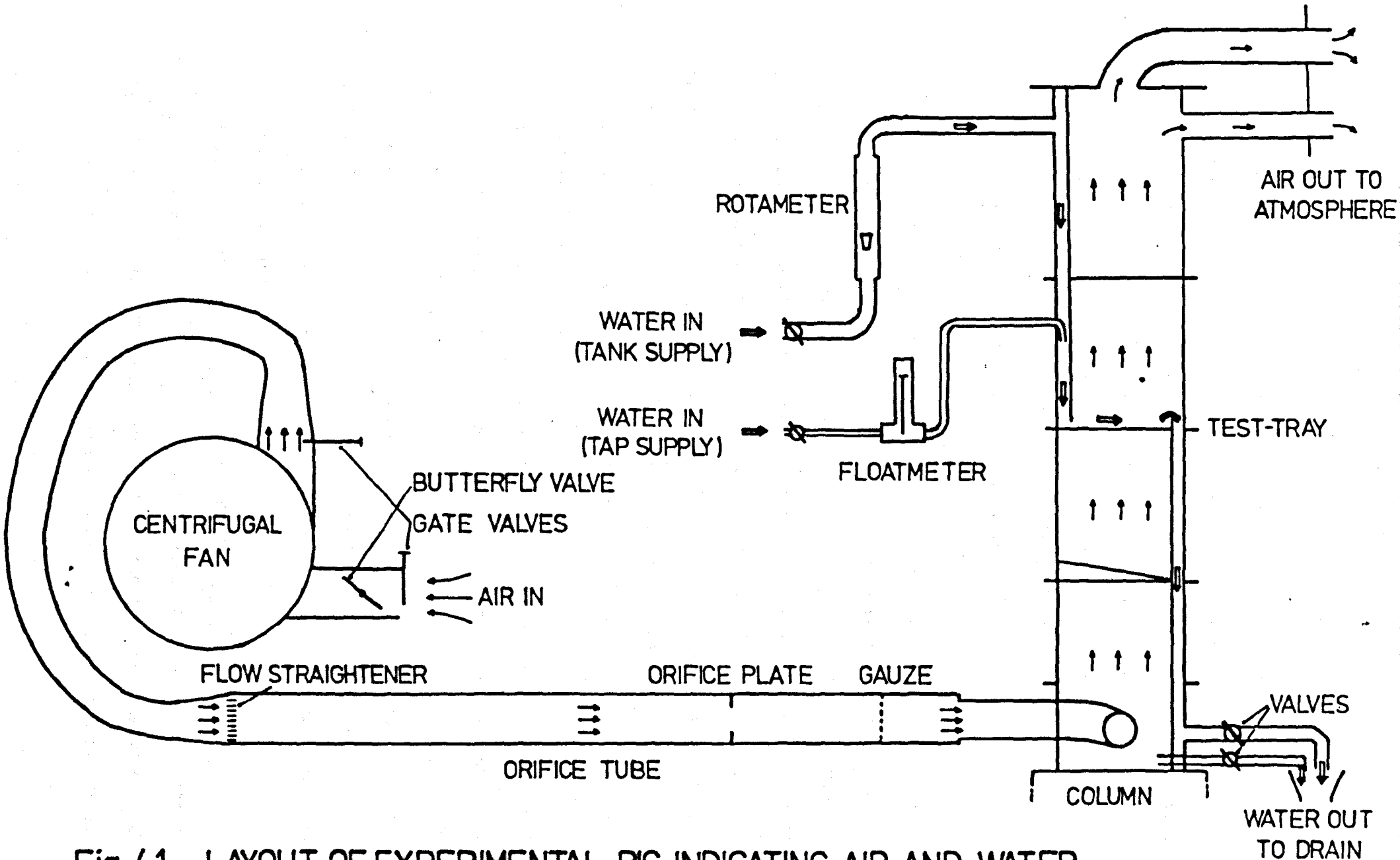

Fig.4.1 LAYOUT OF EXPERIMENTAL RIG INDICATING AIR AND WATER FLOW PATHS

air flow system and the water flow system. The fluid flow systems are described in the next two sections of this chapter.

The model column was a modification of that used by Waddington (2). Waddington used three active sieve-trays; however, in most of this research, only the centre tray was active, water by-passing the other two trays. Details of the column design and dimensions are given in Figure 4.2. Figure 4.3 shows an overall view of the column.

4.1.1 Column Construction.

The column was made up of four rectangular sections between which were fixed three sieve-trays. The sections were made from stress-relieved clear perspex sheet 6.35 mm. thick welded with polyvinyl chloride (P.V.C.) cement. The sections were bolted together at flanges made from 12.7 mm. thick clear perspex sheet welded to the walls of each section and stiffened by 4.76 mm. thick mild steel backing-plates. The flanges were bolted together by 22, bolts, 9.53 mm. in diameter and spaced 101.6 mm. (4 ins.) apart.

A sieve-tray, sealed between two 3 mm. thick neoprene rubber gaskets, was located at each flange connection.

The top of the column was a 3 mm. thick sheet of mild steel clamped to the upper flange of the top column section, and sealed with a 3 mm. thick neoprene rubber gasket.

The column was raised 0.5 m. above the ground on a stand made from mild steel tubing of 38 mm. square cross-section.

To increase column stability the top section was clamped to a concrete beam in the laboratory ceiling.

4.1.2 Downcomer system and adjustable weir mechanism.

There was a water downcomer, 50.8 mm. wide, in each column section, as shown in Figure 4.2. The downcomers of the two top sections were on the same side of the column and were sealed where they met at the top tray, to

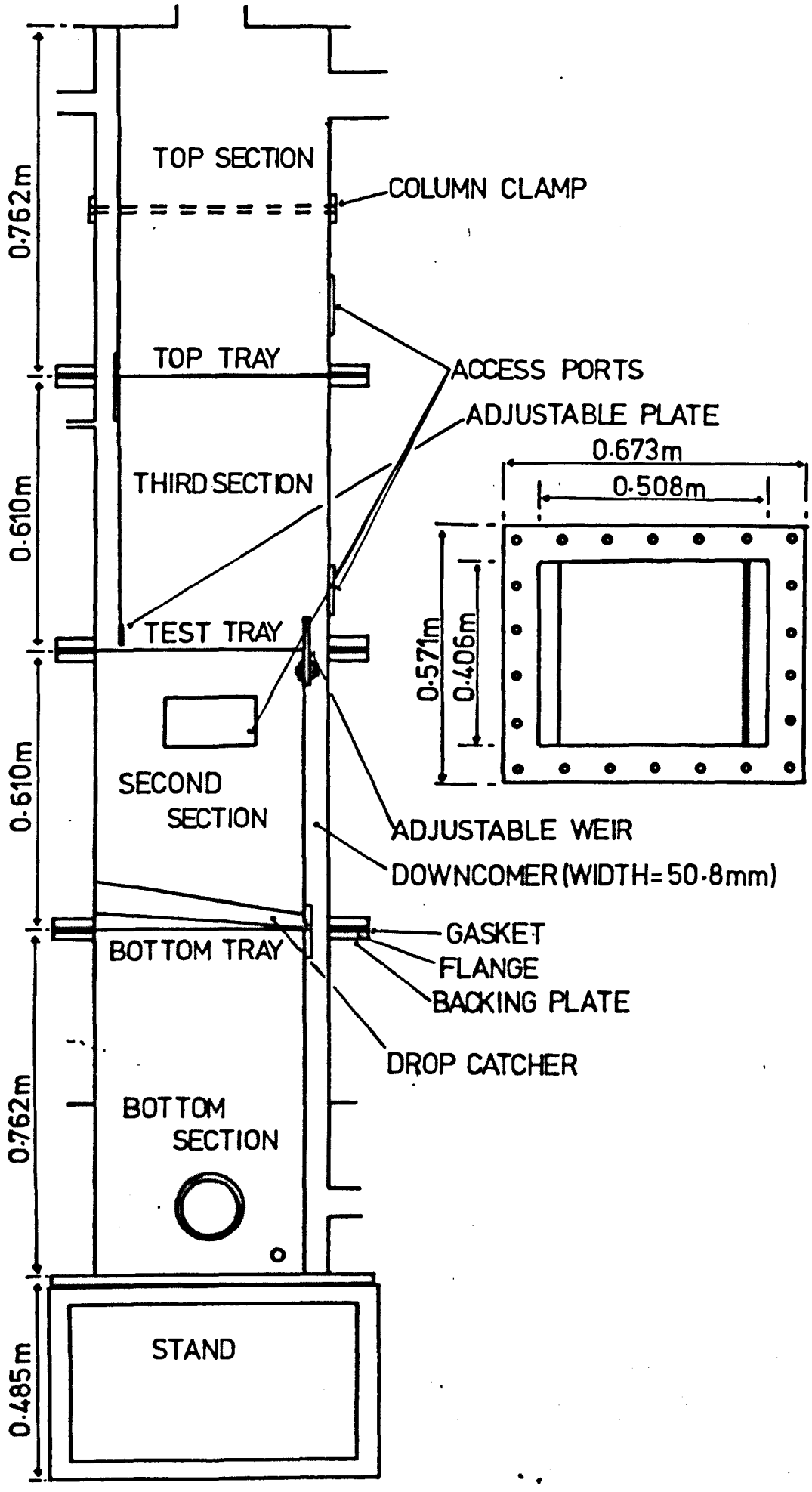

Fig.4.2 DESIGN AND DIMENSIONS OF MODEL SIEVE-TRAY COLUMN

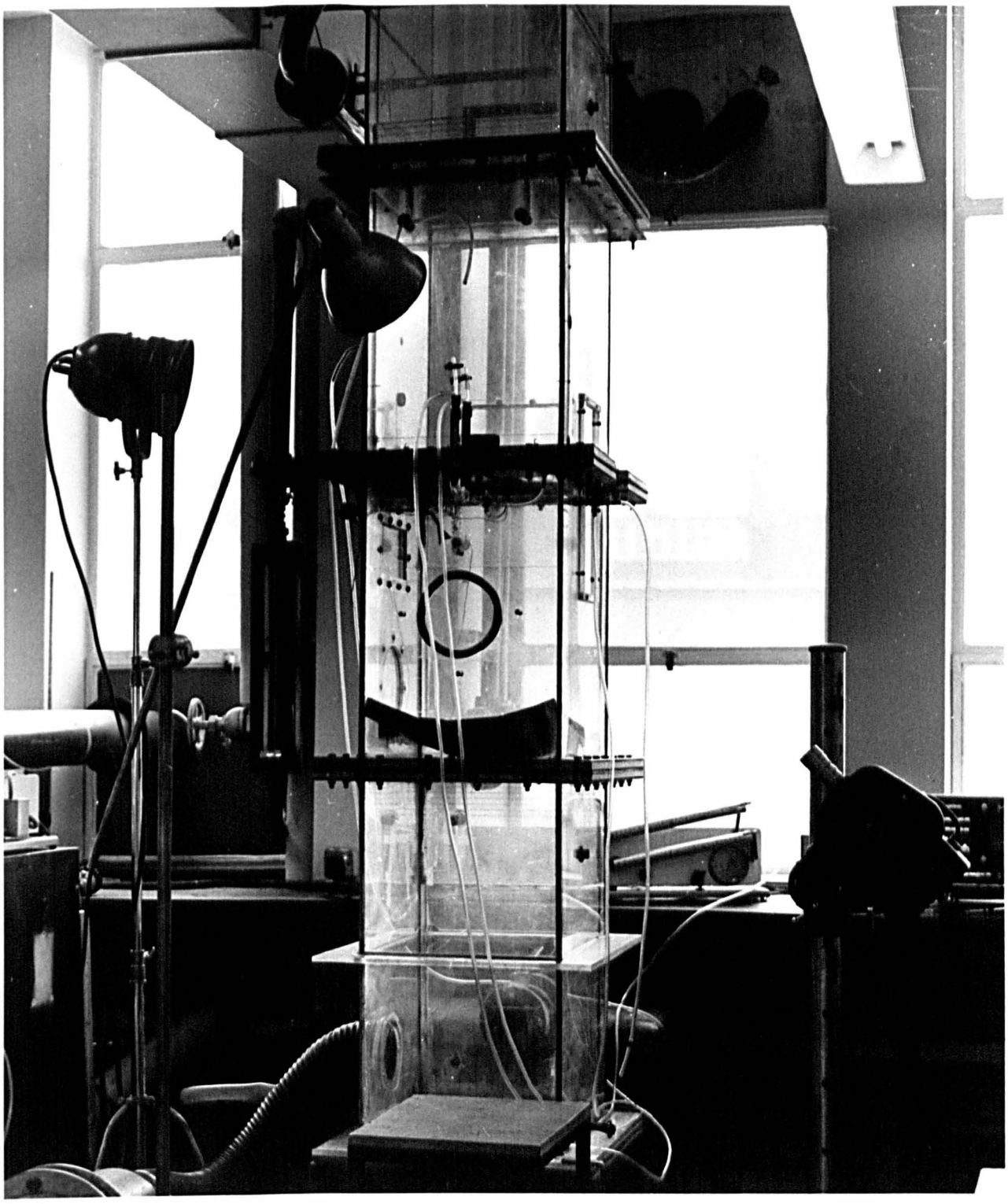

Fig. 4.3 EXPERIMENTAL RIG WITH CINE CAMERA IN POSITION BELOW THE TRAY

form a single downcomer from the water inlet to the test-tray. At the test-tray, an adjustable plate screwed to the bottom of the downcomer and used for varying the gap between the downcomer and the tray, was set to give a gap of 6.35 mm. This gap was sufficiently small so as to maintain a liquid seal and prevent gas leakage into and up the downcomer.

The downcomers of the two bottom sections were on the same side of the column. They were sealed where they met at the bottom tray so as to form a single downcomer from the test-tray to the water outlet.

Water leaving the test-tray flowed over an adjustable outlet weir, as shown in Figure 4.4. The weir height could be varied between 0 and 114 mm. Two slots allowed vertical adjustment, with two locking nuts fastening the weir at the selected height.

Two strips of soft rubber, bonded to the edges of the weir, provided a partial liquid seal between the edges of the weir and the column walls. Plasticine was used to complete the seal, and adhesive vinyl tape was used to seal the joint between the edge of the tray and the bottom of the weir.

4.1.3 Column pipe connections and access hatches.

Two drainage pipes for water and the air inlet pipe were connected to the bottom column section. The air inlet pipe was connected to a 12.7 cm. diameter hole positioned centrally in a side wall and 15 cm. above the base. A 2.5 cm. diameter water drainage pipe was connected on the same side 3 cm. above the base. The main drainage pipe for water was connected to a 5 cm. diameter hole positioned centrally in the downcomer outer wall, 18 cm. from the base.

The second column section had an 11 cm.by 20 cm. rectangular access port positioned centrally in a side of the column, its upper edge being 12 cm. below the test-tray. The port cover was made from clear perspex sheet, 12.7 mm. thick and was secured by ten bolts 6.35 mm. in diameter

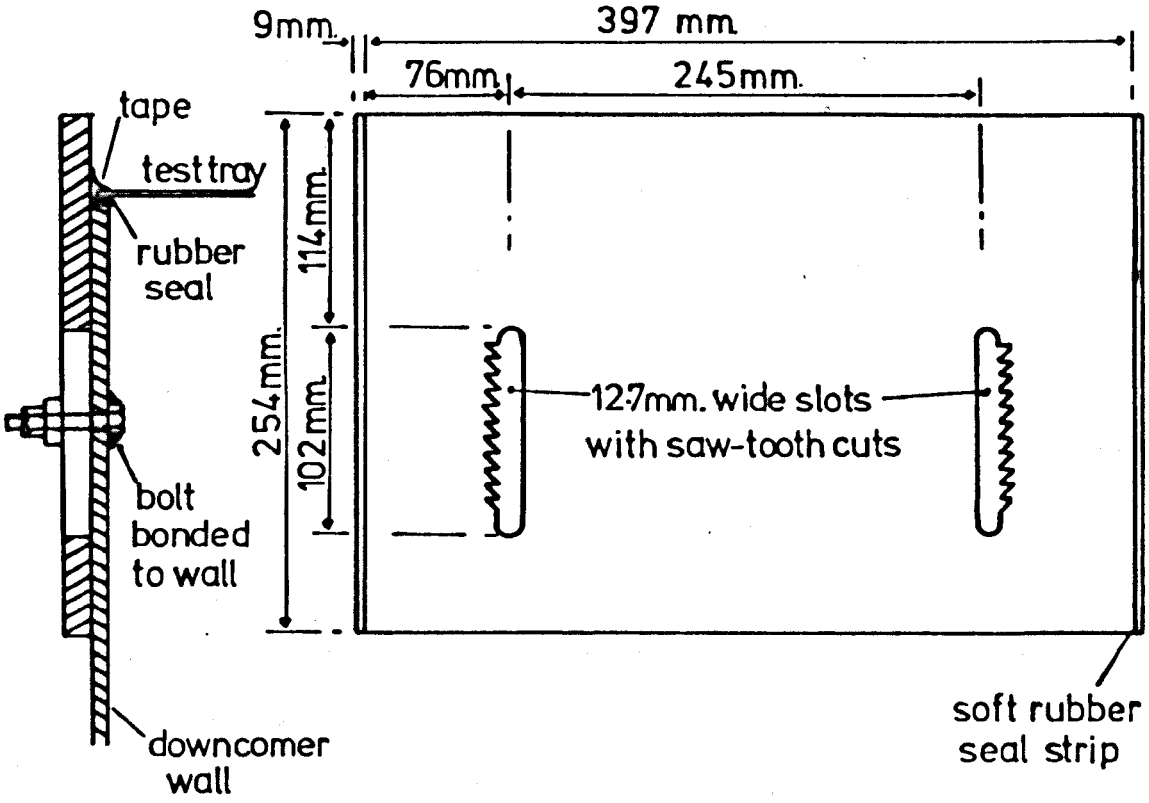

Fig.4.4 ADJUSTABLE WEIR DESIGN

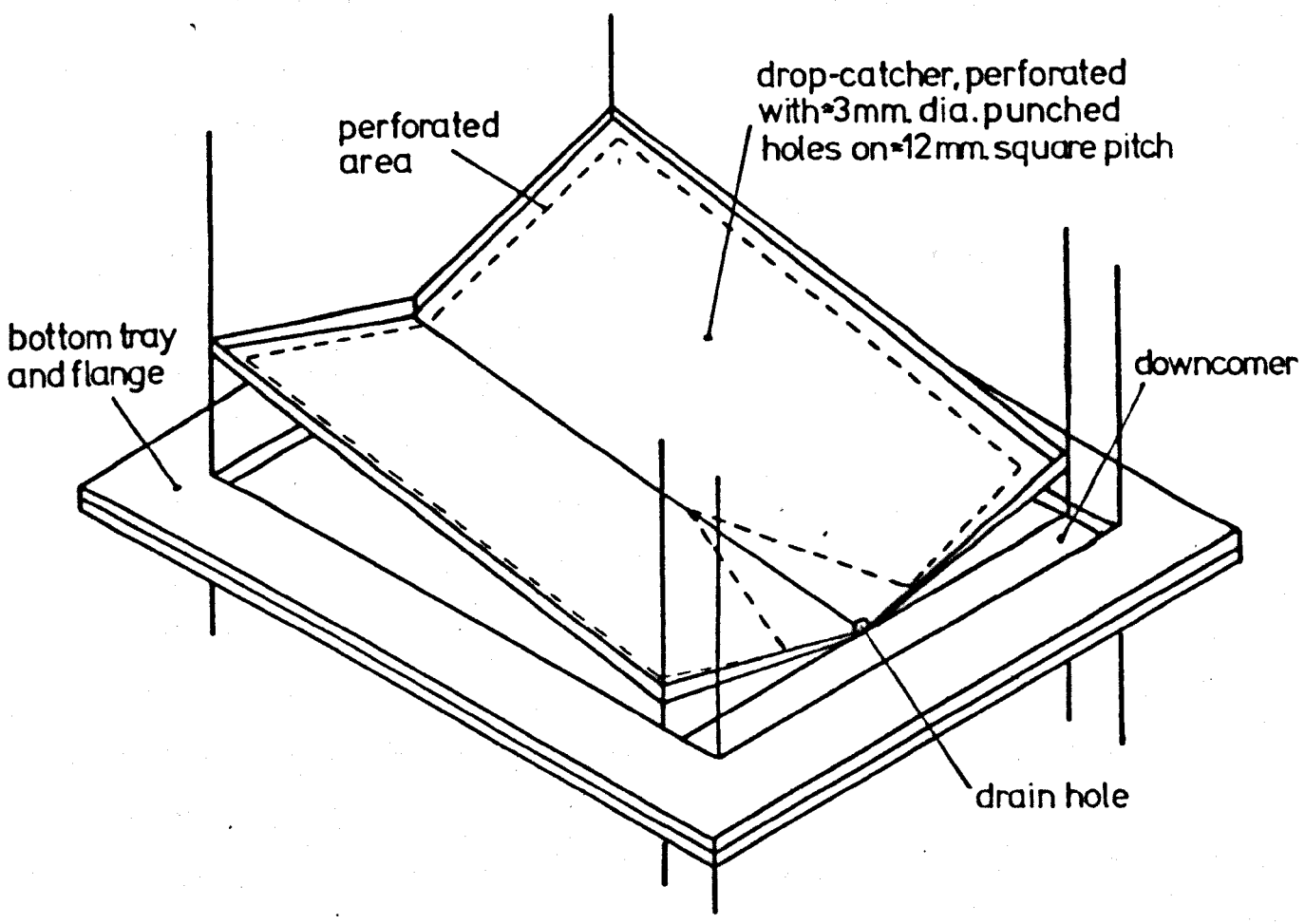

Fig.4.5 DROP-CATCHER DESIGN

set in the column wall. A rubber gasket provided a seal.

The third column section had an access port and a water inlet pipe connection. The port was of the same design as the one described above. It was positioned centrally in the wall of the column opposite the section downcomer, its bottom edge being 6 cm. above the test-tray. The water inlet pipe was an 8 mm. diameter polythene tube which passed into the downcomer via a bored brass plug screwed into the column wall. The tube protruded about 10 cm. into the downcomer.

The top column section had an access port, a water inlet pipe connection, and two air outlet pipe connection. The access port was of similar construction to the other ports; it was positioned centrally in the wall of the column opposite the section downcomer, its bottom edge being 8 cm. above the top tray. The water inlet pipe was connected to a 5 cm. diameter hole positioned centrally in the downcomer outer wall, 15 cm. from the top of the column. One air outlet pipe was connected to a 7.6 cm. diameter hole positioned centrally in the column wall opposite the section downcomer, 15 cm. from the top of the column. The other air outlet pipe was connected to a 15 cm. diameter hole positioned centrally in the top of the column.

4.1.4 'Drop catcher' design.

A 'drop catcher' was installed in the column, immediately above the bottom tray in order to prevent gas-liquid interaction on that tray. It collected water which had'wept'through the test-tray and it then drained away into the downcomer.

The design of the drop catcher is shown in Figure 4.5. It was made from two thin steel sheets punched with holes of approximately 3 mm. diameter on approximately 12 mm. square pitch. The hole burrs were left protruding upwards to increase the efficiency of water collection. The steel sheets were jammed in position and fastened to the column walls by adhesive vinyl tape.

The collected water drained towards the downcomer and passed through a small drain hole into the downcomer. Under weeping conditions a water seal tended to prevent air leakage through the drain hole. In the absence of weeping the hole was sealed with plasticine.

4.1.5 Sieve-tray design and instalment.

Full details of the sieve-tray design, the range of tray geometries used, and the procedure for changing the test-tray are given in Appendix I. Figure I.1 shows the basic sieve-tray design.

The trays were made from 3.175 mm. thick steel plate; the holes were drilled with sharp edges, and were all on equilateral triangular pitch (equ.tri.pitch).

The top and bottom trays in the column were bypassed by the water flow, and acted as constant gas flow resistances. The top tray contained 403, 4.76 mm. diameter holes on 19.05 mm. equ.tri. pitch. The bottom tray contained 403, 6.35 mm. diameter holes on 19.05 mm. equ.tri. pitch. Various test-tray geometries were used as defined in Table I.1. The ranges covered were: hole diameters between 4.76 mm. and 15.87 mm., equi.tri. pitch between 19.05 mm. and 66.04 mm. and number of holes between 38 and 403.

4.2 AIR FLOW SYSTEM AND MEASUREMENT.

The air flow system in shown in Figure 4.1. The air was supplied from atmosphere by a 3.1 H.P. centrifugal fan. Details of the fan are contained in Appendix II. Column volumetric air flow rates of up to 0.33 m^3/s. were possible.

The air flow rate was regulated at the fan inlet by a 20 cm. diameter gate valve and a 20 cm. diameter butterfly valve, in series. A further gate valve, attached to the fan outlet, was permanently open.

Air leaving the fan passed, through a 2.75 m. length of 15 cm. diameter flexible plastic pipe, into the orifice tube for flow measurement.

Details of the orifice tube and flow measurement are given below. Air leaving the orifice tube passed through a 1.0 m. length of 15 cm. diameter flexible pipe into the bottom column section.

After flowing up the column the air left through two flexible plastic pipes connected to the top column section. One, a 2.0 m. length of 15 cm. diameter pipe connected to the top of the column, and the other, a 2.0 m. length of 10. cm. diameter pipe connected to the side of the column. Both exit pipes passed through a laboratory window and the air was vented to atmosphere.

4.2.1 Airflow rate measurement.

Gas flow rate measurement was by orifice plate and conformed to British Standard 848 part 1, 1963 'Methods of testing fans: General purposes.'

The 11.43 cm. (4.50 inches) diameter brass orifice plate was located in the orifice tube, as shown in Figure 4.6.

The pressure drop across the orifice plate was measured at D, D/2 pressure tappings, using two inclined gauge manometers. One had a pressure range of 0 to 152 mm. (0 to 6 in.) of water, with graduations every 0.58 mm. (0.02 in.) of water. The other manometer had two pressure ranges, one from 0 to 25 mm. of water and the other from 0 to 12.5 mm. of water with graduations every 0.1 mm. of water and 0.05 mm. of water respectively. The choice of manometer was determined by the hole free area of the test-tray; high free area trays required a greater column gas volumetric flowrate for a given superficial hole gas velocity.

The orifice plate was calibrated using a rotating vane type anemometer. Details of the calibration are given in Appendix II.

4.3 WATER FLOW SYSTEM AND MEASUREMENT.

The quantity of water used was considered to be sufficiently small for it to be drained away and not recycled. Water flow rates of up to 0.467 m^3/hr. (500 galls/hr.) were possible.

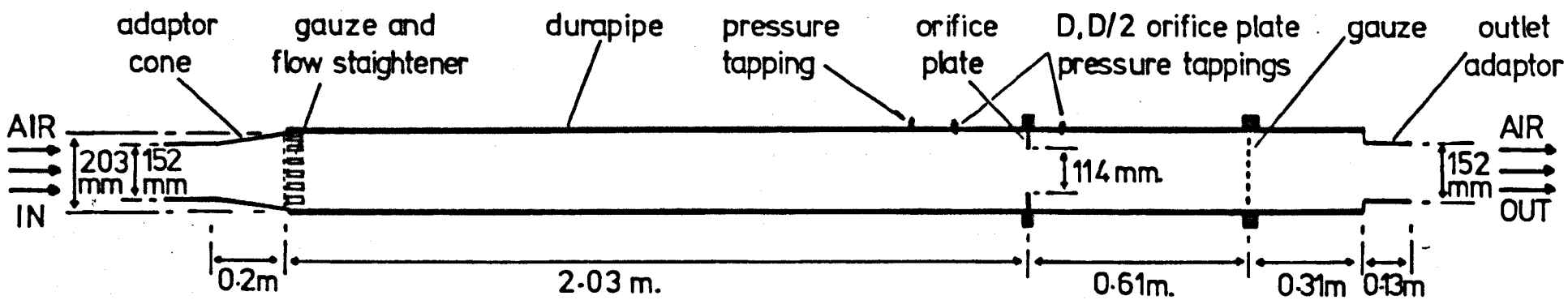

Fig. 4.6 AIR FLOW MEASUREMENT ORIFICE TUBE

Two water supplies were used, as shown in Figure 4.1.

For low flow rates, the water was supplied and regulated by a laboratory bench tap. From the tap, the water flowed through a 12 mm. diameter rubber tube into a Drayton flow indicator for measurement. The flow indicator had a range of 0 to 0.234 m^3/hr.(50 galls/hr.) with 0.00934 m^3/hr. (2 galls/hr.) graduations. Its calibration is described in Appendix III. From the meter the water flowed through an 8 mm. diameter polythene tube into the third column section downcomer.

For higher flowrates, the water was supplied from the main water tank on the roof of the building. The water flowed through a regulator valve into a rotameter for flow measurement. The rotameter had a range of 0.234 m^3/hr. to 2.34 m^3/hr. (50 galls/hr. to 500 galls/hr.) with 0.0467 m^3/hr. (10 galls/hr.) graduations. Its calibration is described in Appendix III. From the rotameter the water flowed through a length of 50.8 mm. diameter flexible plastic pipe and then through a length of 50.8 mm. diameter plastic 'durapipe' into the downcomer of the top column section.

After flowing down the column and across the test-tray, the water left through the 50.8 mm. diameter plastic 'durapipe' attached to the bottom section downcomer. A valve regulated the exit flow and the water went to drain. The valve was used to ensure a permanent liquid seal at the pipe exit, thus preventing gas leakage from the column.

Water which passed through the drop catcher and the bottom tray and into the gas chamber of the bottom column section, left through a 2.5 mm. diameter plastic pipe at the base of the column. A valve regulated the exit flow and the water went to drain.

4.4 STATIC PRESSURE DROP MEASUREMENTS.

Chapter 3, section 3.1 identified the three main static pressures which should be measured:

i) The pressure in the gas chamber beneath the test-tray, P_1;

ii) The pressure at the top surface of the test-tray, as measured by pressure tappings mounted in the tray, P_2;

iii) The pressure in the gas chamber above the test-tray and gas-liquid mixture, P_3.

Figure 4.7 gives details of the pressure tappings used. Those mounted in the column wall (P_1 and P_3) were made from 3 mm. i.d. copper tube and were flush with the inside surface of the wall. Because water droplets tended to block these pressure tappings, leading to incorrect readings, two 'blow' tubes were introduced, as shown in Figure 4.7, to enable any droplets to be blown away before a measurement was taken. The nine tray-mounted tappings (P_2) were made from 3 mm. i.d. brass tube. They were screwed into threaded holes in the tray and secured by two nuts. The tops of the tappings were filed down until they were flush with the upper tray surface. The nine tappings were interconnected using polythene tubing and glass junction pieces.

The total tray static pressure drop, (P_1-P_3) was measured using an inclined gauge manometer, (Airflow Developments Ltd.). It had a pressure range of 0 to 100 mm. of water with 0.2 mm. of water graduations.

The static pressure drops, P_1-P_2 and P_2-P_3, were measured by using the limbs of a glass U-tube as vertical manometers. A wall pressure tapping was connected to the top of each limb, and a glass tube, joined to the bottom of the u-tube, connected it to the tray pressure tappings. The U-tube was filled with water from the tray. Each limb had a mm. scale and readings were taken through a magnifying eye-piece using the bottom of the water meniscus as a reference.

Vertical movement of the u-tube allowed it to be calibrated directly. With water in the tray tappings just level with the damp tray surface, the

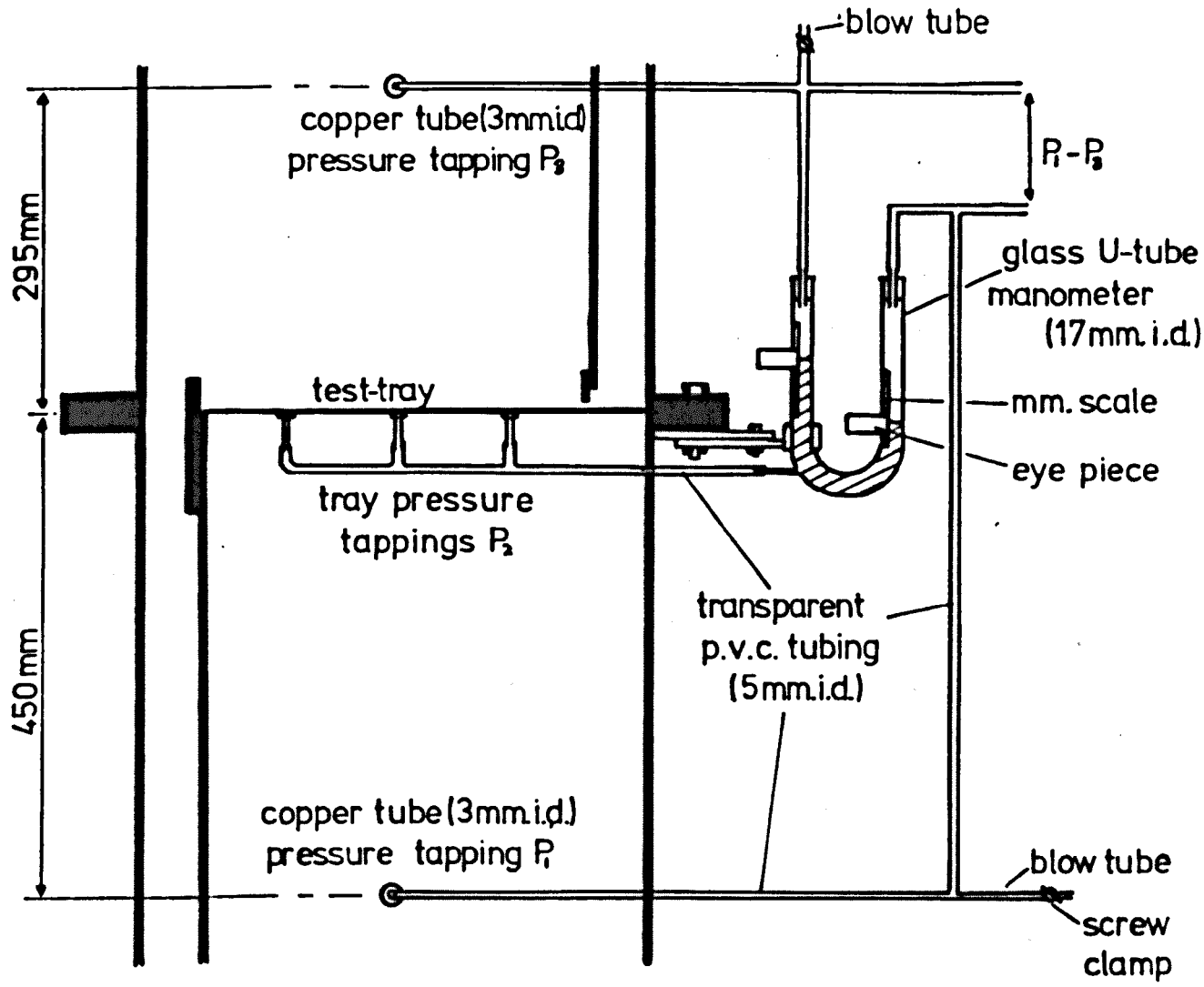

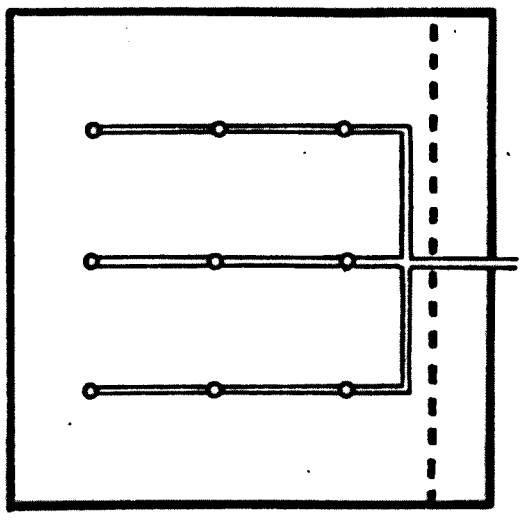

typical location of
tray pressure tappings

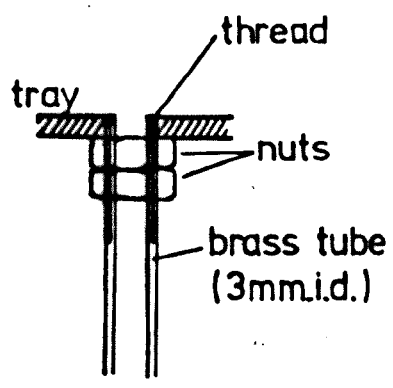

tray pressure
tapping

Fig.4.7. STATIC PRESSURE TAPPINGS AND MEASUREMENT

tube was moved until the bottom of the water meniscus in each limb corresponded to zero on the mm. scale. This calibration accounted for any surface tension effects. A spirit level was used to ensure that the u-tube was vertical.

4.5 MEASUREMENT OF THE HEIGHT OF THE GAS-LIQUID MIXTURE ON THE TRAY.

The height of the gas-liquid mixture was measured visually using three vertical scales with 6.35 mm. (0.25 inch) graduations. Two scales were marked on the column walls, one on each side of the test-tray, and the third scale was marked on a strip of clear perspex fixed to the flange. The scales were arranged in a line, halfway along the liquid flowpath, so that it was possible to view all three scales simultaneously across the tray.

Height measurements were not taken for operation in the spray regime.

4.6 DYNAMIC PRESSURE MEASUREMENTS.

Dynamic pressure measurements were made using two Kistler quartz pressure transducers (Type 412). The charge signal from the transducers was amplified and transformed to a voltage by charge amplifiers. Pressure transducer 1 had a Universal Kistler electrostatic charge amplifier, Model 568; and pressure transducer 2 had a Vibro-Meter Corporation Piezo-amplifier type TA-2/C. The amplifier gains were adjusted to give an output voltage of 10 mV. per 1.0 mm. of water pressure impulse. The transducers were calibrated as described in Appendix IV.

Typical transducer positions and details of the probe attachments are given in Figure 4.8. The transducer support brackets were rigidly bolted to the flange, and a simple test showed the mechanical vibration response of the transducers to be negligible for this arrangement.

The copper gauze hood and cone were attached to the copper probes to prevent water droplets forming at the tip of the probe and interfering

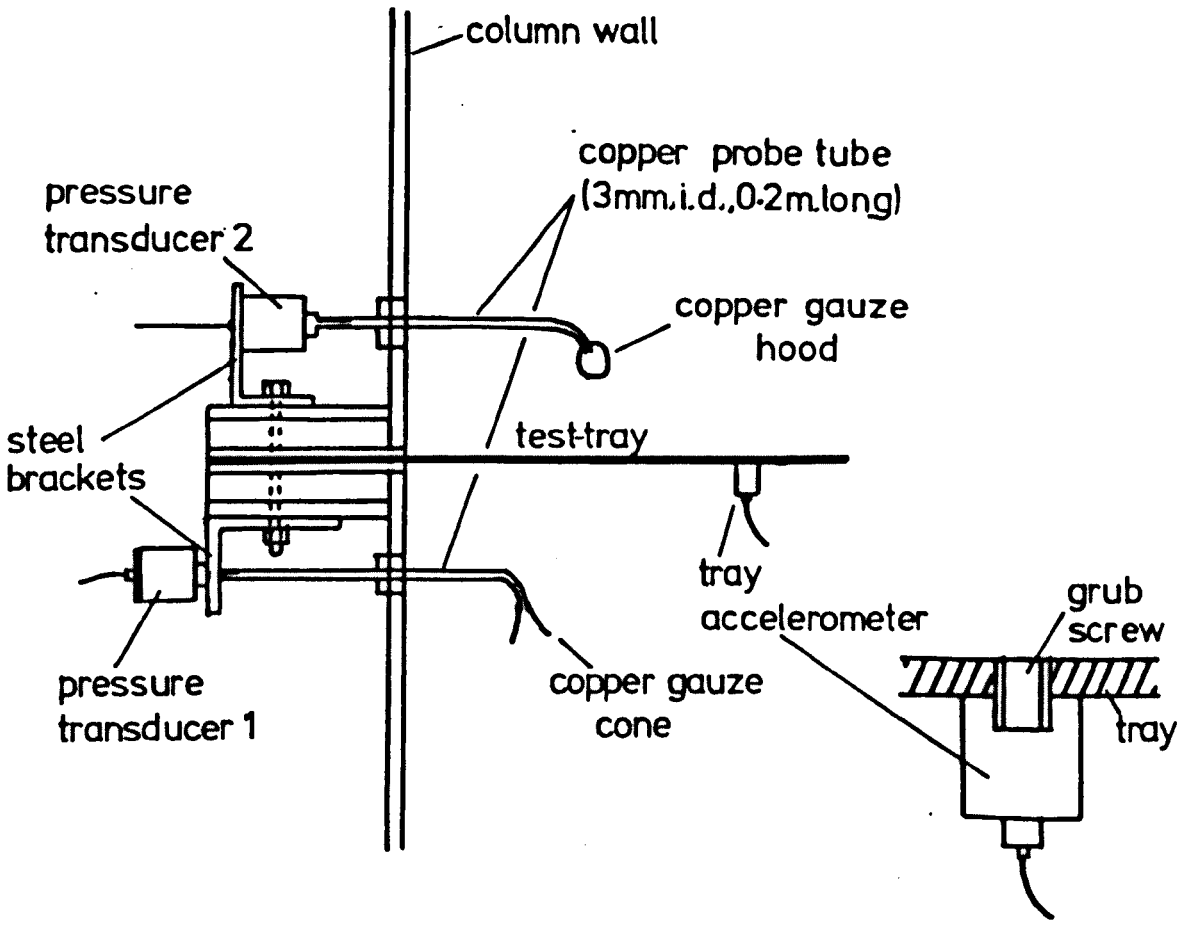

Fig. 4.8. TYPICAL POSITIONS OF PRESSURE TRANSDUCERS AND TRAY ACCELEROMETER

with the pressure readings. It was shown experimentally that the probe length did not affect the dynamic pressure reading.

4.7 MEASUREMENT OF THE TEST-TRAY AND COLUMN WALL MECHANICAL VIBRATION LEVEL.

Mechanical vibration levels were measured using two Bruël and Kjoer lightweight piezo-electric accelerometers, type 4334, and a Bruël and Kjoer vibration pick-up preamplifier type 2625.

One accelerometer was secured to the underside of the test-tray by a screw tapping, as shown in Figure 4.8. The other accelerometer was similarly secured to the outer column wall of the test-tray outlet downcomer, 12 cm. below the level of the tray.

The accelerometer system was calibrated to give an output of 150 mV for an input velocity of 0.3 m/s., as described in Appendix IV.

4.8 SIGNAL ANALYSIS AND DISPLAY.

Most of the analyses were performed using a real time analyser, although some were carried out using a Bruël and Kjoer frequency analyser and level recorder.

Signals were displayed on a storage cathode ray oscilloscope. A polaroid camera was used to obtain photographic records of the signal traces.

4.8.1 Real time signal analysis.

A Spectral Dynamics Corporation, model SD335, spectroscope II, real time analyser was used. This had a built-in oscilloscope giving signal display in the time or frequency domains.

Of the ten frequency ranges available, analyses were carried out with a range of 0.06 Hz. to 100 Hz. full scale, which gave a 3 dB. resolution bandwidth of 0.3 Hz. Three frequency domain channels were available; real time, average memory and storage memory. One or any two channels could be displayed simultaneously.

A linear average of four successive 5 second processed signal periods was carried out, the average being updated with subsequent 5 second periods, in an exponential manner.

A hand-operated movable cursor, linked to a digital display, gave direct readout of the spectrum component frequencies ($\pm$ 0.2 Hz.) and r.m.s. amplitudes ($\pm$ 0.1% full scale). The total signal r.m.s. amplitude was shown on the extreme right of the display. A full scale deflection of 0.1 v. was used for most of the analyses, (for pressure signal analyses this was equivalent to a full scale deflection of 10 mm. of water or 98.1 $N./m^2$).

Some real time frequency analysis was carried out using a Schlumberger, 1510, Solatron spectrum analyser. For a frequency range with 51.2 Hz. full scale, this gave a 1.76 dB. bandwidth of 1.5 Hz. Four, 5 second signal periods were averaged. It had an oscilloscope with a hand-operated movable cursor linked to a digital display. This gave direct readout of the spectrum component frequencies ($\pm$ 0.2 Hz.) and amplitude ($\pm$ .1% full scale). A full scale deflection of 0.1 v was used.

Figure 5.3 shows examples of real time analyser signal displays.

4.8.2 Other signal analysis techniques.

Some frequency analyses were carried out using a Bruël and Kjoer frequency analyser, type 2107, combined with a Bruël and Kjoer level recorder type 2305.

The level recorder paper output gave a permanent record of the frequency analyses. The lower limits of the frequency analysis was 20 Hz. Frequencies could be measured to an accuracy of $\pm$ 0.5 Hz, with a 3 dB. bandwidth of 6%. R.m.s. amplitudes were measured on a dB scale ($\pm$ 0.5 dB).

Analysis by this method was time-consuming and less accurate than that using the real time analyser.

4.8.3 Signal display.

Signals were displayed on a Textronix storage cathode ray oscilloscope, type 564, with a type 3A74 amplifier unit and a type 2B67 time base unit.

Simultaneous display of up to 4 signals was possible.

8.5 cm. x 10.5 cm. photographs of stored signal traces were taken with a Polaroid CR-9 Land camera ('B' shutter setting; f/11), using Polaroid Land film type 107 C.

4.9 ELECTRICAL CONDUCTIVITY PROBES.

Gas-liquid interaction at individual holes on the test-tray was monitored using electrical conductivity probes, of a similar design to those used by Pinczewski and Fell (28).

Probes were made from p.v.c. coated copper wire (0.6 mm. diameter), and were mounted, as shown on Figure 4.9, on tray pressure tappings. Various probe heights were used.

The probes measured the electrical conductivity between the tray surface and the exposed probe tip. With a 24 volt D.C. potential difference applied across the probe and the test-tray, current flowed when there was a liquid bridge between the tray and the tip. The voltage across the probe was monitored on the oscilloscope.

A maximum of six probes was used, as shown in Figure 4.9, with up to four probe signals being displayed simultaneously on the oscilloscope. Probes 1 and 2 were each connected to an oscilloscope channel, the other two channels being connected to six-way switches, each of which could select any one of the six probes.

Examples of probe signals are given in Figure 6.1, 6.2 and 6.3.

4.10 HIGH SPEED CINE-PHOTOGRAPHY.

The gas-liquid interaction at holes over part of the test-tray was studied directly using high speed cine-photography. This required modification of the column and test-tray.

4.10.1 Modifications to the Model Column and test-tray.

In order to permit direct photography from above and below and level with the test-trays, two main modifications were necessary. A section of

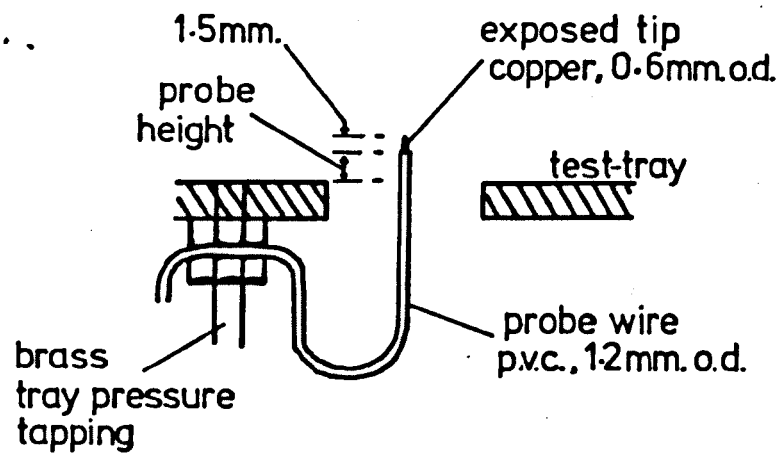

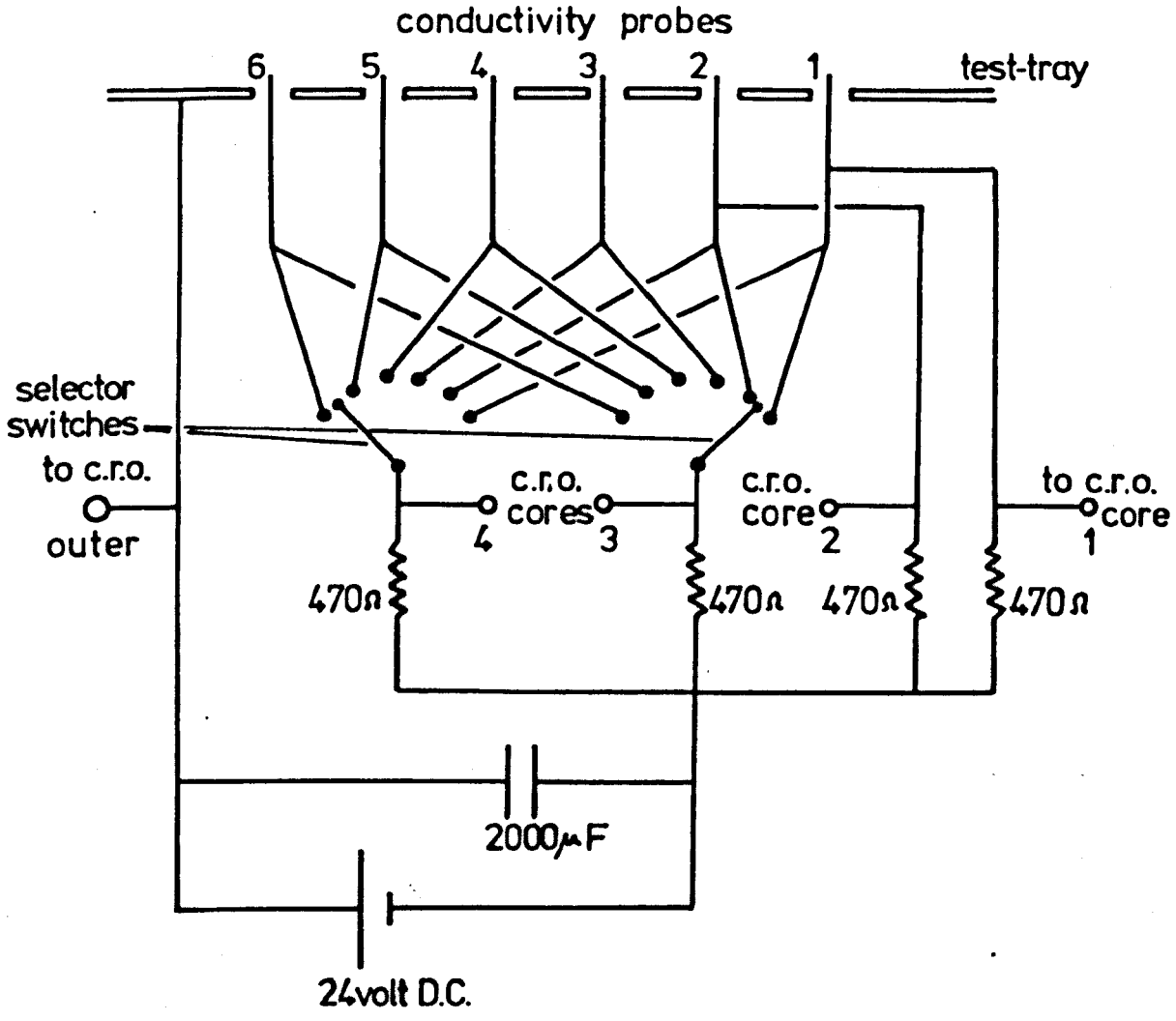

Fig. 4.9. ELECTRICAL CONDUCTIVITY PROBE DESIGN AND CIRCUIT

column wall and flange was removed and replaced by a 3 mm. thick glass plate,and a section of the test-tray was removed and replaced by a 3 mm. thick perforated glass plate. Figure 4.10 gives details of the modifications and Figure 4.11 shows a typical camera view from beneath the test-tray, with the camera position being similar to that shown in Figure 4.3.

The wall glass plate was secured by grooved perspex brackets screwed to the column and it could be easily removed to allow the test-tray to be changed. Two tight-fitting 6.35 mm. diameter steel locating rods set in the flange, enabled the bracket grooves to be easily re-aligned following a tray change.

The glass tray inserts were drilled so as to ensure the production of square-edged holes, without chipping, as described in Appendix I. Glass was used because it is wetted by water, (perspex is not wetted and could have affected the gas-liquid interaction at the holes.)

The tray insert was glued into position, and rested on five metal lugs welded to the underside of the test-tray. Care was taken to ensure that the top of the insert was level with the upper tray surface, and that the holes conformed with the tray hole pattern. The joint between the tray insert and the wall glass plate was sealed with perspex cement.

4.10.2 Cine-photography.

Films were taken using a Kodak high speed camera (Ser. No. 1978) with a Kodak 63 mm., f/2.0 luminized lens. The film used was 16 mm. Ilford Mark V motion picture safety film, type 782. An entire film length of 30.48 m. (100 ft.) had to be used for each run.

Film speeds of between 350 frame/second and 2250 frames/second were used. The camera internal timing lamp marked the edge of the film at 10 millisecond intervals, enabling the exact film speed to be calculated. The length of film required to reach constant frame speed varied from 12 m. at the lower speeds to 20 m. for the higher film speeds.

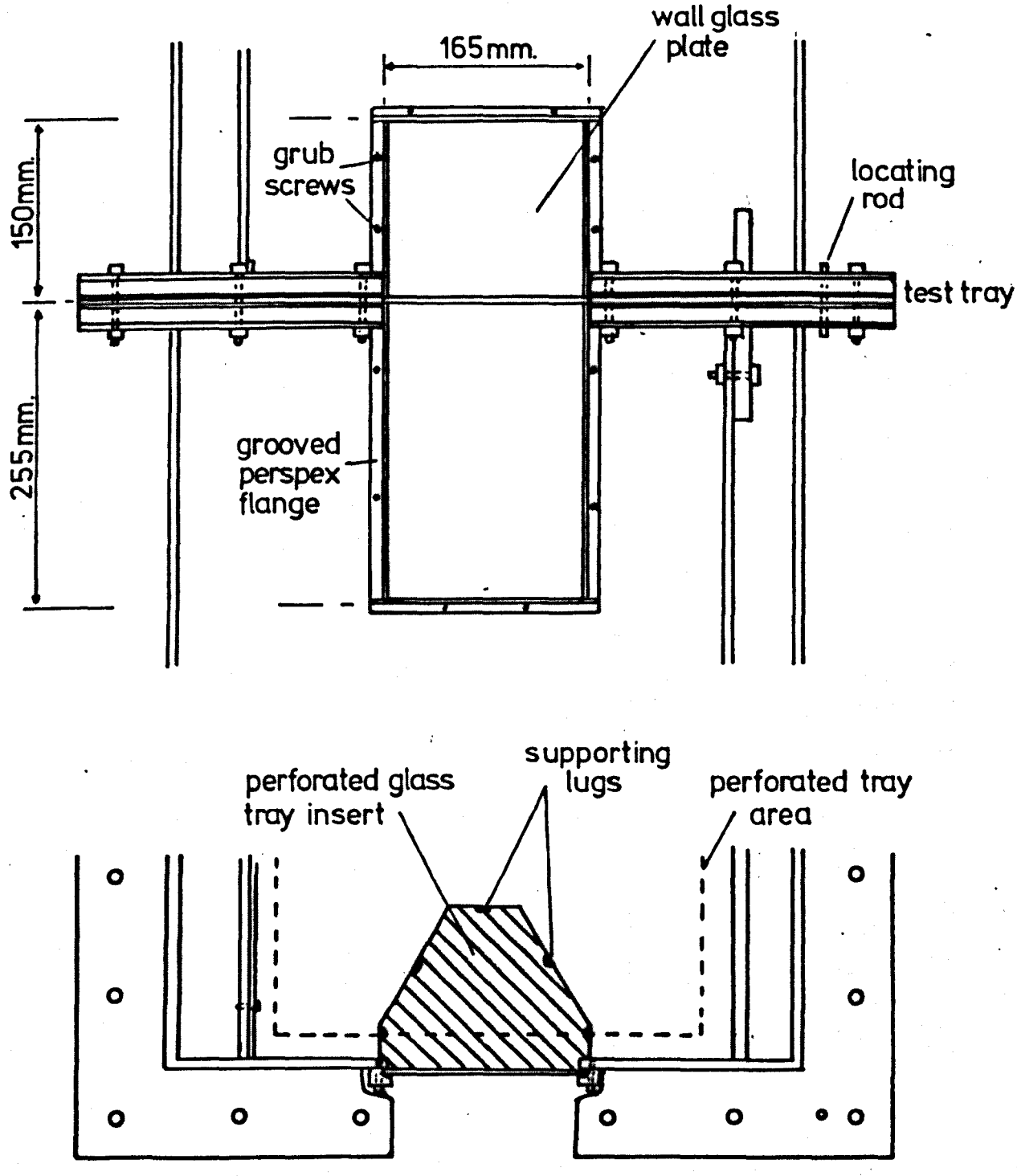

Fig. 4.10. RIG MODIFICATIONS FOR CINE-PHOTOGRAPHY

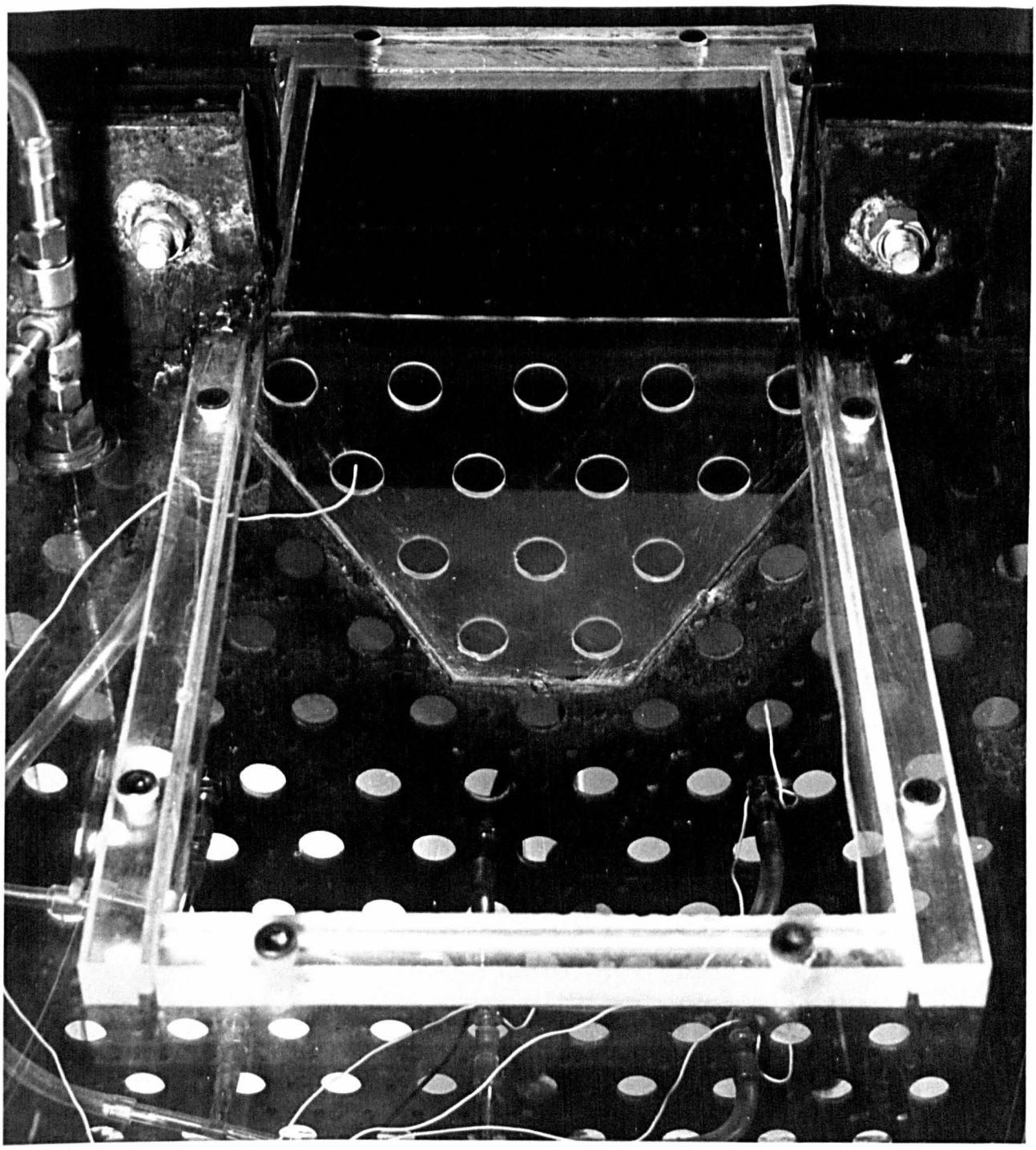

Fig. 4.11 VIEW FROM BELOW THE MODIFIED TEST-TRAY

Lighting was provided by two 1000 w. Colortran flood lamps.

The films were developed by the departmental photographer, and analysis was carried out using film negatives. Some film prints were obtained but did not prove to be more useful for analysis than the negatives.

4.10.3 Film analysers used.

Detailed measurements on the film were carried out using two film analysers, a Vangard Motion Analyser and an L.W. Photo-optical Data Analyser, Model 224-A.

The Vangard Motion Analyser was located in the Department of Metallurgy, University of Newcastle. The analyser had a Model M-16C projection head. This gave motorised, variable speed, projection up to 30 frames/second in forward or reverse directions and it had a digital frame counter with zero reset,which added or subtracted. The analyser had a Model C-11 projection case. The image was back-projected on to a screen which had two, hand controlled, movable cross-hairs for X-Y measurements. The X and Y coordinates were displayed on a variable gain digital voltmeter readout system, which had a zero reset. The voltmeter gain selected gave X-Y coordinates to an accuracy of $\pm$ 0.1 mm. (tray/column dimensions).

The Photo-optical Analyser was located in the University of Sheffield Traffic Engineering Laboratory, Department of Civil and Structural Engineering. The image was back-projected on to a plain screen. It had a variable speed control giving forward or reverse frame speeds of 1, 2, 4, 6, 8, 12, 16 and 24 frames/second. It had a forward/reverse digital frame counter with a zero reset.

4.11 SUMMARY.

The experimental rig allows the study of a single active sieve-tray of various hole geometries, contained in a large model column and operating over a wide range of air and water flow rates.

The measurement techniques allow accurate determination of the column static and dynamic pressures and mechanical vibration levels, with real time signal analysis and display.

Electrical conductivity probes and high speed cine photography allow the direct study of the gas-liquid interaction at individual holes on the tray.

The next two chapters describe the experimental work carried out using the above apparatus and measurement techniques.

Chapter 5.

EXPERIMENTAL WORK AND RESULTS - I.

EFFECTS OF SYSTEM VARIABLES ON THE REGULAR GAS PULSATIONS.

Introduction.

Damaging column vibrations have been found to result from regular pulsations in the column gas flow, induced by the gas-liquid interaction on the sieve-tray.

The major system parameters affecting the gas-liquid behaviour on the tray have been identified as:

i) Superficial hole gas velocity;

ii) Tray liquid head;

iii) Hole pitch;

iv) Hole diameter;

v) Number of holes;

vi) Tray liquid crossflow velocity;

vii) Capacitance of the chamber beneath the test-tray.

In this chapter is described the experimental investigation carried out to determine the effects of these system variables on the amplitude and frequency of the column gas pulsations. The results of this investigation are also given.

The effects on the pulsations of the tray vibrational response and the system acoustics were also investigated.

Experimental work carried out to determine why and how the gas pulsations are produced by the gas-liquid interaction on the tray is described in the next chapter.

Some preliminary experimental work was carried out using three active sieve-trays. The main findings of this work are given in the next section.

5.1 PRELIMINARY EXPERIMENTAL WORK.

Preliminary experimental work showed that when the model column was operated with three active sieve-trays, the operating conditions on each tray were different. Furthermore, gas pulsations produced by one tray could be

detected throughout the column, and it was not possible to be certain from which tray the measured pulsations emanated. When more than one tray produced pulsations, more than one pulsation frequency could be detected at any point in the column. It was therefore decided to carry out the experimental work using only one active sieve-tray, the water flow bypassing the top and bottom trays.

Appendix V contains a description of work carried out, using a single active tray, in an attempt to reproduce some of the results obtained by Waddington (2), using three active trays. It was found that the pressure pulsations reported by Waddington for a weir height of 76.2 mm. could not be reproduced by a single active tray operating at the same water flow rate. It is possible that liquid leakage past the weir on the top tray may have reduced the tray liquid head sufficiently to allow the production of the reported pulsations there. This exemplifies the difficulty in obtaining accurate results using three active trays.

Good agreement was found with the pulsations reported by Waddington at a weir height of 25.4 mm. However, there was an indication that Waddington underestimated the airflow rate by about 10%.

5.2 EXPERIMENT I. INVESTIGATION OF THE EFFECT OF THE SUPERFICIAL HOLE GAS VELOCITY, THE TRAY LIQUID HEAD AND THE TRAY GEOMETRY ON THE GAS DYNAMIC PRESSURE BENEATH THE TEST-TRAY.

The tray geometrical parameters considered were hole diameter, hole pitch and the number of holes. The trays used are listed in Appendix I, Table I.1. They were all 3 mm. (0.125 in.) thick and could be termed 'thin trays'.

Measurements were taken over a range of superficial hole gas velocity and tray liquid head for each tray, using the procedure described in section 5.2.1. A weir height of 76.2 mm was used to minimise tray liquid crossflow, and there was normal chamber capacitance. (Normal chamber capacitance refers to that of the chamber beneath the test-tray with the column arranged as shown in Figure 4.2.)

The tray liquid head was calculated from the tray static pressure drop measurements using the procedure described in Appendix VI.

5.2.1 Experimental Procedure.

For a given tray geometry, chamber capacitance and weir height, the experimental procedure used was as follows.

The air flow rate was set at a constant value, corresponding to a superficial hole gas velocity of x m/s. and the orifice plate pressure drop was recorded. The water was then turned on (the tap water supply was used, unless flowrates greater than 0.234 m^3/hr. (50 galls./hr.) were required, when the main tank supply was used), and the water level on the tray built up until gas-liquid interaction occurred over part or all of the test-tray. The water flow rate was recorded and the system allowed to reach steady state, this being indicated by a constant tray total static pressure drop, $P_1 - P_3$. The air flow rate was then adjusted, if necessary, to maintain a velocity of x m/s. At steady state conditions, the following measurements were carried out and recorded:

i) The tray total static pressure drop, $P_1 - P_3$;

ii) The tray hole static pressure drop, $P_1 - P_2$;

iii) The gas-liquid mixture static pressure drop, $P_2 - P_3$;

iv) The height of the gas-liquid mixture;

v) The frequency and amplitude of the main components in the frequency spectrum of the dynamic pressure in the chamber beneath the test-tray. Pressure transducer 1 was used to monitor the dynamic pressure, and it was positioned as shown in Figure 4.8. Most of the frequency analysis was carried out using the Spectral Dynamics Corporation (S.D.C.) real time analyser. When a different analysis instrument was used this is indicated in the presentation of the results;

vi) A visual description of the gas-liquid regime and the weep rate. Details of the terms used are given in Appendix VII.

The above procedure was then repeated using a slightly higher water flow rate, sufficient to increase the value of $P_1 - P_2$ by about 1.0 mm. of water. However, if this increase resulted in an unusually large change in the dynamic pressure frequency spectrum, water flow rates giving intermediate values of $P_1 - P_2$ were used also.

The water flow rate was increased in this manner until the dynamic pressure frequency spectrum no longer exhibited detectable components in the frequency range 0.06 Hz. to 100 Hz.

Measurements were also taken at conditions corresponding to the point at which the amount of liquid on the test-tray had fallen to the point where the gas-liquid interaction at the tray holes just ceased.

Having taken measurements over the range of water flow rates, the air flow was adjusted to give a gas velocity of (x+1) m/s or (x-1) m/s., and the above procedure was then repeated.

The air flow rate was varied in this manner over the necessary range of gas velocities. The maximum gas velocity used was that at which no frequency component could be detected for any water flow rate. The minimum gas velocity was determined by the onset of serious liquid dumping.

All the air flow rates used were above that corresponding to the limit of the orifice plate coefficient, as calculated in Appendix II, section II.3.

Care was taken to ensure that no gas-liquid interaction occurred on the top or bottom sieve-trays. For high gas flow rates, entrained water built up on the top tray, and had to be removed.

It was shown experimentally that the measurements taken at steady state conditions did not depend upon whether the air or water flow rate had just been increased or just been decreased; i.e., there was no hysteresis effect of fluid flow rate.

The measurements taken were recorded on data sheets, a completed one being shown in Figure 5.1.

DATE 22/x/76 WEIR HEIGHT 3 INS

MEASUREMENT OF - pressure transducer 1 below test-tray M HOLE DIAMETER 5/8 INS 38, 1½

Run no.	L galls/hr	v m/s	P_1-P_2 mm. of water	P_1-P_2 mm. of water	P_2-P_3 mm. of water	f Hz.	A N/m^2	h mmHg	froth mm.	two-phase comments
45	10	8	18·0	18·0	4·5	19·0	26	4·75		(F) S
46	11	8	19·5	13·0	6·0	19·4	28	6·25		(B) S, (low)
47	13	8	22·5	13·25	8·75	19·2	28	9·0		(B) S, ow
48	13	8	24·5	13·5	10·5	19·2	22	10·75		BS, ow
49	15	8	26·5	13·25	13·0	19·0	8	13·25		(Fr) BS, (MW)
50	15	8	29·0	13·5	15·5	—	—	15·75		Fr B(S), (MW)
	$\Delta P_{orifice}$ = 6·5 mm of water									
51	—	9	14·0	12·5	1·0	—	—	1·5		No TP
52	7	9	4·6	12·75	1·5	—	—	2·0		¾ FS
53	8	9	15·5	13·5	1·75	19·6	6	2·25		FS
54	10	9	16·5	14·25	2·0	20·8	20	2·5		FS
55	10	9	17·8	14·75	2·75	21·2	20	3·25		FS
56	11	9	19·2	15·0	3·75	21·2	16	4·25		(F) S
57	12	9	20·8	15·0	5·5	21·0	12	6·0		(F) S
58	12	9	21·8	15·0	6·5	21·2	15	7·0		S
59	14	9	24·5	15·25	8·75	21·0	18	9·25		S
60	14	9	26·5	15·75	10·5	21·0	10	11·0		(B) S, (low)
61	15	9	28·8	15·75	12·5	(21)	(4)	13·0		BS, (low)
62	15	9	30·0	15·75	14·0	—	—	14·5		(Fr) BS, (low)
	$\Delta P_{orifice}$ = 8·1 mm of water									
63	—	10	16·4	14·75	1·25	—	—	1·75		No TP
64	10	10	17·0	15·25	1·25	—	—	1·75		¾ FS
65	12	10	18·5	16·5	1·75	22·8	10	2·25		FS
66	12	10	19·6	17·0	1·75	23·2	14	2·25		FS
67	15	10	22·0	18·0	3·5	23·8	10	4·0		FS

Fig.5.1. TYPICAL EXPERIMENTAL DATA SHEET

5.2.2 Results of Experiment I. - Part I, The occurrence and amplitude of the regular pressure pulsations.

The operating conditions over which pressure pulsations were detected are identified in terms of the superficial hole gas velocity and the tray liquid head. Details are given of the variation in pulsation amplitude, within that region of operation, and an indication is given of the corresponding gas-liquid regime on the tray. Details of the measured pressure pulsation frequencies are given in the second part of these results.

The test-trays are referred to by letters (A to O), as defined in Appendix I, Table I.1., which lists details of the geometry of the trays.

5.2.2.1 The nature of the pressure pulsations.

Figure 5.2 shows the dynamic pressure beneath three of the test-trays, operating at various values of gas velocity and tray liquid head. The frequency f(Hz), and the root mean square amplitude, A(N/m^2), are for the pressure pulsation fundamental frequency.

Figure 5.3 shows the frequency spectrum for some of the pressure signals, as displayed on the S.D.C. real time analyser. The fundamental frequency is clearly defined in all cases, and is seen to have a r.m.s. amplitude just less than that of the total signal (given at the extreme right of the display).

The harmonics of the fundamental frequency may result from the irregular shape of the pressure pulse. For example, a pure sine wave, when transformed into the frequency domain, will produce a frequency spectrum exhibiting a single component at the fundamental frequency, f_o. However, the spectrum of a triangular wave form of the same fundamental frequency will exhibit components at f_o, $3f_o$, $5f_o$ etc.; and a sawtooth wave form will exhibit peaks at f_o, $2f_o$, $3f_o$, $4f_o$ etc. The pulse shape of signal (e) in Figure 5.2 clearly resembles a sawtooth signal, and would be expected to have harmonics in its frequency spectrum.

	Tray	v m/s.	h mm.of water	f Hz.	A N/m²
(a)	B(g)	5·1	12·0	27·8	20
(b)	B(g)	5·1	22·0	–	–
(c)	B(g)	9·2	4·5	32·8	37
(d)	L(g)	5·0	12·5	18·0	60
(e)	L(g)	7·0	5·25	19·4	45
(f)	L(g)	9·0	5·75	23·6	16
(g)	L(g)	11·0	5·5	–	–
(h)	H(g)	5·0	5·75	14·0	20
(i)	H(g)	5·0	12·25	16·6	5
(j)	H(g)	7·0	5·0	19·6	25
(k)	H(g)	9·0	5·25	25·0	28

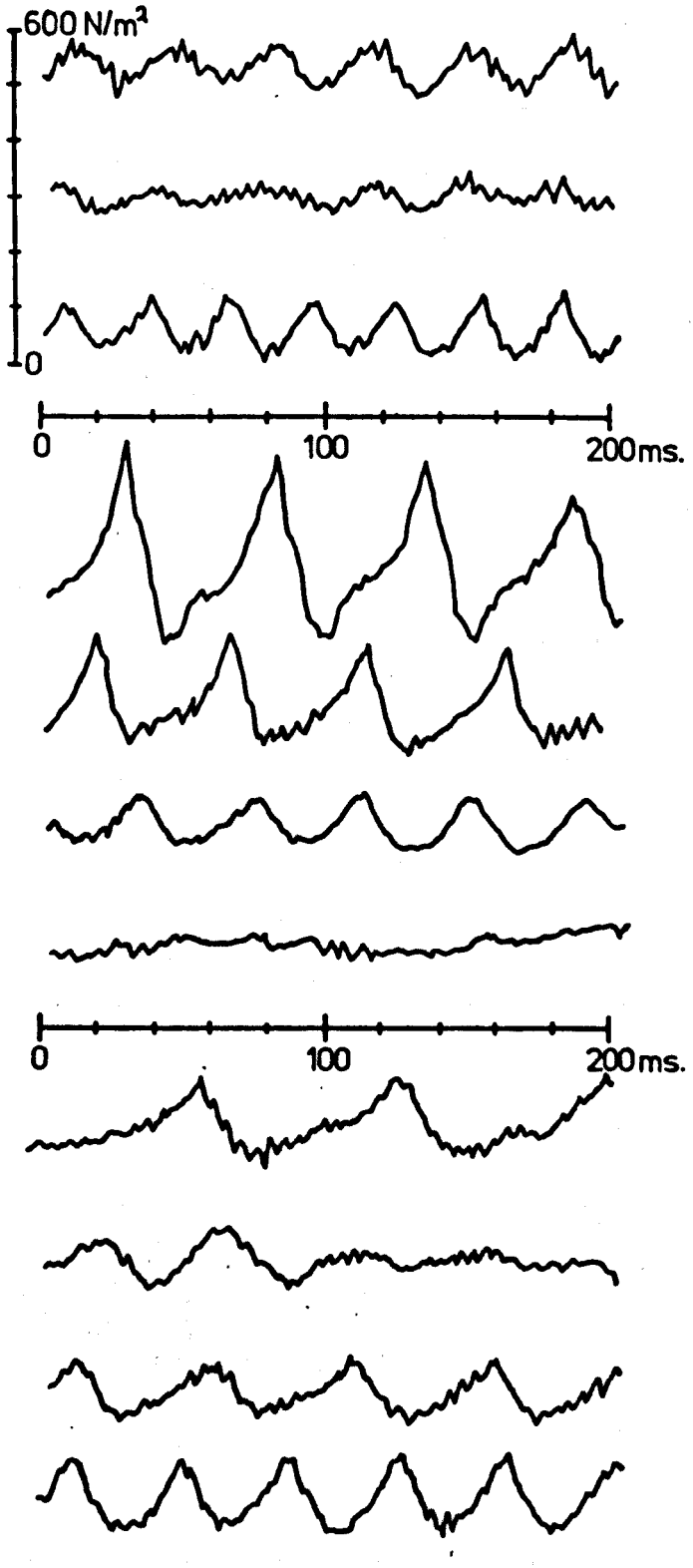

Fig.5.2. DYNAMIC PRESSURE IN THE CHAMBER BENEATH THE TEST-TRAY

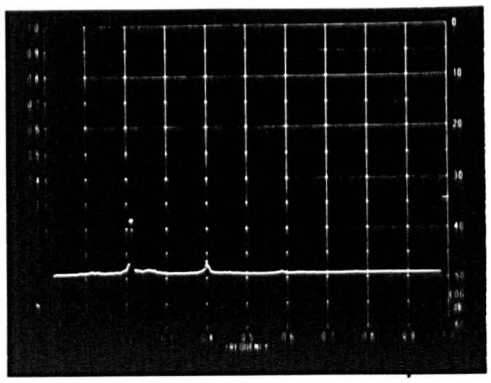

(a)

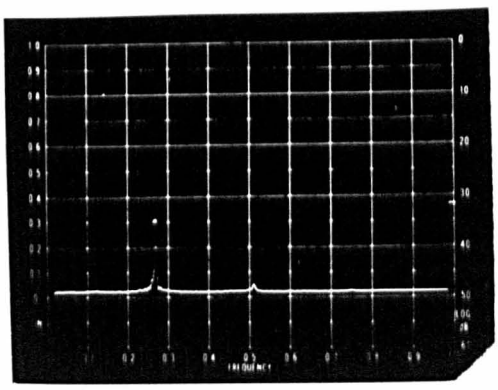

(b)

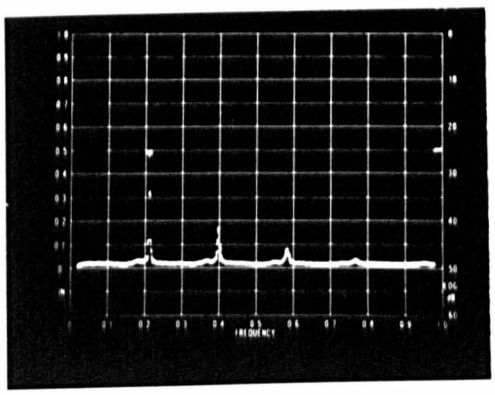

(c)

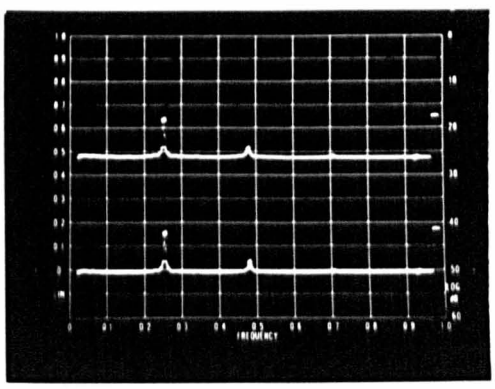

(d)

	tray	v m/s	h mm H_2O	f Hz	A N/m^2	
(a)	H(g)	7·0	5·0	19·6	24	memory
(b)	H(g)	9·0	5·25	25·0	31	memory
(c)	L(g)	7·0	5·0	19·4	50	memory
(d)	L(g)	9·0	5·75	23·8	20	real time & memory

Fig. 5.3 FREQUENCY SPECTRUM OF DYNAMIC PRESSURE BENEATH TEST-TRAY AS DISPLAYED ON S.D.C. REAL TIME ANALYSER

System 'noise', measured at about 200 Hz, can be detected in the pressure signals. No significant system 'noise' was detected below 150 Hz, and it is therefore assumed to have negligible effect on the pressure pulsations at a much lower frequency.

5.2.2.2 The range of operation corresponding to pulsation production.

Regular pulsations of the gas pressure beneath the test-tray were produced by all of the trays investigated. Figure 5.4 shows the range of operation over which pulsations were produced for different test-trays, in terms of the gas velocity and the tray liquid head. The variation in the r.m.s. amplitude of the pulsation fundamental frequency component is indicated by lines or contours representing 10 N/m^2 increments in the amplitude. For example, between the '10' and '20' lines the measured pulsation amplitude was in the range 10 N/m^2 to 20 N/m^2.

Excessive liquid dumping prevented operation at gas velocities much below 4 m/s. The lower limit of the tray liquid head corresponds to the cessation of gas-liquid interaction on the tray.

All the plots in Figure 5.4 are seen to exhibit a specific area of operation over which pulsations of the highest amplitude are produced. An increase in either the gas velocity or the tray liquid head, beyond this area of operation, tends to decrease the pulsation amplitude.

The gas velocity above which no pulsations were detected is seen to be in the range 11 m/s.to 12 m/s. for most of the trays, with no apparent dependence on the corresponding gas volumetric flowrate.

The maximum tray liquid head at which pulsations were detected was in the range 15 mm. of water to 20 mm. of water, except for trays N and O,for which relatively low amplitude pulsations were detected at heads of up to 40 mm. of water.

Most of the measured pressure pulsations had an r.m.s. amplitude of below 40 N/m^2, although amplitudes of up to 60 N/m^2 were detected.

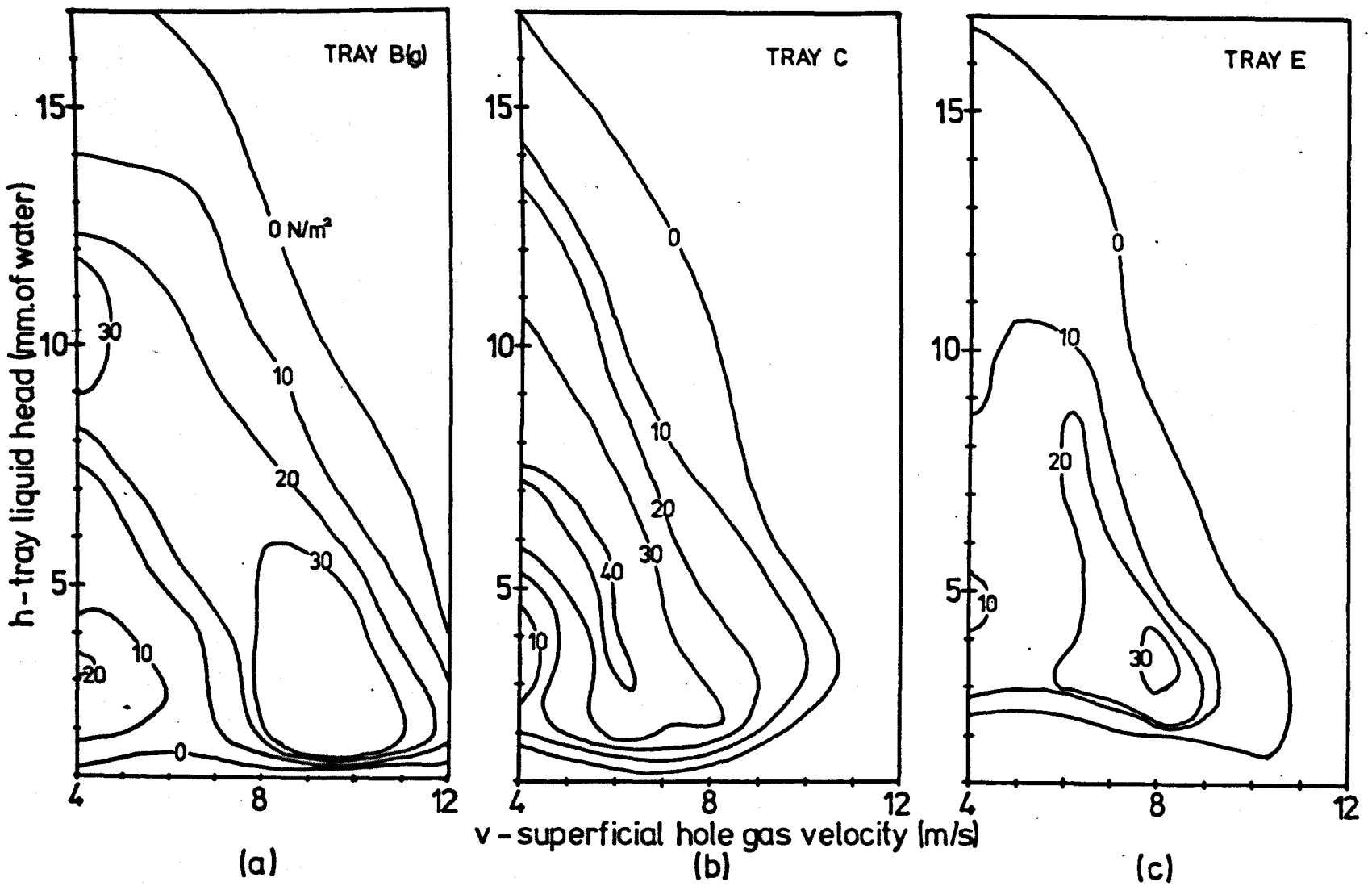

Fig.5.4. R.M.S. AMPLITUDE OF THE PRESSURE PULSATION BENEATH THE TEST-TRAY

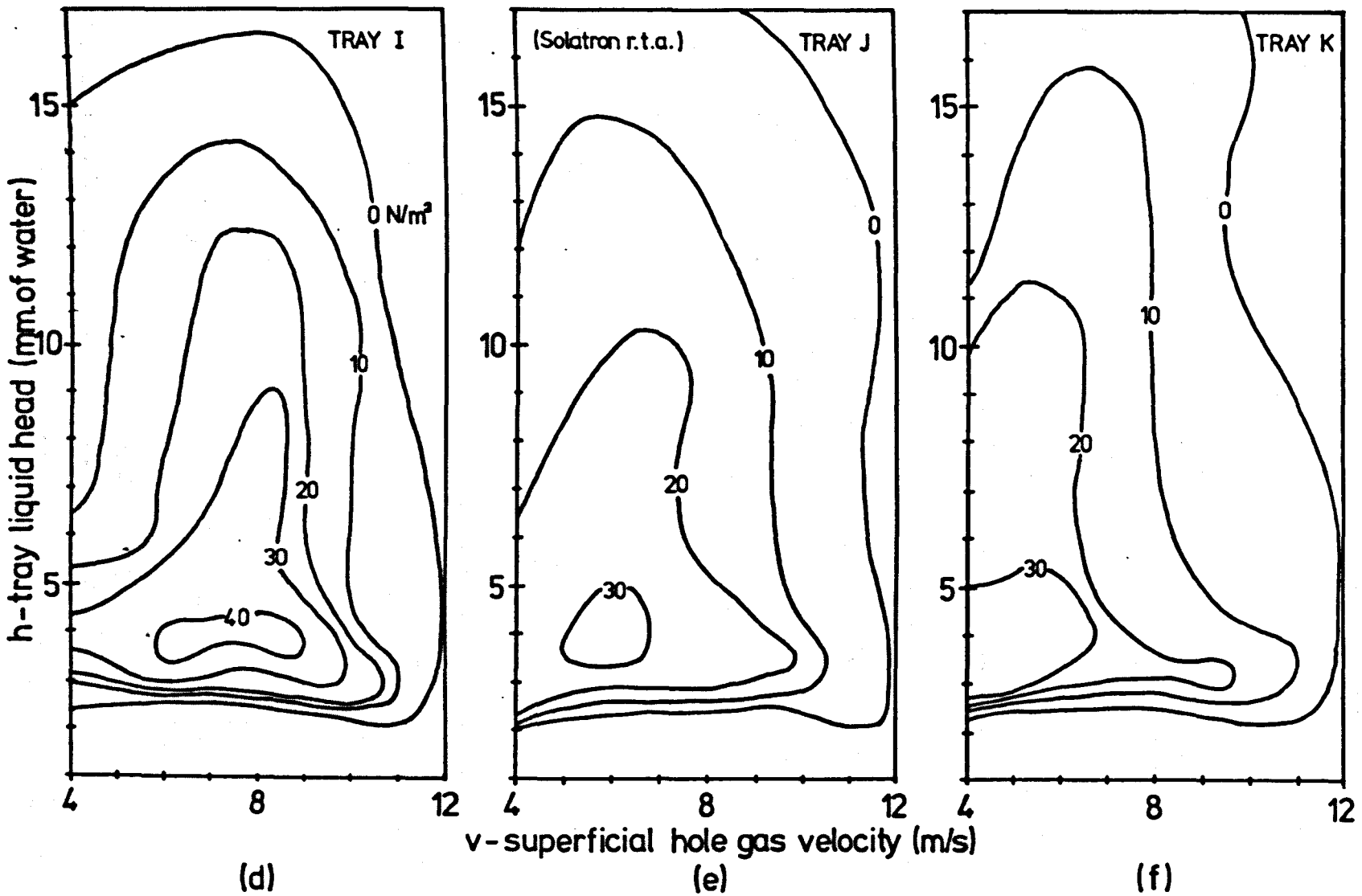

Fig. 5.4. R.M.S. AMPLITUDE OF THE PRESSURE PULSATION BENEATH THE TEST-TRAY

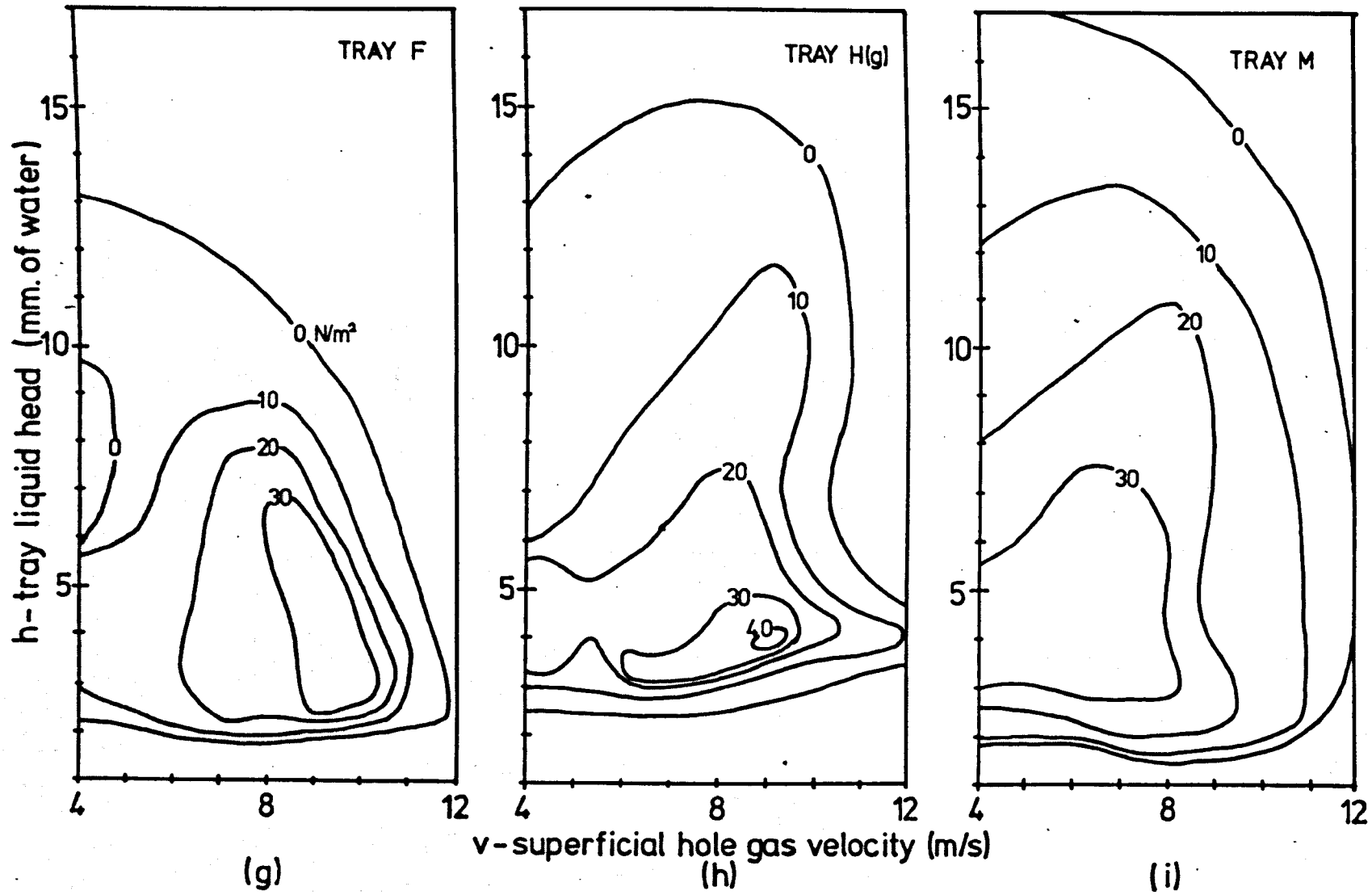

Fig. 5.4. R.M.S. AMPLITUDE OF THE PRESSURE PULSATION BENEATH THE TEST-TRAY

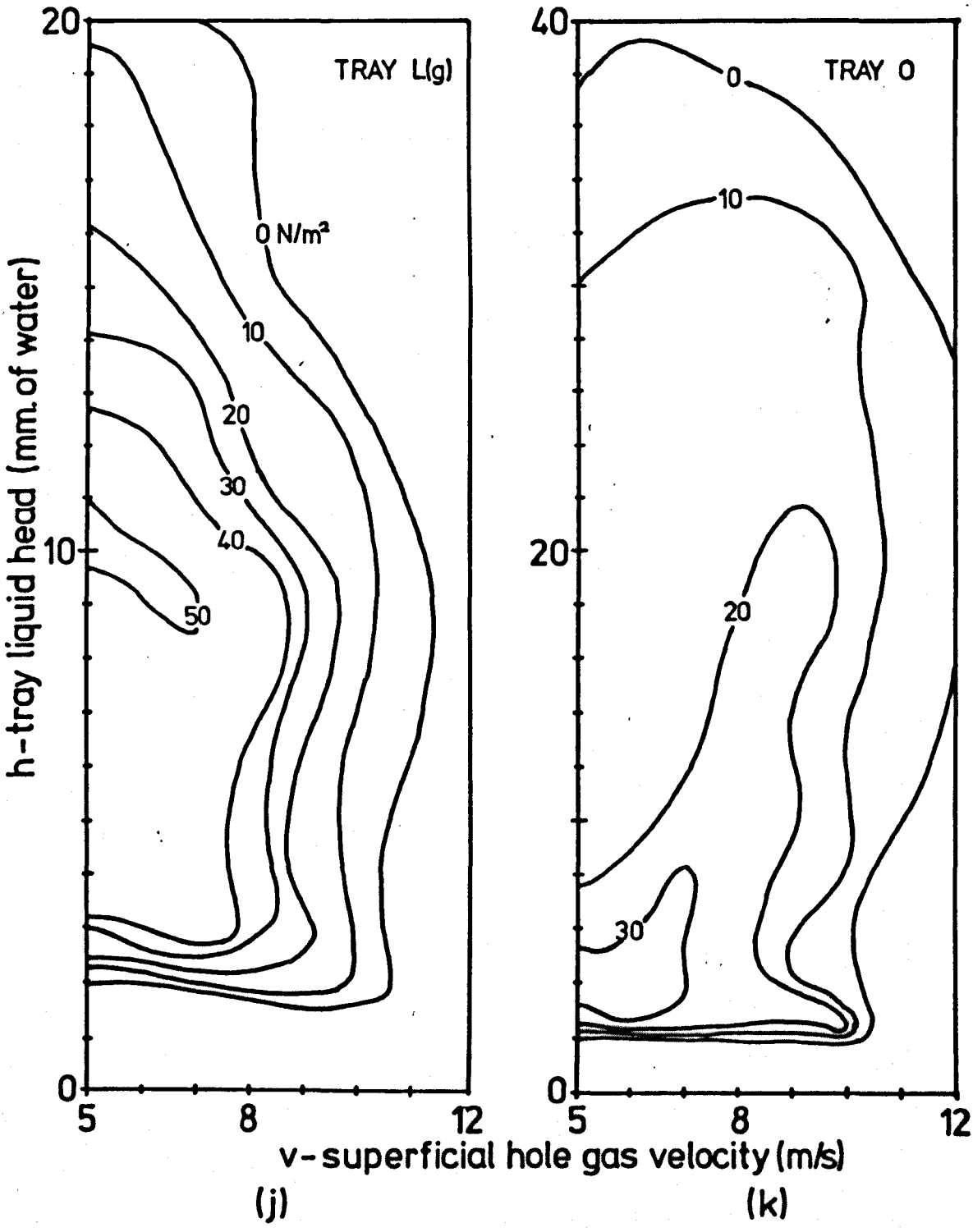

Fig. 5.4. R.M.S. AMPLITUDE OF THE PRESSURE PULSATION BENEATH THE TEST-TRAY

5.2.2.3 The effect of the tray geometry on the occurrence and amplitude of the pulsations.

i) Number of holes. In Figure 5.4, comparison of the three series of plots: (b) and (c); (d) (e) and (f); and (i) and (j); shows that decreasing the number of holes in the tray, whilst the hole diameter and hole pitch are kept constant, has the general effect of reducing the pulsation amplitude, but has little affect on the operating range over which pulsations occur.

Decreasing the number of holes in the tray decreases the gas volumetric flowrate corresponding to a given superficial hole gas velocity. This decrease in flowrate could account for the drop in pulsation amplitude.

ii) Hole diameter. A reduction in the corresponding volumetric flowrate, for a given velocity, also occurs when the hole diameter is decreased, for a constant number of holes. In Figure 5.4, comparison of the two series of plots: (a) and (b); and (h), (i) and (j); shows that a reduction in the hole diameter does result in a general decrease in the pulsation amplitude.

A decrease in the hole diameter is also seen to increase the gas velocity at which pulsations of the maximum amplitude occur, and, generally, to decrease the tray liquid head above which no pulsations are produced.

iii) Hole pitch. In Figure 5.4, comparison of the series of plots (c), (d) and (e), shows that a change in the hole pitch has no major effect on the pulsation amplitude. However, there is an indication that an increase in pitch generally raises the gas velocity at which pulsations of the highest amplitude are produced, particularly for the range of tray liquid head from 5 mm. of water to 12 mm. of water. Comparison of plots (i) and (k) in Figure 5.4 shows that the increase in pitch nearly doubles the maximum tray liquid head up to which pulsations are produced. The same trend was apparent for trays K and N.

5.2.2.4 The operating regimes corresponding to pulsation production.

Figure 5.5 indicates the types of gas-liquid regime which prevail on the

tray,during operation at conditions for which pulsations are produced. The regimes were determined visually and therefore the boundaries for regime transition can only be taken as approximate. Comparison of these regime boundaries with Figure 2.2 shows them to be in general agreement with the froth-spray transition points reported by other workers. It can be seen that pulsations are produced predominantly for conditions corresponding to some form of spraying regime. This varied from a fine spray of droplets (fine spray regime), to a condition in which there was still substantial droplet formation but in which bubble formation was apparent over part or all of the tray (bubble-spray regime). Further build up of liquid on the tray resulted in froth formation.

For gas velocities of up to 12 m/s., Figure 2.4 indicates that, for a single 6.35 mm. diameter hole, the meniscus regime (with minimal gas-liquid interaction) occurs at tray liquid heads up to about 4 mm. of water, and that at higher liquid heads, imperfect bubbling predominates.

Figure 5.5(a) shows that there is apparently a spraying or jetting regime occurring at liquid heads as low as 1.5 mm. of water. This disagreement with Figure 2.4 at low liquid heads could be due either to the relatively close proximity of holes on the tray, or to the possibility that the single hole in perspex of Muller and Prince (37) was not properly 'wetted'. On the metal sieve-trays the holes were 'wetted', with a thin layer of water clinging to the inner surface of the holes. When tray F was operated with oil contamination of the holes, which prevented them from wetting, the tray liquid head at which gas-liquid interaction began was raised, from about 2 mm. of water, to nearly 4 mm. of water. Furthermore, the frequency (see Figure 5.8(b)) and amplitude of the pulsations were changed, this change being greatest for gas velocities above 8 m/s., for which the amplitude of pulsation was considerably reduced. These results indicate hole 'wetting' to be an important factor affecting tray behaviour and further study of this wetting phenomenon may be worthwhile.

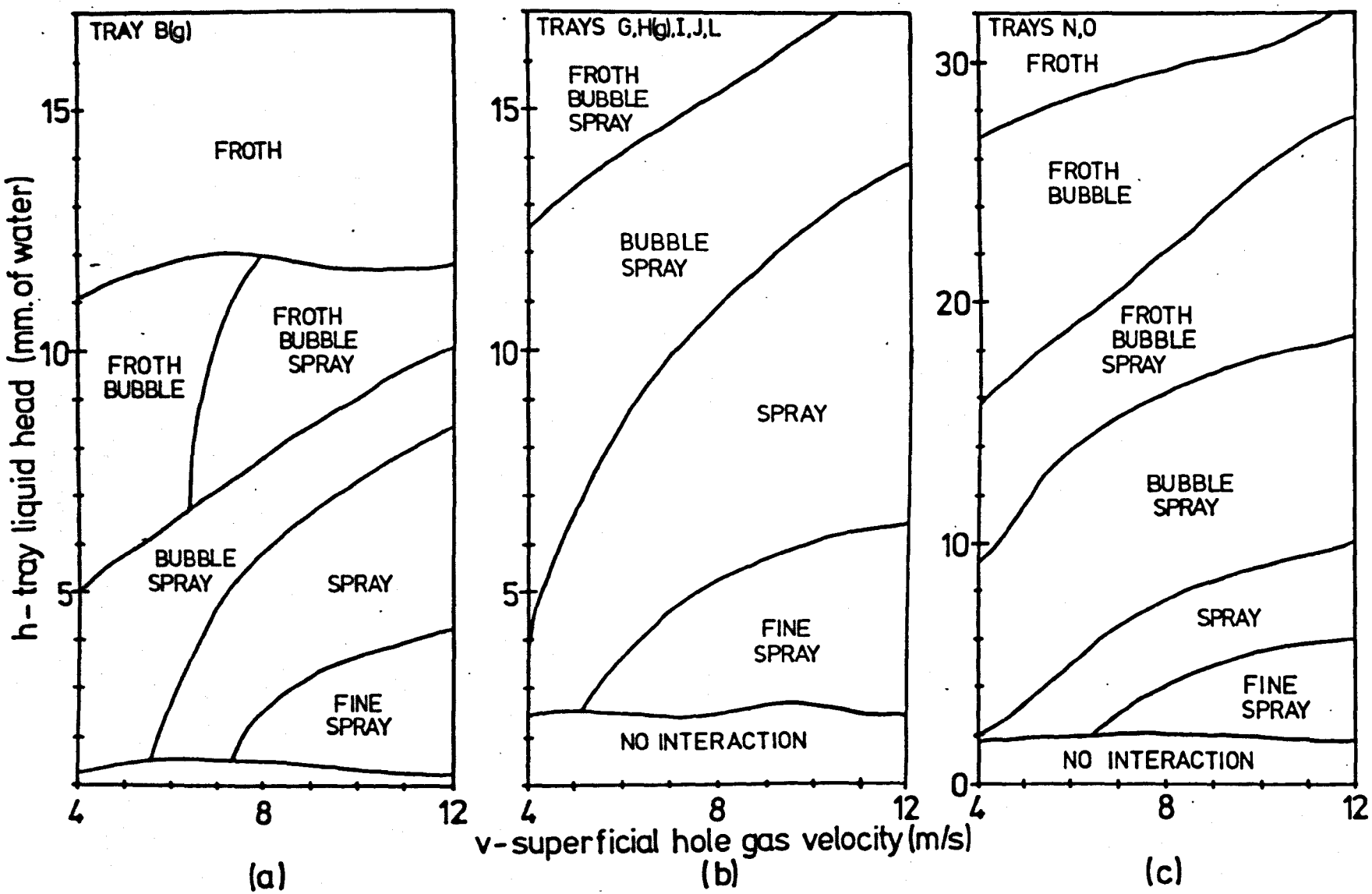

Fig. 5.5. REGIMES OF GAS-LIQUID INTERACTION OBSERVED ON THE TEST-TRAYS

It has been reported that increasing the hole diameter tends to favour the spraying or jetting regimes. For the larger hole sizes, therefore, this is likely to be an important regime of operation during which pulsations may occur.

Apart from the initial build up of liquid on the tray, the amplitude plots in Figure 5.4 exhibit no sudden changes in amplitude, indicating any change of interaction mechanism at the hole, over this area of operation, to be either gradual or to have little effect on pulsation production.

Figure 5.6 indicates the weep points for several of the trays. Comparison of these points with Figure 5.4 shows the pulsations to be produced independently of weeping, with no specific variation in amplitude corresponding to the weep points.

The weep points were determined visually, and represent the point at which all weeping ceases. They are seen to be quite similar for most of the trays. That found for the 6.35 mm. diameter holes is seen to agree fairly well with the correlation of Eduljee (34) (section 2.1.7; equation 2.1). However, some disagreement with the correlation is apparent for the larger hole sizes, for operation at lower liquid heads. This disagreement may be because the correlation of Eduljee was based upon data obtained using hole diameters $\leq$ 7.93 mm. (5/16 inches) and for operation at tray liquid heads above 14 mm. of water. The correlation was therefore not claimed to be accurate for low liquid heads.

5.2.3 Results of Experiment I - Part II, The Effects of System Variables on the Pressure Pulsation Frequency.

The fundamental frequency component of the pressure pulsations beneath the test-tray was determined, over the full range of pulsation production operation, for each test-tray. Typical results are presented to illustrate the effects of the major system variables on the frequency.

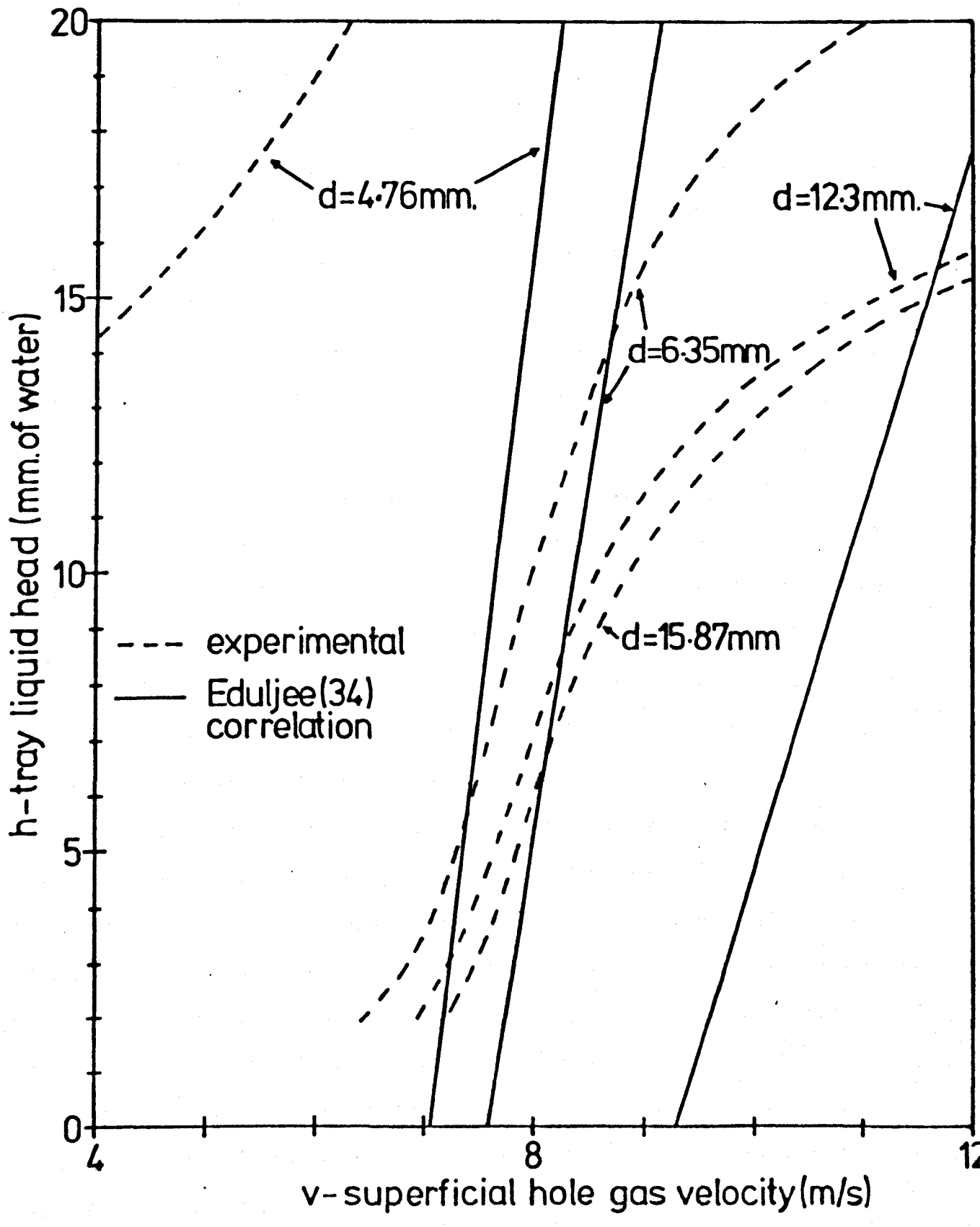

Fig. 5.6 COMPARISON OF EXPERIMENTAL WEEP POINTS WITH EDULJEE CORRELATION(34)

All of the frequencies found were in the range 12 Hz. to 40 Hz., which corresponds to the frequencies reported to be associated with tray damage.

The effects identified for each variable are treated in turn.

5.2.3.1 Superficial hole gas velocity.

In all cases the frequency increased with increasing gas velocity. This can be seen in Figure 5.7, which shows the frequency plotted against tray liquid head for various values of gas velocity (test-tray B).

In Figure 5.9, plots (c) and (d) show that the rate of increase of frequency with increasing gas velocity, (for operation at a constant value of tray liquid head) to be little affected by changes in tray geometry or the value of tray liquid head.

Waddington (2) reported a similar increase of frequency with increasing gas velocity. Comparison of the frequencies reported by Waddington (2) in Figure 3.1, with those in Figure 5.7, make it apparent that the Waddington frequencies were produced at a tray liquid head of between 5 mm. of water and 6 mm. of water. For this tray liquid head there is also reasonable agreement between the overall r.m.s. pressure amplitude reported by Waddington in Figure 3.1, and the amplitudes shown in Figure 5.4(a).

The frequencies reported by Brown (54) for trays containing 41 and 49 holes of 6.35 mm. diameter, (Figure 3.2), are plotted on Figure 5.9(d). The frequency dependence on gas velocity is seen to be very similar to that of the other results shown. There is also good agreement of the frequencies with those found for tray B, even though Brown's results were reported to have occurred at a tray liquid head of 50 mm. of water.

The frequencies reported to be associated with single hole operation are generally much lower than those found for the multi-hole trays. This is illustrated by the frequencies for a single 6.35 mm. diameter hole (from Figure 3.3) which are plotted on Figure 5.9(d). Furthermore, it can be seen that for a single hole, increasing the tray liquid head leads to a fall in the

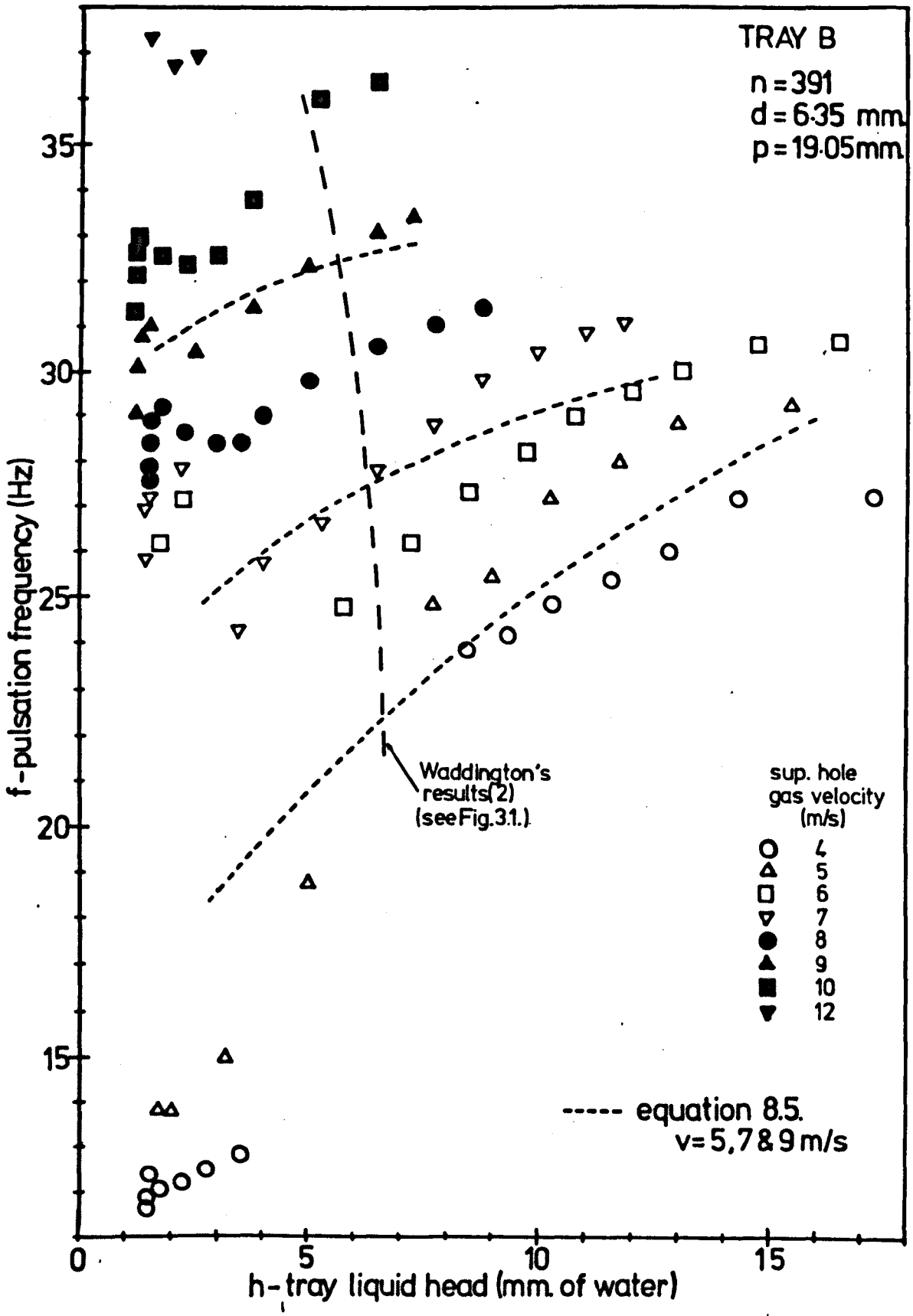

Fig. 5.7. PULSATION FREQUENCY AGAINST TRAY LIQUID HEAD AND GAS VELOCITY; TEST-TRAY B

rate at which the frequency increases with increasing gas velocity. Such behaviour was not found for multi-hole trays operating at a tray liquid head below 20 mm. of water, but did occur at higher heads for trays N and O, as shown in plots (e) and (f) of Figure 5.8.

5.2.3.2 Tray liquid head. The tray liquid head was found to have a definite effect on the pulsation frequency. Figure 5.7 shows that the frequency increases with increasing tray liquid head ('small pitch' behaviour). This dependence was found for all the trays with a 19.05 mm. hole pitch, Figures 5.8(a) and 5.10(a) giving further illustration of this. However, for the larger pitches, the frequency was found to be either little affected or to decrease, with increasing liquid head ('large pitch' behaviour). This is shown in Figures 5.8(d) and plots (b) and (c) of Figure 5.10.

For operation at a relatively low liquid head, and particularly in the region of initial liquid build-up, many trays exhibit local fluctuations in the pulsation frequency with changing liquid head. Also, for operation at low gas velocities, for some trays, there is a rapid decrease in frequency as the liquid head is decreased below about 7 mm. of water. Such behaviour can be seen in Figure 5.7 and in plots (b), (c) and (d) of Figure 5.8.

Brown (54) reports that there is no recognisable effect of liquid depth on frequency, for depths of water between 25 mm. and 100 mm. He did report however, that the frequency decreased with increasing liquid density, with frequency being proportional to $\rho_l^{-0.84}$ in his correlation.

For a single 6.35 mm. diameter hole, Muller and Prince (37) reported that for operation in the pulsating jet regime, the frequency decreased with increasing liquid depth, but that for operation in the bubbling regime, frequency is independent of depth. This is shown in Figure 3.3.

5.2.3.3 Hole pitch.

It has been shown that the value of the hole pitch has a significant effect on the way in which the tray liquid head affects the pulsation frequency.

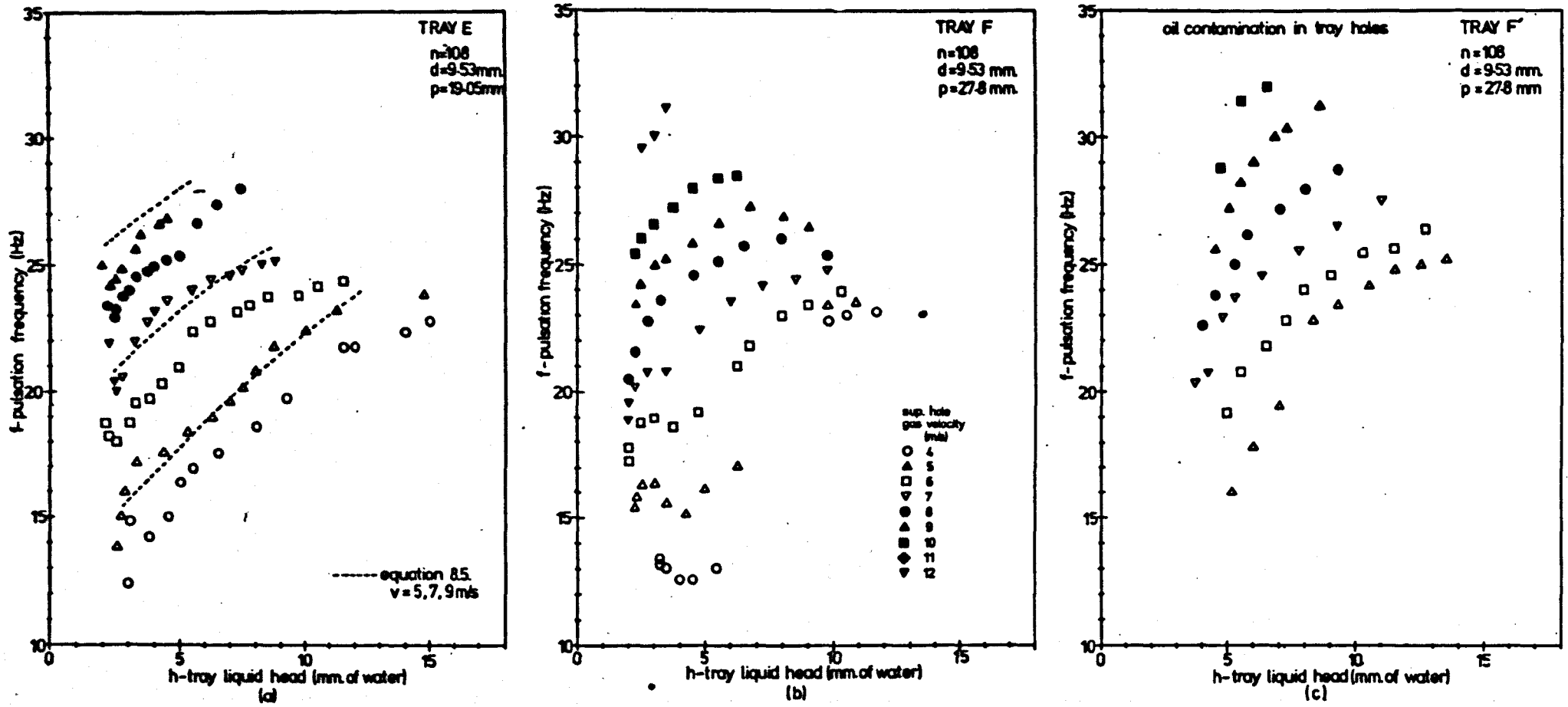

Fig.5.8. PULSATION FREQUENCY AGAINST TRAY LIQUID HEAD AND GAS VELOCITY

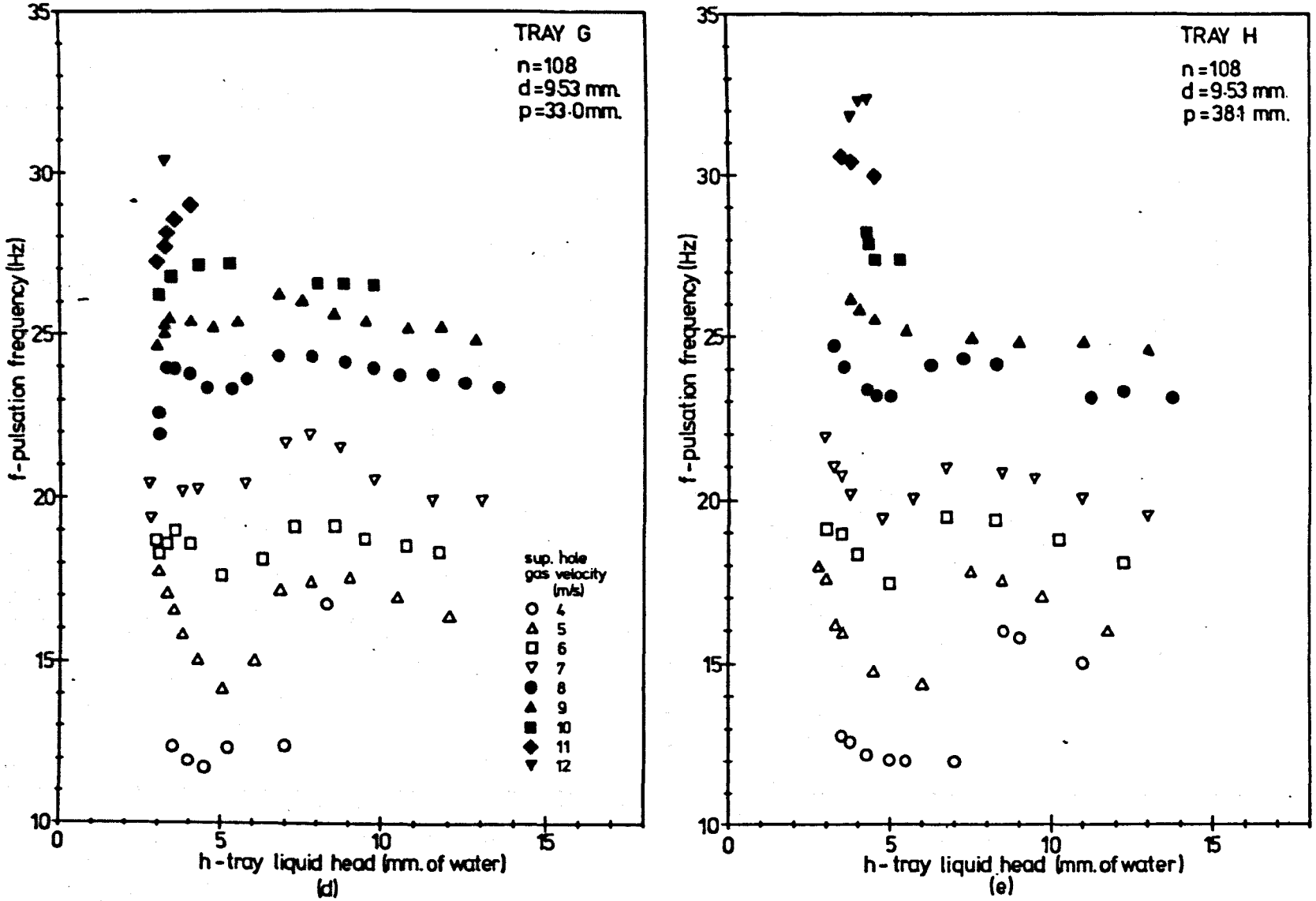

Fig.5.8. PULSATION FREQUENCY AGAINST TRAY LIQUID HEAD AND GAS VELOCITY

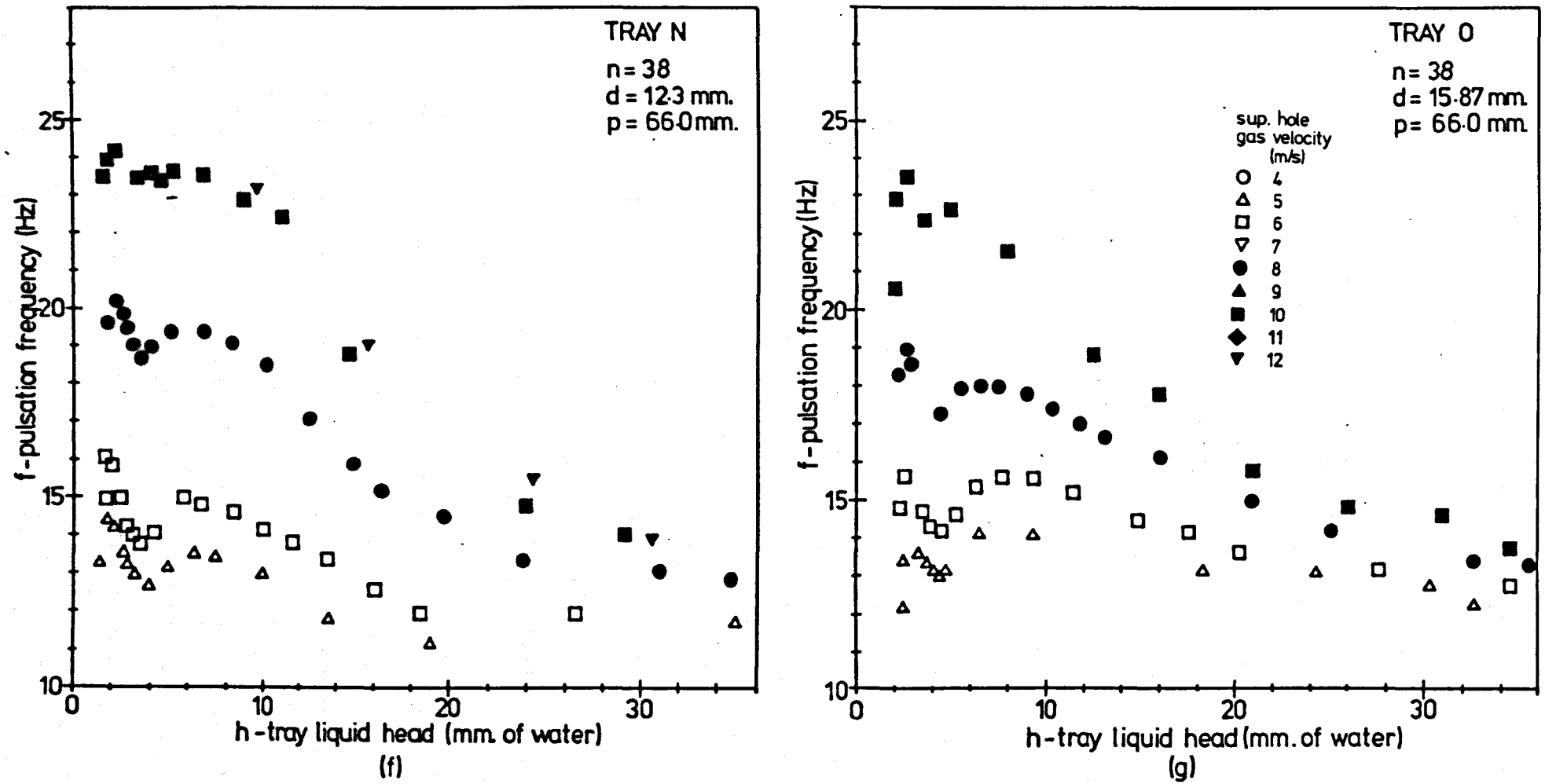

Fig.5.8. PULSATION FREQUENCY AGAINST TRAY LIQUID HEAD AND GAS VELOCITY

Plots (a), (b), (c) and (d) of Figure 5.8 show pulsation frequencies for a series of trays containing 108, 9.53 mm. diameter holes,with hole pitches of 19.05 mm., 27.8 mm., 33.00 mm., and 38.1 mm., respectively. The changes in the dependence of frequency on tray liquid head from a 'small pitch' behaviour to a 'large pitch' behaviour is clearly evident, with most of the change occurring between hole pitches of 27.8 mm. and 33.0 mm. However, at the lowest gas velocities the 27.8 mm. pitch tray exhibits some 'large pitch' behaviour, and, for the highest gas velocities, the 33.0 mm. pitch tray exhibits some 'small pitch' behaviour. This indicates that the change between the two types of behaviour is also dependent upon the gas velocity.

Apart from changing the effect of liquid head on pulsation frequency, increasing the hole pitch can also be seen to decrease the frequency slightly.

Figures 5.10(b) and 5.8(e) allow the comparison of two trays containing 38, 12.3 mm. diameter holes, with hole pitches of 38.1 mm. and 66.0 mm. respectively. Both show 'large pitch' liquid head behaviour, with the frequencies for the smaller pitch being slightly higher. Figures 5.10(c) and 5.8(f) allow a similar comparison for trays containing 15.87 mm. diameter holes. The 38.1 mm. pitch tray shows some evidence of 'small pitch' liquid head behaviour. This tray has an edge to edge hole separation of 22.2 mm. A tray containing 9.53 mm. diameter holes, with this separation, would have a pitch of 31.7 mm., which is a value lying in the transition area. This indicates that the hole edge to hole edge separation is perhaps more important than the actual centre to centre hole pitch, in determining the liquid head dependence. These results indicate that interference of the gas-liquid interaction at neighbouring holes may be occurring at, or below, a critical value of the hole edge to hole edge separation, and that such interference may be responsible for the change in the effect of liquid head on pulsation frequency.

Brown (54) reported the frequency to increase as the pitch increased. However, this was based on experiments with trays containing only three holes, and furthermore, the results were correlated by using frequency as proportional to $(\text{pitch})^{-0.16}$.

5.2.3.4 Hole diameter.

Figure 5.9 shows that a change in hole diameter has little effect on the pulsation frequency. In Figure 5.9, plot (a) is for small hole pitch (19.05 mm.) and plot (b) for large pitch (38.1 mm.). These show some evidence of a very small decrease in frequency as diameter is increased, for operation at a gas velocity of 9 m/s. In plot (b), the higher frequencies produced with the 15.87 mm. diameter holes, at the 7 m/s gas velocity, could be due to the smaller hole edge to edge separation.

Plots (c) and (d) of Figure 5.9 again show evidence of a slight decrease in frequency with increasing hole diameter at the higher gas velocities, but there is an opposite effect at the lower gas velocities, this being particularly evident for the 19.05 mm. pitch trays in plot (c).

Brown (54), McCann and Prince (42) and Kupferberg and Jameson (55), all reported little dependence of frequency upon hole diameter.

The apparent lack of dependence on diameter indicates that the gas momentum through the holes is much more important in determining the pulsation frequency than is the gas volumetric flowrate.

5.2.3.5 Number of holes.

Figure 5.10 shows a series of results obtained for trays in which only the number of holes was changed. It is clear that increasing the number of holes tends to increase the pulsation frequency and that changing the number of holes does not affect the dependence of the frequency on the tray liquid head.

Plots (b) and (c) in Figure 5.10 show that an increase in the frequency of between 2 Hz. and 3 Hz. occurs as the number of holes in the tray is

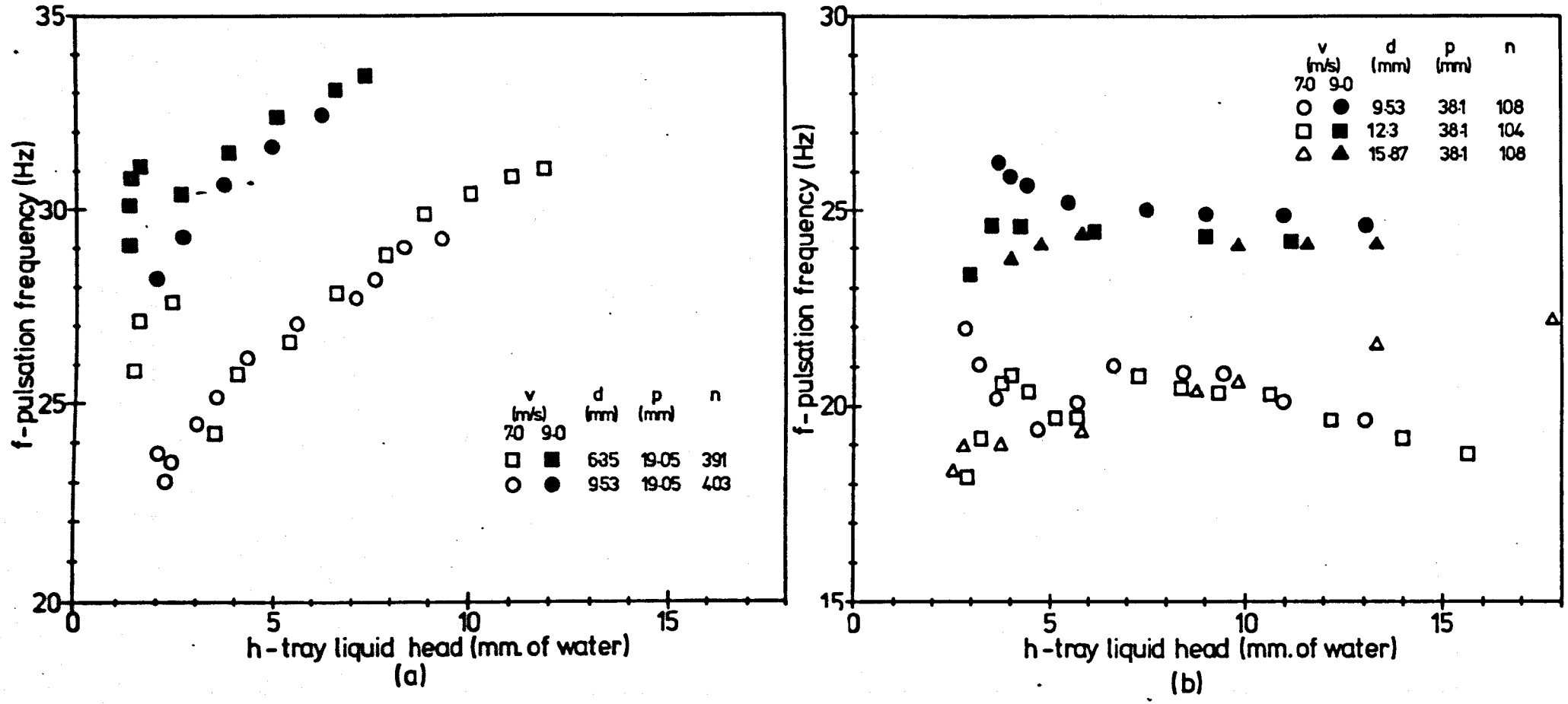

Fig. 5.9. EFFECT OF HOLE DIAMETER ON PULSATION FREQUENCY

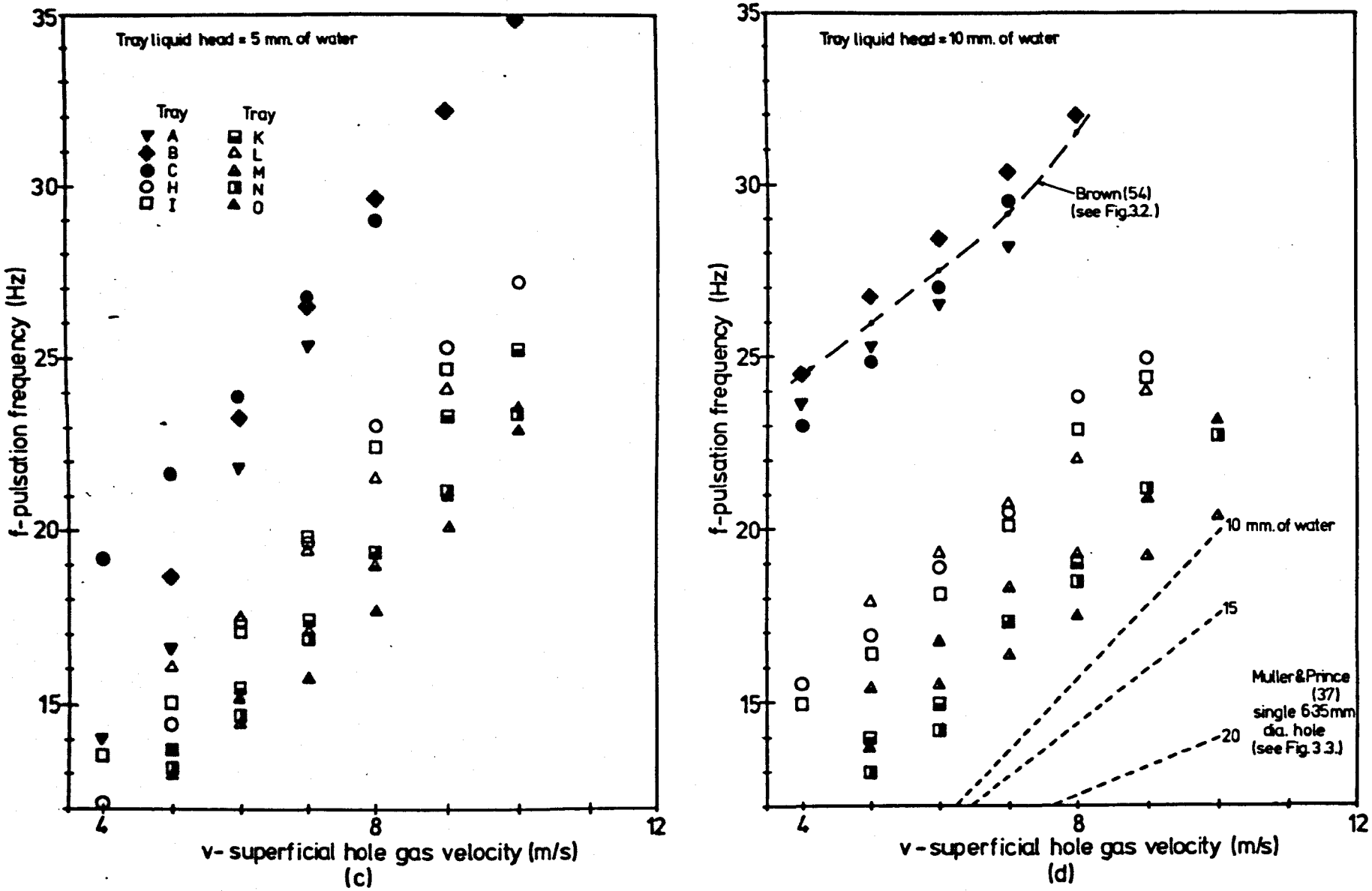

Fig. 5.9. EFFECT OF HOLE DIAMETER ON PULSATION FREQUENCY

increased from 38 to 108. Plot (a) shows a similar frequency increase to result from an increase in the number of holes from 108 to 403, with more than half of this frequency increase occurring between 108 and 256 holes.

It has been shown (section 5.2.2.3(i)) that a decrease in the number of holes reduces the pulsation amplitude, and it was suggested that this was due to the associated decrease in the gas volumetric flowrate corresponding to a given superficial hole gas velocity. It is possible that this change in flowrate could also account for the observed change in the pulsation frequency. However, this is unlikely, as changes in the hole diameter, which also affect the corresponding gas flowrate, have been found to have little affect on the frequency.

Kupferburg and Jameson (55) reported that a change in the number of holes had little affect on the frequency. Brown (54) found the frequency to increase as the number of holes was increased from 3 to 7, and he suggested that the chamber volume per hole was an important factor. This is considered further in section 5.4.2. Brown (54) correlated his findings using frequency proportional to (number of holes)$^{0.46}$. Such a dependence would lead to a frequency ratio of 1:1.62, as the number of holes was increased from 38 to 108, and this ratio is clearly too high.

Changing the number of holes also affects the tray resistance coefficient and this may result in a change in frequency.

5.2.4 Summary of the Results of Experiment I.

The results of this experiment clearly demonstrate that the amplitude and frequency of the regular gas pressure pulsations are dependent upon those system variables which effect the nature of the gas-liquid interaction on the tray.

Pulsations were found to occur over a specific range of operating conditions, determined by the superficial hole gas velocity and the tray liquid

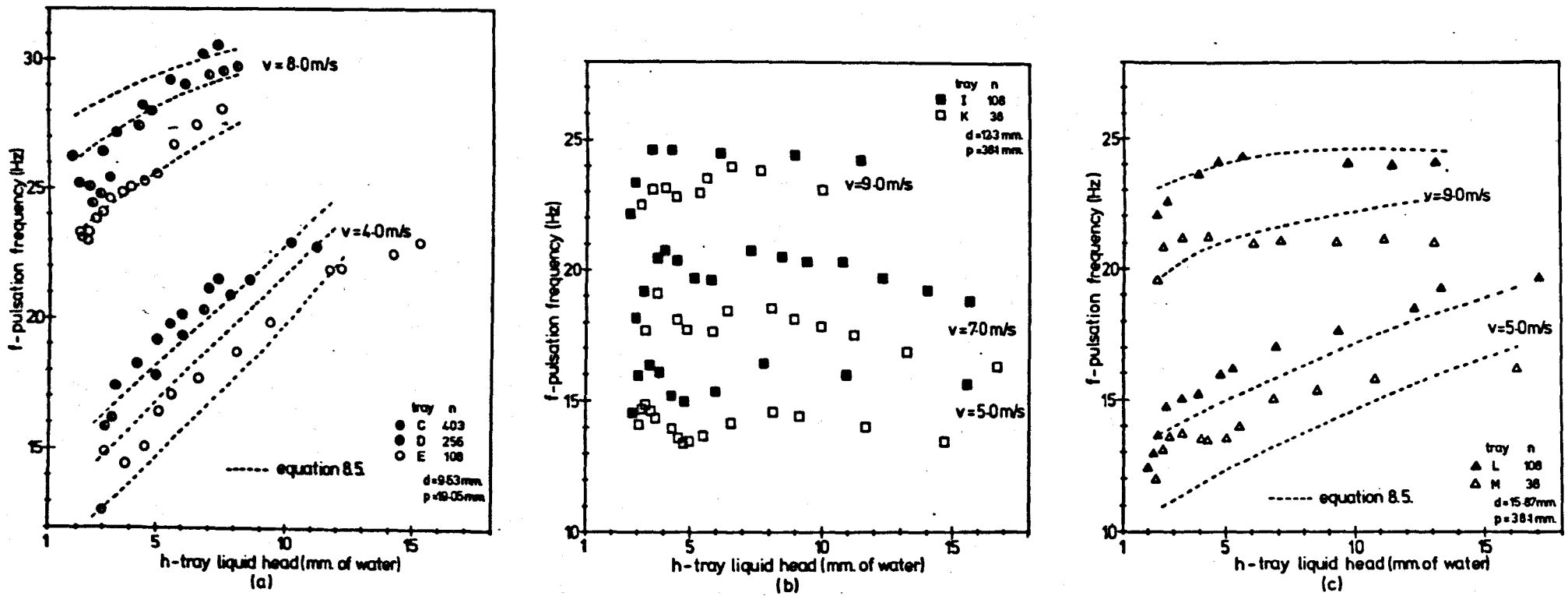

Fig.5.10. EFFECT OF NUMBER OF HOLES ON PULSATION FREQUENCY

head. These parameters were also shown to have a major effect on the pulsation frequency, with the effect of tray liquid head being dependent upon the value of hole pitch or separation. The number of holes and the hole pitch were found to be important parameters affecting the pressure pulsations, with hole diameter being of lesser importance.

The fundamental frequency of pressure pulsation varied between 12 Hz. and 40 Hz., with an r.m.s. amplitude of up to 60 N/m^2.

Most of the pulsations were produced when spray formation was evident on the tray, the conditions being those found by other workers to correspond to a form of jetting or imperfect bubbling at the holes.

This experiment was conducted with minimal tray liquid crossflow and with a constant chamber volume beneath the test-tray. These two factors will be considered in the next two sections.

5.3 EXPERIMENT II. INVESTIGATION OF THE EFFECT OF TRAY LIQUID CROSSFLOW ON THE PRODUCTION OF REGULAR PRESSURE PULSATIONS.

For operation above the seal point, the lower the weir height is, then the greater is the liquid flowrate, and tray liquid crossflow velocity, required to maintain a given tray liquid head. The effect of tray liquid crossflow velocity on the gas dynamic pressure in the chamber beneath the test-tray was investigated by taking measurements at different weir heights.

5.3.1 Experimental Procedure.

For a given tray geometry and normal chamber capacitance, measurements were taken according to the procedure described in section 5.2.1, but using only a single constant gas velocity. Various weir heights were used between 0 mm. and 76.2 mm., with test-trays B(g), H(g) and L(g). Table 5.1 gives details of the conditions used.

The tray liquid crossflow velocity, ℓ, was calculated using the equation:

$$\ell = 36 \times 10^6 \cdot \frac{L}{h} \quad \text{mm./s.} \qquad (5.1)$$

Table 5.1 Conditions used in Experiment II.

Test-Tray (d, p., p)	Weir heights (mm.)	v (m/s)
B(g) (6.6;19.05;391)	0;3.18;6.35;9.53;12.7;76.2	5.0
H(g) (9.53;38.1;108)	0;6.35;12.7;76.2	6.0
L(g) (15.87;38.1;108)	0;6.35;12.7;19.05;76.2	6.0

5.3.2 Results of Experiment II.

The results are plotted in Figure 5.11, which gives the frequency and r.m.s. amplitude of the pressure pulsation fundamental, and also indicates the higher values of the tray liquid crossflow velocity. A variation in behaviour can be seen between the three trays investigated.

In Figure 5.11, plot (a) shows that for tray B(g) the pressure pulsations are affected by crossflow velocities greater than about 20 mm./s. with both the frequency and amplitude increasing with increasing crossflow velocity. The effect is quite uniform, with an increase in frequency of up to 4 Hz. occurring at the highest crossflow.

Plot (b) shows that for tray H(g) there is no significant effect of tray liquid crossflow velocity on the pulsations for velocities below about 80 mm./s. Above this velocity, however, there is a significant increase in the frequency and amplitude of the pulsations with increasing crossflow velocity.

Plot (c) shows that for tray L(g) there is no significant effect of crossflow velocity on the pulsations up to the highest value used, which was 190 mm./s. There is some evidence of a small increase in pulsation amplitude with increasing crossflow velocity, but the frequency tends to be lowest at the highest crossflow velocities.

It is possible that the different behaviour of trays B(g) and H(g) is due to the change in frequency dependence upon tray liquid head, resulting from the increase in hole pitch. However, it would then be expected that tray L(g),

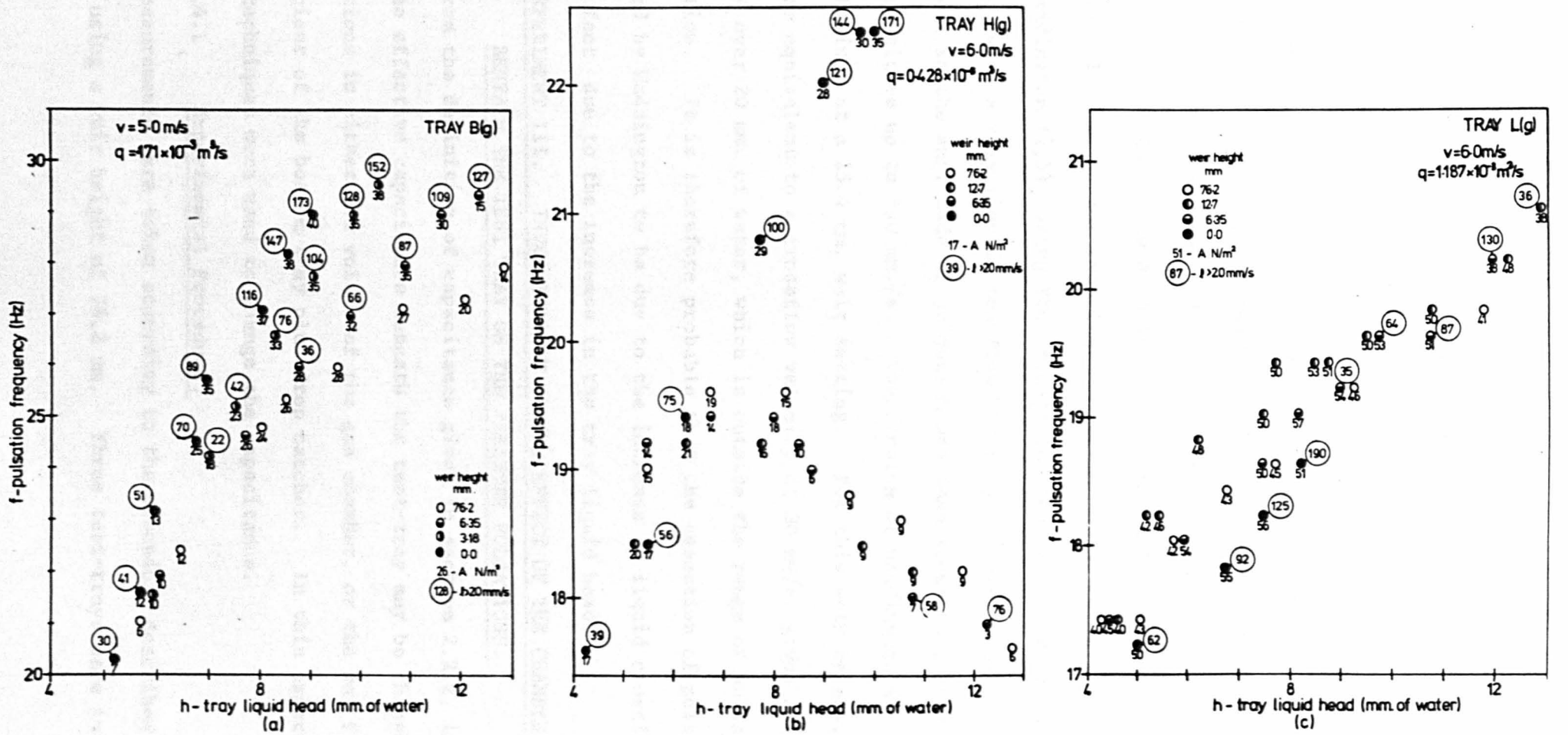

Fig. 5.11. EFFECT OF TRAY LIQUID CROSSFLOW VELOCITY ON PRESSURE PULSATIONS

which showed evidence of 'small pitch' behaviour, would exhibit an increase in frequency with increase in liquid head, similar to tray B(g). This does not occur.

It is possible that the change in behaviour is due to the increase in the average gas hole volumetric flowrate which results from an increase in the hole diameter, a higher crossflow velocity being needed to affect the higher volumetric flowrate. The hole volumetric flowrates are indicated in Figure 5.10, and can be seen to increase from 0.171×10^{-3} m^3/s.for tray B(g) to 1.187×10^{-3} m^3/s. for tray L(g).

Waddington (2,5), using tray B,reported that no pressure pulsations were produced with a tray liquid crossflow velocity of over 30 mm./s. This is not the case, as the amplitude of pulsation has been shown to increase with crossflow velocities up to 190 mm./s. The finding of Waddington was based upon data obtained at a 25.4 mm. weir setting. For this weir height, the liquid flowrate equivalent to a crossflow velocity of 30 mm/s. gives a tray liquid head of over 20 mm. of water, which is outside the range of pulsation production. It is therefore probable that the cessation of pulsations, reported by Waddington to be due to the increase in liquid crossflow velocity, was in fact due to the increase in the tray liquid head.

5.4 EXPERIMENT III. INVESTIGATION OF THE EFFECT OF THE CHAMBER CAPACITANCE BENEATH THE TEST TRAY ON THE PRESSURE PULSATIONS.

From the definition of capacitance given in section 2.2.2, it follows that the effective capacitance beneath the test-tray may be changed by alterations in either the volume of the gas chamber, or the gas flow resistance coefficient of the bottom tray plus drop catcher. In this experiment both of these techniques were used to change the capacitance.

5.4.1 Experimental Procedure.

Measurements were taken according to the procedure described in section 5.2.1, using a weir height of 76.2 mm. Three test-trays were investigated,

with various values of chamber volume and bottom tray resistance coefficient. Details of the conditions used are given in table 5.2.

Two measures of the coefficient of resistance of the bottom tray plus drop catcher are given. The coefficient K_B is based upon the test-tray superficial hole gas velocity, and K_{BC} is based upon the superficial column gas velocity.

In run 1, only the resistance coefficient was changed. This was done by placing a 25 mm. thick layer of foam rubber on top of the drop catcher. In the other runs the chamber volume was changed.

Reduction in the chamber volume was achieved by inserting a known volume of expanded polystyrene into the chamber. In run 2 the polystyrene was supported, above the drop catcher, on a small 'table', and therefore did not affect the resistance coefficient. In this case the volume of polystyrene was determined using a water displacement technique. For the other runs in which the volume was reduced (3, 4, 5 and 7), 25.4 mm. thick polystyrene slabs were used. These were built up on top of the drop catcher and therefore increased the resistance coefficient. Figure 5.12 shows the polystyrene in position for run 3. The volume of the polystyrene packing was calculated from a knowledge of the area of the slabs used. Because of the packing the static pressure tapping beneath the test-tray, (P_1), had to be moved up the side of the column, to a position 70 mm. below the test-tray.

The chamber volume was increased in runs 6 and 8. This was achieved by attaching an 8.95 m. length of 0.15 m. internal diameter p.v.c. tubing to the side of the chamber. Further details of this tube are given in Appendix IX.

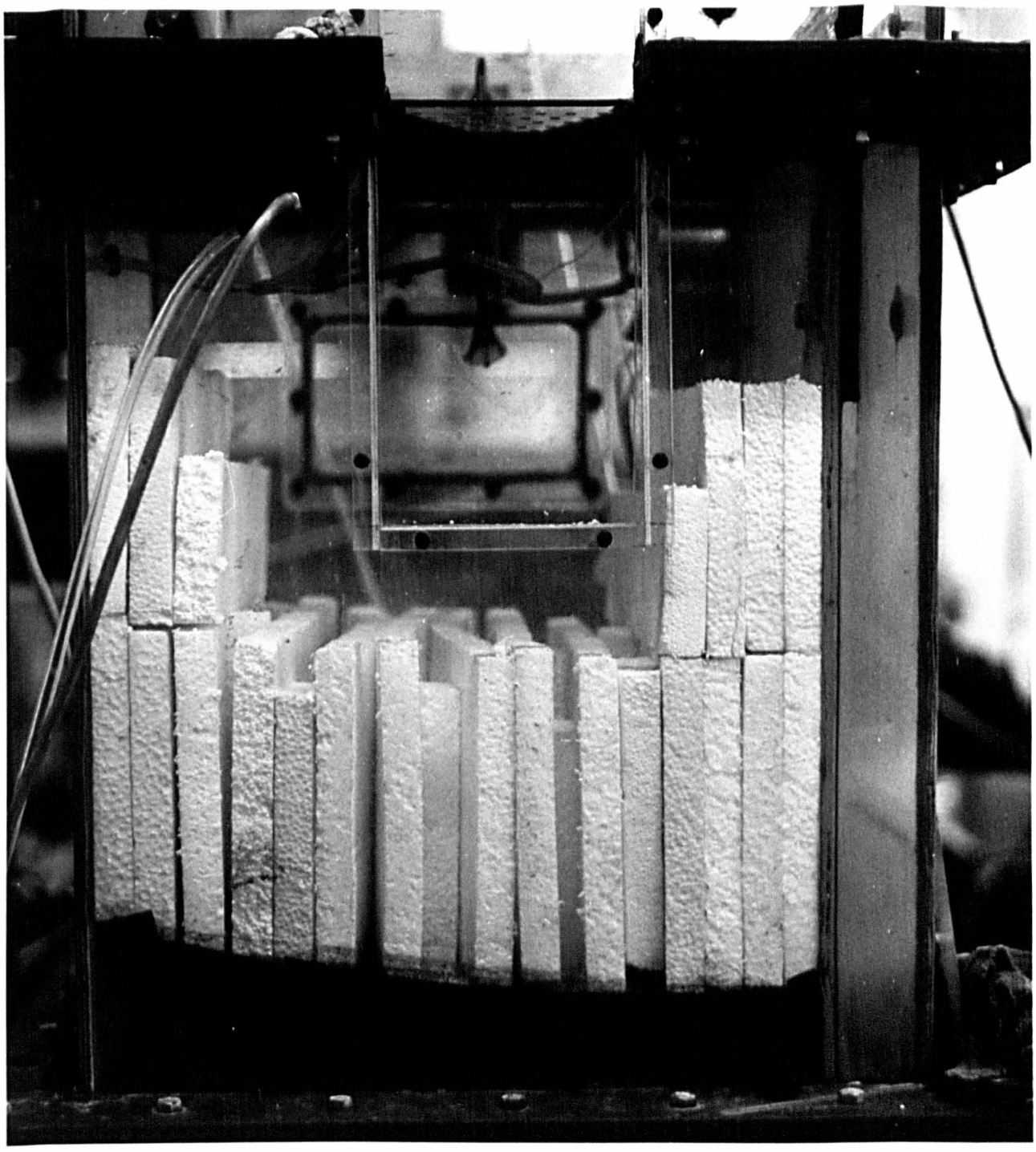

Fig. 5.12 EXPANDED POLYSTYRENE PACKING USED TO REDUCE THE CHAMBER CAPACITANCE IN EXPERIMENT III, RUN 3

Table 5.2 Conditions used in Experiment III.

Run Number	Test-Tray	Chamber Volume beneath test-tray m^3	Resistance Coefficient of the Bottom Tray plus drop catcher K_B	K_{BC}
1	B	0.11	7.4	1900
2	B	0.097	4.1	1050
3	B(g)	0.066	7.8	1700
4	B(g)	0.052	6.7	1450
5	H(g)	0.052	2.3	1340
6	H(g)	0.268	1.7	990
7	L(g)	0.052	17.5	1320
8	L(g)	0.268	13.3	1000

5.4.2 Results of experiment III.

The fundamental r.m.s. amplitude and frequency of the pressure pulsations measured in the experiment are compared in Figures 5.13 and 5.14 with those measured under conditions of normal capacitance.

Figure 5.13 shows that the amplitude of pulsation is apparently independent of the changes in capacitance. This suggests either that the changes in capacitance were too small, or that the magnitude of the pulsation is controlled or 'limited' primarily by the nature of the gas-liquid interaction on the tray.

Figure 5.14 shows that some of the changes in capacitance have a definite effect on the pulsation frequency. Plot (a) shows the frequency to be increased slightly by the 80% increase in the bottom tray resistance coefficient in run 1. Increasing the bottom tray resistance tends to reduce the capacitive influence of the bottom chamber and the orifice tube on the gas pressure pulsations in the chamber beneath the tray. Only when the resistance becomes very high will the effective capacitance beneath the test-tray be due only to the gas chamber volume below the test-tray.

The 11% reduction in chamber volume in run 2 is seen to have no significant effect on the pulsation frequency.

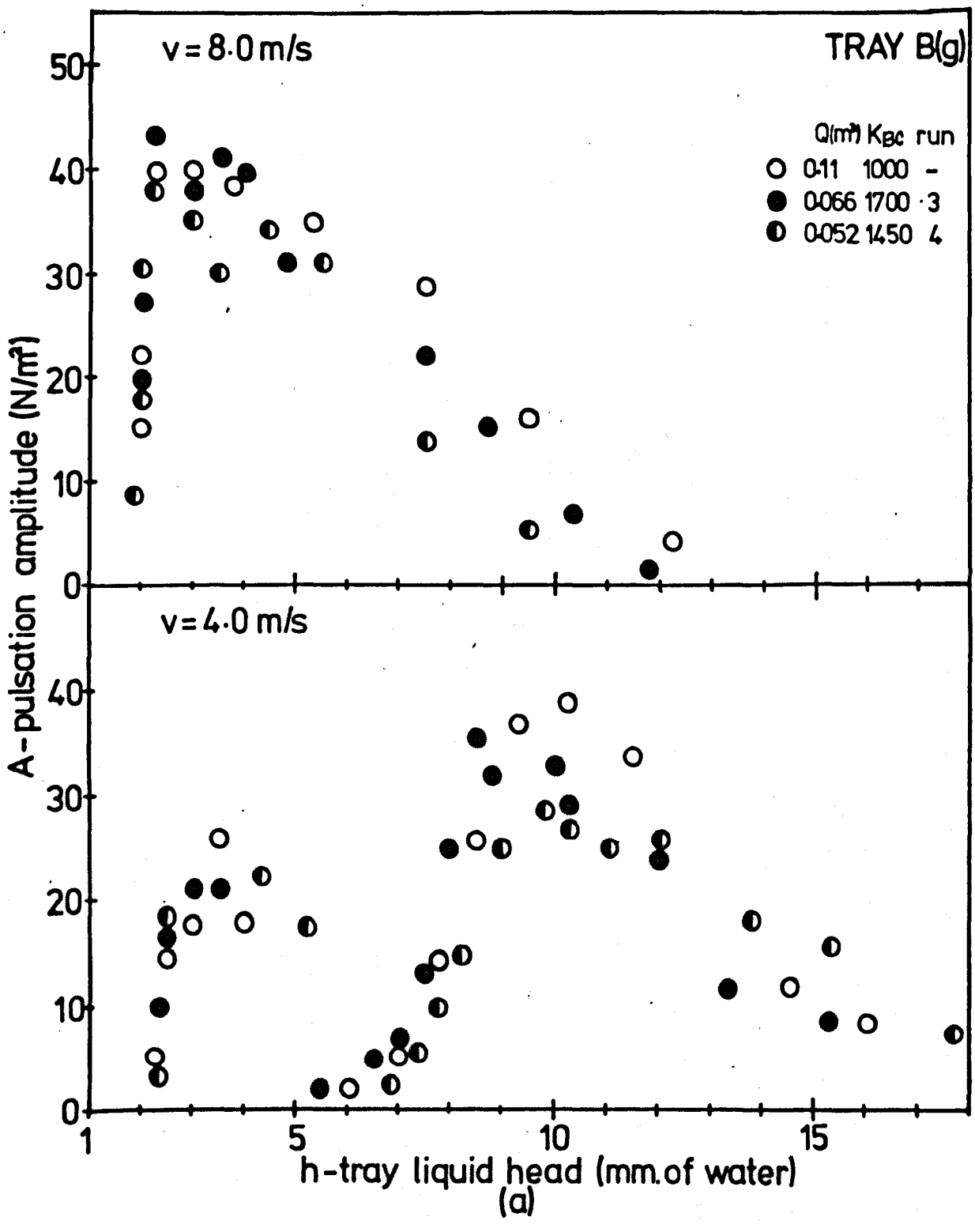

Fig.5.13. EFFECT OF CHAMBER CAPACITANCE ON PULSATION AMPLITUDE

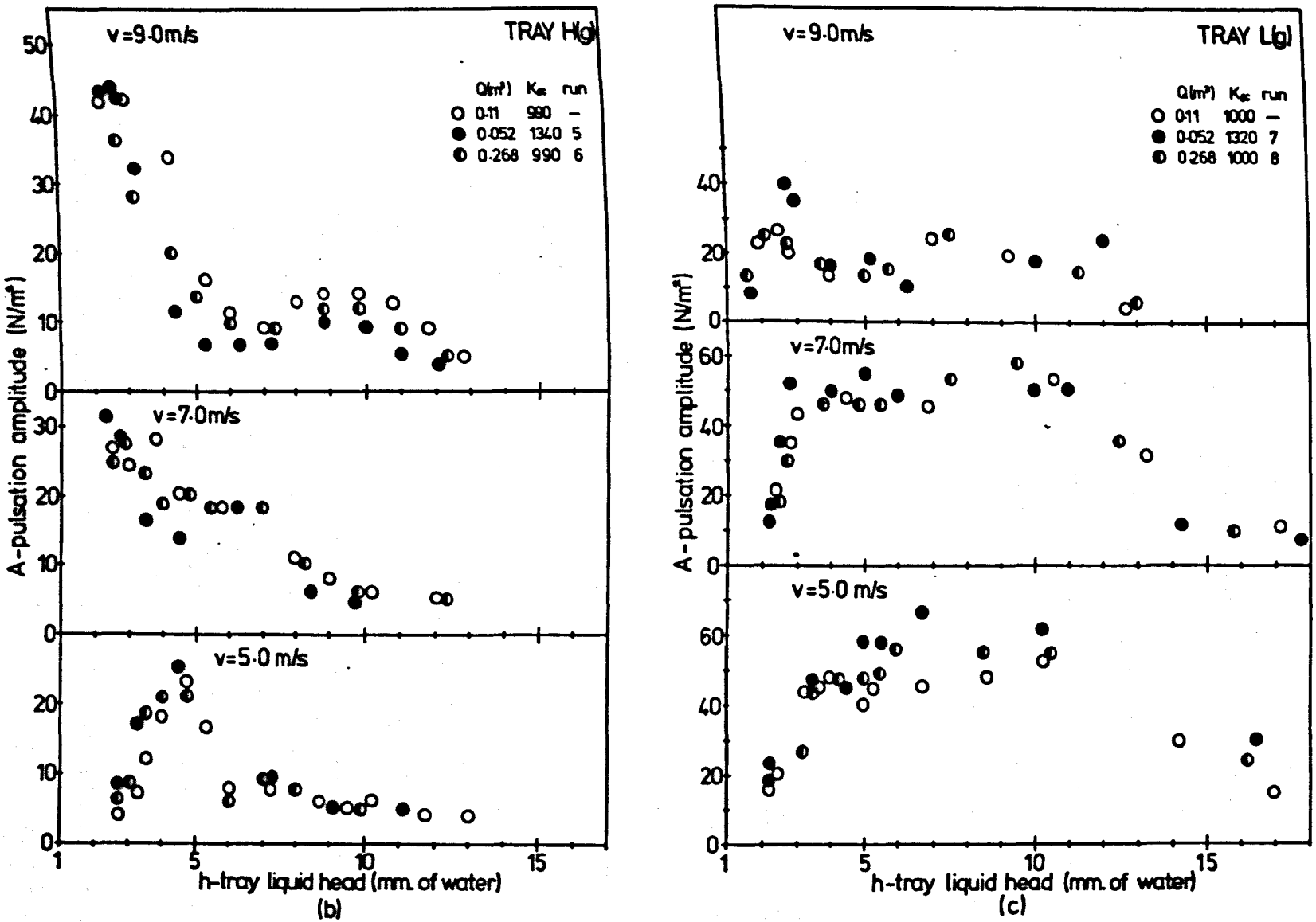

Fig.5.13. EFFECT OF CHAMBER CAPACITANCE ON PULSATION AMPLITUDE

In run 3 a 67% increase in the resistance coefficient and a 40% volume reduction resulted in an increase in the frequency which was greater than that found for run 7. This indicates that the frequency has been increased by the volume reduction. This finding is supported by the results of run 4, in which a further frequency increase resulted from an overall increase of 38% in the tray resistance and a 50% reduction in the volume.

Runs 5 and 7 show a similar increase in frequency for a 50% volume reduction and an increase in the resistance of 35% and 32% respectively. The increase in frequency, as in run 4, was up to 2 Hz., and tended to be more pronounced at the higher gas velocities.

The fact that an 11% reduction in volume in run 2 had no effect on the frequency, whilst the 10% reduction between runs 3 and 4 did have an effect, suggests that the frequency becomes more dependent upon chamber volume changes as the volume becomes small. This idea is supported by the results of runs 6 and 8, in which a 140% increase in the chamber volume had no apparent effect on the frequency other than at the highest gas velocity, for which a slight decrease in frequency can be detected.

Because of the uncertainty in knowing the exact magnitude of the changes in the capacitance beneath the test-tray brought about in the experiment, it is difficult to compare the results obtained with those of other workers. However, for the 50% volume reductions, the resulting increase in frequency is below that given by a relationship of frequency proportional to $(\text{volume})^{-0.1}$ ($f \propto Q^{-0.1}$). Brown (54) correlated the volume effect by $f \propto Q^{-0.46}$, and the results of McCann and Prince (42) for single hole bubbling, indicate a relationship of approximately $f \propto Q^{-0.25}$.

Brown (54) used a volume per hole basis to correlate his results. In experiment I, the frequency dropped by about 2.5 Hz. as the number of holes in the tray dropped from 108 to 38, equivalent to an increase in the volume

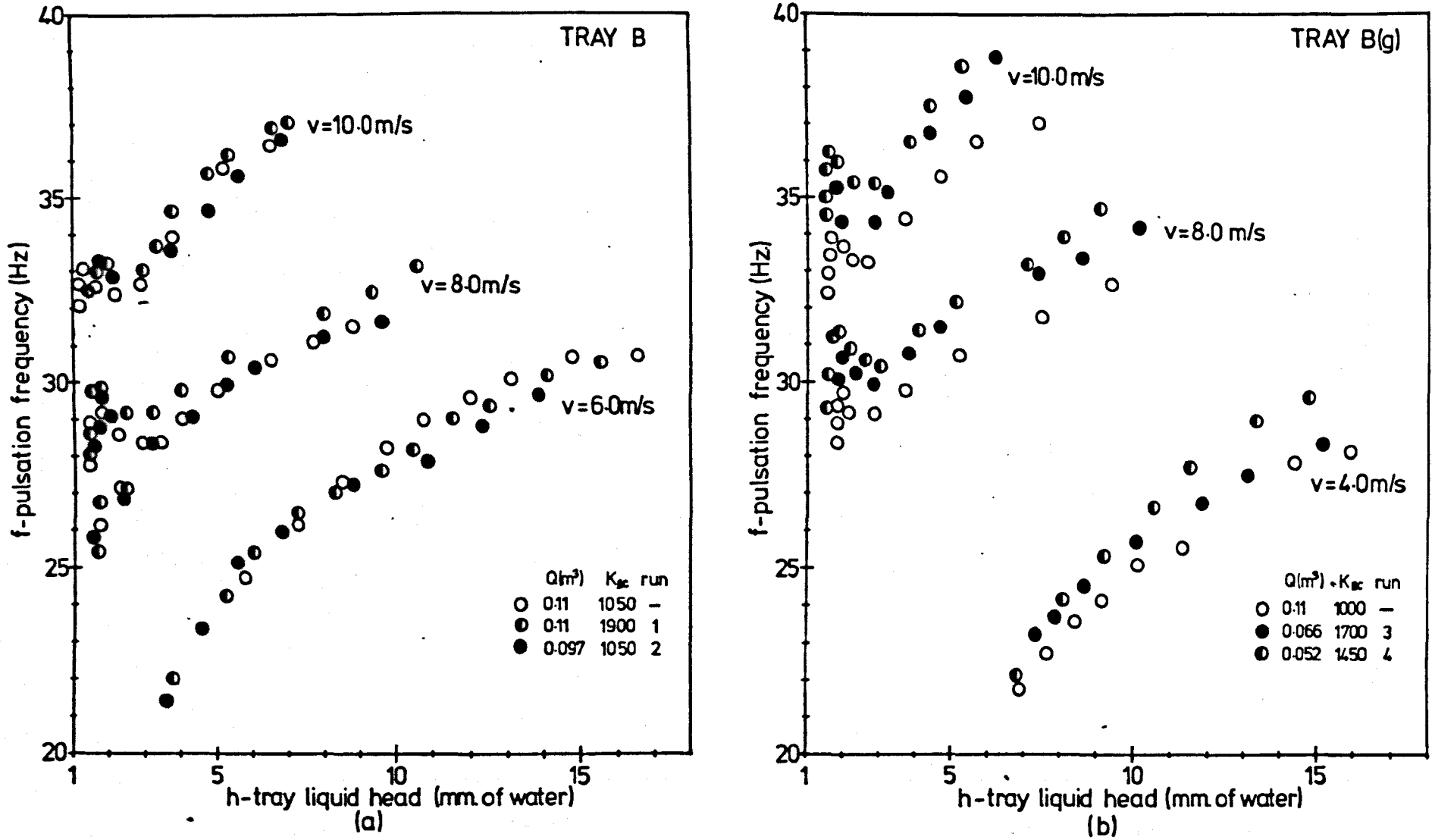

Fig. 5.14 EFFECT OF CHAMBER CAPACITANCE ON PULSATION FREQUENCY

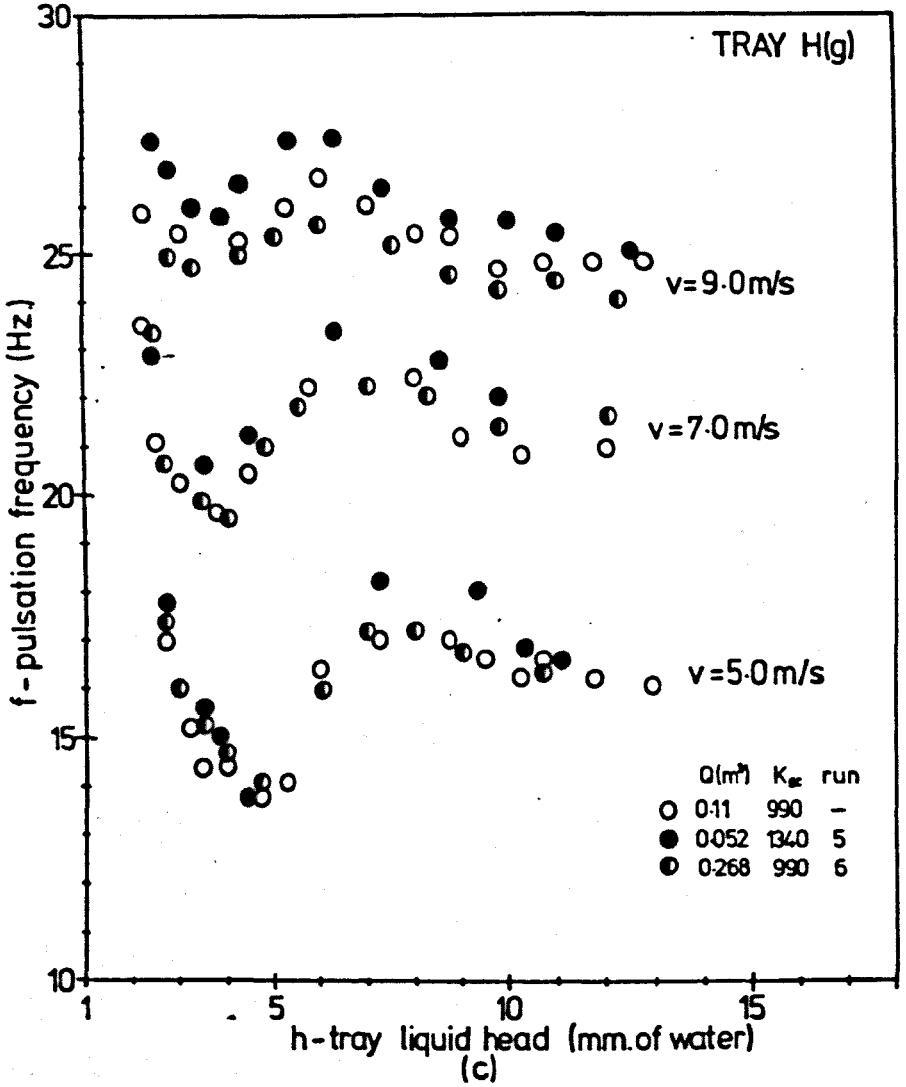

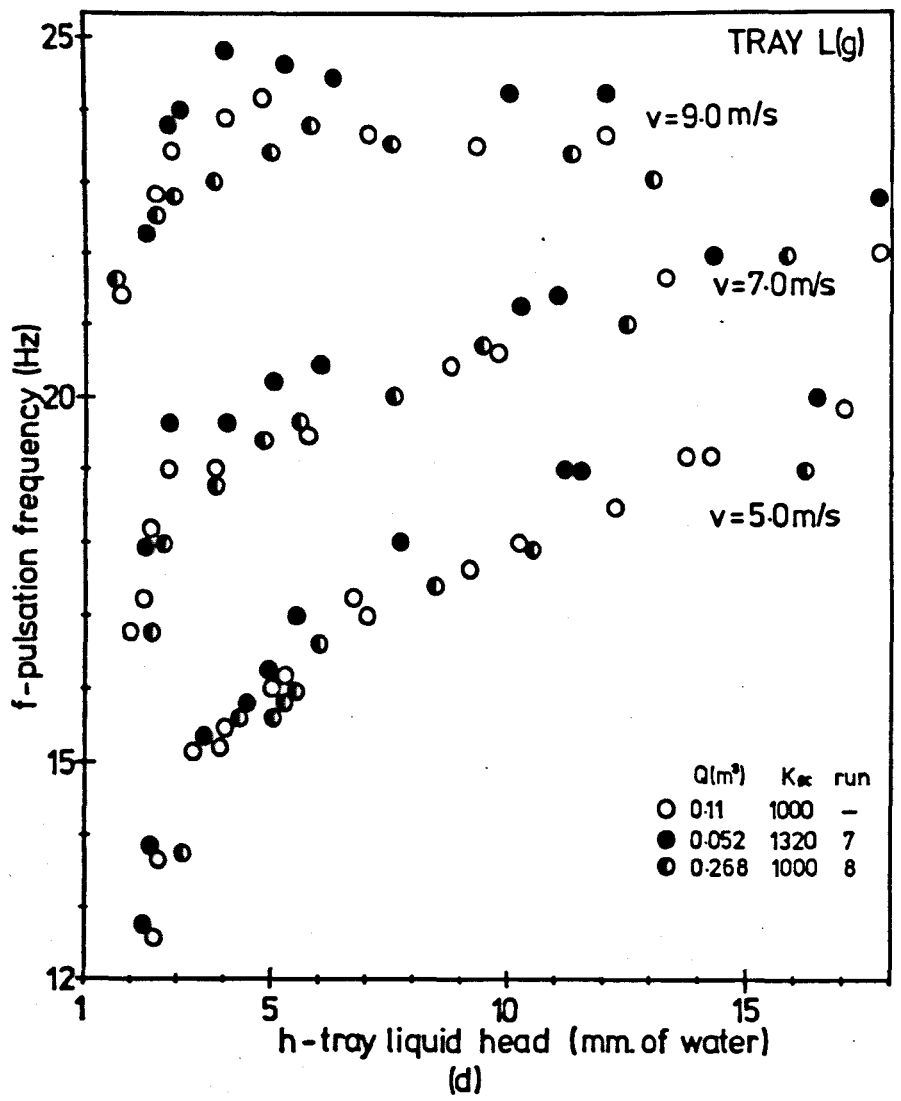

Fig. 5.14 EFFECT OF CHAMBER CAPACITANCE ON PULSATION FREQUENCY

per hole from 1.02 x 10^{-3} m^3 to 2.89 x 10^{-3} m^3, based on the volume of the chamber beneath the test-tray. However, the addition of the side tube in runs 6 and 8 resulted in a similar increase in the volume per hole (1.08 x 10^{-3} m^3 to 2.50 x 10^{-3} m^3), and this is seen to have had no appreciable effect on the frequency. This indicates that the volume per hole ratio is not primarily responsible for the reduction in frequency associated with the decrease in the number of holes.

It can be concluded that changes in the capacitance beneath the test-tray have no appreciable effect on the pulsation amplitude, but the pulsation frequency is increased by up to 10% for a 50% reduction in the volume of the chamber beneath the test-tray together with a 30% increase in the bottom tray resistance coefficient. The frequency is largely unaffected by increases in chamber volume of up to 140%.

5.5 EFFECT OF THE TEST-TRAY MECHANICAL VIBRATIONAL CHARACTERISTICS ON THE GAS PULSATIONS.

An experimental investigation of the effect of changing the tray vibrational characteristics on the gas pressure pulsations was carried out, and is detailed in Appendix VIII.

The test-tray was stiffened using two diagonal metal struts to link it to the top tray, raising its fundamental vibration frequency from about 110 Hz. to about 155 Hz. The tray was also loosened by cutting slots along its sides, reducing its fundamental frequency to about 90 Hz. with two slots, and about 60 Hz. with three slots, these frequencies being in the range of the second and first harmonics of the pulsation frequency spectrum respectively.

It was found that these changes to the tray vibrational characteristics had no effect on the amplitude or frequency of the pressure pulsations.

The tray was found to be excited by both the fundamentals of the pressure pulsations and the harmonics exhibited in its frequency spectrum. The highest levels of tray vibration occurred when a harmonic approached the tray fundamental frequency.

Although the tray fundamental frequency was not lowered sufficiently to correspond to the fundamental frequency of the pressure pulsations, it is to be expected that when the correspondence occurs, very high levels of tray vibration will result.

5.6 EFFECT OF SYSTEM NOISE AND SYSTEM ACOUSTICS ON THE PRESSURE PULSATIONS.

A certain amount of pressure variation is generated within the experimental apparatus, even in the absence of gas-liquid interaction within the column. Measurement of this 'system noise' is detailed in Appendix IX, in which is described work carried out to investigate the system acoustic resonant frequencies, including attempts to change these.

It was found that the system noise was primarily at a relatively high frequency (> 150 Hz.) and low amplitude, with respect to the regular pressure pulsations generated by gas-liquid interaction (12 Hz. to 40 Hz.). The 'system noise' was found to be produced mainly by the centrifugal fan and orifice tube.

There were no significant acoustic resonances below 150 Hz. An attempt to introduce low frequency acoustic resonance, by attaching a long side tube to the chamber beneath the test-tray, was unsuccessful and had no apparent effect on the regular pressure pulsations.

5.7 SUMMARY.

Regular pulsations of the gas pressure beneath the test-tray have been found to be produced by each of the fifteen sieve-tray geometries investigated. They occurred over a specific range of operating conditions as determined by the superficial hole gas velocity and the tray liquid head, most of the pulsations were produced at gas velocities below 12 m/s and tray liquid heads below 20 mm. of water. The pulsation fundamental frequency varied between 12 Hz. and 40 Hz., with an r.m.s. amplitude of up to 60 N/m^2.

Superficial hole gas velocity and tray liquid head were found to be the major flow parameters affecting pulsation frequency, with the effect of

tray liquid head being dependent upon the hole pitch or separation. The number of holes and the hole pitch were found to be the major geometrical parameters affecting the pulsations, with hole diameter being of minor importance.

Increasing the tray liquid crossflow velocity was found to increase both the frequency and amplitude of the pressure pulsations for crossflow velocities of over 20 mm/s. for tray B(g) and over 80 mm/s. for tray H(g). Crossflow velocities of up to 190 mm/s. failed to effect pulsations produced by tray L(g).

Changes in the capacitance beneath the test-tray affected the pulsation frequency, but had no appreciable effect on the pulsation amplitude. The frequency increased by up to 10% for a 50% reduction in the volume of the chamber beneath the test-tray together with a 30% increase in the bottom tray gas resistance coefficient. However, increasing the chamber volume by up to 140% had no appreciable effect on the frequency.

Changes in the test-tray vibrational characteristics had no effect on the amplitude or frequency of the pressure pulsations.

The major system 'noise' and acoustic resonances were found to be of a relatively high frequency (> 150 Hz.) with respect to the pressure pulsations.

It is now necessary to determine why and how the gas pulsations are produced by the gas-liquid interaction on the tray. An investigation aimed at solving this problem is described in the next chapter.

Chapter 6.

EXPERIMENTAL WORK AND RESULTS - II.

STUDY OF THE GAS-LIQUID INTERACTION ON THE SIEVE-TRAY.

Introduction.

Regular gas pulsations have been found to be produced, over a specific operating range, by fifteen different tray geometries, and the effects of the important system variables on the frequency and amplitude of these pulsations have been determined. The production of the pulsations is associated with the gas-liquid interaction on the sieve-tray. This chapter gives details of an investigation carried out to try to determine why and how the regular pulsations are produced.

Two main methods of investigation were used. Firstly, electrical conductivity probes were used to monitor the frequency of the gas-liquid interaction at individual holes. Secondly, a direct study of the gas-liquid interaction was carried out by high speed cine-photography. The experimental procedures are described and main results are presented and discussed. Further discussion of the results is given in the next chapter.

It was reported in Chapter 5 that the mechanism of gas-liquid interaction on the tray which occurred during the occurrence of the regular pulsations was likely to be some form of periodic 'jetting' or 'bubbling'. However, because of the uncertainty as to the exact mechanism of the interaction, the term 'hole event' is introduced, a hole event being a single period of gas-liquid interaction at an individual hole on the tray. Under certain conditions, for example, the hole event may be an imperfect bubble, and under other conditions, a jet pulse.

6.1 INVESTIGATION OF THE GAS-LIQUID INTERACTION AT THE TRAY HOLES USING ELECTRICAL CONDUCTIVITY PROBES.

The construction and operation of the electrical conductivity probes is described in section 4.9. Similar probes were used by Pinczewski and Fell (28), and Yeo (41), who reported that the probes accurately monitored the liquid 'bridging' at the hole. The frequencies reported by Yeo can be compared, in Figure 3.4, with those found by McCann and Prince (42), who

measured the pressure variations beneath the hole. There is good agreement between the two sets of frequencies, indicating that the conductivity probe correctly monitors the hole event frequency.

6.1.1 Experimental Procedure.

Conductivity probes were used with all of the trays investigated. They were positioned centrally in specific holes on the tray, with the probe tip at a measured height above the tray surface.

Output signals from up to four probes were displayed simultaneously on the cathode ray oscilloscope, although one channel on the C.R.O. was usually used to display continually a dynamic pressure signal. Photographic records of displayed signals were taken. Some frequency analysis of the probe signals was carried out using the Solartron real time analyser.

6.1.2 Results from the Electrical Conductivity Probes.

Results are given in the form of tracings of signal display photographs. Although this presents only a relatively short time period of signal, the traces shown are representative ones.

The hole in which each probe was located is defined in terms of the hole identification system given in Appendix I. Unless otherwise specified, the results were obtained for operation with a 76.2 mm. weir height, giving minimal liquid crossflow.

Figure 6.1 compares signals from two conductivity probes with the pressure pulsations measured beneath test-tray H(g), for operation in the spray regime. Probe 1 was at a constant height of 5 mm., and the height of probe 2 was varied from 0 mm. in trace (a) to 14 mm. in trace (d).

All the peak signals in Figure 6.1 exhibit short regular pulses which correspond with the gas pressure pulsations beneath the tray. This is positive evidence that the occurrence of the pressure pulsations is closely linked with the gas-liquid interaction on the tray, and indicates that the 'hole events' are of a regular periodic nature, synchronised with the pressure pulsations.

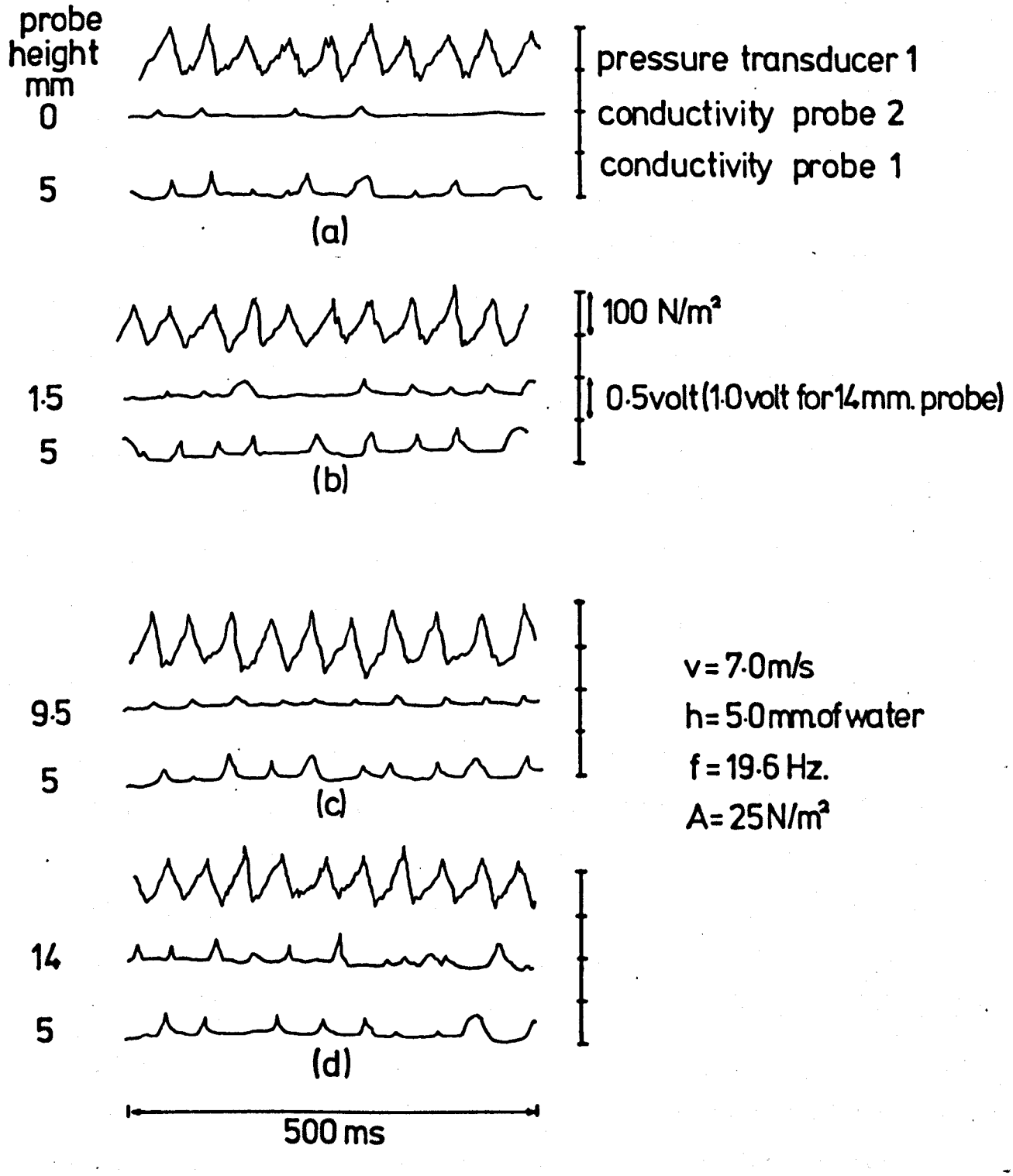

Fig. 6.1 CONDUCTIVITY PROBE SIGNALS AND DYNAMIC PRESSURE BENEATH TEST-TRAY H(g)

Occasionally a probe pulse can be seen to fail to occur during a particular pressure pulsation, indicating extended continuous gas flow through the hole. The probe pulse immediately following such an absence is again usually well synchronised with a pressure pulsation, indicating that the moment of occurrence of a hole event is strongly influenced by the pressure pulsations, and little affected by the history of behaviour at that hole.

Very few pulses could be detected with a probe height of 0 mm., on average only 2 or 3 pulses per second being apparent. The other traces indicate that at greater heights, up to 14 mm., there is little variation of signal with probe height, apart from a decrease in pulse amplitude for large heights. The probe pulses are seen to correspond approximately with the peak of the pressure pulsation, and there is some indication that as the probe height is increased, the pulse occurs at a later time with respect to the pressure pulsation. It is evident from Figure 6.1 that a probe height of about 5 mm. gives a representative signal.

Figure 6.2 shows four traces of signals produced by test-tray B(g) operating at various conditions. Again there is strong evidence of regular periodic hole events, synchronised with the pressure pulsations. Trace (a) is for operation in the fine spray regime, and yet there is still an apparent indication of liquid bridging at the holes. Again probe pulses occasionally fail to occur at individual pressure pulsations, with some indication, particularly in trace (b) that a pulse is more likely to be absent immediately after a large or extended pulse.

Table 6.1 presents the results of frequency analyses carried out on probe signals produced by test-tray J, operating at various conditions with a 50.8 mm. weir height. The number in parenthesis is a relative linear amplitude of the frequency component. It can be seen that during regular pressure pulsation production, a main frequency component is present in the probe

TABLE 6.1 FREQUENCY ANALYSIS OF ELECTRICAL CONDUCTIVITY PROBE SIGNALS.

Test tray J; Weir height = 50.8 mm.

Probe height = 6 mm. ; probe hole, F5.

Gas velocity v m/s	Tray liquid head h,mm.of water	Pulsation frequency f.Hz.	Pulsation amplitude A N/m^2	Probe frequencies Hz (amplitude)
4.3	3.0	14.4	26	14.2(10)
4.3	4.0	14.0	25	14.0(14)
4.3	8.25	14.4	11	7.4(15); 14.4(9)
6.4	2.75	16.8	20	16.8(4)
6.4	5.0	17.0	30	9.0(10); 17.0(10)
6.4	9.25	17.4	22	8.6(10); 17.4(10)
6.4	28.0	-	-	-
7.5	3.25	20.0	29	20(3)(5)(4)(3)*
10.7	4.0	27.0	5	-

*Also probes: (hole) D9 , height 3 mm.; I10 , 9 mm; D15 , 3 mm.

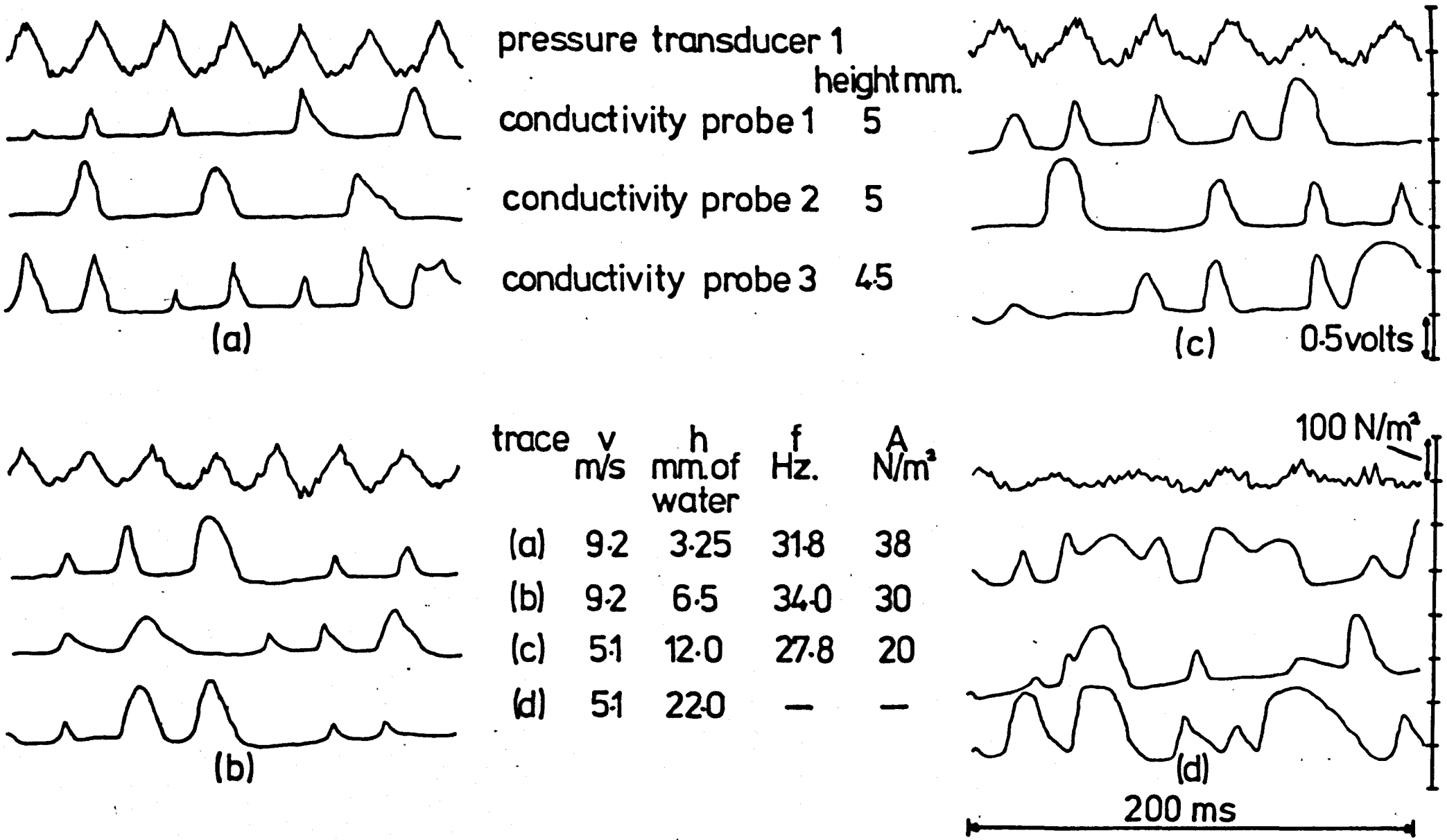

trace	v m/s	h mm. of water	f Hz.	A N/m²
(a)	9·2	3·25	31·8	38
(b)	9·2	6·5	34·0	30
(c)	5·1	12·0	27·8	20
(d)	5·1	22·0	—	—

Fig. 6.2. CONDUCTIVITY PROBE SIGNALS AND DYNAMIC PRESSURE BENEATH TEST-TRAY B(g)

spectrum, at the same frequency as the pressure pulsations. Also, at the higher tray liquid heads, a second main frequency component is present, at about half the pressure pulsation frequency. This can be taken to indicate a substantial number of pulses being absent for a single pressure pulsation, that is, a substantial number of hole events of approximately double the normal duration.

In Figure 6.2., trace (d) shows probe signals for conditions of heavy liquid weeping and no pressure pulsations. These signals are erratic and show no definite regular behaviour. Under such conditions some preference for liquid weeping at the probe holes was evident. However, for conditions of moderate weeping with pressure pulsation production, as for trace (c), the probes were little affected by the weeping.

Signals produced by probes in test-tray L(g) are shown in Figure 6.3. Again there is strong indication of regular periodic hole events synchronised with the pressure pulsations beneath the tray. Trace (d) shows how the probe output became much less regular when the gas velocity was increased sufficiently to stop the pressure pulsations.

Although the signals shown in Figures 6.1, 6.2 and 6.3 exhibit regular, synchronised pulses, there is some variation both in the size of the pulses and in the interval between successive pulses. This indicates that there is some variation both in the extent of the apparent liquid bridging and in the duration of individual hole events, particularly for those hole events indicated by a large or extended probe pulse with subsequent pulse absence. Thus, although use of the conductivity probes has established a definite link between the regular pressure pulsations and the gas-liquid interaction on the tray, much more detailed information is required about the exact behaviour of the gas and liquid. In an attempt to obtain this information, a photographic study of the gas-liquid behaviour on the tray was carried out.

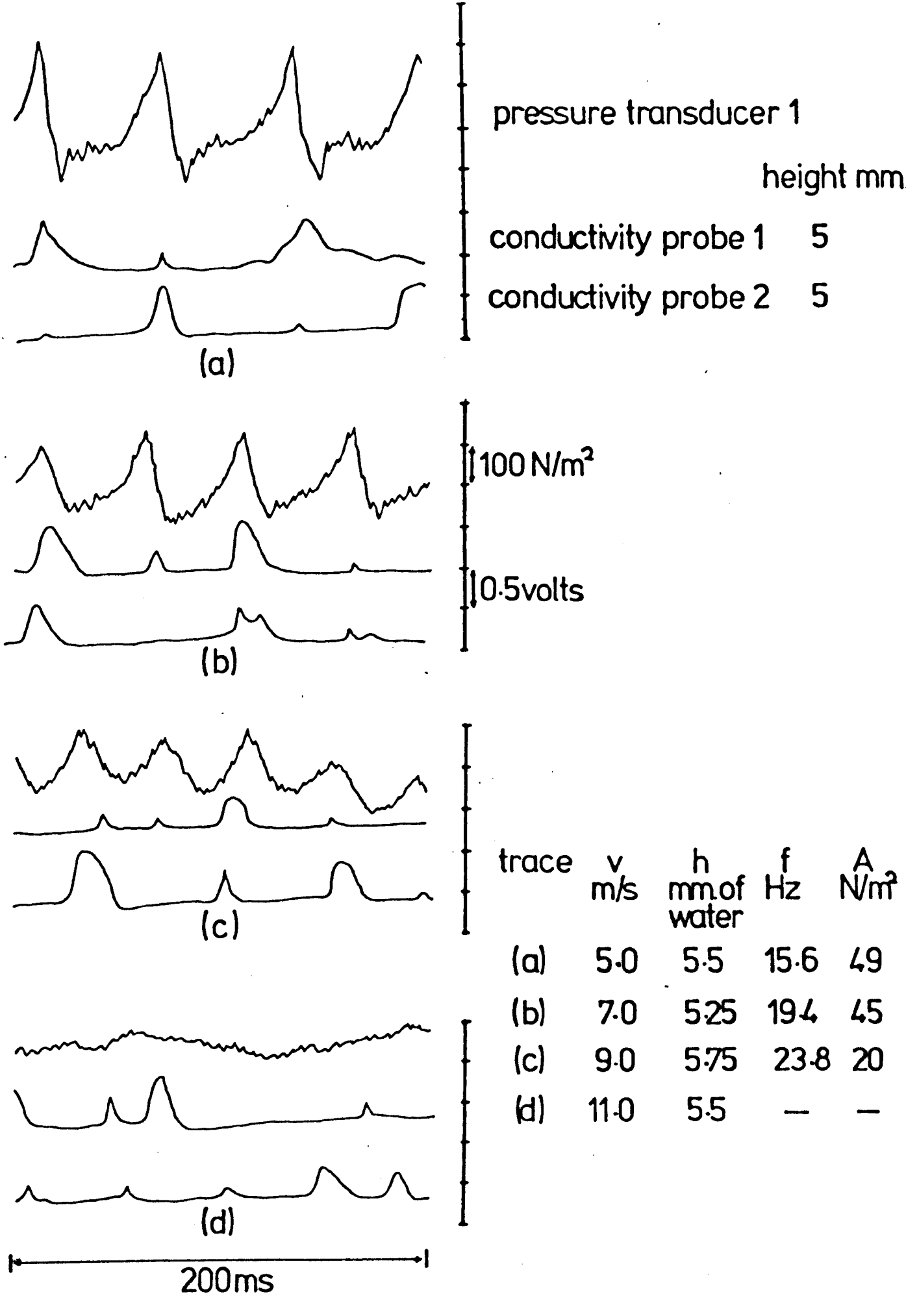

trace	v m/s	h mm of water	f Hz	A N/m²
(a)	5·0	5·5	15·6	49
(b)	7·0	5·25	19·4	45
(c)	9·0	5·75	23·8	20
(d)	11·0	5·5	—	—

Fig.6.3. CONDUCTIVITY PROBE SIGNALS AND DYNAMIC PRESSURE BENEATH TEST-TRAY L(g)

6.2 STUDY OF THE GAS-LIQUID INTERACTION AT THE TRAY HOLES USING HIGH SPEED CINE-PHOTOGRAPHY.

The evidence obtained using electrical conductivity probes has shown the regular column gas pulsations to be associated with regular periodic hole events of the same frequency. High speed cine-photography was used to obtain detailed information about the nature of the hole events and about how they are related to the gas pulsations.

Details of the photographic equipment used and the rig modifications carried out are given in section 4.10. Films were taken, at various operating conditions, for test-trays B(g), H(g), L(g) and O(g). Those for tray H(g) were synchronised with a u-v recorder which recorded the dynamic pressure beneath the test-tray and a conductivity probe signal.

6.2.1 Experimental Procedure.

Details of the films taken are given in Table 6.2. Three camera positions were used; most of the films were taken with the camera positioned beneath (B) the test tray, as shown in Figure 4.3. The other films were either taken from the side (S) or from above (A) the test-tray.

For each film, measurements were taken of the prevailing column static and dynamic pressures, (according to the procedure described in section 5.2.1) and photographic records were taken of the C.R.O. display of column dynamic pressure and conductivity probe signals.

The film speeds given in table 6.2 correspond to that portion of the film which was analysed.

6.2.1.1 Film synchronisation with a u.-v. recorder.

To provide a direct link between the film, the pressure pulsations and a conductivity probe signal, the films taken for test-tray H(g) were synchronised with a Honeywell 1706 Visicorder ultra-violet recorder. An electronic flash and photocell were used to synchronise the time bases of the camera and the u. v. recorder.

TABLE 6.2 DETAILS OF CINE FILMS TAKEN.

Film No.	Camera position	Gas velocity v m/s	Tray liquid head h mm.of water	Pulsation frequency f Hz.	Pulsation amplitude A N/m^2	Film speed frames/s.
TRAY B(g)						
1	B	5.1	12.0	27.8	21	341
2	S	5.1	12.0	27.8	19	
3	A	5.1	12.0	27.8	25	
4	B	7.2	4.25	27.0	18	365
5	B	9.2	3.25	31.8	38	437
6	S	9.2	3.25	31.8	36	
7	B	9.2	4.5	32.8	40	342
TRAY B'(g) (6.6; 33.0 ;138)						
8	S	4.0	37.25	-	-	
9	S	5.0	12.0	-	-	
TRAY L(g)						
10	B	5.0	5.5	15.4	49	2145
11	S	5.0	5.5	15.6	47	1034
12	B	5.0	12.25	18.0	60	2250
13	B	5.0	27.0	-	-	960
14	B	7.0	5.25	19.4	45	2082
15	B	9.0	5.75	23.8	20	2062
16	S	9.0	5.75	23.6	16	959
17	B	11.0	5.5	-	-	1100
TRAY O(g)						
18	B	5.1	6.75	14.2	45	1015
19	B	9.0	12.25	19.4	26	1149
20	B	9.0	32.0	14.0	13	1100
21	S	9.0	32.0	14.0	12	948
TRAY H(g)						
22	B(u.v.)	5.0	5.25	14.0	20	810
23	B(u.v.)	5.0	12.5	16.6	5	1000
24	B(u.v.)	7.0	5.0	19.6	25	850
25	S(u.v.)	7.0	5.0	19.6	24	965
26	B(u.v.)	9.0	5.25	25.0	28	960
27	B(u.v.)	6.0	10.25	18.0	7	987
28*	B(u.v.)	6.0	10.5	22.6	30	870

*Weir height = 0 mm.

The three signals recorded were from the pressure transducer (1) in the chamber beneath the test-tray (trace 1); the photocell positioned next to the camera lens (trace 2); and a 4 mm. high conductivity probe in hole 5 of the glass insert (trace 3). Figure 6.4 shows the experimental arrangement used.

The u.v. recorder was switched on just before the film was run and switched off just after the film had finished. A u.v. recorder paper speed of 407 mm./s. (16 ins./s.) was used and an internal timer marked the paper. The marker separation was given as 100 ms; however, a check using a standard 50 Hz. input signal showed the separation to be 104 ms.

The electronic flash was operated by hand several times, at random intervals, whilst the film was running. It had a flash duration of 0·5 ms. Each flash blacked out all or part of a single film frame. (Some flashes occurred whilst the camera shutters were closed and therefore did not affect the film).

The u.v. recorder galvanometers and terminal connections are specified in Figure 6.4. They were such that representative signal traces were obtained. This is shown in Figure 6.5, which compares signals recorded simultaneously on the u.v. recorder and the oscilloscope. There is seen to be no evidence of any time lag between the pressure signal trace and the photocell trace, on the u.v. recorder.

The time interval between flashes on the u.v. paper were calculated using the u.v. internal timer, and the time interval of successive blacked frames on the film were calculated from the film time markers. As the flashes were at random time intervals, it was then possible to match up the flashes on the paper with those on the film. This allowed the gas-liquid interaction on the tray, as recorded on the film, to be matched in time exactly with the corresponding pressure pulsations beneath the tray and conductivity probe signal,

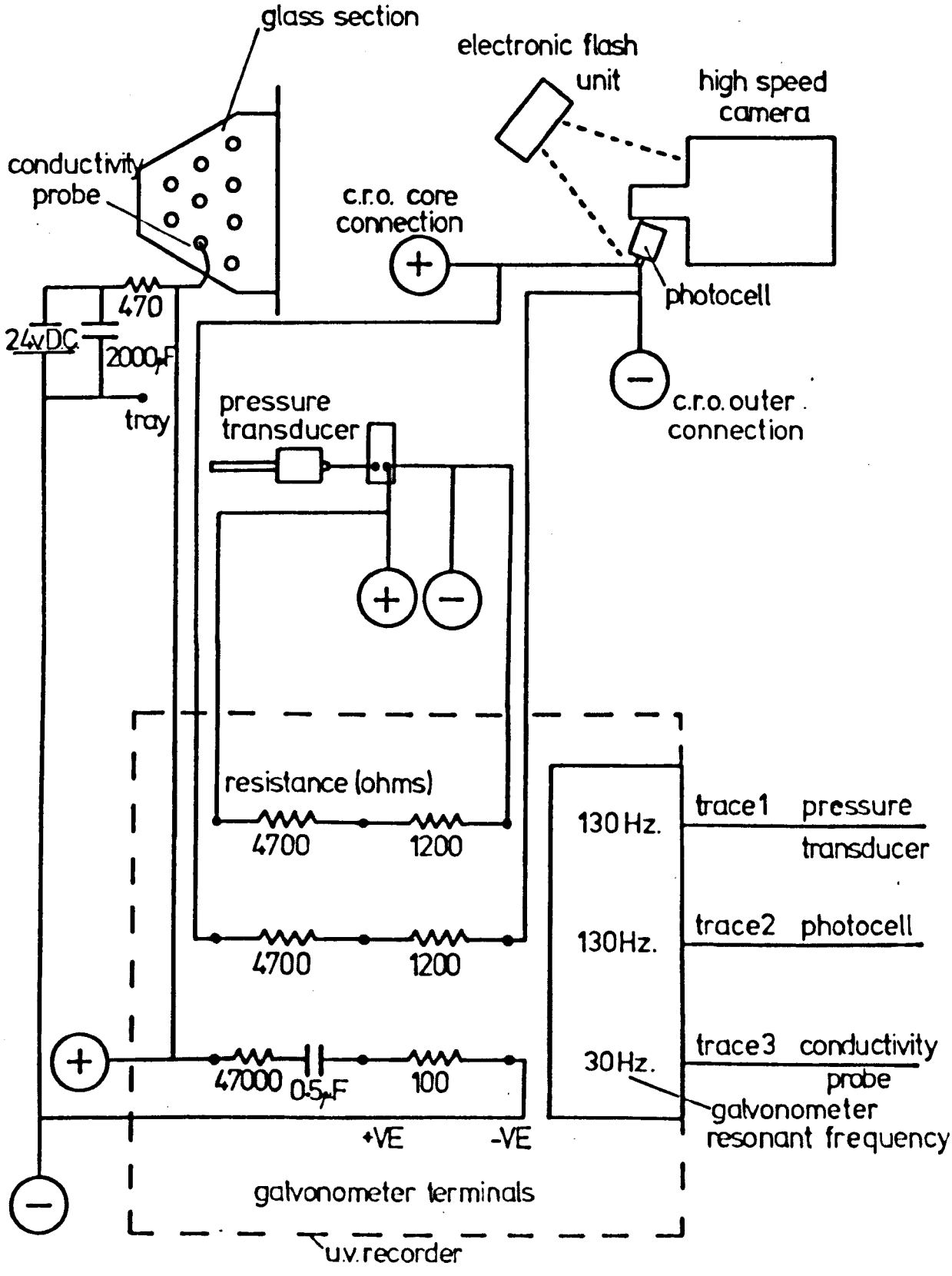

Fig.6.4. USE OF CAMERA IN CONJUNCTION WITH ULTRA-VIOLET RECORDER

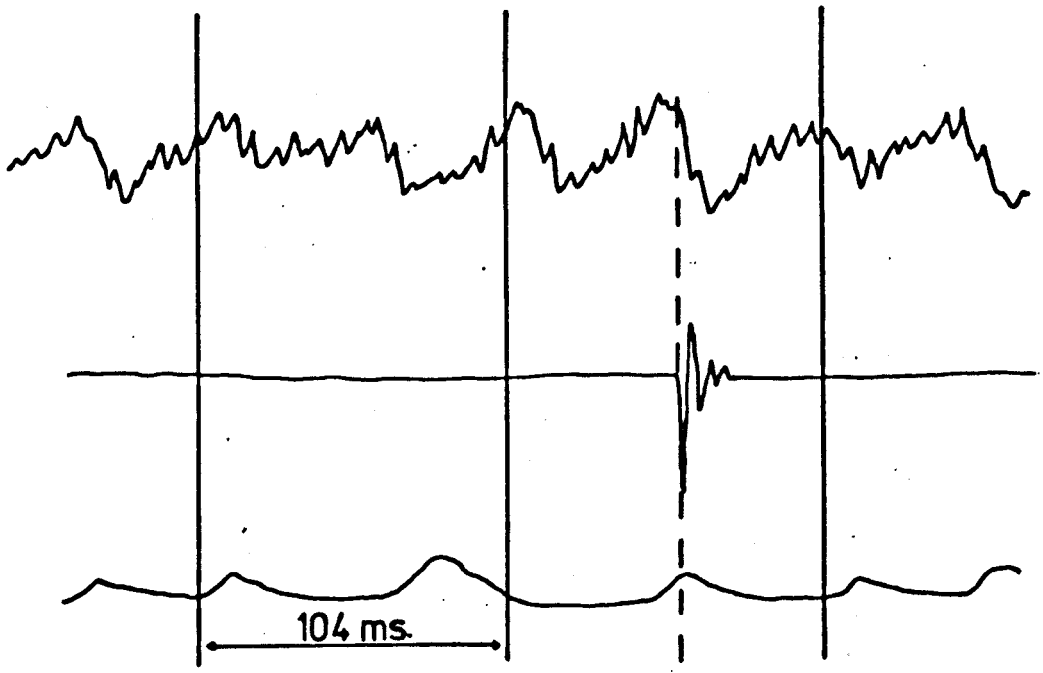

U-V RECORDER

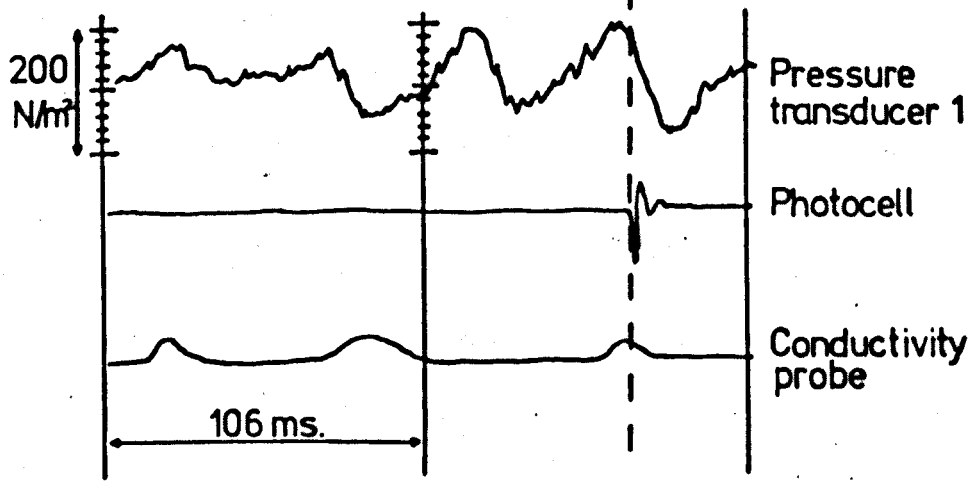

C.R.O.

TRAY H(g)
v = 7·0 m/s
h = 5·0 mm of water

f = 19·6 Hz
A = 25 N/m²

Fig. 6.5. COMPARISON OF U.-V. RECORDER AND C.R.O. TRACES

as recorded on the u.v. recorder. The film timing light gave a u.v. timing marker separation of 104 ms. which is in agreement with the experimental calibration.

6.2.2 Film Analysis.

The main objective of the film analysis was to obtain information about the following factors:

i) The nature of the individual hole events;

ii) The extent of hole event synchronisation on the tray;

iii) The relationship between hole events and the regular gas pulsations;

iv) The effect of system variables on the above three factors.

Details of the film analysers used are given in section 4.10.3. Analysis was performed on a length of film negative (usually 400 frames) which had been marked off using two pieces of vinyl tape.

The films taken from beneath the test-tray showed the nature of the gas-liquid interaction at all the holes in the glass insert. Examples of the view seen in the film are given in Figure 6.6.

Although the nature of the hole events varied with changes in the gas velocity, the tray liquid head and the tray geometry, the start of a hole event could usually be detected as radial spread of the water being 'pushed' by the air away from the hole. The point at which this event growth could first be detected (at the edge of the hole) was termed the 'hole event initiation point'.

The photo-optical analyser was used to identify each frame in which a hole event initiation point occurred. Taking the frame of the first vinyl tape marker as zero, the frame numbers of event initiations were recorded for each of the holes shown in all of the films taken from beneath the test-tray. The holes were numbered as shown in Figure I.3.

The hole event duration was calculated from the number of frames between each event initiation point, and the degree of hole event synchronisation was

Frame from film 24 - tray H(g)

Fig.6.6 SAMPLE FILMS TAKEN FROM BELOW TEST-TRAY

Frame from film 7 - tray B(g)

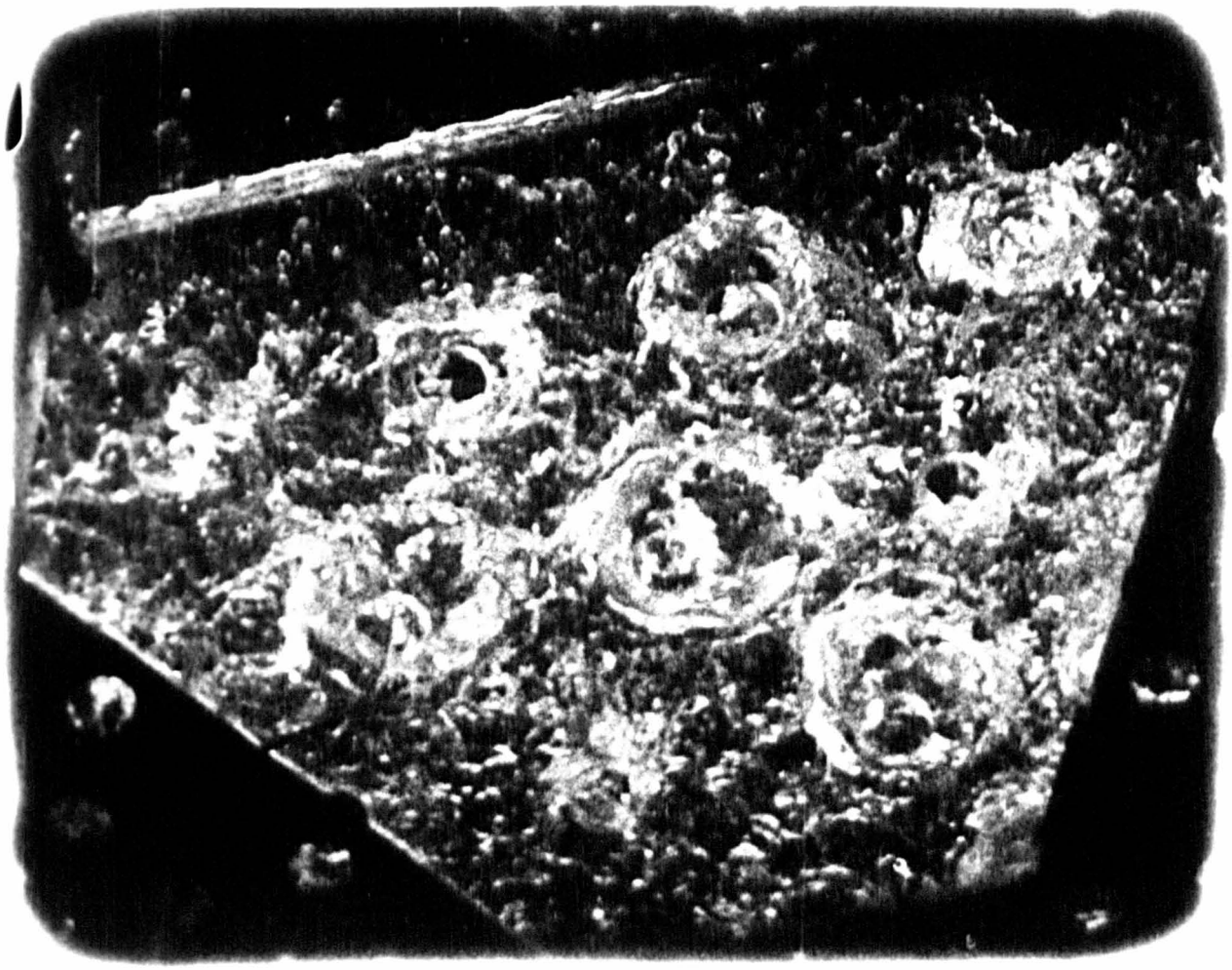

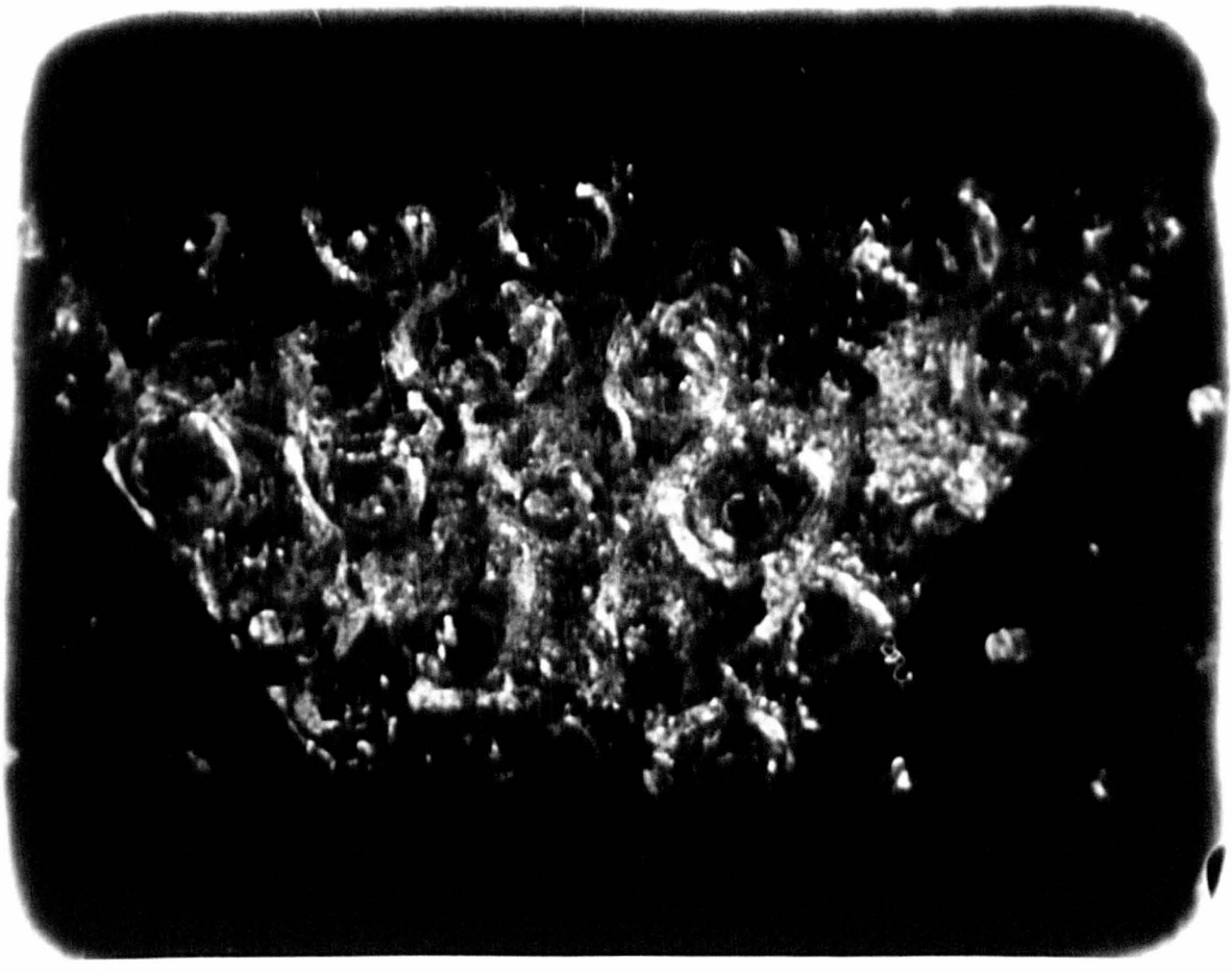

estimated from the correspondence between event initiation points for the different holes in the glass insert.

Individual hole events were studied more closely using the Vangard film analyser. The extent of the liquid radial spread was measured at short time intervals during event growth. The measurements were made using the x-y cross hairs to record the edge of the liquid spread at the points above, below, to the right and to the left of the hole. The cross hairs were calibrated using the hole diameter and the hole pitch, as shown on the film, as reference distances. On some films only the maximum liquid radial spread was measured.

Analysis of many hole events on each film enabled the estimation of the variation and average of the hole event dimensions at particular operating conditions.

6.3 RESULTS OF THE FILM ANALYSIS.

Due to the close interrelationship of the four main objectives of the film analysis, given in section 6.2.2, these objectives will not be considered individually. Instead, the results will be presented in the following order, as determined by the type of camera view used and the kind of analysis performed.

The analyses of the films taken from beneath the test-tray will be considered first. Identification of the event initiation points on these films allowed the determination of the event duration and the extent of the event synchronisation. Information about the relationship between the hole events and the pressure pulsations was obtained from analysis of the films which were synchronised with the u.v. recorder. These films also provided information about the monitoring of hole events by an electrical conductivity probe. More detailed information about the nature of the hole events and their dependence on system variables was obtained from measurements of the liquid radial spread of the hole events as seen from beneath the test-tray.

The analyses of the films taken from a position level with the test-tray are then presented. These provided some useful information about the nature of the hole events, and how this depended upon the tray liquid head and the superficial hole gas velocity. Several different types of hole event are identified and preliminary physical descriptions of these events are given.

6.3.1 The duration and synchronisation of hole events.

The hole event initiation points, as identified in the analyses of the films taken from beneath the test-tray, are presented in Figures 6.7, 6.8,6.9 and 6.10. The initiation points are given for each hole in the glass tray insert for a period of operation of between 200 ms. and 600 ms. The accuracy with which the initiation points could be determined was generally less than $\pm$ 2 ms. Some of the holes in the insert were partially obscured on the film and could not be analysed accurately and therefore are not included in the results.

For the films taken during regular pulsation production, the initiation points are seen to occur usually in fairly well defined lines, termed initiation lines, whose separation is approximately equal to the period of the pressure pulsation. This is direct evidence that the hole events are synchronised with the pressure pulsations. The mean and standard deviation of the initiation lines are indicated, the standard deviation being a measure of the extent of the hole event synchronisation.

For most of the films, the majority of the hole events had a duration similar to the interval between the initiation lines. Such events are termed single events. The percentage of the hole events identified in each analysis which were found to be single events is given in Figures 6.7 to 6.10. Also given are the mean and standard deviation, (in parentheses), of the single event duration, the standard deviation being a measure of the variation of the hole event duration.

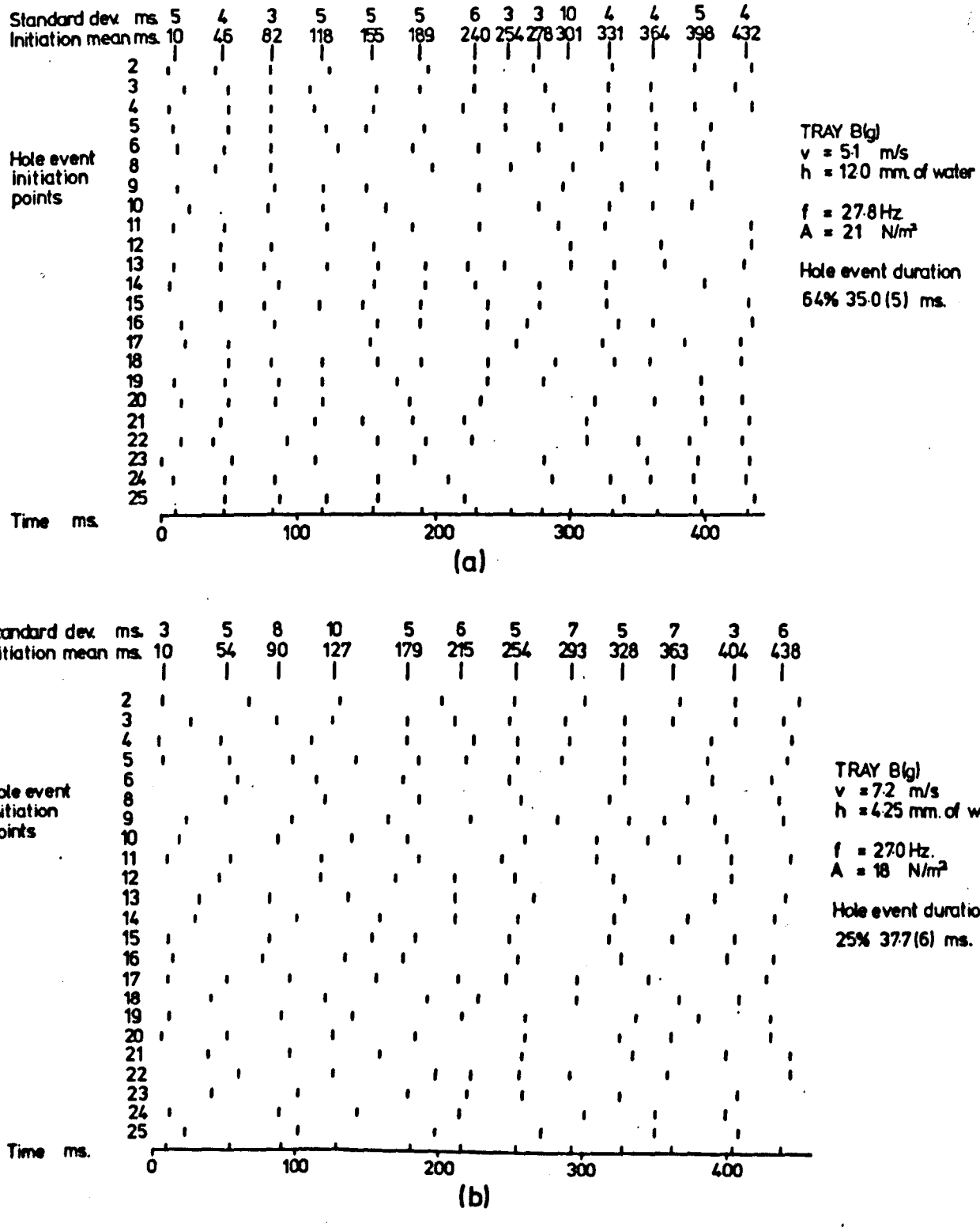

Fig. 6.7 HOLE EVENT INITIATION POINTS, TEST-TRAY B(g)

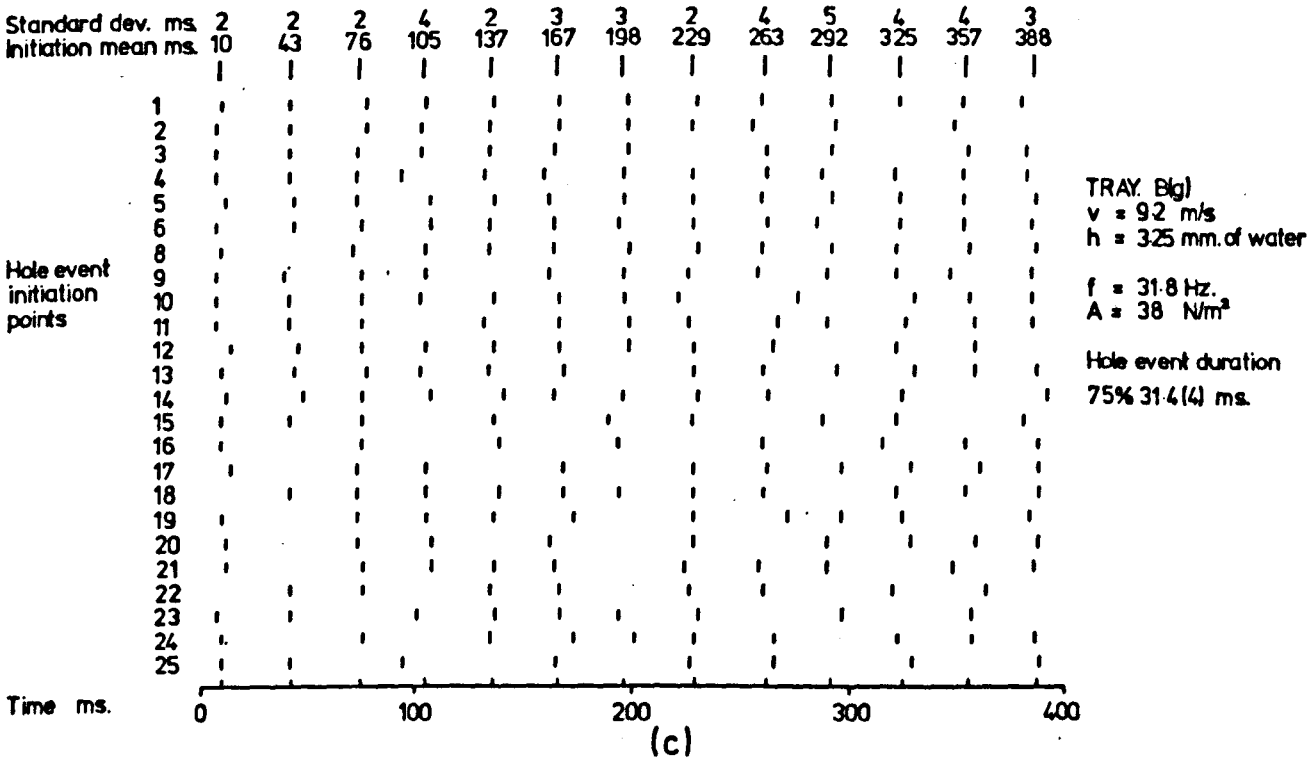

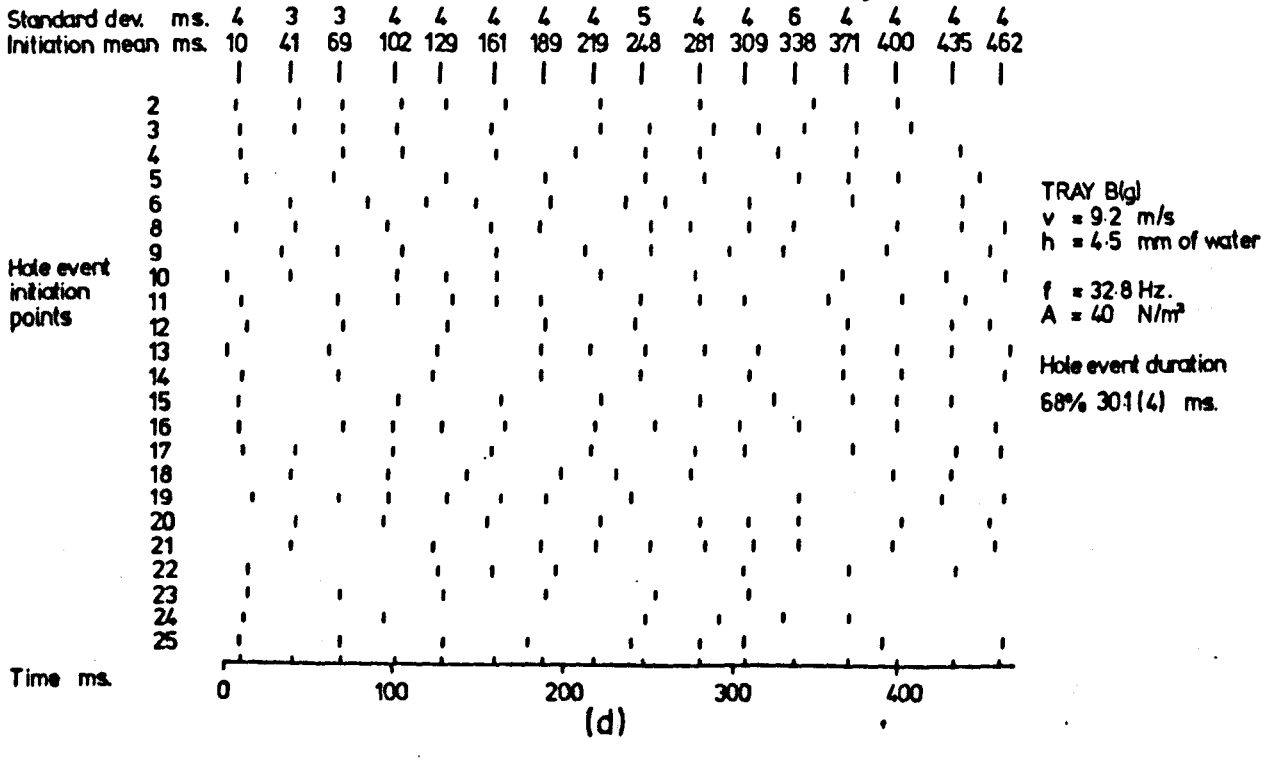

Fig. 6.7. HOLE EVENT INITIATION POINTS, TEST-TRAY B(g)

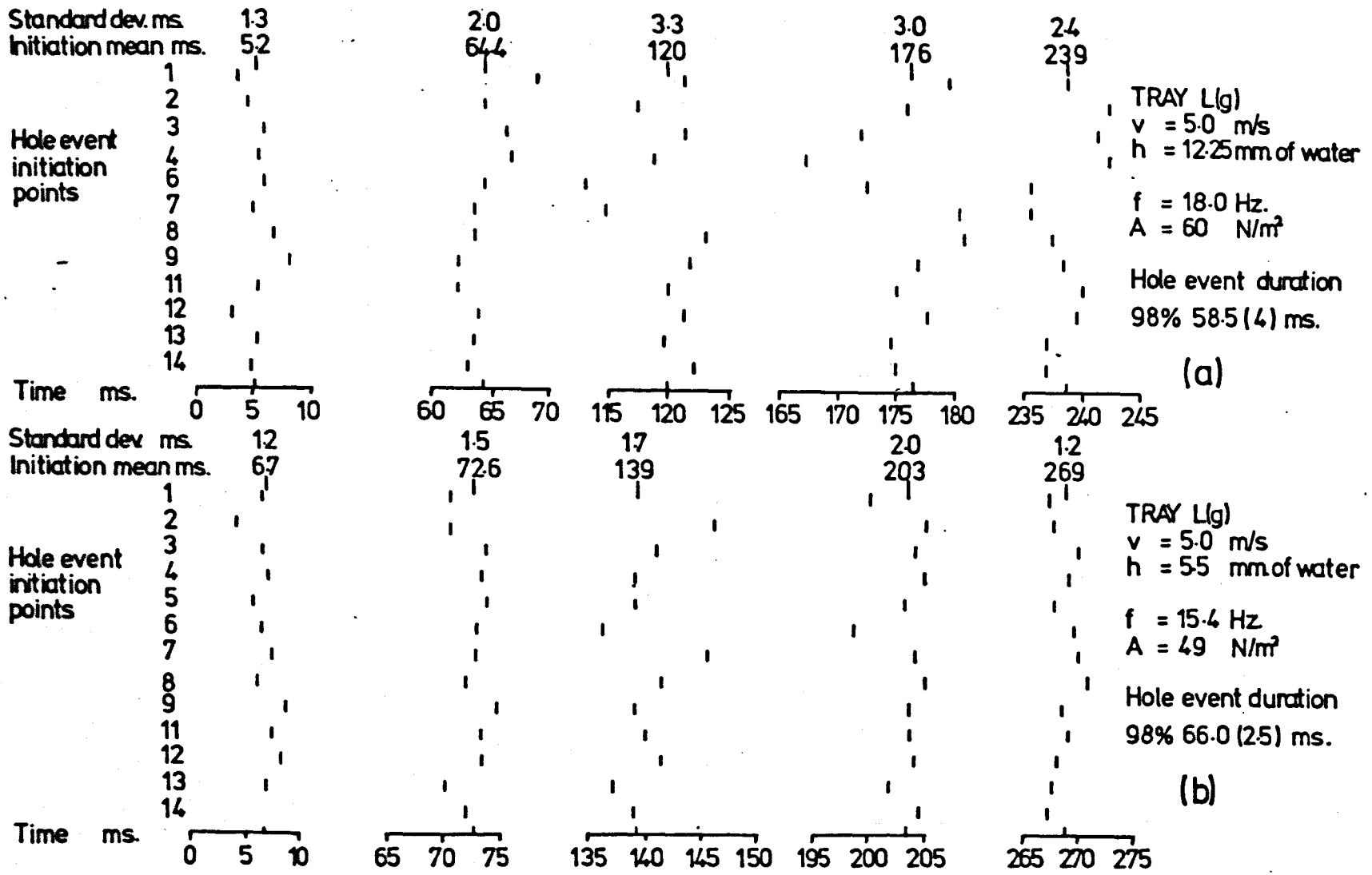

Fig. 6.8. HOLE EVENT INITIATION POINTS, TEST-TRAY L(g)

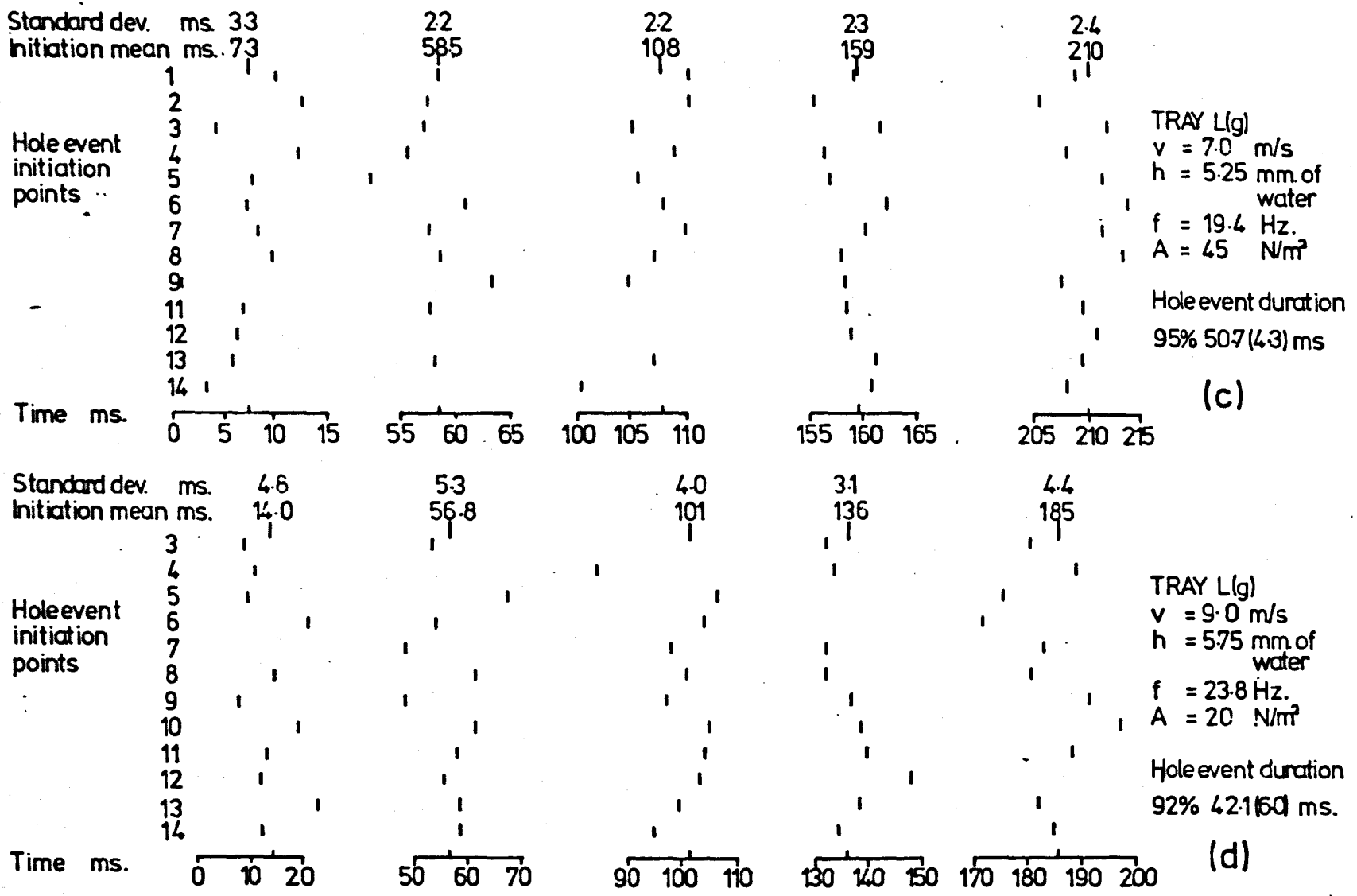

Fig. 6.8. HOLE EVENT INITIATION POINTS, TEST-TRAY L(g)

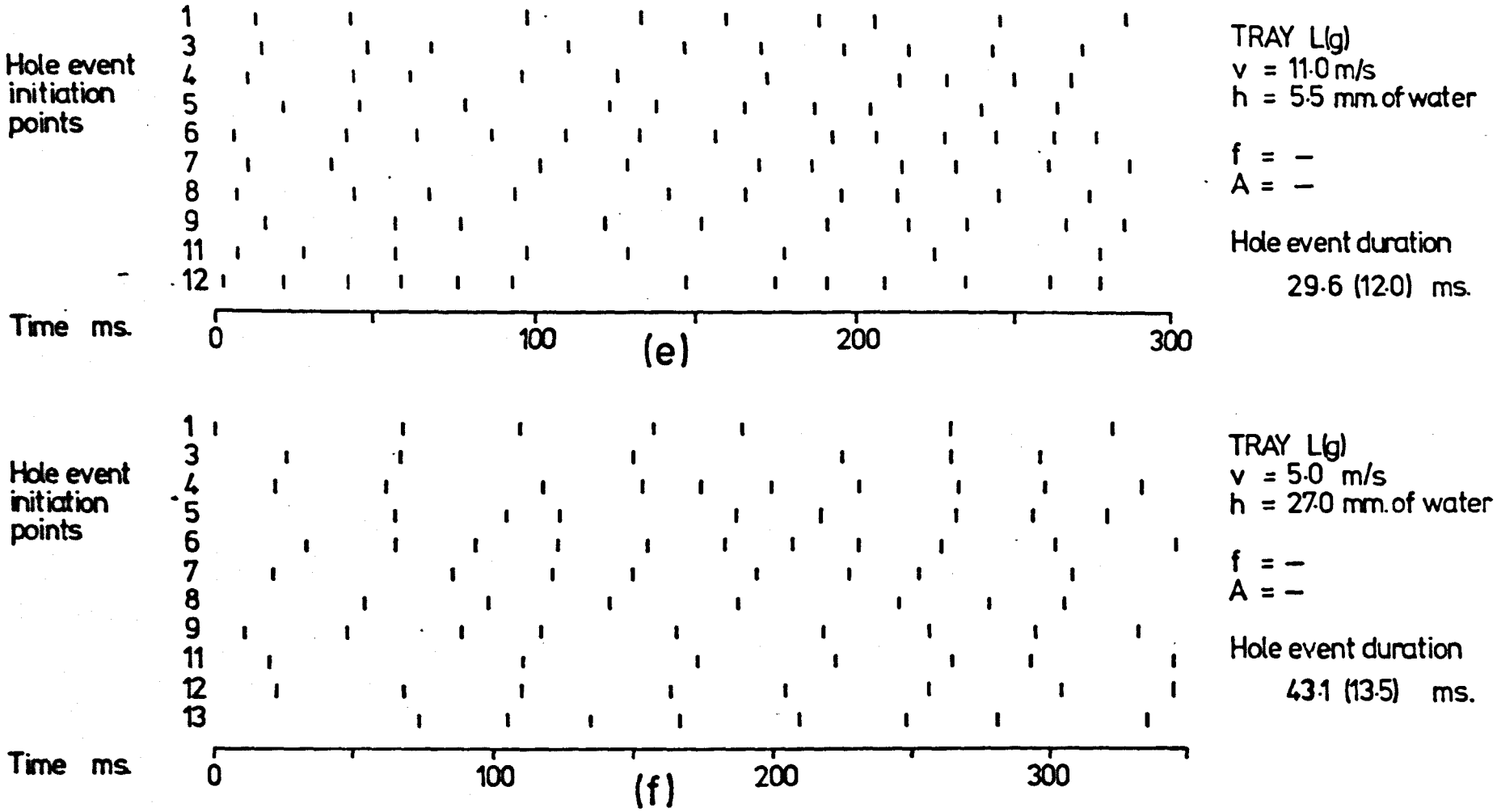

Fig. 6.8. HOLE EVENT INITIATION POINTS, TEST-TRAY L(g)

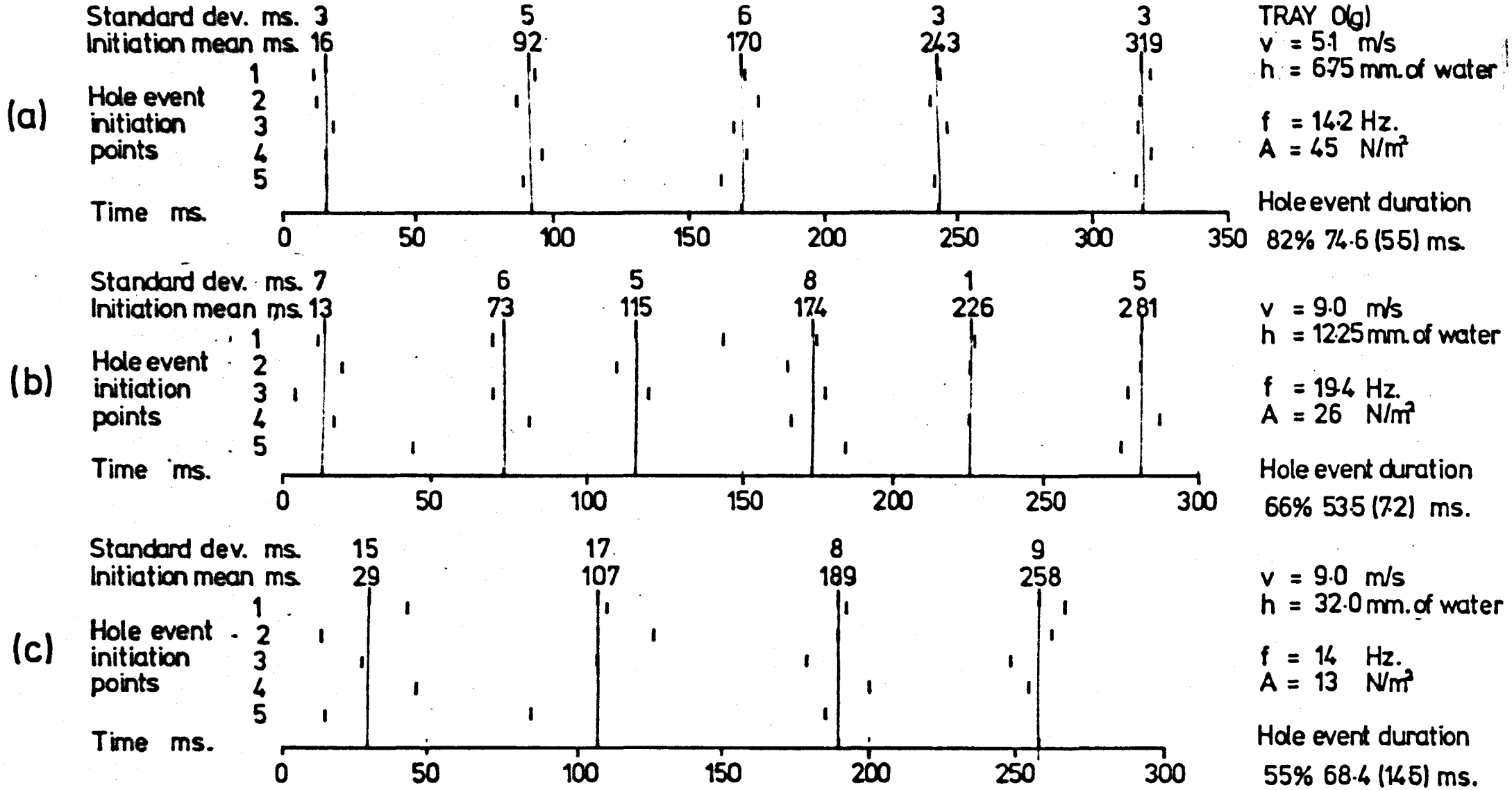

Fig. 6.9. HOLE EVENT INITIATION POINTS, TEST-TRAY 0(g)

Some hole events were identified which had a duration of approximately double that of a single event. These are termed double events. Some of the observed double events could result from a failure, in the film analysis, to identify all of the initiation points. However, this number is likely to be small as Figure 6.8 indicates that, under certain conditions, the analysis technique can identify well over 90% of the initiation points. The occurrence of double events is in agreement with the results obtained using the electrical conductivity probes, which, under certain conditions, indicated the occurrence of a substantial number of double events.

Details of the hole event durations are listed in Table 6.3, which also gives the frequency and amplitude of the pressure pulsation fundamental at each operating condition. There is seen to be very good agreement between the period of the pressure pulsation and the mean event duration, with most of the differences being consistent with the experimental accuracy.

As would be expected, in general the higher amplitude pulsations are seen to correspond to a high percentage of single events with small variation in their duration. However, there are some anomalies within this behaviour, particularly in the operation of test-tray B(g) which exhibits a lower percentage of single events than the other trays.

Figure 6.7 gives the initiation points for test-tray B(g) at four different operating conditions. Plot (b) shows that, of all the events, about 25% were single events and 30% were double events with the remainder being mostly of intermediate duration. This relatively large number of double events is consistent with the results given in Figure 5.7 which show that for gas velocities below about 7.0 m/s and tray liquid heads below about 6.0 mm. of water, the pulsation frequency falls to a value of approximately half that found for higher gas velocities or liquid heads. This drop in frequency can be taken to indicate a transition from a predominance of single events to one

TABLE 6.3 DETAILS OF HOLE EVENT DURATIONS.

Film Number	Pulsation frequency f. Hz.	Pulsation amplitude A N/m^2	Pulsation duration 1000/f ms.	Event duration mean ms.	Event duration standard deviation ms.	Percentage single events %
Tray B(g)						
1	27.8	21	36.0	35.0	5.0	64
4	27.0	18	37.0	37.7	6.0	25
5	31.8	38	31.5	31.4	4.0	75
7	32.8	40	30.5	30.1	4.0	68
Tray L(g)						
10	15.4	49	64.9	66.0	2.5	98
12	18.0	60	55.6	58.5	4.0	98
13	-	-	-	43.1	13.5	-
14	19.4	45	51.5	50.7	4.3	95
15	23.8	20	42.0	42.1	6.0	92
17	-	-	-	29.6	12.0	-
Tray O(g)						
18	14.2	45	70.4	74.6	5.5	82
19	19.4	26	51.5	53.5	7.2	66
20	14.0	13	71.4	68.4	14.5	55
Tray H(g)						
22	14.0	20	71.4	71.2	5.2	85
23	16.6	5	60.2	63.4	6.0	10
24	19.6	25	51.0	53.0	6.3	92
26	25.0	28	40.0	39.5	4.0	94

of double events. This area of transition can also be identified on plot (a) of Figure 5.4 as a trough in the pulsation amplitude data.

It is of note that in plot (b) of Figure 6.7, of those events which occurred at the row of holes next to the column wall (1 to 7), 50% were single events and only 10% double events. This difference from the overall average values may result from either a local increase in tray liquid head due to liquid draining down the column wall or a local increase in the gas velocity due to wall edge effects.

Plots (c) and (d) in Figure 6.7 show that at the higher gas velocity of 9.2 m/s there is a predominance of single events. Again there is evidence of more single events next to the column wall. However, the small increase in liquid head between plots (c) and (d) is seen to decrease the overall percentage of single events. This indicates that it is a local increase in gas velocity that accounts for the anomaly at the edge of the tray and not a local increase in tray liquid head.

Plot (a) of Figure 6.7 shows a much higher percentage of single events, with smaller variation in duration, than plot (b), and yet the corresponding pulsation amplitude is only slightly higher, suggesting that the amplitude has been affected by a change in the nature of the hole event and also, perhaps, by the change in the gas volumetric flowrate.

Between 240 ms. and 300 ms. on plot (a) there is evidence of intermediate hole event synchronisation, which would be likely to reduce and distort the pressure pulsation signal. All of the plots in Figure 6.7 show the extent of the event synchronisation to vary slightly with time. This is consistent with the small fluctuations in the amplitude of the pressure signals shown in Figures 5.2 and 6.2.

Figure 6.8 gives the hole event initiation points for test-tray L(g) at six different operating conditions. In plots (a) to (d) the time axis

has been made discontinuous in order that the initiation points can be presented more accurately. These four plots were for conditions with regular gas pulsation production and they show a high percentage of single events with very good synchronisation. Plots (e) and (f), which were for conditions at which no gas pulsations could be detected, show very little evidence of event synchronisation, and there is seen to be a relatively large variation in the hole event duration.

The very high percentage of single events in plots (a) to (d) of Figure 6.8, is consistent with the conductivity probe signals shown in Figure 6.3, which indicate only occasional double events. Figure 5.3 gives the pressure frequency spectra corresponding to plots (c) and (d).

The well defined harmonic series present in these spectra was attributed, in section 5.2.3, to the shape of the pressure signal. The film analyses support this assumption because no evidence was found of short duration hole events which could have produced the harmonic frequencies.

Figure 6.10 gives the hole event initiation points for test-tray H(g), at six different operating conditions. Plots (a) to (d) are at very similar conditions to the equivalent plots given in Figure 6.8 for test-tray L(g), allowing comparison of the behaviour for these two trays.

For test-tray L(g), it can be seen that at a tray liquid head of about 5.5 mm. of water, increasing the gas velocity tends to decrease slightly the percentage of single events and to increase the variation in event duration. These changes are consistent with the observed fall in pulsation amplitude. A similar relationship between the hole events and the pulsation amplitude is exhibited by test-tray H(g) in Figure 6.10. However, for this tray, the fall in amplitude occurs as the gas velocity is decreased. It is possible that this anomaly results from the greater volumetric gas flowrate associated with the larger holes in tray L(g).

Neither tray L(g) nor tray H(g) exhibit the tendency shown by tray B(g), to change to a predominance of double events at low gas velocity or liquid head.

For tray L(g), increasing the liquid head from 5.5 mm. of water to 12.25 mm. of water, at a constant gas velocity of 5.0 m/s, is seen to have no effect on the percentage of single events, but does result in an increase in the pulsation amplitude. This is despite an increase in the variation in event duration, indicating that a slight change in the nature of the hole events has occurred. Tray H(g) shows very different behaviour for the same change in conditions, with a large drop in the percentage of single events, and a substantial decrease in both the extent of the event synchronisation and the pulsation amplitude. Again this difference in behaviour between the two trays may be a result of the differing gas volumetric flowrates.

The results obtained for test-tray O(g), shown in Figure 6.9,are in general agreement with the results for tray L(g). However, plot (c) shows the occurrence of regular gas pulsations when there is a relatively large variation in the hole event duration.

It was found in experiment 2, section 5.3, that a sufficient increase in the tray liquid crossflow velocity resulted in an increase in both the frequency and the amplitude of the pressure pulsations. Plot (f) of Figure 6.10 shows details of the analysis of film 28, which was taken with a 0 mm. weir height and an average tray liquid crossflow velocity of 170 mm/s. Film 27, detailed in plot (e), was taken at the same gas velocity and tray liquid head as film 28, but with a 76.2 mm. weir height, giving minimal tray liquid crossflow.

The hole events formed under conditions of liquid crossflow are seen to be much more regular and more synchronised than those formed in the absence of crossflow. It is of note that the few larger pressure pulsations seen in plot (e) correspond to a period of relatively well synchronised hole events.

Some of the films were taken under conditions of liquid weeping at the holes. Analysis of such films showed that weeping was most likely to occur just prior to event initiation. For conditions of relatively heavy weeping,liquid drainage was sometimes observed to occur at either one hole or at a group of several holes, for extended periods up to the duration of one or two single events. During this period hole events would not occur at such holes. For conditions of relatively light weeping, liquid which had 'leaked' through the holes, could be seen to accumulate on the under surface of the tray from where it would fall as large drops.

6.3.2 Correspondence between the Hole Events and the Pressure Pulsation and Conductivity Probe Signals.

In Figure 6.10 the event initiation points for test-tray H(g) are synchronised with the signal from pressure transducer 1, positioned beneath the test-tray, and with the signal from an electrical conductivity probe positioned in hole 5, as recorded on the u.v. recorder. In plot (a) a fault in the photocell prevented the film from being synchronised with the u.v. recorder.

It is clear from plots (b) (c) and (d) of Figure 6.10 that,during the production of regular pressure pulsations, the hole event initiation point occurs, on average, between about 5 ms. and 10 ms. before the peak of the pressure pulse beneath the test-tray. The similarity between both the pressure pulsations and the hole events measured for test-tray H(g) with those measured for other test-trays, makes it reasonable to assume that the event initiation points for these other trays occur at a similar position with respect to the pressure pulsation to that found for tray H(g).

It has been found that the behaviour of the hole events found for trays B(g) and L(g) was consistent with the electrical conductivity probe signals. Figure 6.10 also shows there to be very good agreement between the event

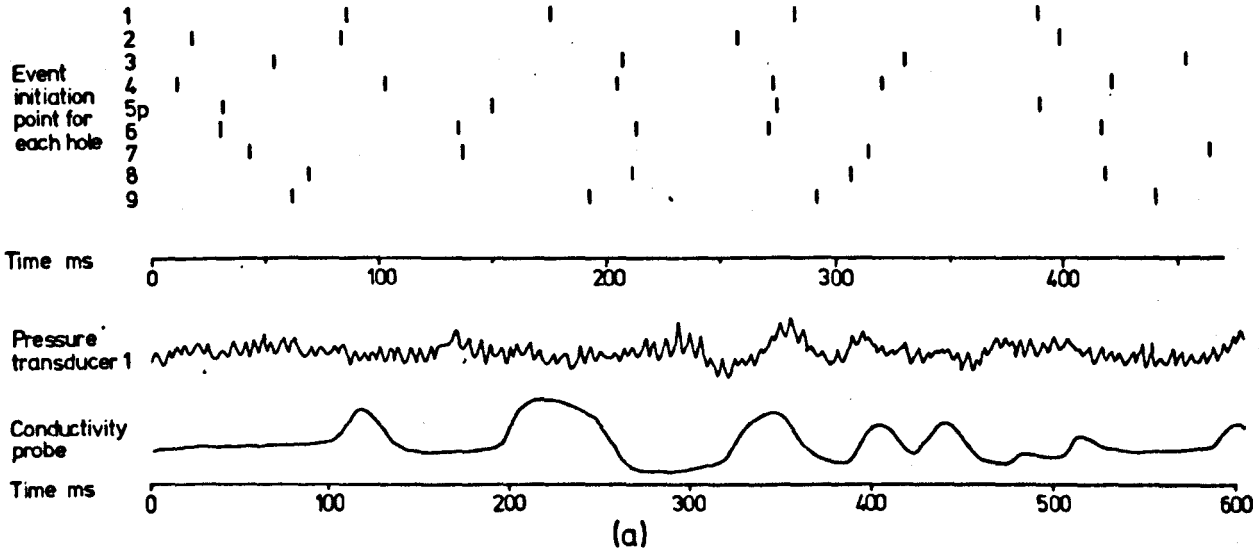

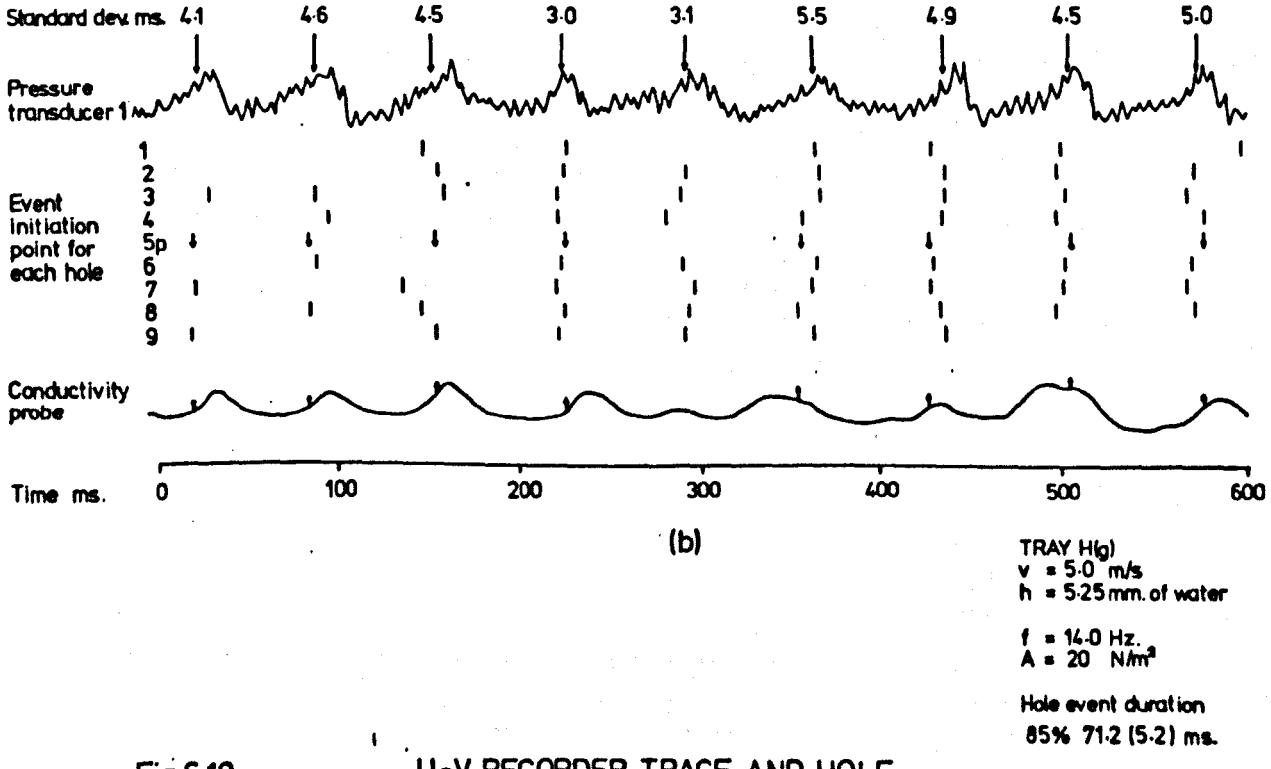

Fig.6.10 U-V RECORDER TRACE AND HOLE EVENT INITIATION POINTS

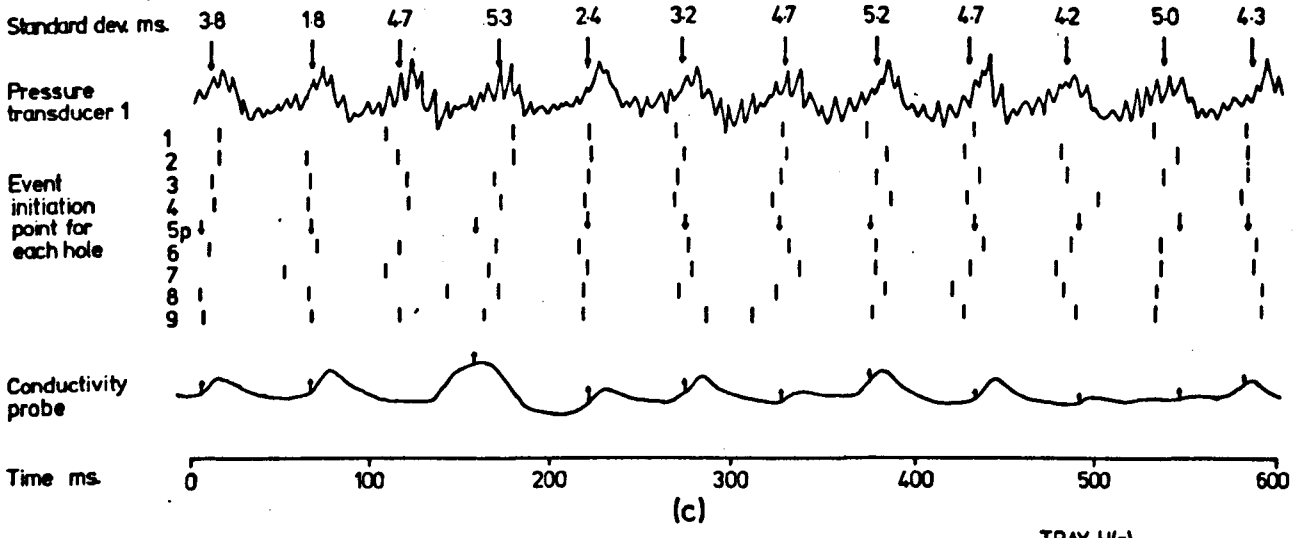

(c)

TRAY H(g)
v = 7·0 m/s
h = 50 mm of water

f = 19·6 Hz
A = 25 N/m²

Hole event duration
92% 53·0(6·3) ms.

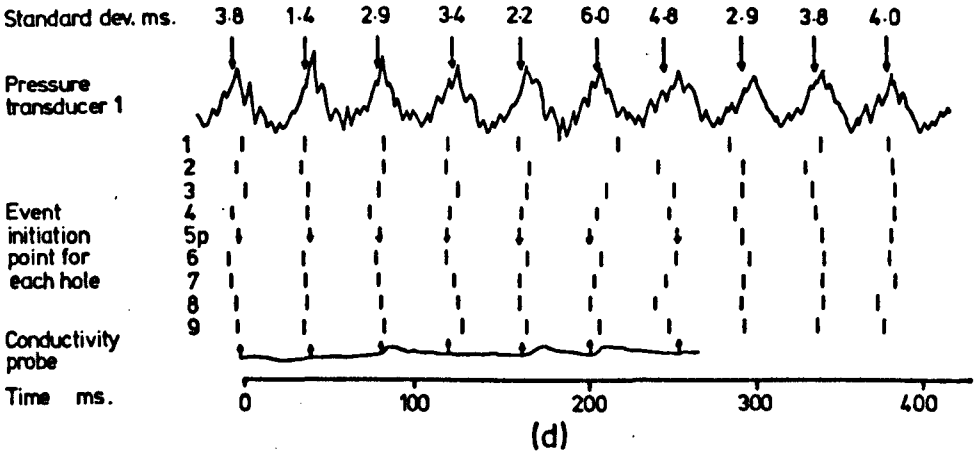

(d)

TRAY H(g)
v = 9·0 m/s
h = 525 mm of water

f = 25·0 Hz.
A = 28 N/m²

Hole event duration
94% 39·5 (4·0) ms.

Fig. 6.10 U-V RECORDER TRACE AND HOLE EVENT INITIATION POINTS

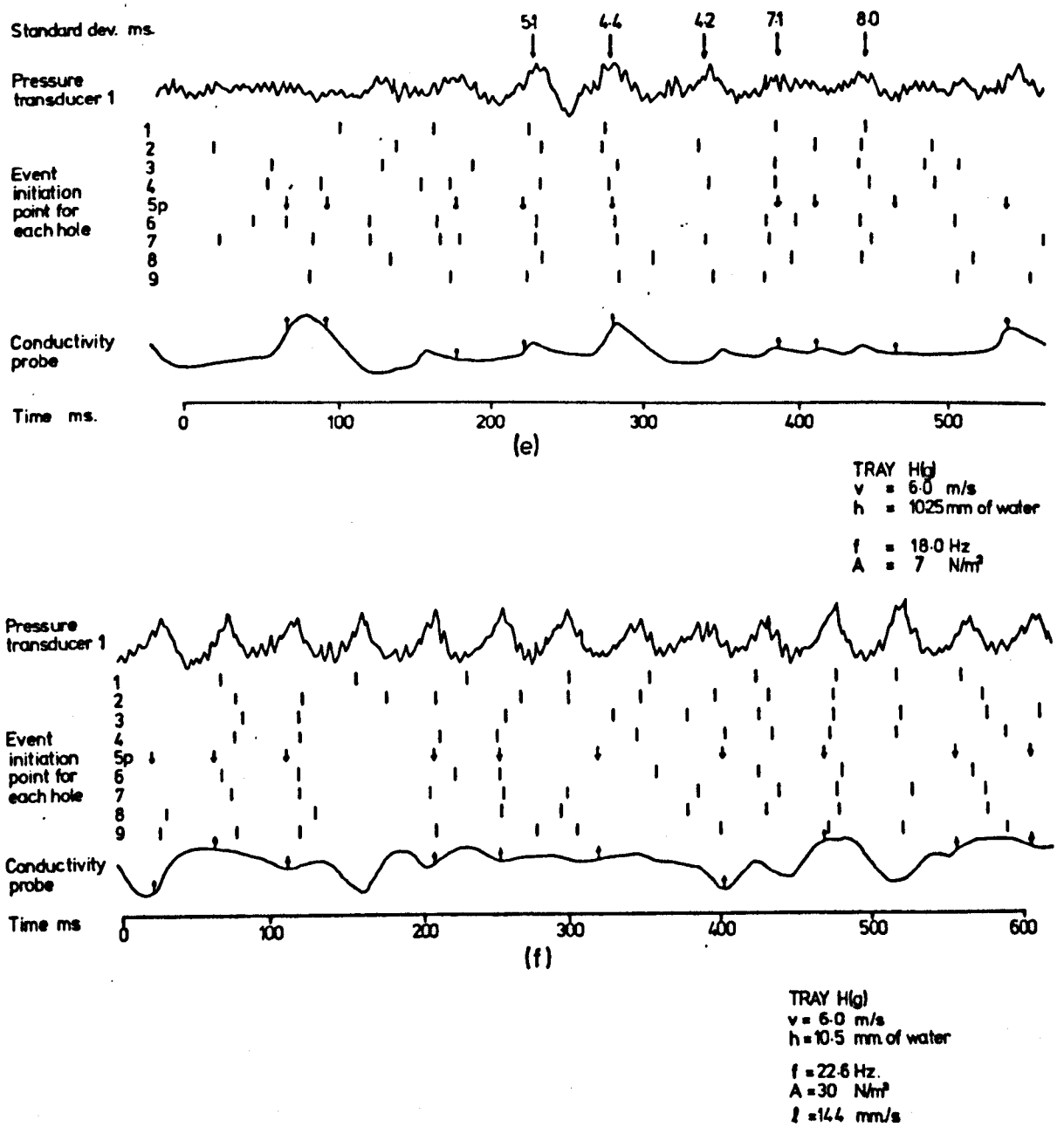

Fig.6.10 U-V RECORDER TRACE AND HOLE EVENT INITIATION POINTS

initiation points determined for hole 5 and the signal from the conductivity probe positioned in that hole. In most cases the initiation point occurs during,or just prior to, the rise in the probe signal. This indicates, as would be expected, that the apparent liquid bridging detected by the probe occurs just after the event initiation point.

On plot (c) of Figure 6.10, at a time between 100 ms. and 200 ms.,a hole event fails to occur at hole 5, and this is consistent with the absence of a pulse in the conductivity probe signal. On plot (d) the probe fails to indicate all of the initiation points, and the pulses shown are smaller than those for lower gas velocities.

Plot (e) shows that the conductivity probe becomes less reliable at higher tray liquid heads, and plot (f) shows the probe to be of little use in predicting hole event behaviour for conditions of high tray liquid crossflow.

6.3.3 Summary.

The main conclusions drawn from the consideration of the hole event initiation points and their relationship with the pressure pulsations and electrical conductivity probe signals, can be summarised as follows:

i) During the production of regular gas pulsations the majority of the hole events are synchronised at the same frequency as the pressure pulsations;

ii) The synchronised hole event initiation points occur, on average, between 5 ms. and 10 ms. before the peak of the pressure pulsation beneath the test-tray;

iii) During the production of regular gas pulsations there is normally a majority of single events whose duration is equivalent to the pulsation frequency;

iv) For operation outside the area of pulsation production there is little synchronisation of the hole events;

v) High amplitude pulsations are favoured by a high degree of hole event synchronisation, a large proportion of single events and a small

variation in the hole event duration. There is an indication that the amplitude of the pulsations also depends upon the gas volumetric flowrate and changes in the nature of the hole event other than those above.

vi) There are sometimes a number of double events having a duration equivalent to about half the pulsation frequency. Under certain conditions double events become predominant leading to a rapid fall in the pulsation frequency.

vii) For operation at relatively low tray liquid heads, in the absence of tray liquid crossflow, electrical conductivity probes provide an accurate indication of hole events, with the probe signal peak occurring several milliseconds after the hole event initiation point. However, there is some indication that the probe fails to monitor all the hole events at low tray liquid head for the higher gas velocities.

For tray liquid heads above about 12 mm. of water or in the presence of high tray liquid crossflow, the probe signal becomes erratic and unreliable.

6.3.4 Dimensions of the Hole Event Liquid Radial Spread.

Hole events have been considered as the periodic radial spread of liquid away from the hole. The nature of this spread, as seen from beneath the test-tray, is now considered in more detail.

The films of test-tray B(g), and those of the other trays taken for operation at the higher tray liquid heads, showed some quite large variation in both the duration and the extent of the radial spread. The growth associated with double events was longer and more extensive than that of the single events produced at the same operating conditions. For operation at the lower liquid head, of about 5 mm. of water, the films of test-trays H(g) and L(g) indicated two types of behaviour of the single events, some of the events having slightly shorter and less extensive liquid spread. This smaller event growth became increasingly evident as the gas velocity was increased, being largely predominant in film 17.

The measurements of the event radial spread permitted the clear distinction of the larger spread associated with double events. However, the relatively small difference in spread between the two types of single events was found to be more difficult to quantify.

Figure 6.11 shows how the diameter, s, of the liquid radial spread, changes during the growth of typical single events. After an initial period of fairly constant growth, the rate of growth decreases until a maximum value of radial spread, s_{max}, is reached. Beyond this point the spread either remains fairly constant or begins to decrease. The point at which each of the plotted lines stops indicates approximately the point at which the radial spready could no longer be detected on the film.

The assumption of circular growth is fairly accurate at low tray liquid heads, but becomes less so at higher heads, where increased distortion occurs.

Several of the hole events in plots (b) and (c) of Figure 6.11 are seen to have longer and more extensive growth than the others, although the difference is small.

Table 6.4 gives average values of the maximum radial spread and the time taken to reach this value, t_{max}. Most of the values are for single events but for some films, those for double events are given also. The values are also expressed in terms of the average maximum spread beyond the edge of the hole, and the average growth rate.

The time taken to reach maximum spread is seen to be usually between 40% and 50% of the hole event duration.

For operation at a given tray liquid head, increasing the gas velocity is seen to decrease the maximum spread. At a given gas velocity, increasing the tray liquid head is seen to have little effect on the maximum spread, although there is some indication of a small decrease.

The average growth rate of the hole events is seen to decrease slightly with increase in either the tray liquid head or the gas velocity.

TABLE 6.4 DETAILS OF HOLE EVENT LIQUID RADIAL SPREAD.

Film Number	Mean event duration ms.	Average maximum spread time $t_{max.}$ ms.	Average maximum spread diameter $s_{max.}$ mm.	$\frac{s_{max.}-d}{2}$ mm.	Average growth rate $\frac{s_{max}-d}{2\ t_{max.}}$ m/s
Tray B(g)					
1	35.0	12.5	13.9	3.6	.29
1	75.0	32.8	20.5	6.9	.21
4	37.7	12.8	13.8	3.6	.28
4	75.5	36.8	19.5	6.4	.18
5	31.4	17.8	13.2	3.3	.19
5	61.5	34.7	17.1	5.2	.15
Tray L(g)					
10	66.0	33.8	30.4	7.3	.21
12	58.5	34.1	28.7	6.4	.19
12	104.2	56.0	37.2	10.7	.19
13	106.1	54.7	33.1	8.6	.16
14	50.7	25.5	26.2	5.2	.20
15	42.1	22.0	24.4	4.3	.19
17	29.6	23.6	23.1	3.6	.15
Tray O(g)					
18	74.6	37.2	40.1	12.1	.33
19	53.5	30.5	29.1	6.6	.22
20	68.4	40.3	28.2	6.2	.15
20	108.0	68.1	45.7	14.9	.22
Tray H(g)					
22	71.2	26.3	24.9	7.7	.29
23	63.4	29.6	24.4	7.4	.25
24	53.0	21.5	20.5	5.5	.26
26	39.5	17.4	18.0	4.2	.24

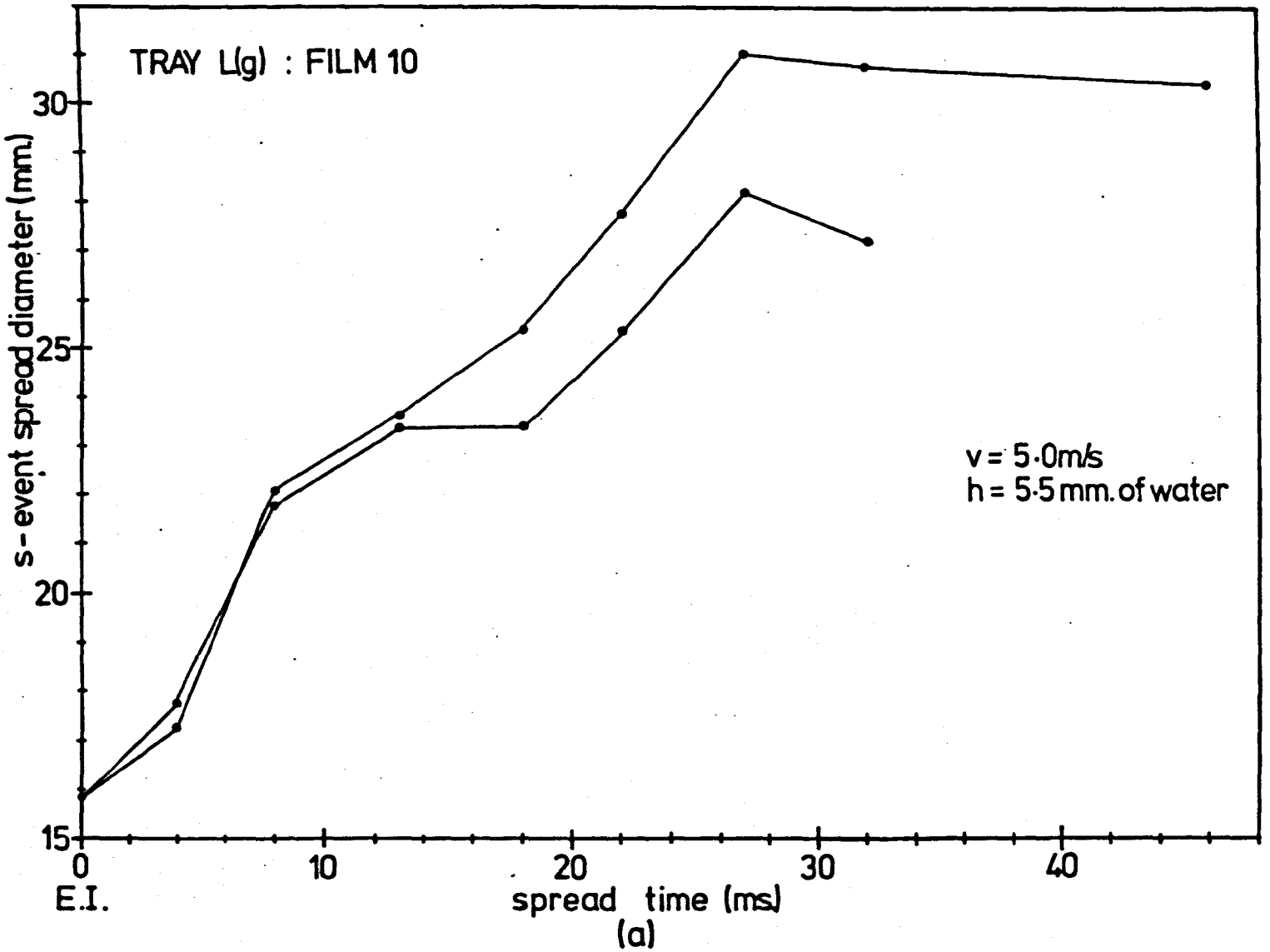

Fig.6.11. SINGLE HOLE EVENT GROWTH

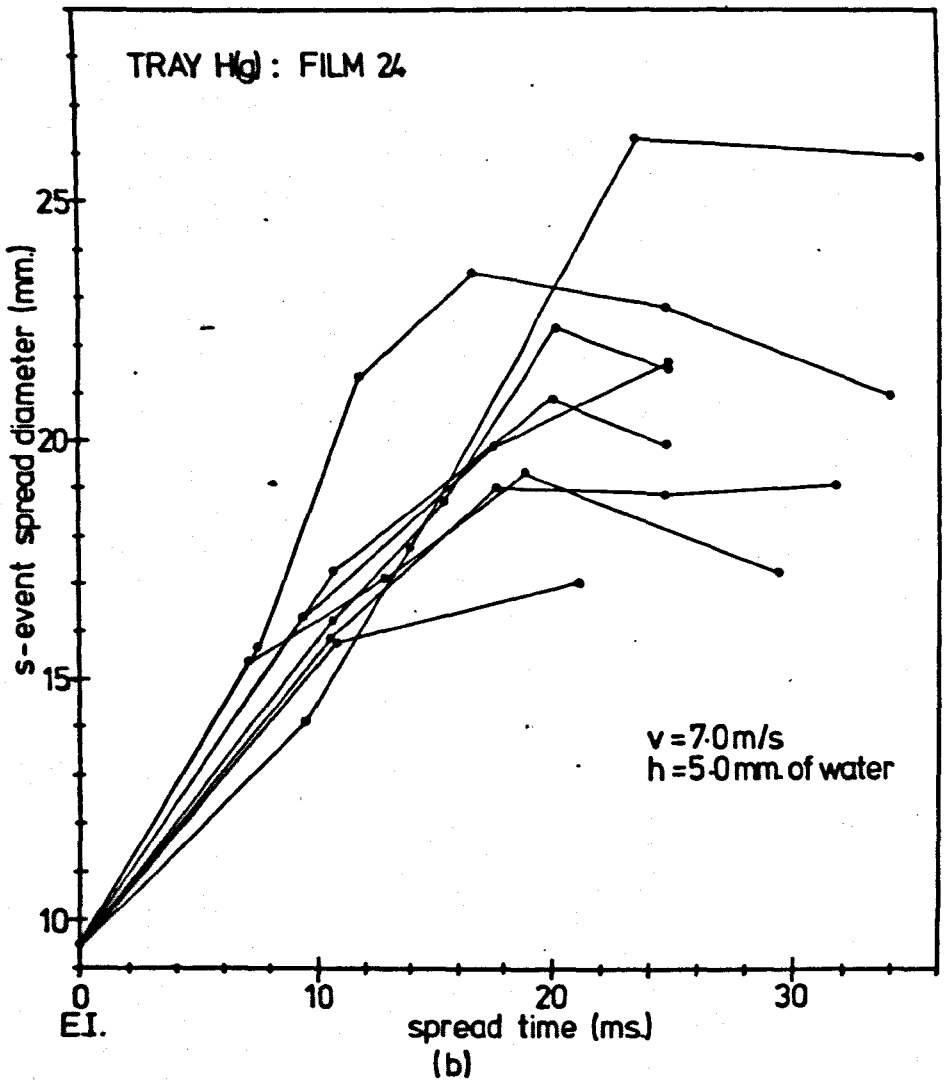

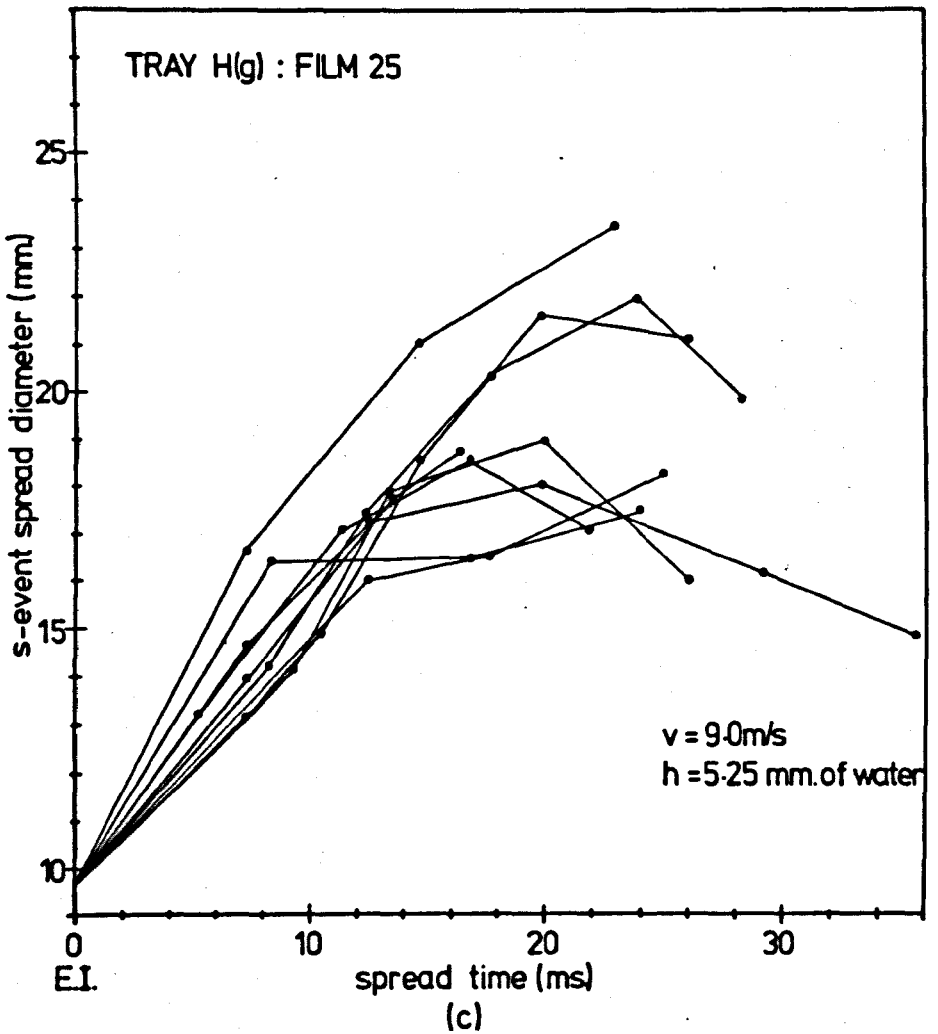

Fig.6.11. SINGLE HOLE EVENT GROWTH

The maximum spread distances measured for equivalent operating conditions on test-trays L(g) and H(g) are seen to be very similar, indicating that the change in hole diameter has little effect on the hole events. This is in agreement with the earlier finding that the frequency of the regular gas pulsations was fairly independent of the hole diameter.

Operation of test-tray B(g) has been found to produce a relatively high number of double events. The maximum radial spread of these events is seen to be comparable to the hole pitch of 19.05 mm., indicating substantial interference between hole events at neighbouring holes. Such interference was clearly evident on the films and can be seen in Figure 6.6(c). This finding verifies the assumption made in section 5.2.3.3 that this was the reason for the marked change in the pulsation frequency found to occur as the hole pitch was reduced. It was postulated that interference became important below an edge to edge hole spacing of about 20 mm. and that some interference occurred on test-tray L(g).

The average maximum spreads measured for tray L(g) indicate that only the double events would be likely to interfere and these were found to be small in number for conditions of pulsation production. However, there was evidence on the films that at the lower gas velocity some interference of the larger single events did occur. Furthermore, the larger growth of the hole events in film 18, as compared with those in film 10, is an indication of restriction of the event growth on tray L(g). Some indication of growth restriction on tray L(g) is also shown by the average growth rates, which are seen to be smaller than those for test-tray H(g). This difference, however, may be due to the greater water volume displaced by radial spreading from a larger diameter hole.

6.3.5 Analysis of the Films Taken Level with the Test-Tray.

Table 6.2 shows that the eight films which were taken level with the test-tray covered a wide range of operating conditions. (Film 3, which was taken from above the test-tray, is also considered in this section.)

All of the films clearly showed that there was a layer of clear liquid next to the tray surface, above which there was either a spray or a froth. The depth of the liquid layer increased with increasing tray liquid head, and for heads above about 10 mm. of water it was possible to detect the gas-liquid interaction at the holes, within this liquid layer. Analysis of the gas-liquid behaviour above the clear liquid, within the froth or spray, was difficult as it was obscured either by a layer of relatively small bubbles which formed next to the column wall in the froth regime, or by the dense spray of liquid droplets formed within the spray regime. Further difficulty arose from the fact that, observed from the side, the holes lay in rows along the line of view; under certain conditions this made it difficult to determine exactly which hole was being observed. Furthermore, analysis was usually restricted to either one or two rows of holes immediately next to the column wall. It was shown in section 6.3.1 that the hole events occurring at the first row of holes next to the wall are not always representative of those occurring at the other holes in the tray, although the differences are small.

The difficulties of the analysis of films taken from level with the test-tray meant that only limited quantitative information could be obtained. However, valuable qualitative observations were possible.

For operation in the spray regime with a relatively low tray liquid head of about 5 mm. of water, the clear liquid layer was too shallow to permit detailed observation of the gas-liquid behaviour at the holes. However, there was some indication of regular liquid spreading in the layer, but it was not possible to see whether hole closure occurred. Within the spray of droplets definite 'bubble' growth, or 'imperfect bubbling', could be detected. Such bubble formation is shown in Figure 6.12. For particular conditions, the extent of the bubble growth varied, with bubble rupture occurring up to a

maximum height of about 40 mm. above the tray. As the bubbles ruptured ligaments and droplets of water were formed, the entrainment of which was enhanced by the surge of gas which usually followed the rupture. This gas surge became increasingly more apparent as the gas velocity was increased. Also, bubble rupture tended to occur sooner and closer to the tray, as the gas velocity was increased.

Quite often, no bubble growth could be detected and continuous pulsed gas flow occurred with regular periodic droplet entrainment, with approximately inverse conical trajectories, being apparent. Such behaviour became more common as the gas velocity was increased and at a velocity of 9 m/s. a relatively small amount of bubble growth was apparent.

These various types of behaviour were all periodic and synchronised at the pressure pulsation frequency, with an apparent degree of synchronisation compatible with that observed from beneath the test-tray at the same operating conditions. Therefore, the imperfect bubble formation with associated gas surge, and the apparent continuous surge or pulse of gas flow, can both be termed single events.

The observed gas-liquid behaviour is largely consistent with regimes observed by other workers (37,38) for a single hole tray, as shown in Figure 2.4. The occurrence of continuous pulsed gas flow at a superficial hole gas velocity below that reported by these other workers may be due either to fluctuations in the gas flow associated with the regular pressure pulsations or to local variations, across the tray, of the gas velocity or the tray liquid head. These factors will be considered more closely in the next two chapters.

It is of note that the liquid entrainment associated with an imperfect bubble event was apparently similar to that of a continuous flow event, indicating that the determination of a transition between these two types of

TRAY L(g) : FILMS 10&11 : v=5·0m/s; h=5·5 mm. of water.

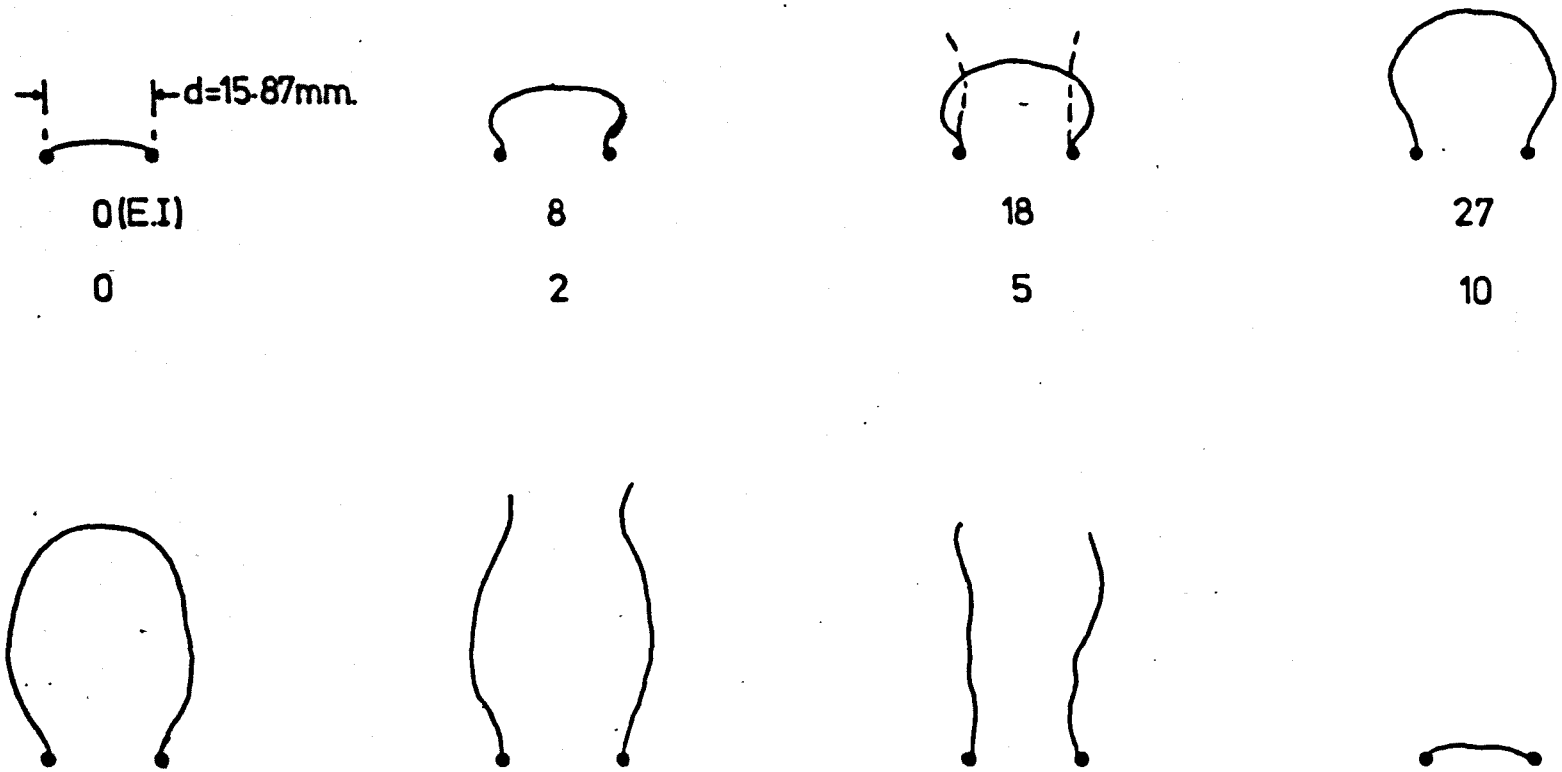

(a)

Fig. 6.12. TYPICAL IMPERFECT BUBBLE EVENT, BASED UPON FILM ANALYSIS MEASUREMENTS

TRAY H(g) : FILMS 24 & 25 : v=7·0 m/s ; h=5·0 mm. of water.

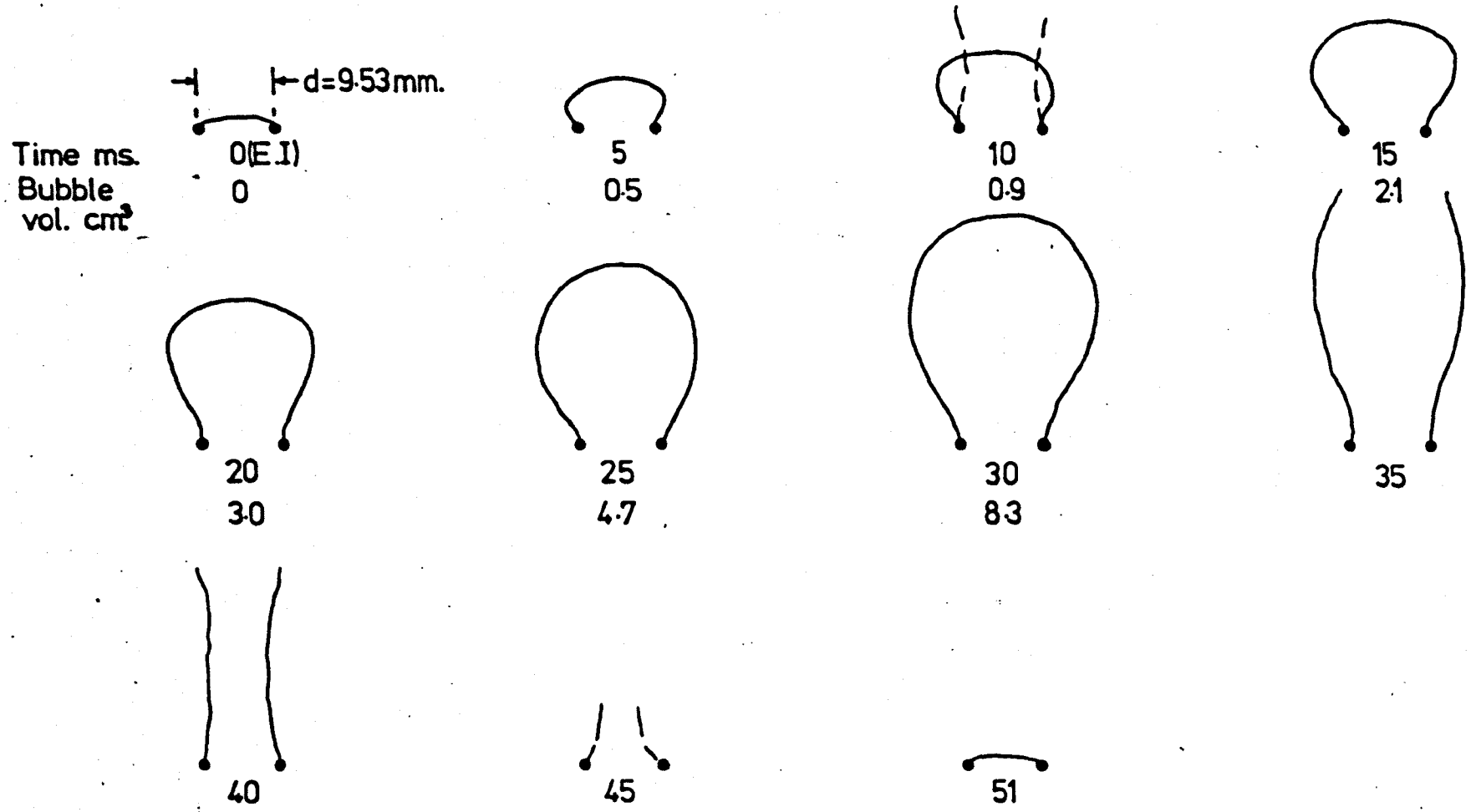

(b)

Fig. 6.12. TYPICAL IMPERFECT BUBBLE EVENT, BASED UPON FILM ANALYSIS MEASUREMENTS

behaviour by detecting changes in the rate of liquid entrainment (39) would be difficult. The observed mechanism of droplet and ligament formation following an imperfect bubble rupture was similar to that reported by Lindsey (29).

Some measurements of imperfect bubble growth were carried out using the photo optical analyser. Tracings of individual bubbles were made at several intervals during their growth. By running the film in reverse a fairly good estimate of the event initiation point could also be obtained. The measurements were largely consistent with the dimensions of the hole event growth as seen from beneath the test-tray. Measurements from films 10 and 11, and films 24 and 25, were each combined to form an average imperfect bubble growth for each of these two operating conditions. These are given in Figure 6.12. Film 25 was synchronised with the u.v. recorder and the event initiation points occurred, on average, between 5 and 10 milliseconds prior to the pressure pulsation peak, the same as was found for the hole events as seen from beneath the test-tray.

The bubble models shown are for the longer observed bubble growth; rupture occurred much earlier in the growth on many occasions.

For the conditions of plot (a) in Figure 6.12,imperfect bubble formation followed by a relatively weak gas surge was the predominant hole event mechanism. However, for the conditions of plot (b), early bubble rupture was common and many continuous gas flow events were observed.

The observation of these two types of single events at low liquid head operation is consistent with the observation made from beneath the test-tray that some single events had a shorter and less extensive liquid radial spread than others. These smaller spreads were most common at the higher gas velocities, and can be associated with the continuous gas flow events, which would be expected to have a smaller liquid spread. The larger spreads can be associated with the larger imperfect bubble events.

Increasing the tray liquid head results in an increase in the clear liquid layer next to the tray, allowing some gas-liquid interaction within this layer to be seen. On film 2, preliminary 'bubble' growth could be seen to occur within the liquid layer, as shown in Figure 6.13(a). Unfortunately, a layer of relatively small bubbles, which formed next to the column wall, obscured much of the remaining bubble growth. However, it was possible to see some imperfect bubble growth above the liquid layer, similar to that observed at the lower liquid heads. As before, bubble rupture occurred up to a maximum height of about 40 mm. and this was usually followed by a relatively weak gas surge. Considerable interference between neighbouring imperfect bubbles was evident. Imperfect bubble growth and rupture could also be seen on film 3, (taken from above the test-tray) as shown in Figure 6.13 (b) in which a bubble rupture is evident. Also, from above, some synchronisation of the bubble ruptures was apparent. Event synchronisation was also evident on film 2, this being most apparent during the initial stages of the bubble growth following a hole closure.

Quite often these hole events (bubble growth and an associated gas surge) were not followed by a complete hole closure. Instead, one or more longer and more pronounced gas surges occurred. These tended to form gas pockets or 'bulges' within the liquid layer, as can be seen to a limited extent in Figure 6.13(a). Such gas surges constituted hole events which were of a similar duration and to some extent synchronised with those events containing imperfect bubble growth. It is possible that these gas surges are equivalent to the 'chain bubbling' reported, by Yeo (41), to occur on a single hole tray.

Some of the hole events observed on film 2 exhibited longer and more extensive bubble growth within the liquid layer, leading to interference between events. This is consistent with the observation, from beneath the

(b) Frame from film 3 - tray B(g)

Fig. 6.13. SAMPLE FILMS TAKEN FROM LEVEL WITH AND FROM ABOVE THE TEST-TRAY

(a) 'still' at conditions of film 2 - tray B(g)

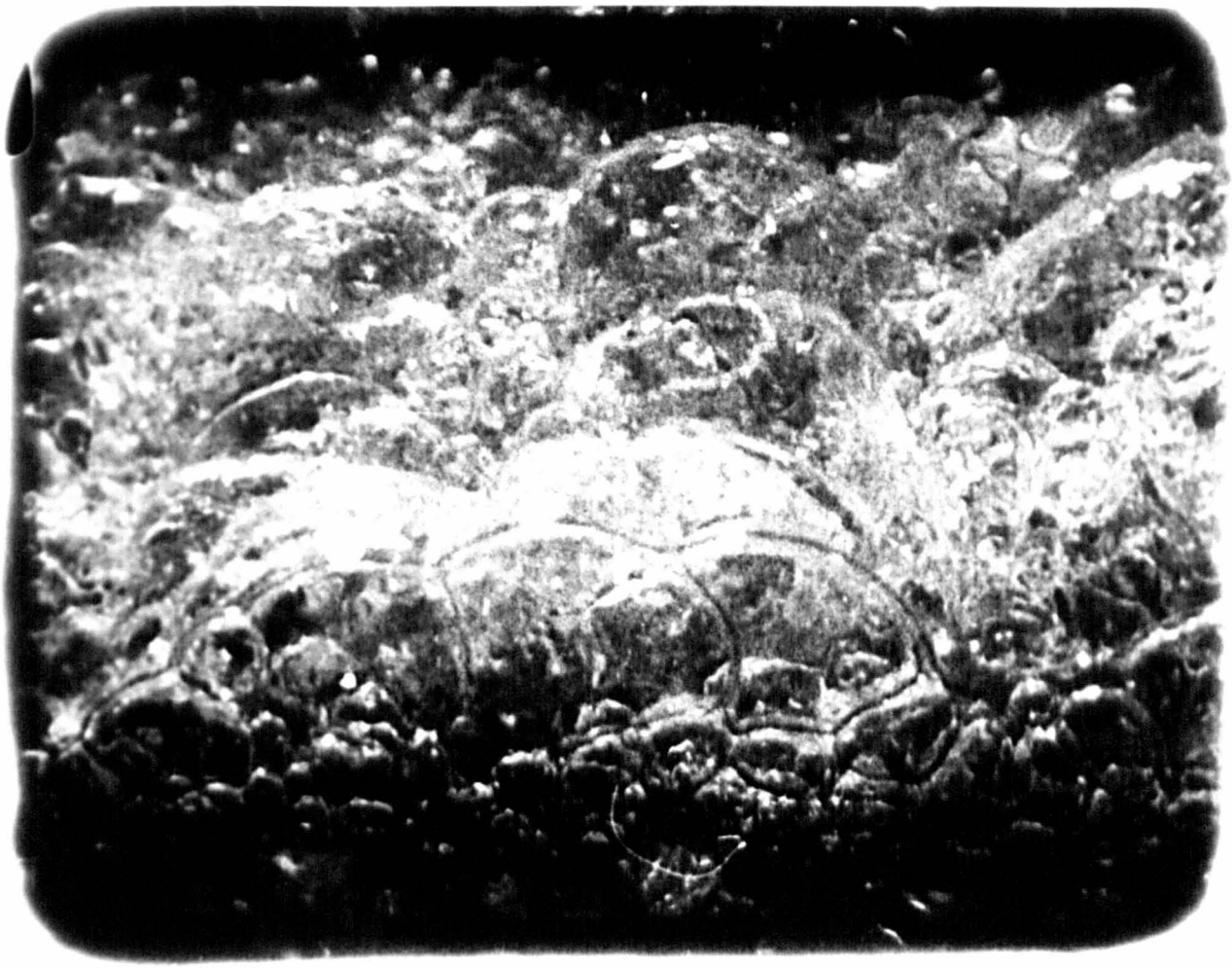

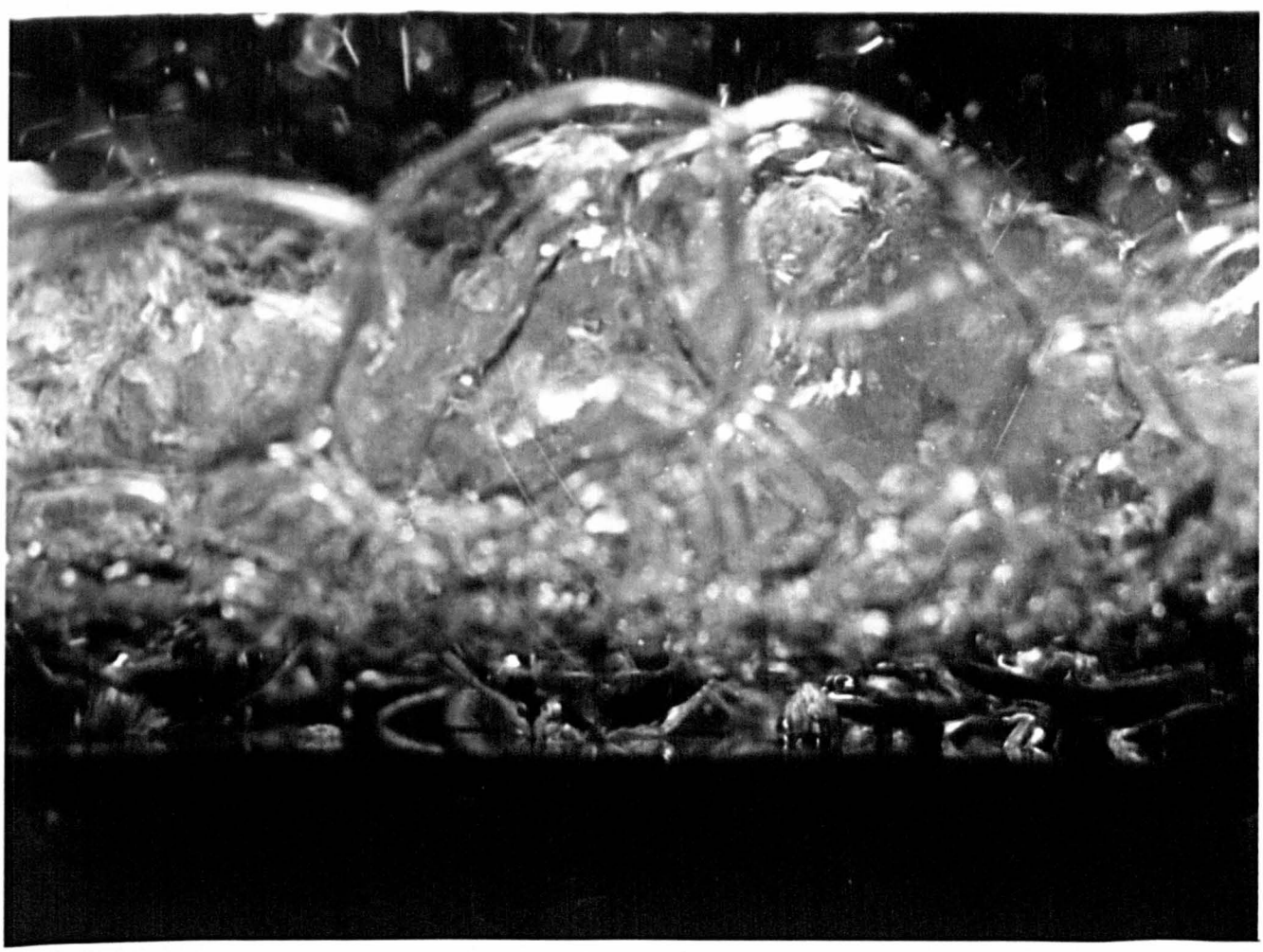

test-tray, of the occurrence of the longer and more extensive liquid spreading associated with the double events.

Films 8 and 9 were taken from level with test-tray B'(g), which contained 138, 6.6 mm. diameter holes on 33.0 mm. pitch, formed by blocking off holes on test-tray B(g). The regular pressure pulsations produced by tray B'(g) were of a much lower amplitude and occurred over a more limited range of operating conditions than those for tray B(g), with no pulsations being detected at gas velocities greater than 7.0 m/s. or at tray liquid heads above 6.0 mm. of water. However, the pulsation frequencies observed were similar to those for tray B(g), and therefore some correspondence between hole events occurring on these trays, at equivalent operating conditions, is to be expected.

Film 9 was taken at the equivalent operating conditions to films 2 and 3. However, no layer of bubbles was formed next to the column wall and a diffuse spray could be seen above the clear liquid layer. The hole events were seen to be very similar to those observed in films 2 and 3. Following a hole closure there was initial bubble growth within the liquid layer which then extended up into the spray, where definite imperfect bubble formation could be seen. As before, the bubbles ruptured up to a maximum height of about 40 mm., this rupture being followed by a weak gas surge. Again, some more continuous gas surging occurred but this was less common than for tray B(g). The event lateral spread was larger than for the smaller pitch tray; however no event interference could be seen. There was little hole event synchronisation and that which could be seen occurred mainly during the initial stages of bubble growth following hole closures.

Film 8 showed the behaviour of tray B'(g) at the higher tray liquid head of 37.25 mm. of water and a slightly lower gas velocity. Bubble growth could be seen in the relatively deep clear liquid layer; however, the froth which existed above this layer obscured all further event growth. Following

a hole closure, well defined bubble growth could be seen, rising through the clear liquid. This was followed by one or more successive surges of gas, which flowed up into the initial bubble, or formed gas 'bulges' as described earlier, with no intervening hole closure. Hole closure was quite common and at times prolonged. Most of the bubble growth was well developed within the liquid layer, and more extensive than for the lower tray liquid heads. No marked event interference occurred and the little synchronisation that was observed occurred, as before, during the initial stages of bubble growth.

Film 21 showed behaviour at a similar tray liquid head but at a much higher gas velocity. Again there was a relatively deep clear liquid layer above which growth was obscured by a layer of bubbles next to the wall. As before, following hole closure, there was bubble growth but the subsequent gas surges were much stronger and more pronounced than at the lower gas velocity. Successive surges with no intervening hole closure,were common; these were of a periodic nature and appeared to induce considerable turbulence within the froth layer. Event synchronisation was apparent, although the hole events were quite varied, with some extended bubble growth giving a larger liquid lateral spread, consistent with the earlier reported double events.

Some measurements of hole event dimensions were made on film 21 using the Vangard film analyser. These were generally consistent with the measurements made on film 20, taken from beneath the test-tray at the same operating conditions. Measurements from the two film analyses were combined to produce a model of typical hole events, as shown in Figure 6.14. The extended bubble growth of a double event is followed by two gas surges and then hole closure. The gas 'bulge' produced by the second gas surge produces a lateral spread interpreted from beneath as a single event. Following the hole closure a more conventional single event occurs, with bubble growth and a single gas surge, followed by hole closure.

TRAY 0(g) : FILMS 20&21 : v=9·0m/s ; h=32·0 mm. of water.

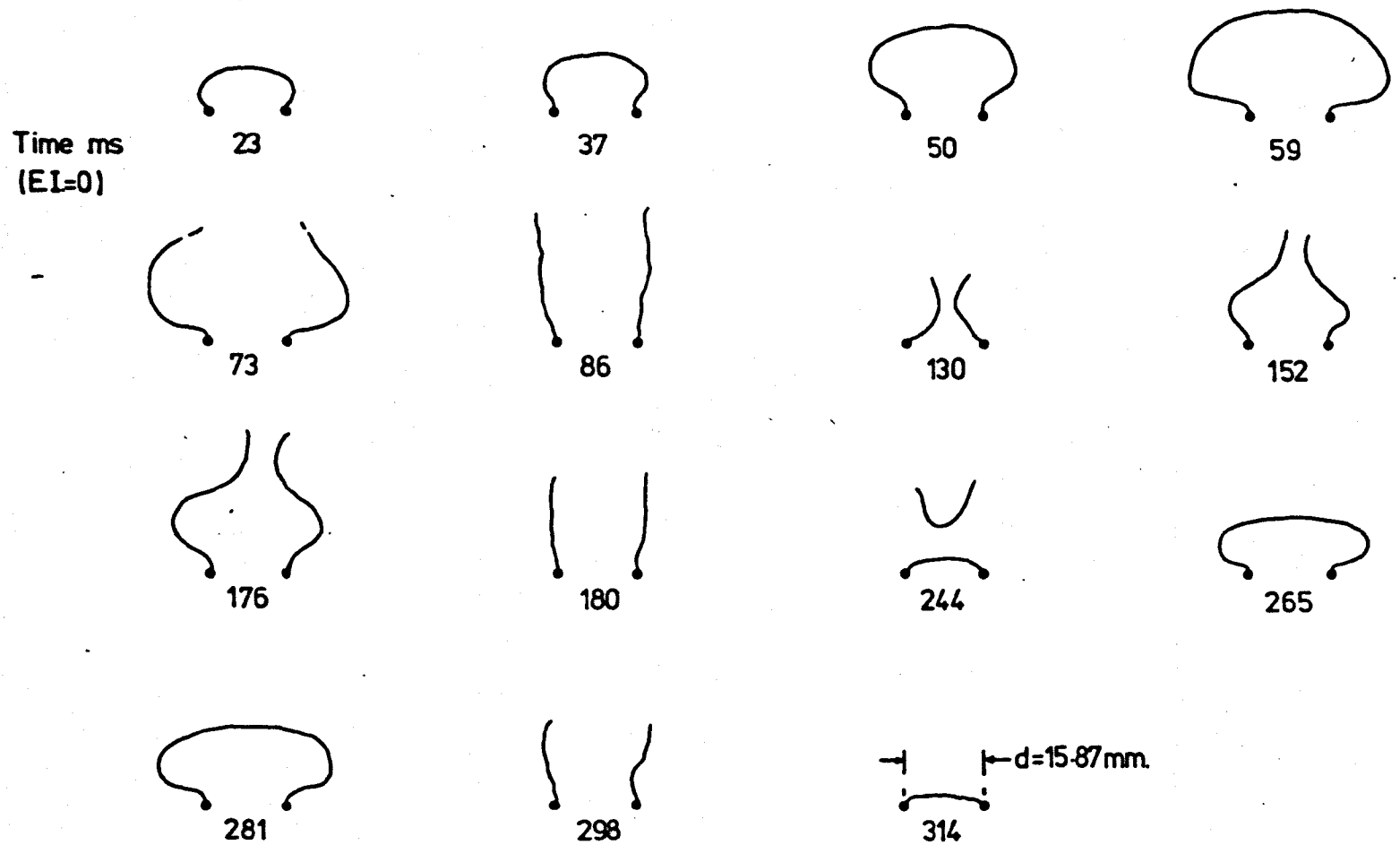

Fig. 6.14. SUCCESSIVE HOLE EVENTS AT HIGH TRAY LIQUID HEAD, BASED UPON FILM ANALYSIS MEASUREMENTS

6.3.5.1 Summary.

The main results of the analysis of films taken from level with the test tray follow.

Under all conditions there was seen to be a layer of clear liquid next to the tray above which was a layer of either spray or froth. The depth of the clear liquid layer increased with increasing tray liquid head.

For the higher tray liquid heads, the gas-liquid interaction at the holes could be observed within the clear liquid layer. Gas-liquid behaviour above this layer was usually obscured, making analysis difficult. However, the following types of events were identified:

i) Pulsed continuous gas flow occurred, with each pulse constituting a single event. This was at low tray liquid head and most gas velocities, being predominant at the higher gas velocities.

ii) There was imperfect bubble growth with rupture up to a height of about 40 mm. followed by a surge of gas, in all constituting a single event. This occurred at moderate or low tray liquid heads and at most gas velocities. At the higher gas velocities bubble rupture tended to occur sooner and nearer the tray with a pronounced gas surge. The surge was much weaker at the low gas velocities. As the tray liquid head was increased, the proportion of submerged bubble growth increased;

iii) There was submerged bubble growth followed by one or more gas surges with some resultant gas 'bulge' formation. The bubble growth and first gas surge, and also the possible subsequent gas surge(s) with possible 'bulge' formation, both constituted individual single events. These occurred at high tray liquid heads, with continuous gas surging becoming more common as the gas velocity was increased;

iv) Extended imperfect or submerged bubble growth occurred, followed by a gas surge. This constituted a double event, and generally occurred at lower gas velocities;

v) Hole events similar to those above but of more variable duration, occurring mainly under conditions of little or no pulsation production.

Normally, more than one of these different types of hole events could be observed at a given operating condition.

The type of hole events observed are in general agreement with the type of behaviour observed, by other workers, to occur on single hole trays.

The nature of the hole events was determined mainly by the gas velocity and the tray liquid head, in the manner indicated in Figure 6.15. Tray geometry had little apparent effect on the hole events, other than at the lower hole separations. where hole event interference occurred

The observed hole event duration and size, and the degree of event synchronisation, was in general agreement with that observed from beneath the test-tray. Some measurements of hole events were possible, and these were combined with the measurements taken from beneath the test-tray to produce a preliminary physical description or model of some types of hole events.

6.4 SUMMARY.

The gas-liquid interaction on the test-tray was investigated using electrical conductivity probes and high speed cine-photography. Both techniques provided valuable information about the nature of the gas-liquid interaction, and its relationship with the regular gas pressure pulsations.

The gas-liquid interaction on the tray was treated in terms of periodic hole events. During the production of regular gas pulsations there was found to be normally a majority of single events whose duration was equivalent to the pulsation frequency. Under most conditions a number of double events also occurred, which had a duration equivalent to about half the pulsation frequency. These double events were predominant under certain conditions.

During the production of regular gas pulsations the majority of hole events were synchronised at the same frequency as the pressure pulsations,

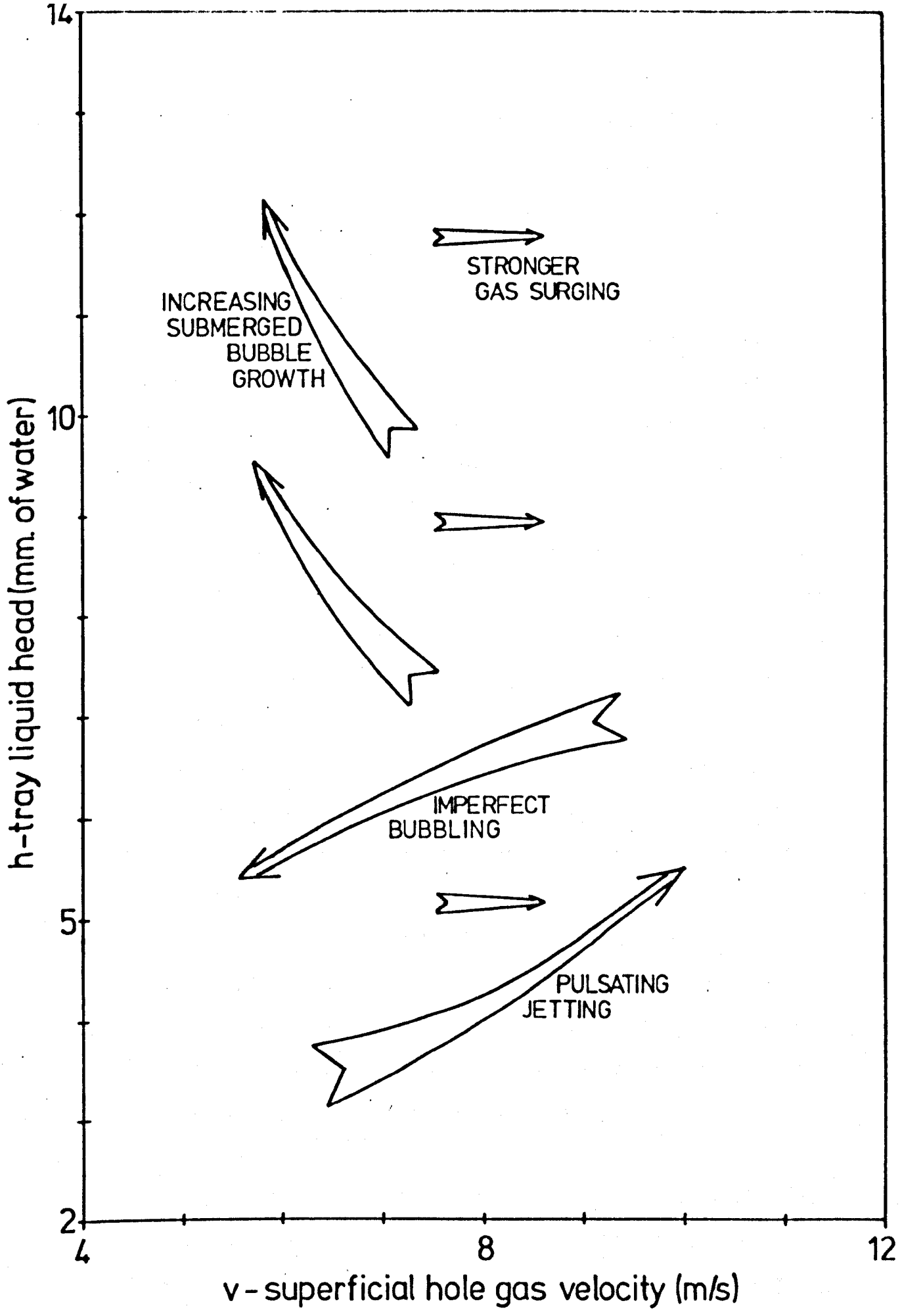

Fig.6.15. EFFECT OF GAS VELOCITY AND TRAY LIQUID HEAD ON THE NATURE OF HOLE EVENTS

with the start of the hole events, or the hole event initiation points, occurring, on average, between 5 ms. and 10 ms. prior to the peak of the pressure pulse beneath the test-tray. For operation outside the area of pulsation production there was little or no synchronisation of the hole events.

High amplitude pulsations were favoured by a high degree of hole event synchronisation, a large proportion of single hole events and a small variation in the hole event duration. There was also some indication that the amplitude depended upon other small variations in the nature of the hole events and upon the gas volumetric flowrate.

For operation at a relatively low tray liquid head, and in the absence of tray liquid crossflow, electrical conductivity probes provided an accurate indication of hole events. For tray liquid heads above 12 mm. of water or in the presence of high tray liquid crossflow, the probe signal became erratic and unreliable.

Average values of the hole event duration, their maximum lateral liquid spread and the time taken to reach this spread, were obtained for events, over a wide range of operating conditions, by detailed measurement of the hole events as seen from beneath the test-tray.

By analysis of films taken from level with the test-tray various types of hole events were identified, whose nature was dependent mainly upon the superficial hole gas velocity and the tray liquid head. Tray geometry was found to have only a secondary effect on the hole events, except at low values of hole separation where some hole event interference and growth restriction occurred.

Preliminary physical descriptions of hole events were developed based upon measurements taken both from level with and from beneath the test-tray. This event description is extended in the next chapter, which relates the observed gas-liquid behaviour on the test-tray to the measured regular gas pressure pulsations.

Chapter 7.

FURTHER ANALYSIS AND DISCUSSION OF THE RESULTS.

Introduction.

This research has been carried out to investigate the occurrence of damaging vibrations in sieve-tray columns. These vibrations have been shown to result from regular pulsations of the column gas flow induced by the gas-liquid interaction on the sieve-tray. In the experimental work described in Chapter 5, regular gas pressure pulsations were produced, over a specific range of operating conditions, with all of the fifteen different tray geometries investigated. The effects of the important system variables on the frequency and amplitude of these pulsations were determined.

The experimental work described in Chapter 6 showed the regular gas pulsations to be associated with synchronisation of the gas-liquid interaction at the individual holes on the sieve-tray. Much qualitative and quantitative information was obtained about how the nature of this gas-liquid interaction and its degree of synchronisation depended upon the major system variables. The predominant mechanism of interaction was found to be one characterised by a period of relatively slow gas flow, restricted sometimes by a growing gas-liquid interface, followed by a period of faster, surging, gas flow.

This chapter relates the measured regular pressure pulsations to the observed mechanism of gas-liquid interaction on the tray in an attempt to produce an understanding of how and why the pulsations are produced. This understanding can then be used in the prediction of the occurrence of the induced damaging column vibrations.

A detailed analysis of column dynamic and static pressures is carried out to determine the fluctuations both in the gas volumetric flowrate through the test-tray and in the test-tray total static pressure drop,

associated with regular pressure pulsations. The findings are related to the gas-liquid interaction on the tray as observed in the film analysis, in particular to the pulsating jet and imperfect bubble events.

The calculated pressures and flows are then combined to produce a measure of the variation in the total test-tray loss coefficient. This variation is then compared with measurements made in the film analysis and related to the gas-liquid momentum transfer on the tray.

7.1 THE CALCULATION OF THE FLUCTUATIONS IN THE GAS VOLUMETRIC FLOWRATE THROUGH THE TEST-TRAY AND IN THE TEST-TRAY TOTAL STATIC PRESSURE DROP.

The calculation of the fluctuations in the gas volumetric flowrate from dynamic pressure measurements requires analysis of the flow system dynamics.

Muller (62) analysed the case of a single hole operating in the pulsating jet regime by using the electrical analogue technique. The low gas volumetric flows associated with single hole operation permitted the installation of a sonic orifice at the entrance to the gas chamber beneath the hole. This gave a constant gas supply flow and thus permitted the fluctuations of the gas flow through the hole to be directly related to the pressure pulsations measured in the chamber. Despite the simplifications to the analysis resulting from having a constant gas supply flow to a well defined chamber beneath a single hole operating in a relatively simple mode, Muller still found it necessary to rely directly upon the measured pulsation frequency for prediction of the system behaviour. Further critical discussion of Muller's work is given in the next Chapter.

The relatively large gas flows required to operate the multi-hole sieve-trays used in this work made it impractical to include a sonic

orifice in the gas supply system. Furthermore, the inclusion of such a high flow resistance would make the system unrepresentative of an industrial column, where pressure drops tend to be minimised and the transmission of flow fluctuations throughout the column occurs. Because of the relatively large pressure fluctuations within the column it is not possible to assume a constant gas supply flow. This makes the simulation of the system by an electrical analogue technique much more difficult.

However, the fluctuations in the column gas volumetric flowrate associated with the regular pressure pulsations can be determined from static and dynamic pressure measurements made at several locations in the column. Furthermore, if the calculated flowrates correspond to highly regular and synchronised gas-liquid behaviour on the test-tray, then the fluctuations in the overall gas flowrate can be directly related to the fluctuation in the gas flowrate through individual holes in the tray.

To calculate the fluctuating flowrate the column gas flow system can be represented simply in terms of gas flow resistances and capacitive volumes, with a variable gas supply flow and with the operating test-tray acting as a variable resistance, as shown in Figure 7.1. Regular column pressure pulsations will therefore result from corresponding fluctuations in the overall resistance of the test-tray to gas flow.

7.1.1 Calculation of the fluctuations in the gas volumetric flowrate into the chamber beneath the test-tray.

From Figure 7.1 it can be seen that the bottom tray and drop catcher may be represented by a constant, non-linear, resistance. Therefore, knowledge of the mean column gas volumetric flowrate, G, and the static and dynamic pressure drops across the bottom tray, enables the calculation of G_o', the fluctuating gas volumetric flowrate through this tray into the chamber beneath the test-tray.

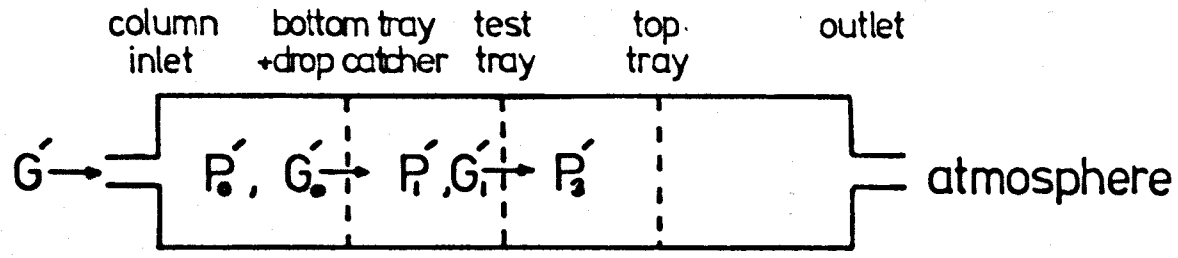

COLUMN GAS FLOW SYSTEM

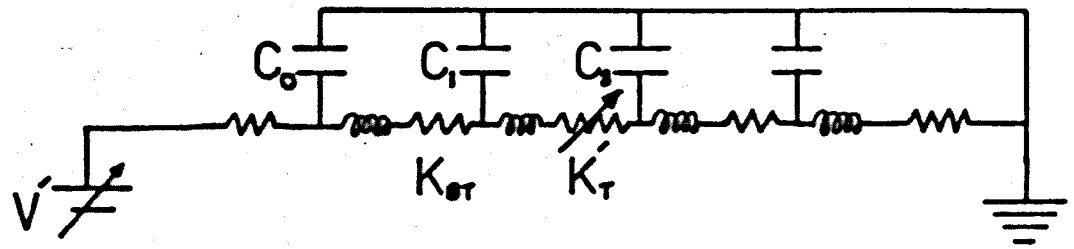

Fig. 71. COLUMN GAS FLOW SYSTEM AND ELECTRICAL ANALOGUE

The static pressure drop (P_o-P_1) was measured using column wall pressure tappings and an inclined manometer gauge. The loss coefficient for the bottom tray and drop catcher, K_{BC}, was calculated assuming a square law flow-resistance dependence. The value of K_{BC} was found to vary slightly with flowrate. These variations may have been due partly to the somewhat varied and irregular perforations in the drop-catcher. Because the drop-catcher was often removed and replaced, or had some holes blocked off, K_{BC} was determined for each experimental run to which the flow analysis was applied.

The dynamic (time varying) pressures in the gas chambers above and below the bottom tray were measured by a pressure transducer in each chamber. Polaroid photographs were taken of the signals from the two transducers as displayed simultaneously on the c.r.o.. The difference between measurements made from tracings of each of the photographed signals, made using a millimetre grid, gave the dynamic pressure drop across the bottom tray, $(P_o-P_1)'$, (i.e. the time varying static pressure drop). The c.r.o. gain settings used permitted the pressure difference to be measured to an accuracy of about 6 N/m^2, at 2.5 ms intervals. The separation of the signal tracings was adjusted so that the calculated dynamic pressure drop had a mean value equal to the measured static pressure drop. Pressure differences measured at equivalent points on several pressure cycles were averaged to produce an average pressure drop fluctuation for one cycle.

To ensure that the two transducer signals had the same calibration, the transducers (and the preamplifiers and the c.r.o. channels) were interchanged and the pressure drop fluctuation recalculated.

Figure 7.2 shows typical pressure traces and the calculated fluctuating pressure drops for operation of test-tray H(g). Figure 7.3 shows measurements taken at the same operating conditions as for Figure 7.2 but with a flow restrictor positioned at the column gas inlet. This flow restrictor was found to have no effect on the production of the pressure pulsations, although it did reduce the transmission of fan noise into the column. This shows the frequency and amplitude of the pressure pulsations measured beneath the test-tray to be unaffected by changes in the flow system upstream of the bottom chamber of the column.

The dynamic gas flowrate through the bottom tray, G_o', was calculated using the equation:

$$G_o' = (2 \cdot (P_o - P_1)' / \rho \cdot K_{BC})^{0.5} \cdot A_C \qquad (7.1)$$

Account was taken of the small variation of K_{BC} with gas flowrate. This method of calculation could not be applied to conditions of heavy weeping on the test-tray when some gas-liquid interaction occurred on the bottom tray and the drop-catcher.

7.1.2 Calculation of the fluctuations in the gas volumetric flowrate through the test-tray.

The dynamic gas flowrate through the test-tray cannot be calculated from a measured dynamic tray pressure drop as the operating test-tray has a varying loss coefficient. To calculate the flowrate it is therefore necessary to relate it to the dynamic gas flowrate entering the chamber beneath the tray, the rate of change of pressure within that chamber and the chamber capacitance.

When the flow entering the chamber beneath the test-tray, G_o, is not the same as that leaving the chamber, G_1, then the chamber pressure will change, the pressure rising when $G_o > G_1$, and falling when

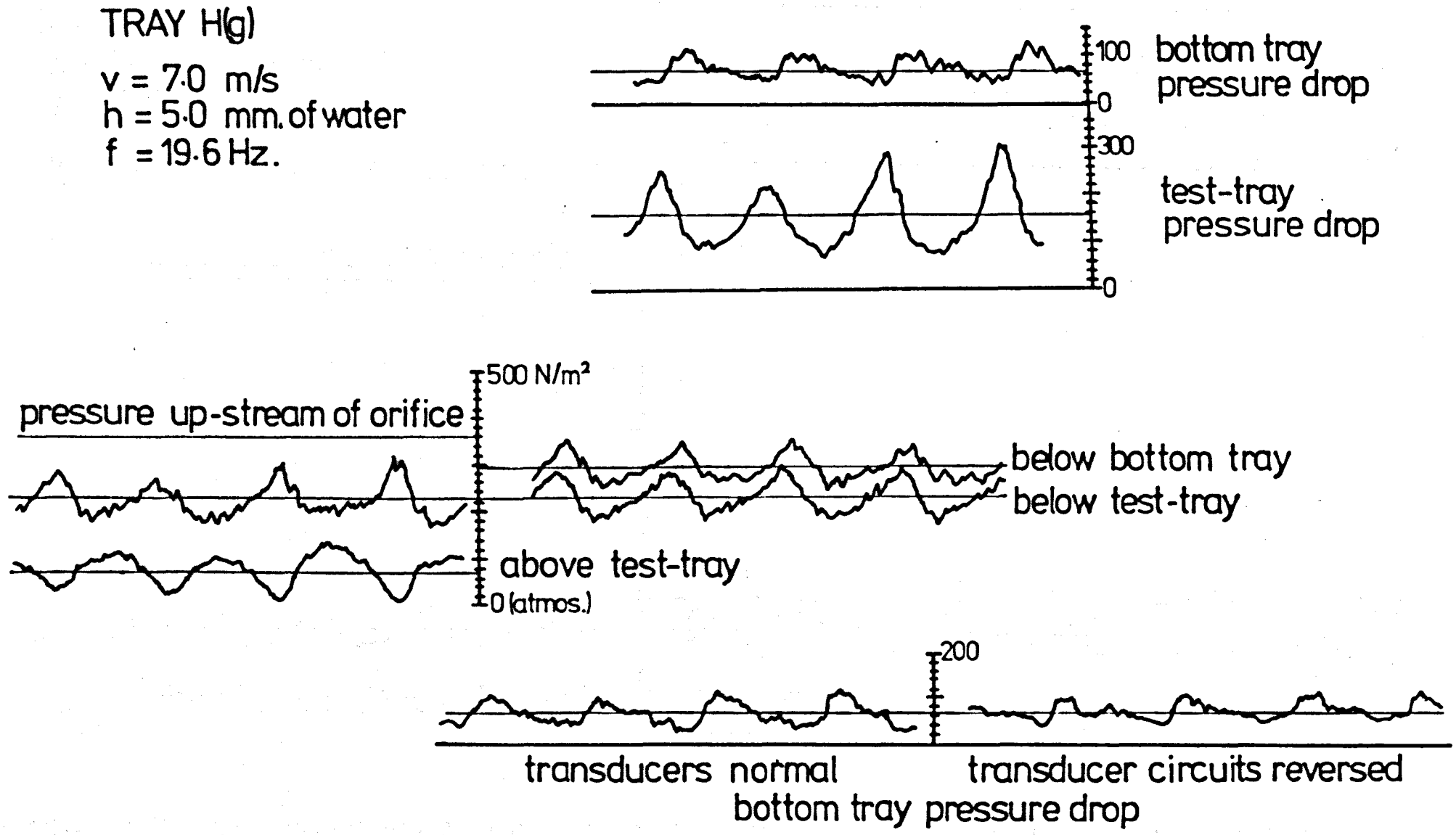

Fig.7.2. FLUCTUATIONS IN COLUMN PRESSURES AND TRAY PRESSURE DROPS

TRAY H(g)

v = 7·0 m/s
h = 5·0 mm. of water
f = 19·6 Hz.

(gas flow restrictor at column inlet)

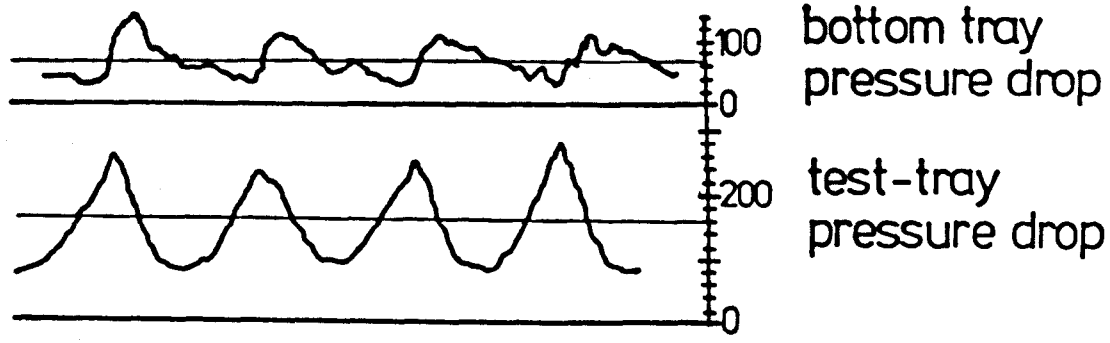

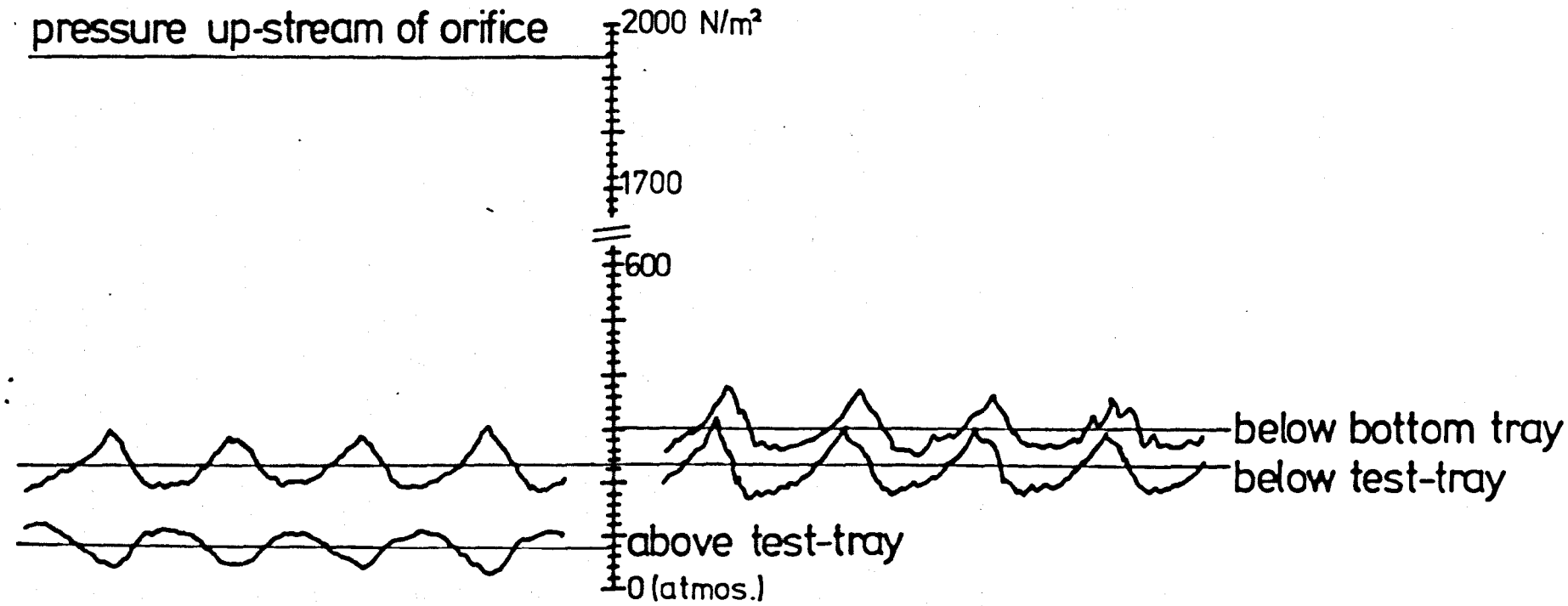

Fig. 7.3. FLUCTUATIONS IN COLUMN PRESSURES AND TRAY PRESSURE DROPS WITH GAS FLOW RESTRICTOR AT COLUMN INLET

$G_o < G_1$. For a given flow difference the rate of change of the pressure is determined by the chamber inverse capacitance, C, as given by the equation:

$$\frac{d P_1}{dt} = C \cdot (G_o - G_1) \qquad (7.2)$$

where; $$\frac{1}{C} = \frac{Q}{\beta_m} + \frac{dQ}{dP} \qquad \text{(ref.63, page 43)}$$

which for constant chamber volume becomes:

$$C = \frac{c^2 \cdot \rho}{Q} \qquad (2.2)$$

The rate of change of the pressure beneath the test-tray, $\frac{dP_1}{dt}$, was obtained by taking measurements from pressure signal tracings using a millimetre grid in a similar manner to that used to obtain the bottom tray pressure drop fluctuations. The change in pressure was assumed to be linear during each successive 2.5 ms. signal period. As before, measurements from several pressure cycles were averaged. The dynamic gas flowrate through the test-tray, G_1', was then calculated using equations (7.2) and (2.2), assuming that any air 'trapped' on the test-tray during hole event growth did not affect the chamber volume.

Figure 7.4 shows the calculated dynamic gas volumetric flowrate through test-trays H(g) and L(g) for operating conditions corresponding to the cine-films 14, 15, 22, 24 and 25, (see Table 6.2). The zero on the time axis corresponds to the peak of the pressure pulsation beneath the test-tray. All of the flowrates are seen to exhibit the same fundamental type of behaviour. That is, there is a relatively rapid rise in the flowrate to a maximum value followed by a more gradual fall in the flowrate to a minimum. The maximum flowrate is seen to occur at a point between 2.5 ms. and 12.5 ms. after the peak pressure beneath the test-tray,

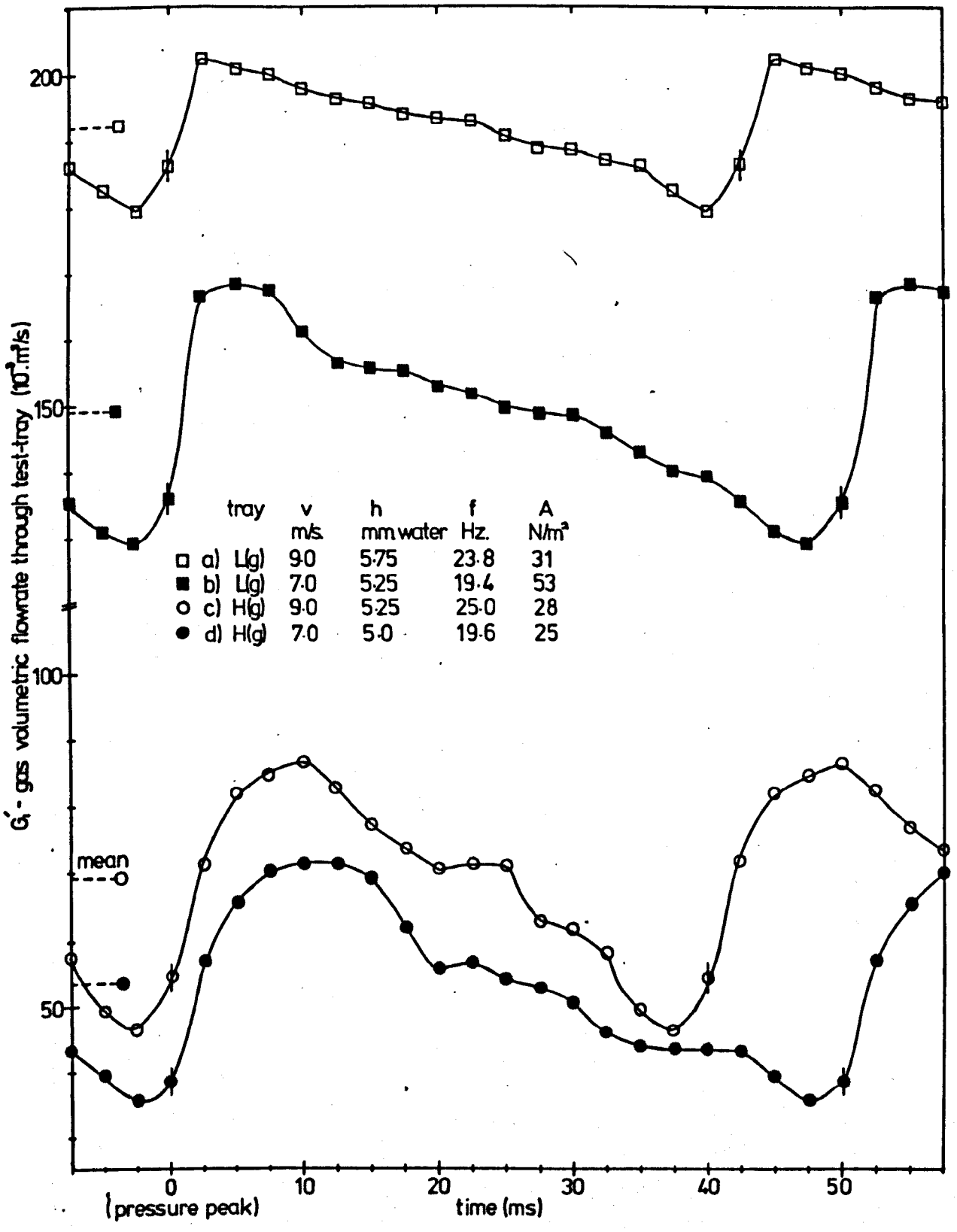

Fig.7.4. FLUCTUATION IN TEST-TRAY GAS FLOWRATE DURING PRESSURE PULSATION CYCLE

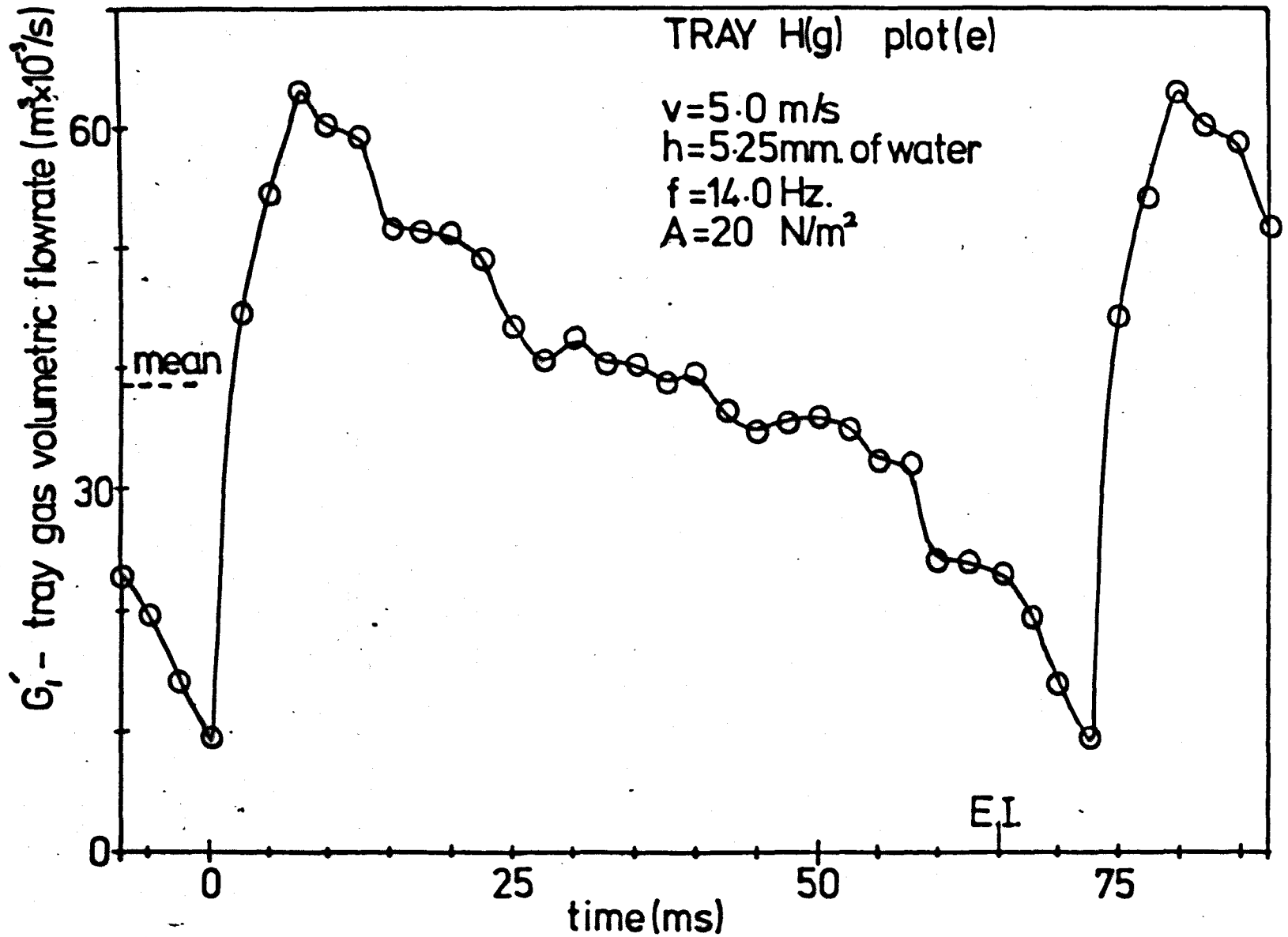

Fig 7.4. FLUCTUATION IN TEST-TRAY GAS FLOWRATE DURING PULSATION CYCLE

with the minimum flowrate occurring about 2.5 ms. before the pressure peak. It is also apparent that, apart from the lowest superficial hole gas velocity of 5 m/s., the minimum flowrate has a value of between 75% and 90% of the mean flowrate.

7.1.3 Calculation of the fluctuations in the test-tray total static pressure drop.

The fluctuations in the test-tray total pressure drop (the dynamic pressure drop) were calculated from static and dynamic pressure measurements made above and below the operating test-tray, using the same analysis procedure as was used to obtain the bottom tray dynamic pressure drop. Figure 7.5 shows the calculated test-tray dynamic pressure drops for conditions corresponding to the dynamic gas flowrates plotted in Figure 7.4.

As with Figure 7.4, the plots in Figure 7.5 all exhibit the same characteristic behaviour, the correspondence between plots (a) and (c) being particularly close, consistent with the similarity between the pressure pulsations measured at these two conditions.

The results shown in Figures 7.4 and 7.5 are discussed in the next section which relates them to the observed gas-liquid interaction on the test-tray.

7.2 COMPARISON OF THE CALCULATED FLUCTUATIONS IN THE TEST-TRAY GAS VOLUMETRIC FLOWRATE AND TOTAL PRESSURE DROP WITH THE OBSERVED GAS-LIQUID INTERACTION ON THE TRAY.

The calculated flowrates and pressure drops plotted in Figures 7.4 and 7.5 were at operating conditions identified by the film analysis as producing over 90% single events with a relatively high degree of synchronisation. It is therefore reasonable to apply these calculated flows and pressure drops to the gas-liquid interaction at individual holes.

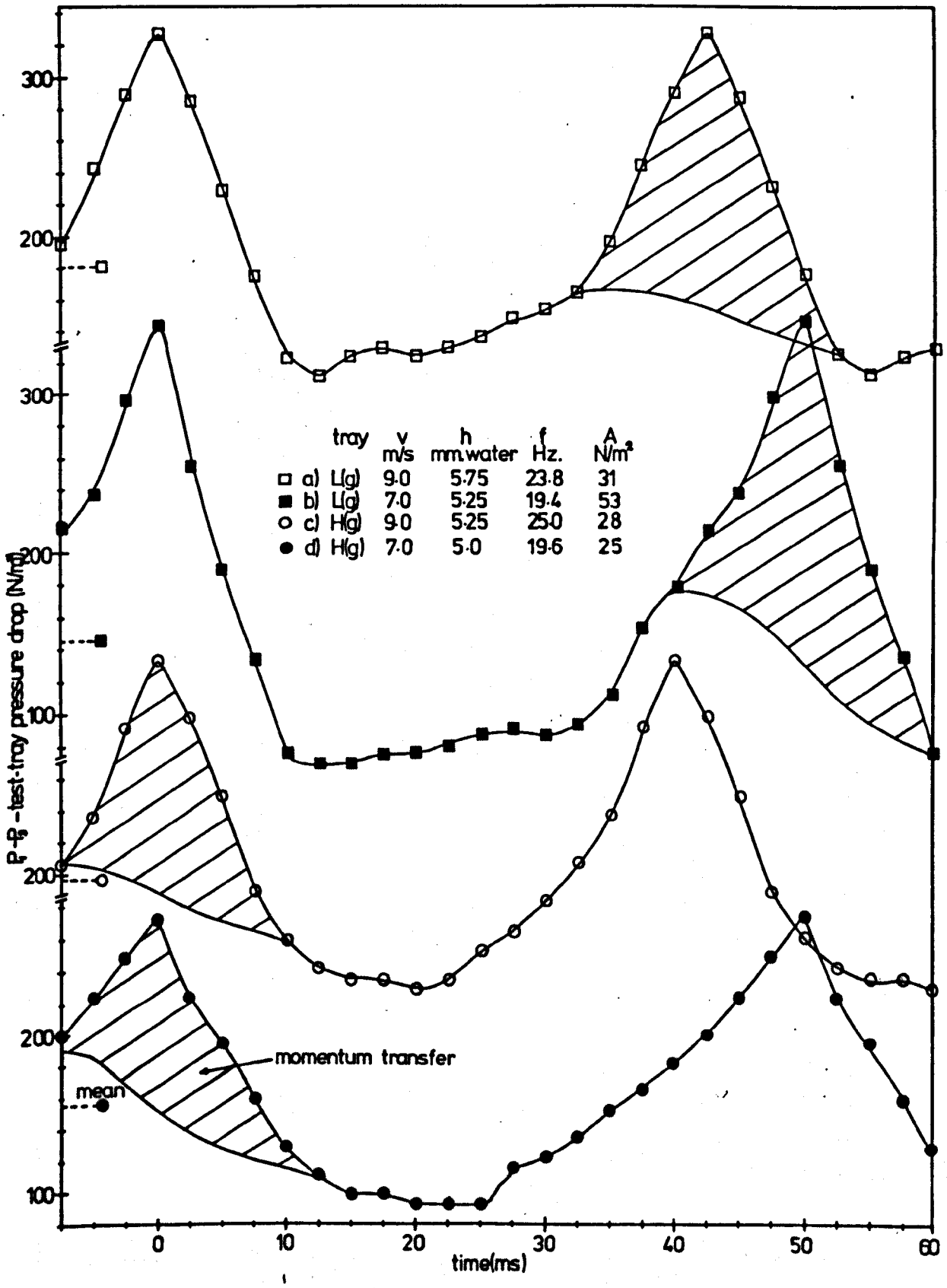

Fig.25 FLUCTUATION IN TEST-TRAY PRESSURE DROP DURING PRESSURE PULSATION CYCLE

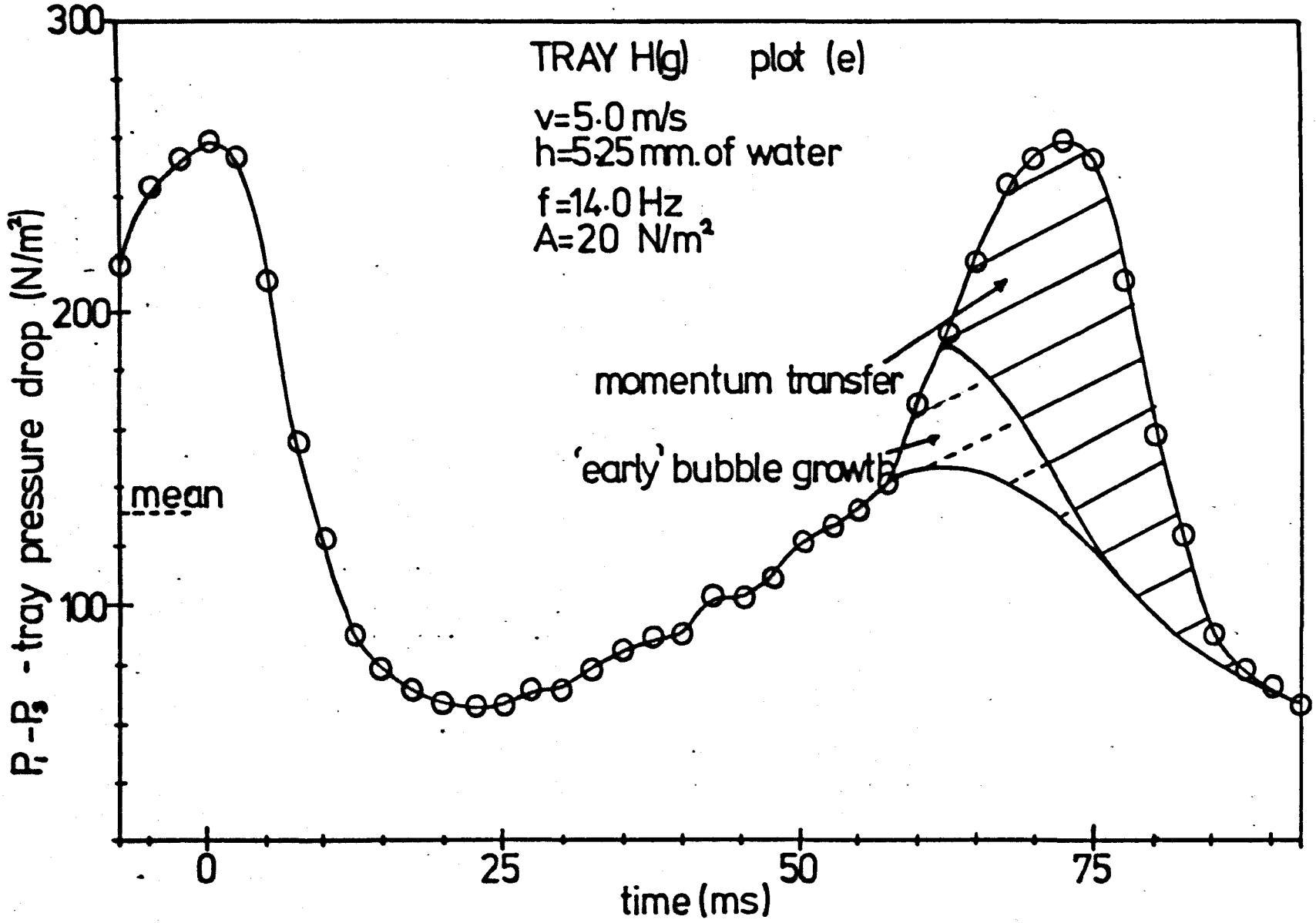

Fig.7.5. FLUCTUATION IN TEST-TRAY PRESSURE DROP DURING PULSATION CYCLE

Analysis of films 24 and 25 identified continuous pulsed gas flow and imperfect bubbling as the two main types of hole event occurring on test-tray H(g), operating with a gas velocity of 7 m/s. and a tray liquid head of 5 mm. of water. Event initiation occurred between 5 ms. and 10 ms. prior to the peak pressure beneath the test-tray. The two types of hole event can be described as follows.

In a pulsating jet event, liquid draining back towards the hole leads to a restriction of the gas flow and results in a build-up of pressure beneath the test-tray. However, before liquid bridging and subsequent bubble formation can occur, the pressure drop across the tray rises sufficiently for the gas to force liquid radially away from the hole and to strip off liquid droplets and ligaments and entrain them upwards. This action reduces the resistance of the hole to gas flow and a surge of gas occurs, releasing the pressure built up beneath the tray. The liquid forced away from the hole eventually comes to rest and then drains back towards the hole, leading to the initiation of the next event.

In an imperfect bubble event, liquid bridging of the hole does occur and this hole closure results in a temporary cessation of gas flow through the hole. The increasing pressure drop across the tray induces immediate bubble growth, with the gas-liquid interface elongating upwards above the layer of liquid on the tray. Eventually, bubble rupture occurs with liquid ligament and droplet stripping and entrainment by the ensuing surge of gas through the hole. After rupture, the liquid forced away from the hole eventually comes to rest and then the liquid motion becomes very similar to that of the pulsating jet events which may be occurring simultaneously on the tray, with the liquid draining back towards the hole leading to the initiation of the next event.

Plot (b) of Figure 6.12 presented a model of imperfect bubble growth based upon measurements taken from films 24 and 25. The gas volumetric flowrate associated with such an event is shown in Figure 7.6. Also shown is the flowrate through a hole based upon the calculated fluctuations in the total tray volumetric flowrate, assuming equal hole loading. Clearly the flow associated with imperfect bubbling is not consistent with that calculated directly from the column dynamic pressure measurements. Even allowing for a large number of early bubble ruptures and for variation in the time of event initiation, the minimum flowrate is too small and the maximum flowrate is too large and occurs at the wrong time. Therefore, as shown by the film, pulsating jet events must also be occurring on the tray.

Figure 7.7 shows a possible combination of the two types of hole events for the operating conditions of films 24 and 25. With, at any instant, 75% of the holes operating in the pulsating jet regime and 25% in the imperfect bubble regime, the total average flow fluctuation equals that calculated from the dynamic pressure measurements. The flows shown for each event include effects due to small variations in the initiation and the duration of the events. These variations prevent a zero overall flowrate for the imperfect bubble events at the average initiation point. The point of bubble rupture also varies and the majority of ruptures are assumed to occur within the first 20 ms.

As already stated, once bubble rupture has occurred and the movement of liquid away from the hole has stopped then the liquid motion associated with pulsating jet and imperfect bubble events is essentially the same, with liquid draining back towards the hole leading to the initiation of the next event. Hence, for a short period of time the gas flow associated with the two types of event will be substantially the same.

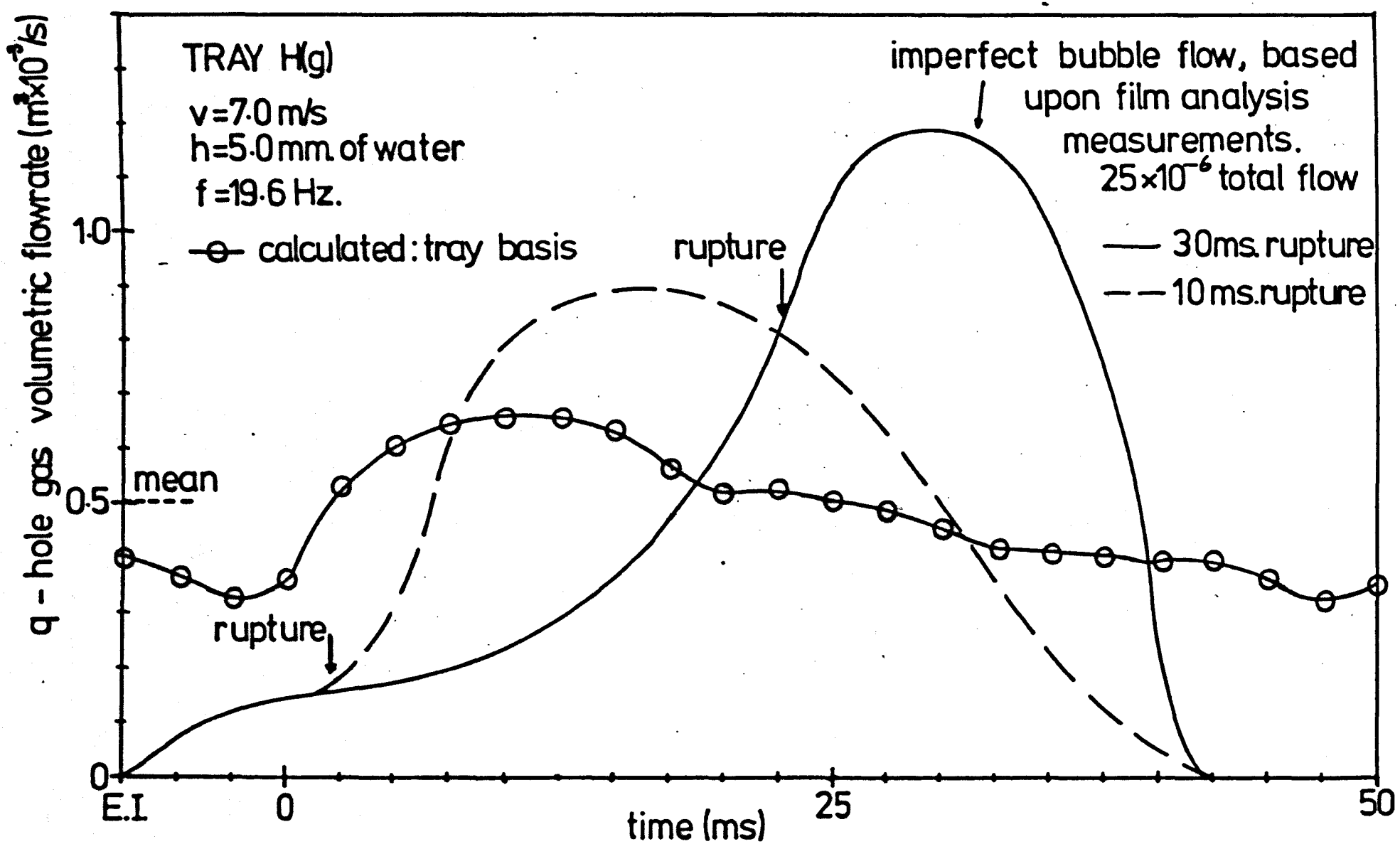

Fig. 76. FLUCTUATING GAS FLOWRATE OF IMPERFECT BUBBLE EVENT

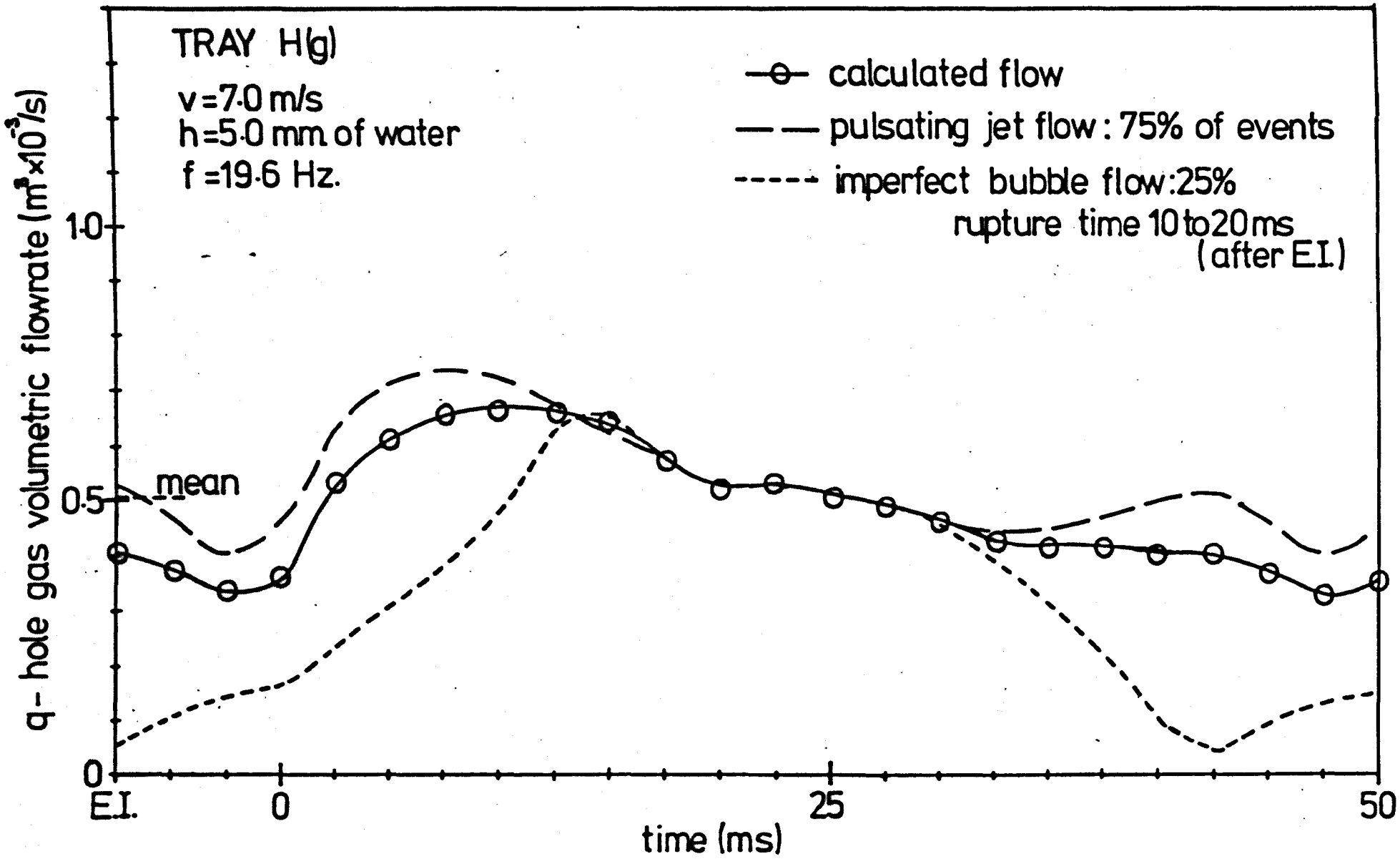

Fig. 7.7. COMPOUNDED GAS FLOWRATES OF PULSATING JET AND IMPERFECT BUBBLE EVENTS

Furthermore, this means that the type of event which occurs at a hole is not dependent upon the previous event at that hole.

A good indication of the type of event which is occurring on the tray is the variation in the resistance of the test-tray to gas flow (the loss coefficient), which relates directly the fluctuations in the tray gas flowrate to those in the pressure drop. It is to be expected that a high proportion of imperfect bubble events would produce a relatively high peak in the tray loss coefficient corresponding to the instant of hole closure, and that a high proportion of pulsating jet events would produce a smaller variation in the loss coefficient. Furthermore, the variation in the loss coefficient should give a good indication of the variation in the gas-liquid momentum transfer.

These factors are examined in the next section in which the test-tray loss coefficient is determined and expressed in terms of a variable equivalent dry tray hole diameter.

7.3 CALCULATION OF THE FLUCTUATIONS IN THE TEST-TRAY LOSS COEFFICIENT AND THE COMPARISON OF THOSE FLUCTUATIONS WITH OBSERVED GAS-LIQUID INTERACTION ON THE TRAY.

As stated in section 3.1, the total static pressure drop across an operating sieve-tray is normally expressed as the sum of a number of terms representing additive resistance to gas flow, i.e.:

$$\Delta P_t = \Delta P_d + \Delta P_r + \Delta P_m \qquad (3.5)$$

Incorporating the residual pressure drop, ΔP_r, and the dry tray pressure drop, ΔP_d, into a velocity dependent loss term gives:

$$\Delta P_t = K_t \cdot \frac{\rho}{2} \cdot v^2 + \Delta P_m \qquad (7.3)$$

This represents the pressure loss due to the passage of gas through the holes in the presence of liquid on the tray plus the loss due to maintaining the static head of liquid on the tray.

When the tray is operating with regular fluctuations of both the tray pressure drop and the gas volumetric flowrate through the tray, equation (7.3) can be expressed in terms of time-dependent variables (indicated by primes) with the inclusion of a term to account for gas inertial changes.

$$\Delta P_t' = P_1' - P_3' = K_t' \cdot \frac{\rho}{2} \cdot \left(\frac{G_1'}{a_h'}\right)^2 + \Delta P_m' + \Delta P_I \qquad (7.4)$$

where:

a_h' = time varying tray free area , m^2.

ΔP_I = inertial pressure loss.

ΔP_I can be expressed in terms of changes in the gas volumetric flowrate in the chamber beneath the test-tray (63, page 56).

$$\Delta P_I = \frac{\rho . b}{A_c} \cdot \frac{d\, G_1}{dt} \qquad (7.5)$$

Muller (62) used a different expression to estimate inertia effects. It was based on changes in the gas hole velocity acting over an estimated gas 'tube' length, and can be written as:

$$\Delta P_I = \rho(t + H + 0.44d) \cdot \frac{dv}{dt} \qquad (7.5a)$$

Both of these expressions give similar values for the gas inertial loss. The former expression is used because it is easier to evaluate. It should be noted that as the changes in the gas flowrate are relatively small, the accuracy to which the gas inertia effect is calculated is not critical.

In equation (7.4) $\Delta P_m'$ represents the instantaneous pressure loss due to maintaining the head of liquid on the tray. The head of liquid can be considered to be maintained in two main ways. Firstly, a small head can be maintained on the tray, in the absence of any gas-liquid interaction, by liquid surface tension forces and the steady flow of gas through the holes. This head was determined experimentally for each test-tray over a range of gas flowrates and was found to usually have a value of between 1 and 3 mm. of water, as shown in Figure 5.5. Secondly, the remaining head of liquid is maintained on the tray by gas-liquid momentum transfer.

The pressure loss due to gas-liquid momentum transfer will vary during the period of a hole event, as will the effective tray hole area, a_h. Therefore, although $(P_1-P_3)'$ and G_l' are known, equation (7.4) cannot be used to calculate K_t' as a_h' and $\Delta P_m'$ are unknown. However, $(P_1-P_3)'$ and G_l' can be used to calculate a time dependent test-tray total loss coefficient K_T' for a hypothetical dry tray having a time dependent hole diameter d'.

7.3.1 Calculation of the test-tray total loss coefficient K_T'.

The test-tray total loss coefficient, K_T', is defined by the equation:

$$K_T' \cdot \frac{\rho}{2} \cdot v'^2 = (P_1-P_3)' - \frac{\rho . b}{A_c} \cdot \frac{dG_l'}{dt} \qquad (7.6)$$

By expressing K_T' in terms of the time dependent hole diameter, d', of a hypothetical dry tray, it is possible to estimate v', assuming equal hole loading, using the relationship:

$$v' = \frac{G_l'}{a_h'} = \frac{4.G_l'}{n.\pi.d'^2} \qquad (7.7)$$

However, apart from affecting the instantaneous gas hole velocity, the value of d' will also affect the instantaneous hypothetical dry tray loss coefficient, K_T'. The nature of this effect can be determined by considering the dry tray loss coefficients found for the test-trays. These loss coefficients are given in Table 7.1 which also shows the coefficients calculated from the tray geometry using the equation:

$$K = 0.95 \cdot \left(\frac{p^2}{t.d}\right)^{0.2} \qquad (7.8)$$

This equation is a modified form of equation (3.4) derived by Cervanka and Kolar (50). For all practical tray geometries equation (7.8) gives a value of K which is within $\pm$ 0.5% of the value of K_c given by equation (3.4).

TABLE 7.1 DRY TEST-TRAY LOSS COEFFICIENTS.

Tray	Experimental K $= \frac{2.\Delta P_d}{\rho \cdot v^2}$	Theorectical K $=0.95\ (\frac{p}{td})^{2\ 0.2}$	Tray	Experimental K $= \frac{2.\Delta P_d}{\rho \cdot v^2}$	Theoretical K $=0.95(\frac{p}{td})^{2\ 0.2}$
A	1.64	1.79	I	2.05	1.96
B(g)	1.56	1.69	J	2.20	1.96
C	1.47	1.56	K	2.40	1.96
D	1.75	1.56	L(g)	1.83	1.86
E	2.00	1.56	M	2.21	1.86
F	1.90	1.82	N	2.52	2.44
G	2.10	1.95	O	2.22	2.32
H(g)	2.12	2.06			

The theoretical coefficients show moderate agreement with the experimentally determined values. Some disagreement is to be expected because the theoretical value assumes perforation of 100% of the column cross

sectional area, whereas the trays tested only had perforated areas of between 20% and 75% of the column area. However, good agreement with the diameter dependence, $K \propto d^{-0.2}$, is shown by the two series of trays, A, B(g), C; and H(g), I, L(g). Therefore, as K_T' is for a dry tray in which only the diameter varies we can assume that:

$$K_T' \propto (d')^{-0.2} \tag{7.9}$$

Modifying the coefficient in order to obtain the experimentally determined loss coefficient at $d' = d$, equation (7.8) becomes for trays H(g) and L(g):

$$H(g) - \quad K_T' = 0.978 \left(\frac{P}{td}\right)^{2\ 0.2} \tag{7.10a}$$

$$L(g) - \quad K_T' = 0.935 \left(\frac{P}{td}\right)^{0.2} \tag{7.10b}$$

The small difference between the two coefficients may be due to errors in the experimentally determined loss coefficients or perhaps to equation (7.8) being less applicable to the relatively high free area of tray L(g).

Now, knowing $(P_1-P_3)'$ and G_1'; using equations (7.6), (7.7) and (7.10) it is possible to evaluate K_T' expressed in terms of the hypothetical hole diameter, d'.

It must be remembered that, as indicated by equation (7.4), variations in d' will result from changes both in the resistance of the actual tray holes to gas flow and in the magnitude of the gas-liquid momentum transfer.

Figure 7.8 shows d' calculated for trays L(g) and H(g) operating at the same conditions as the flows and pressures shown in Figures 7.4 and 7.5.

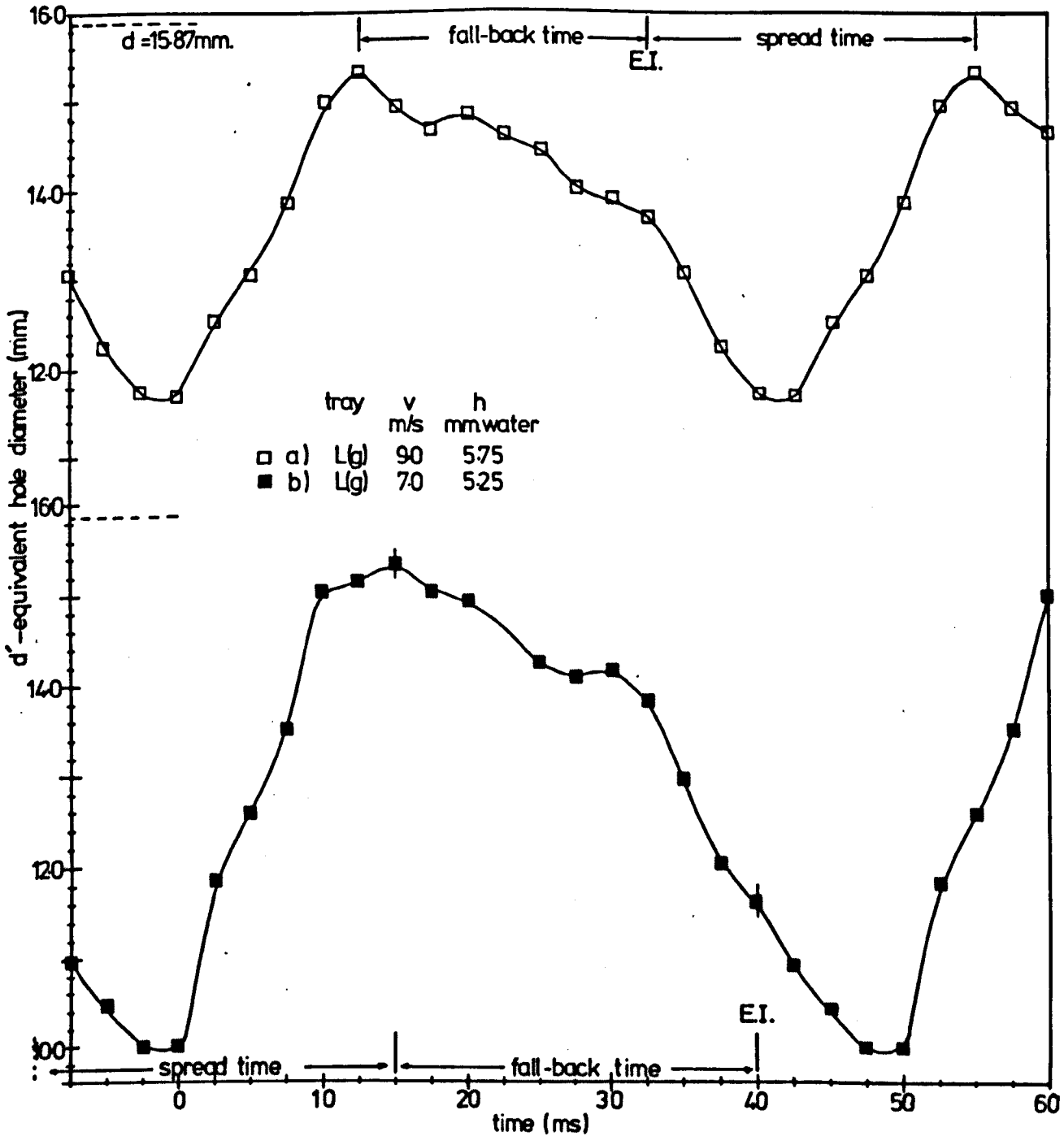

Fig.7.8. VARIATION IN EQUIVALENT HOLE DIAMETER DURING PRESSURE PULSATION CYCLE

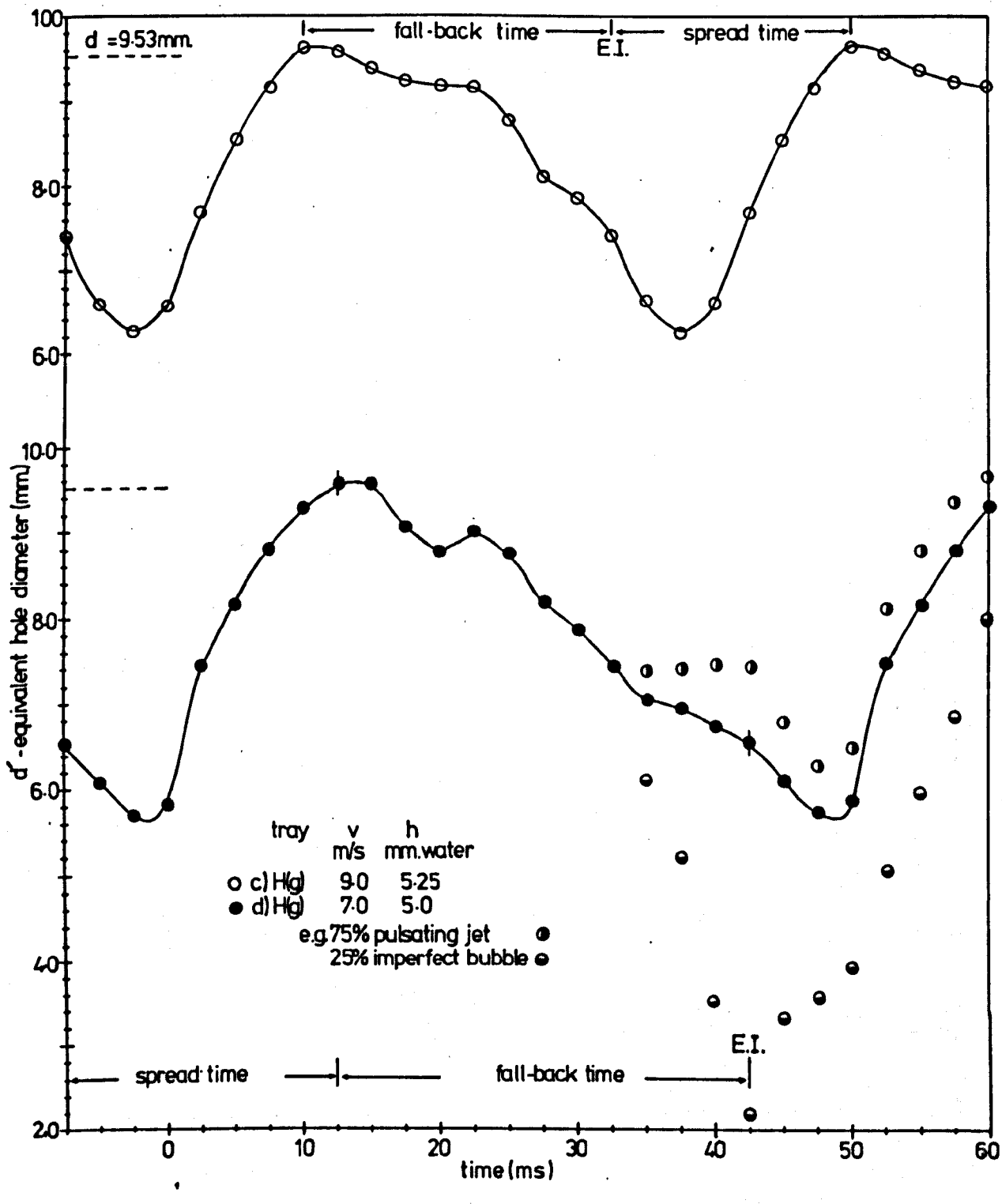

Fig. 7.8. VARIATION IN EQUIVALENT HOLE DIAMETER DURING PRESSURE PULSATION CYCLE

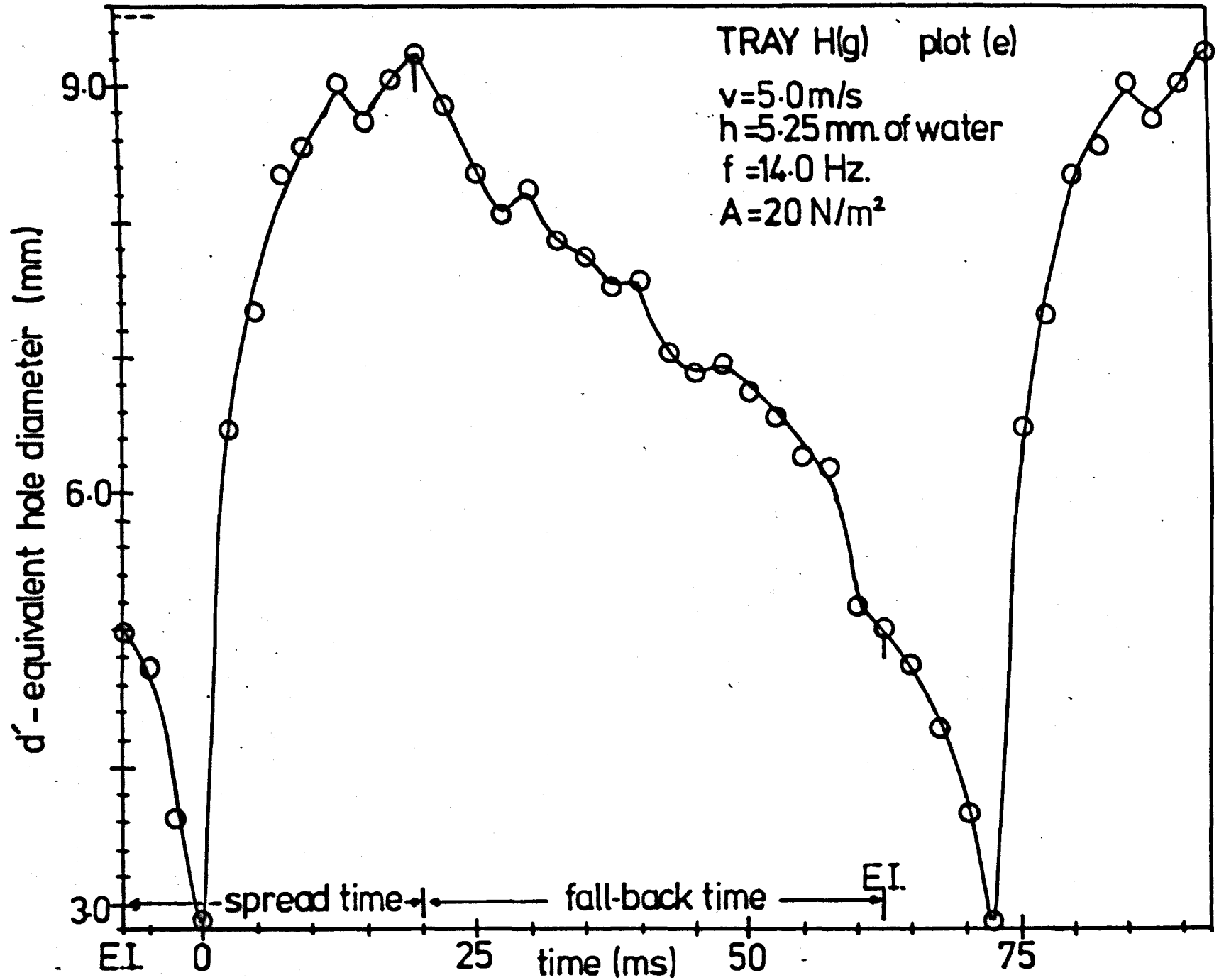

Fig 7.8. FLUCTUATION IN TEST-TRAY EQUIVALENT HOLE DIAMETER DURING PULSATION CYCLE

7.3.2 Interpretation of the Variation in Test-Tray Total Loss Coefficient.

Plot (a) of Figure 7.8 is for test-tray L(g) operating at a gas velocity of 9 m/s. and a tray liquid head of 5.75 mm of water, under which conditions it is reasonable to assume that the great majority of hole events are pulsating jets. The minimum resistance (maximum value of d') is seen to occur after about 12.5 ms and is close to the actual dry tray resistance. This point can be taken to represent the moment at which the liquid pushed back away from the hole reaches its maximum radial spread. Following this minimum value the resistance is seen to slowly increase, which is consistent with the concept of liquid falling back towards the hole. During this fallback period the gas-liquid momentum transfer will be minimal. After about 32.5 ms the resistance is seen to increase more rapidly. This can be taken to represent the onset of gas-liquid momentum transfer, the pressure drop across the tray having reached a value sufficient to induce event initiation with the liquid being forced away from the hole and entrained upwards. Figure 7.5 indicates the pressure drop at this point to be about 165 N/m^2. Beyond this point the actual pressure loss across the tray holes will decrease because the liquid is being pushed back away from the holes. Hence, the further increase in tray resistance must result from increased gas-liquid momentum transfer, this reaching a maximum value after about 42 ms. The variation in the total tray resistance coefficient indicates that event initiation occurs about 10 ms. prior to the peak pressure beneath the test-tray, and gives the time to reach maximum radial spread as about 22.5 ms. This agrees very well with the findings of the film analysis, which gave a maximum radial spread time of 22.0 ms. (see Table 6.4).

In plot (a) of Figure 7.5 is indicated the pressure loss which, from the analysis of the tray resistance, can be attributed to gas-liquid momentum transfer, (the net change in gas inertia over this period is relatively small and can be ignored). This pressure loss has a mean value, over the period of the hole event, which is equivalent to a head of about 4.0 mm of water. This is less than the measured tray liquid head by 1.75 mm of water, which is the head found to be supported on the tray in the absence of gas-liquid interaction, (see Figure 5.5).

Plot (b) of Figure 7.8 is for test-tray L(g) operating at the lower gas velocity of 7.0 m/s and a tray liquid head of 5.25 mm of water. Again a high proportion of pulsating jet events should occur, more than the 75% estimated to occur on the smaller hole tray H(g) operating at the same conditions. Plot (b) is seen to have a very similar shape to plot (a), with the value of the minimum resistance being almost identical. The plots also show remarkable agreement during the fallback period. This is to be expected in that although a small number of imperfect bubble events may be occurring at the lower gas velocity, these will be essentially the same as pulsating jet events during the fallback period. The lower gas flowrate in plot (b) means that it will take longer for the tray pressure drop to build up to a value sufficient to induce event initiation. The pressure drop reaches the value required to induce initiation at the higher gas flowrate after about 40 ms. This gives an average initiation point about 10 ms prior to the peak pressure and a maximum radial spread time of about 25 ms, again in good agreement with the findings of the film analysis (t_{max} = 25.5 ms.). The corresponding tray pressure loss attributable to gas-liquid momentum transfer is shown on plot (b) of Figure 7.5. This is equivalent to an average head of 3.5 mm of water which is again very close to the measured total tray

liquid head less the head found to be supported on the tray in the absence of gas-liquid interaction. The change in the rate of increase of the tray resistance, taken in plot (a) to indicate event initiation, is more likely in plot (b) to result from hole closures associated with the small number of imperfect bubble events which may be occurring. Results for tray H(g), for which imperfect bubble events are more common, should show this more clearly.

In Figure 7.8 the plots for test-tray H(g) (c, d and e) are seen to have a very similar shape to those for the larger hole diameter tray. The minimum resistance in plots (c) and (d) is seen to correspond to an equivalent diameter slightly smaller than the actual hole diameter, which is impossible. However, the error is small and within the limits of the experimental measurements and analysis technique.

As with the results for tray L(g), the plots for tray H(g) show a gradual increase in resistance during the fallback period, and as before the rate of increase is similar for the different gas velocities.

At the highest velocity of 9 m/s (plot (c)), a high proportion of the hole events can be expected to be pulsating jets. On plot (c) event initiation can be taken to occur after about 32.5 ms., at which point the tray pressure drop is about 207 N/m^2. This initiation point is in good agreement with that indicated by Figure 6.10 and the maximum spread time of about 17.5 ms agrees very well with the value of 17.4 ms found in the film analysis. The pressure loss indicated on plot (c) of Figure 7.5 to be due to gas-liquid momentum transfer, as before, corresponds well with the measured tray liquid head minus the head maintained in the absence of gas-liquid interaction.

Plot (d) of Figure 7.8 is for tray H(g) operating at conditions indicated by previous analysis to produce about 25% imperfect bubble

events and 75% pulsating jet events. As well as the average variation in resistance, plot (d) also indicates the variation for these two types of event, based upon the flowrates shown in Figure 7.7. The occurrence of the minimum resistance after about 12.5 to 15 ms indicate that most of the bubble ruptures must have occurred by this time. During the fallback period the variation in resistance for the two types of event is the same until after about 32.5 ms at which point the onset of the hole closure of the imperfect bubble events causes their resistance to increase rapidly, reaching a maximum value after 42.5 ms. This maximum value is not equivalent to zero hole diameter (complete hole closure) because of the assumed variation of the event initiation points. The flow model for the imperfect bubble events was based upon measurements from the film analysis and hence the average point of event initiation corresponds to the value found in the analysis, i.e.7.5 ms before the pressure peak. However, it should be noted that, unlike the pulsating jet events,which initiate at a certain pressure drop, imperfect bubble events will start limited bubble growth almost immediately after hole closure.

The occurrence of some complete hole closure tends to increase the gas loading of the other holes,which maintain a fairly constant resistance during this period. Following event initiation, at 42.5 ms., the resistance variation of the pulsating jet events is very similar to that exhibited by trays H(g) and L(g) operating at v = 9 m/s (plots (c) and (a)), when pulsating jets are highly predominant.

Although the indication of event initiation after 42.5 ms in plot (d) relates directly to the results of the film analysis, the tray pressure drop at this point is about 200 N/m^2 which agrees well with the value found for tray H(g) operating at v = 9 m/s. The maximum spread time of plot (d) (20.0 ms.) agrees well with the value from the film analysis (21.5 ms.).

Plot (e) of Figure 7.8 is for tray H(g) operating at v =5.0 m/s, and can therefore be expected to exhibit evidence of a large number of imperfect bubble events. The variation in resistance clearly indicates this, with the sharp increase in resistance to a relatively high value being similar to the behaviour shown for the imperfect bubble events in plot (d). The minimum resistance occurs after about 20 ms., and event initiation after about 63 ms., assuming it to occur at the same pressure drop as for the higher gas velocities ($\simeq$ 200 N/m^2). This indicates bubble rupture to occur slightly later than at the higher gas velocity, and gives a maximum spread time (28.5 ms.) which agrees fairly well with the film analysis (26.3 ms.).

The pressure loss indicated on plots (d) and (e) of Figure 7.5 as being associated with the gas-liquid momentum transfer are equivalent to liquid heads which are slightly less than the total tray liquid head minus the head maintained in the absence of gas-liquid interaction. This could be due both to the occurrence of gas-liquid momentum transfer in single events (particularly imperfect bubbles) prior to the average initiation point, and to the occurrence of double or intermediate events (likely to be most important for v = 5.0 m/s.). It should also be noted that some gas-liquid momentum transfer will occur as the gas flows past entrained liquid droplets temporarily suspended above the tray.

The above analysis and discussion shows conclusively that, for the conditions considered, calculations based upon measured column gas pressures and flowrates (assuming regular synchronised gas-liquid behaviour) give results which are in very good agreement with the measurements from the film analysis and with the proposed descriptions of prevailing hole events (pulsating jet and imperfect bubble).

7.4 THE HOLE EVENT INITIATION PRESSURE DROP.

It has been found that, for trays H(g) and L(g) operating at a gas velocity of between 5 and 9 m/s and a tray liquid head of between 5 and 6 mm. of water, event initiation occurs as the total tray pressure drop rose past a critical value of between about 170 and 210 N/m^2, this occurring at a time of between 10 and 7.5 ms. prior to the maximum pressure beneath the tray.

The value of the initiation pressure may depend upon the tray liquid head and perhaps upon the dry tray loss coefficient. The lower value of the critical pressure drop for tray L(g) as compared with tray H(g) supports the idea of dependence on the tray loss coefficient, although the apparent independence of the critical value on average gas velocity indicates the reverse. This second indication however is partially invalid in that the instantaneous hole gas velocity at event initiation is not proportional to the average value.

Table 7.2 lists the calculated tray pressure drops plotted in Figure 7.5 and also gives values calculated for tray L(g) operating at another five sets of conditions, in particular at different values of tray liquid head. If it is assumed that the initiation pressure drop is independent of tray liquid head then Table 7.2 indicates that event initiation occurs increasingly earlier, with respect to the maximum tray pressure drop, as the tray liquid head is increased. This agrees, to some extent, with the assumption that the pressure loss immediately after initiation, attributed to gas-liquid momentum transfer, is proportional to the tray liquid head. Conversely, if it were assumed that the initiation pressure drop increases in proportion to the increase in tray liquid head, then Table 7.2 indicates the initiation to occur at an approximately constant time prior to the maximum pressure drop.

TABLE 7.2 THE VARIATION IN TOTAL PRESSURE DROP ACROSS THE TEST-TRAY DURING A PRESSURE PULSATION CYCLE.

Tray	H(g)	H(g)	H(g)	L(g)	L(g)	L(g)	L(g)	L(g)	L(g)	L(g)
v(m/s)	5.0	7.0	9.0	5.0	5.0	7.0	7.0	7.0	7.0	9.0
h(mm.H_2O)	5.25	5.0	5.25	5.5	12.0	2.75	5.25	8.5	10.75	5.75
f (Hz.)	14.0	19.6	25.0	15.4	18.0	19.2	19.6	20.4	21.2	23.8
A(N/m^2)	20	25	28	46	58	34	47	54	49	25
Time (ms.)	Time dependent tray pressure drop $(P_1-P_3)'$									
0	259	272	333	380	478	365	344	414	393	327
2.5	253	224	297	260	334	156	254	312	339	285
5.0	211	194	249	164	262	90	188	264	285	228
7.5	157	158	189	92	166	65	134	222	237	174
10.0	124	128	159	38	94	59	74	150	189	123
12.5	91	110	141	32	88	65	68	96	159	111
15.0	79	98	135	38	70	65	68	108	129	123
17.5	73	98	135	38	58	59	74	108	99	129
20.0	67	92	129	32	58	65	74	108	105	123
22.5	67	92	135	38	94	59	80	108	129	129
25.0	67	92	153	32	106	71	86	120	129	135
27.5	73	116	165	50	118	77	90	120	129	147
30.0	73	122	183	56	106	77	86	114	135	153
32.5	79	134	207	56	118	83	92	90	153	162
35.0	85	152	237	62	130	101	116	114	189	195
37.5	91	164	291	80	142	125	152	162	213	243
40.0	91	182		92	190	137	176	198	249	288
42.5	103	200		86	202	143	212	234	297	
45.0	103	224		92	238	161	236	276	351	
47.5	109	248		110	274	211	296	330		
50.0	121			122	346	283				
52.5	127			146	418					
55.0	133			188						
57.5	139			218						
60.0	169			260						
62.5	193			326						
65.0	217									
67.5	244									
70.0	253									
Static (P_1-P_3) (N/m^2)	131	155	196	118	186	116	145	182	206	181

Further experimental work is required in order to define the precise relationship of initiation pressure drop on tray liquid head, which is likely to be a form of compromise of the two proposed alternatives. The work in section 8.1 however, indicates that the initiation pressure drop may be largely independent of changes in the tray liquid head provided no significant changes of hole event mechanism occur.

7.5 SUMMARY.

The fluctuations both in the gas volumetric flowrate through the test-tray and in the total tray pressure drop, have been calculated from static and dynamic (time varying) pressure measurements. The column gas flow system was represented in terms of several gas flow resistances and capacitive volumes with a variable gas supply flow and with the operating test-tray acting merely as a variable resistance. The calculations were carried out for test-trays H(g) and L(g) operating at conditions identified by the film analysis as producing regular, synchronised, pulsating jet and imperfect bubble events. Physical descriptions of these two types of event were proposed based upon the findings of the film analysis.

It was shown that for test-tray H(g) operating with a gas velocity of 7.0 m/s and a tray liquid head of 5.0 mm of water about 75% of the single events were pulsating jets and the remainder imperfect bubbles, the calculated gas flowrate then agreeing with measurements of imperfect bubble growth obtained from the film analysis.

The calculated pressures and flows were combined to give the variation in the test-tray total loss coefficient, this being expressed in terms of the time dependent diameter, d', of a hypothetical dry tray. This analysis showed conclusively that, for the conditions considered, the measurements made in the film analysis and the proposed descriptions of imperfect bubble and pulsating jet events, were in very good agreement with the calculations based solely upon static and dynamic pressure measurements.

The minimum tray loss coefficient was found to be close to that of a dry tray, this minimum value occurring at a time after event initiation corresponding well to the point of maximum radial liquid spread as determined by the film analysis. Such a minimum value of loss coefficient is further evidence of a high degree of event synchronisation across the tray.

The analysis showed that, for the conditions considered, the tray liquid head is maintained on the tray mainly by the gas-liquid momentum transfer occurring immediately after event initiation, although a small head of liquid (1 to 3 mm of water) can be maintained on the tray by liquid surface tension forces and the flow of gas through the holes, even in the absence of any gas-liquid interaction.

The analysis also indicated that, for tray liquid heads of between 5 and 6 mm of water, event initiation occurred as the total tray pressure drop rose past a critical value in the range 170 to 210 N/m^2, with some indication that this range may depend upon the tray liquid head and perhaps the tray geometry.

Having demonstrated that the column dynamic pressure measurements are consistent with results of the film analysis and are in general agreement with the proposed description of the gas-liquid interaction, it is possible to attempt to correlate the amplitude and frequency of the pressure pulsations using these results and descriptions.

Chapter 8.

CORRELATION AND DISCUSSION OF THE RESULTS.

Introduction.

The results of the film analysis presented in Chapter 6 and the findings of the system analysis carried out in Chapter 7 are used as a basis for explaining and predicting the pressure pulsation measurements given in Chapter 5. The occurrence and amplitude of the pulsations are examined first, followed by consideration of the pulsation frequency.

8.1 EXAMINATION OF THE OCCURRENCE AND THE AMPLITUDE OF THE REGULAR PRESSURE PULSATIONS.

In Chapter 6 it was shown that high amplitude pulsations are favoured by a high degree of hole event synchronisation, a large proportion of single events and a small variation in the hole event duration. Conversely, it could be said that these three factors would result from high amplitude pressure pulsations. However, as it is the gas-liquid interaction which produces the pulsations then it is only when regular, synchronous, gas-liquid behaviour can be established and maintained that pulsations will occur. Therefore, to examine the occurrence of the pressure pulsations it is necessary to determine how the tray operating conditions affect the uniformity of hole events and the process of event synchronisation.

8.1.1 The Basic Mechanism of Event Synchronisation.

The analysis in Chapter 7 indicated that, for conditions of relatively low tray liquid head corresponding to pulsating jets and imperfect bubbles, events were synchronised by the total tray pressure drop rising past a critical value, ΔP_i, at which event initiation occurred.

This initiation process, in which the pulsating jet event is of primary importance, is illustrated in Figure 8.1 for four sets of operating conditions. Its main points can be explained by considering plot (a), which is for operation with 100% single events, the majority (or all) being pulsating jet events and the remainder imperfect bubbles.

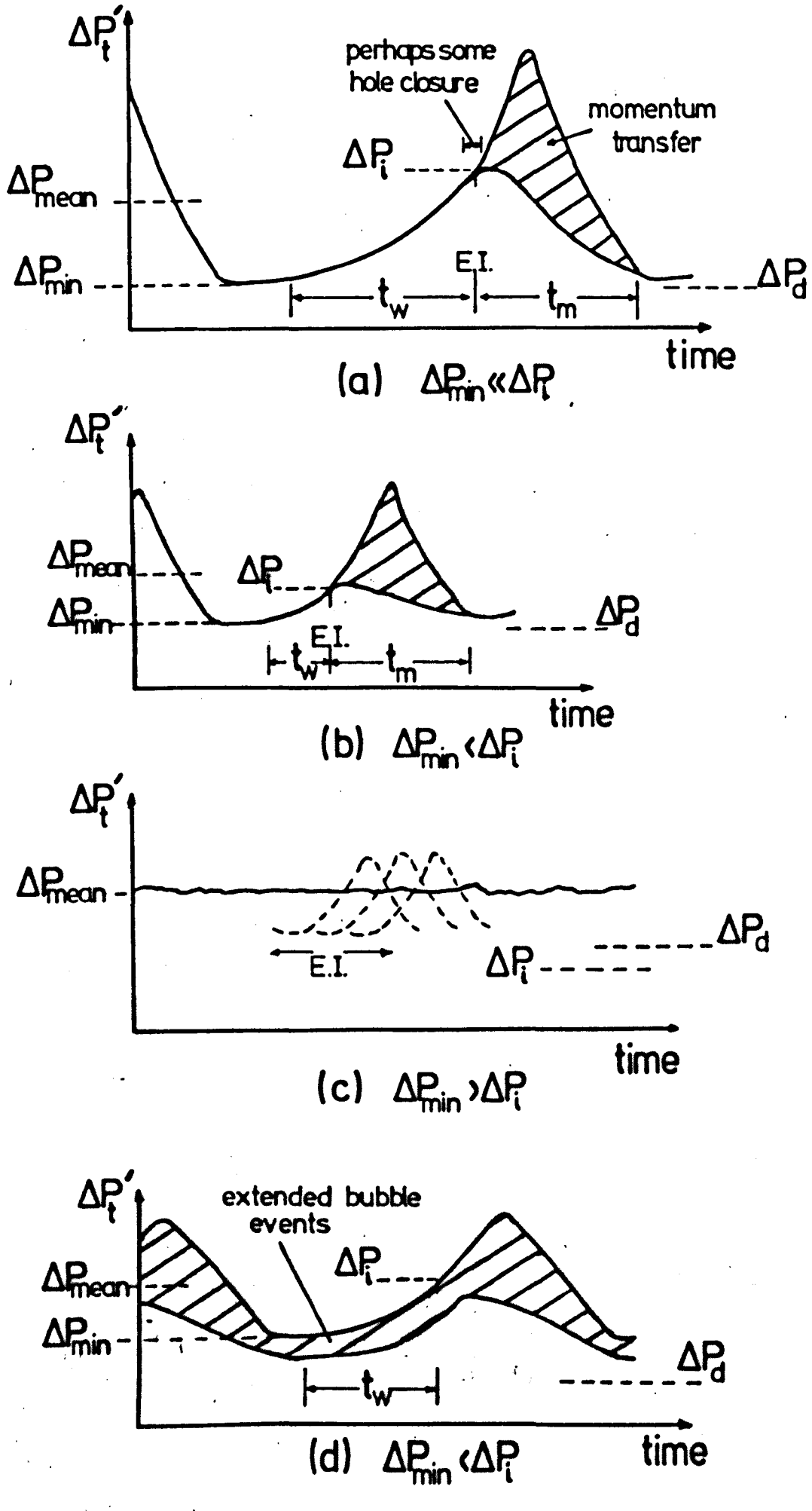

Fig. 8.1. TRAY PRESSURE DROP FLUCTUATIONS AND EVENT SYNCHRONISATION

Firstly let it be assumed that no imperfect bubbles occur. With the cessation of gas-liquid momentum transfer the total tray pressure drop falls until it reaches a minimum value, ΔP_{min} (which for plot (a) is significantly below ΔP_i). A simplified gas flow analysis described in Appendix X shows that if the tray resistance falls to its minimum possible value (i.e. that corresponding to the dry tray), then the value of ΔP_{min} will equal the dry tray pressure drop, i.e.

$$\Delta P_{min} = \frac{1}{2} K.\rho. v^2. \qquad N/m^2 \qquad (X.5)$$

This represents the lower limit of the value of ΔP_{min}. The liquid draining back towards the tray holes eventually causes restriction of the gas flow through the tray and this causes the total tray pressure drop to rise. The pressure drop rises due to this process until the initiation pressure drop is reached. This period of pressure rise is termed the 'waiting period' in that event initiation is 'waiting' for the pressure drop to reach the necessary value. Once initiation has occurred the rapid onset of gas-liquid interaction associated with the pulsating jet event will result in a sharp rise in the overall tray pressure drop. (The pressure loss due solely to the passage of gas through the tray holes will fall).

The occurrence of a minority of imperfect bubble events will have little affect on this process of synchronisation as the nature of the bubble events will be strongly influenced by that of the pulsating jets. With increasing hole closure during the waiting period eventually a certain proportion of complete hole closures will occur followed almost immediately by the onset of bubble growth. The extra flow resistance resulting from these hole closures, plus the small amount of associated gas-liquid momentum transfer, will lead to a rapid rise in the tray pressure drop, thus quickly

inducing pulsating jet initiation. The ensuing rapid rise in pressure drop due to momentum transfer will tend to 'overwhelm' the bubble events, inducing accelerated bubble growth and probably premature bubble rupture. Therefore, the great majority of events are still well synchronised, with rapid occurrence of most of the gas-liquid momentum transfer. In this case the overall tray pressure drop fluctuation, although controlled primarily by the pulsating jet events, strongly influences and synchronises another type of event occurring on the tray. This 'domination' by the pulsating jet event is an important factor of the synchronising process. Several factors will affect this synchronisation process, eventually causing it to cease. These factors are now considered.

8.1.2 Factors Controlling the Mechanism of Event Synchronisation.

8.1.2.1 The minimum tray pressure drop, ΔP_{min}.

In plot (a) of Figure 8.1 ΔP_{min} was significantly below ΔP_i, which resulted in a relatively long waiting period, t_ω, during which liquid restriction could occur at all of the tray holes, thus enabling relatively rapid initiation at all of the holes. In plot (b) (which is also for 100% single events, the majority or all being pulsating jets), ΔP_{min} is just below ΔP_i and as a result the waiting period is much shorter. In this case variation in the liquid motion of individual events will become important in that at the initiation pressure drop not all of the holes may have a significant restriction by liquid. Initiation at these holes will be delayed until further liquid inflow occurs or until a higher pressure drop is reached. The degree of synchronisation is therefore reduced with event initiation occurring over an increased period of time. As the onset of momentum transfer is more gradual, the rate of rise of pressure drop is decreased and the peak tray pressure drop probably reduced. Furthermore, this smaller

rate of pressure drop increase will reduce the influence of the pressure fluctuations on any other types of events.

In plot (c) of Figure 8.1 ΔP_{min} is higher than ΔP_i and there is therefore a negligible waiting period. Variation in the event liquid motion now becomes dominant, with event initiation occurring immediately sufficient liquid restriction occurs at an individual hole. As individual event initiations will have a negligible effect on the overall tray pressure drop, no significant pressure drop fluctuations will occur and there will therefore be negligible event synchronisation. In this case event initiation 'waits' for sufficient liquid hole blockage to occur and not for the tray pressure drop to rise to the initiation value. Such unsynchronised behaviour is evident on plot (e) of Figure 6.8.

It can therefore be concluded that the process of event synchronisation cannot occur when $\Delta P_{min} > \Delta P_i$.

It is therefore necessary to consider the factors controlling the value of ΔP_{min} and also those affecting the degree of variation of event liquid motion, i.e. the event uniformity.

8.1.2.2 Event uniformity.

It has been shown that small variations in the liquid motion of events become increasingly important when the value of ΔP_{min} approaches ΔP_i. Small variations in the event liquid motion can be seen in Figure 6.11 in which hole event growth measured in the film analysis is plotted. These variations will result from small differences in the extent of the gas-liquid momentum transfer which lead to variations in the extent and shape of the liquid radial spread and hence in the motion of the liquid draining back toward the hole.

At the smaller values of hole separation, the liquid motion of single events will be influenced by the more extensive growth of any double events occurring at neighbouring holes.

Perhaps the most important factor affecting the uniformity of events is the general liquid disorder or turbulence on the tray. This factor can be expected to become more important as the disorder is increased by increase in either the tray liquid head or the gas velocity. The cine films showed that in general the hole events became less uniform as the tray liquid head was increased.

It is also to be expected that even when the waiting period is relatively long, large turbulence-induced variations in event uniformity will make synchronisation more difficult. Event initiation will tend to occur over a longer period resulting in a more gradual pressure drop rise and a lower peak pressure drop. Therefore liquid disorder or turbulence is another factor tending to stop event synchronisation, with the effect being most marked when ΔP_{min} approaches ΔP_i.

8.1.2.3 Factors affecting ΔP_{min}.

As previously mentioned, the lower limit of ΔP_{min} corresponds to the dry tray pressure drop (see equation X.5). Therefore the superficial hole gas velocity is the main factor affecting ΔP_{min}, with the dry tray loss coefficient also being important. The pressure drops listed in Table 7.2 agree well with this lower limit for ΔP_{min}.

It is to be expected that at the higher values of tray liquid head, increased general restriction of the gas flow by the liquid will occur. This will increase the minimum tray resistance above the dry tray value and therefore increase the value of ΔP_{min}. Evidence of this effect can be seen in Table 7.2, in particular for tray L(g) operating at v = 5.0 m/s, with the film analysis showing 98% single events to occur at both of the heads used (see Table 6.3, films 10 and 12).

The lower limit of ΔP_{min} corresponds to 100% single events with complete bubble rupture. The occurrence of double or intermediate events

will tend to increase ΔP_{min}. This will be because, at the point of minimum tray pressure drop, these longer events may still have a growing gas-liquid interface, which will tend to restrict gas flow and increase the gas loading of the other (single event) holes. Also, the extended gas-liquid momentum transfer of such events will tend further to increase the minimum tray pressure drop. (The same effect will be produced by single imperfect bubble events with extended bubble growth). As an example, if hole blockage due to extended bubble growth induced 85% of the column gas flow to pass through 60% of the tray holes, then the minimum tray pressure drop would be at least twice the lower limit given by equation (X.5). Plot (d) of Figure 8.1 illustrates how ΔP_{min} is increased by extended bubble growth.

Plot (d) also demonstrates how the occurrence of these bubble events decreases the pressure peak, as a lesser proportion of the total gas-liquid momentum transfer is being synchronised. This effect is less marked in that, as shown by the film analysis, the initiation of many of the double and intermediate events is synchronised with that of the single events by the pressure fluctuations. However, as the proportion of pulsating jet events becomes smaller and early imperfect bubble rupture less common, then event synchronisation will become increasingly difficult and eventually stop.

Therefore, the occurrence of extended bubble events will not only increase the value of ΔP_{min} but also lead eventually to the cessation of event synchronisation.

8.1.2.4 Summary.

Three main mechanisms have been identified which will stop the synchronisation of events. These can be summarised as follows:

A) Event synchronisation stops when the minimum tray pressure drop equals the event initiation pressure drop.

B) Pronounced non-uniformity of events, mainly induced by liquid disorder or turbulence, will eventually stop event synchronisation. The influence of event non-uniformity is particularly great when ΔP_{min} approaches ΔP_i.

C) Increased occurrence of double and intermediate events and of more extensive bubble growth in single events, eventually stops event synchronisation.

These factors thus represent three modes by which the occurrence of pressure pulsations will cease. These modes are considered in the next section which relates them to the observed ranges of pulsation occurrence as detailed in Figure 5.4.

8.1.3 Modes of Pulsation Cessation.

8.1.3.1 Mode A. Cessation of pulsations when $\Delta P_{min} = \Delta P_i$.

In Chapter 7 the initiation pressure drop for operation at relatively low tray liquid heads was found to be in the range 170 to 210 N/m^2. For the trays used, the dry tray pressure drop is in this range for gas velocities of between about 11 m/s and 14 m/s, depending upon the dry tray loss coefficient. Hence, at such gas velocities, the lower limit of ΔP_{min} will equal ΔP_i and so, as explained in section 8.1.2.1, the pressure pulsations will cease. This area of cessation is indicated on Figure 8.2.

Such a range of maximum gas velocities is seen to correspond very well with the maximum velocities of pulsation occurrence found experimentally, as shown on Figure 5.4. It is of note that the plots for trays I, J, L(g), M and O show the maximum velocity to be fairly independent of tray liquid head for heads up to about 10 mm of water, indicating that the initiation pressure drop is fairly constant over this range.

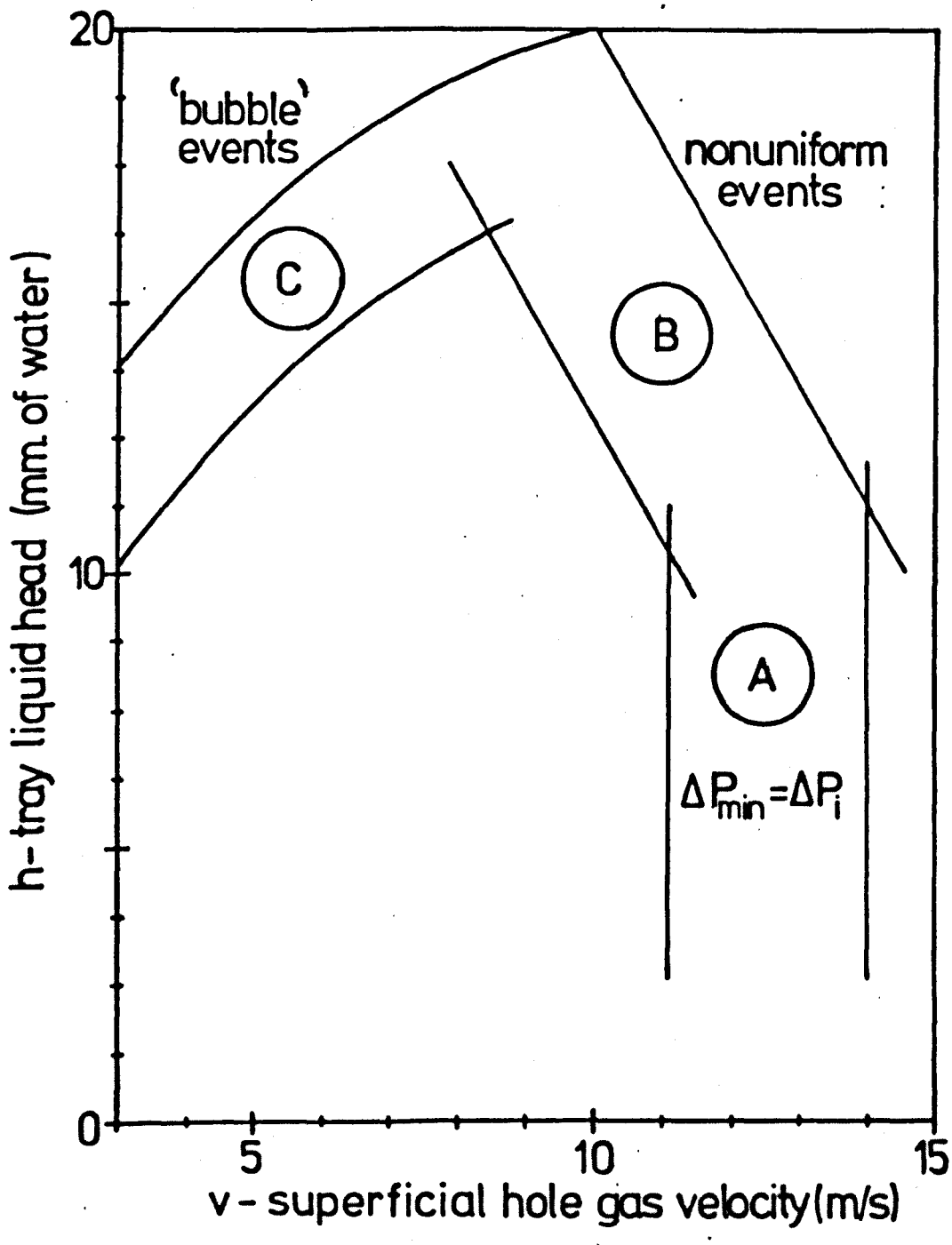

mode

A - minimum pressure drop = initiation pressure drop

B - decreased event uniformity

C - dominance of 'bubble' type events, depends upon gas volumetric flowrate

Fig. 8.2. MODES OF PRESSURE PULSATION CESSATION

This apparent lack of head dependence is not evident on the plots for trays with the smaller hole separations (B(g), C, E, F). These plots also show that the pulsations stop at a slightly lower gas velocity than expected. Although this may be partly due to the lower dry loss coefficients for these trays resulting in a lower initiation pressure drop, it is more likely to be due to extra variation in the single events occurring on these trays, as described in the next section.

8.1.3.2 Mode B. Cessation of pulsations due to decreased event Uniformity.

This mode of cessation is closely related to mode 'A' as the variations in the liquid motion of events is a primary factor with that mode.

The event uniformity is largely dependent upon general liquid disorder on the tray which, in turn, depends upon the magnitude and the rate of the gas-liquid momentum transfer and upon the quantity of liquid to which the transfer occurs.

The magnitude of the momentum transfer increases with increasing liquid head. The rate of momentum transfer will in general increase with increasing hole event frequency, which increases with increasing gas velocity. Thus, the level of liquid disorder required to stop pulsations will occur at lower tray liquid heads as the gas velocity is increased. This factor combined with the increasing association with mode 'A' cessation at the higher gas velocities, results in an area of Mode B cessation as indicated on Figure 8.2. All of the plots in Figure 5.4 show a line of pulsation cessation corresponding to this area. It is seen to be most marked and occurs at the lowest values of tray liquid head for those trays having the smaller hole pitch to diameter ratios. This is to be expected in that these trays have a smaller quantity of liquid per hole (this depends on the tray area per hole, given by $\frac{2\sqrt{3}}{\pi}\left(\frac{p}{d}\right)^2$), and also produced higher

event frequencies. As indicated earlier, this increased liquid disorder is likely to account for the occurrence of Mode A cessation at a slightly lower gas velocity than expected.

The amplitude plot for tray 0 shows the cessation due to this mode to occur at relatively high values of tray liquid head. This is possibly due to its large hole pitch/diameter ratio and the low hole event frequencies measured on this tray (and tray N).

At the higher values of tray liquid head prolonged 'bubble' events become more numerous and cessation Mode 'C' becomes more important.

8.1.3.3 Mode C. Cessation of pulsations due to the increased occurrence of double and intermediate events and to the extended bubble growth of single events.

These types of events result from the occurrence of complete hole closure during the waiting period. Several factors have an important effect on the extent of hole closure. The superficial hole gas velocity is important as it largely determines the minimum tray pressure drop. The lower this pressure drop the longer will be the waiting period and the greater the hole closure. Hole diameter is important with small diameters both facilitating hole closure and stabilising bubble growth due to increased surface tension effects. Tray liquid head is clearly important with higher heads favouring hole closure. The overall column gas volumetric flowrate also has an important effect on hole closure.

From equation (X.1) it follows that a given rate of tray pressure drop increase corresponds to a given fall in column volumetric flowrate. The maximum rates of pressure increase shown in Chapter 7 require falls in the flowrate of up to about 2 to 3 x 10^{-2} m^3/s, with the maximum value during the waiting period being about 10^{-2} m^3/s. In the range of pulsation production, the actual flowrates used were from 3 to 23.5 x 10^{-2} m^3/s,

except for trays K and N operating at gas velocities of 5 and 6 m/s (2.26 to 2.71 x 10^{-2} m^3/s). Therefore, in the vast majority of cases most of the gas flow passes continually through the tray. Thus, for synchronised behaviour, pulsating jet events will be dominant at the higher gas flowrates and will still occur at the lower values. However, for the trays of lower free area operating at low gas velocities, the flow reductions could constitute a substantial part of the overall flow and therefore there is scope for fairly widespread bubble formation. For example, in Figure 7.4 plot (e) (tray H(g), v = 5 m/s) the total volumetric gas flowrate through the tray falls from a mean value of just below 4 x 10^{-2} m^3/s to a minimum value of about 10^{-2} m^3/s, a substantial change in flowrate. However, for tray L(g) operating at the same gas velocity, a similar reduction in volumetric flowrate would still leave a minimum of about 8 x 10^{-2} m^3/s flowing through the tray. It is clear that bubble formation will be much more widespread for the lower free area trays such as tray H(g).

Results for film 23 (Table 6.3) showed a predominance of double and intermediate events to occur on tray H(g), whereas film 12 showed virtually none to occur on tray L(g) operating at the same conditions. The occurrence of imperfect bubble single events was also found to be more widespread on tray H(g) as compared with tray L(g), with much earlier bubble rupture occurring on the latter tray. (Also see evidence of double events in Table 6.1).

The area of pulsation cessation resulting from the dominance of 'bubble' events is shown on Figure 8.2, although its location will depend critically upon the gas volumetric flowrate. There is definite evidence in Figure 5.4 for pulsation cessation by this mode, although its effect is most manifest as a tendency gradually to reduce the pulsation amplitude. This factor is considered further in section 8.1.4.

This mode of pulsation cessation corresponds approximately to the spray-froth transition. The results support the idea presented in Chapter 2 that this transition is a gradual process with no definite sudden transition point. The correlations developed to predict froth-spray transition (e.g. Payne and Prince (32)), are in general based upon data obtained using high gas velocities and small hole diameters and are not really applicable to the operating conditions corresponding to pressure pulsation production.

8.1.4 Variation in the Amplitude of Pressure Pulsation.

The amplitude plotted in Figure 5.4 is the r.m.s. amplitude of the fundamental frequency component of the pressure pulsations measured in the chamber beneath the test-tray. This has no direct relationship to the actual magnitude of either the pressure pulsations beneath the tray or the fluctuations in the total tray pressure drop. However, there is an indirect order of magnitude relationship.

Because the components in the frequency analysis form a power spectrum their mean value will correspond to the mean chamber pressure. The r.m.s. amplitude of the fundamental component is therefore largely determined by the magnitude of pressure deviation from the mean value. As the pressure fluctuations above and below the tray are very similar (but inverted), it is fairly accurate to relate the measured r.m.s. amplitude to the deviations of the total tray pressure drop from its mean value. For the case of equal sinusoidal fluctuations occurring 180^{o} out of phase above and below the tray, the r.m.s. amplitude measured below the tray equals $1/2\sqrt{2}$ times the peak deviation of the tray pressure drop from its mean value.

The observed pressure fluctuations are not sinusoidal and the minimum and maximum pressure deviations are not generally the same. The largest minimum deviation equals $\Delta P_{mean} - \Delta P_{min}$ and this has an upper limit

corresponding to the tray liquid head plus the residual pressure drop (see equations (X.5) and (3.5).). As shown in Figure 8.1 the largest maximum deviation corresponds to $(\Delta P_i - \Delta P_{mean})$ plus the height of the pressure peak above ΔP_i, which will increase with increases in both the tray liquid head and the degree of event synchronisation. Figure 8.3 illustrates how these factors will influence equivalent sinusoidal fluctuations with the minimum value having a greater influence than the much more transient peak value. Assuming the minimum pressure deviation to be dominant gives a very approximate guide to the value of the measured r.m.s. amplitude, i.e.

$$A \simeq \frac{1}{2.5} (\Delta P_m + \Delta P_r) \qquad N/m^2 \qquad (8.1)$$

The pressure drops in Table 7.2 indicate a residual pressure drop of about 40 N/m^2, giving the relationship:

$$A \simeq \frac{1}{2.5} (H.\rho_\ell.g. + 40) \qquad N/m^2 \qquad (8.2)$$

The amplitudes predicted by equation (8.2) agree fairly well with the maximum measured r.m.s. amplitudes (Figure 5.4) particularly for tray L(g).

As the degree of event synchronisation and the percentage of single events decrease, the pulsation r.m.s. amplitude will fall below the value predicted by equation 8.1 The difference $\Delta P_i - \Delta P_{mean}$ is also important and when this becomes small at the higher gas velocities then the pulsation amplitude can be expected to fall. The same factors which were responsible for the actual cessation of the pulsations, as indicated on Figure 8.2, will therefore tend gradually to decrease the pulsation amplitude prior to complete cessation. The results in Figure 5.4 demonstrate this, with decreases in the amplitude associated with cessation modes A, B and C being clearly evident on most of the plots. The amplitude decrease at the higher

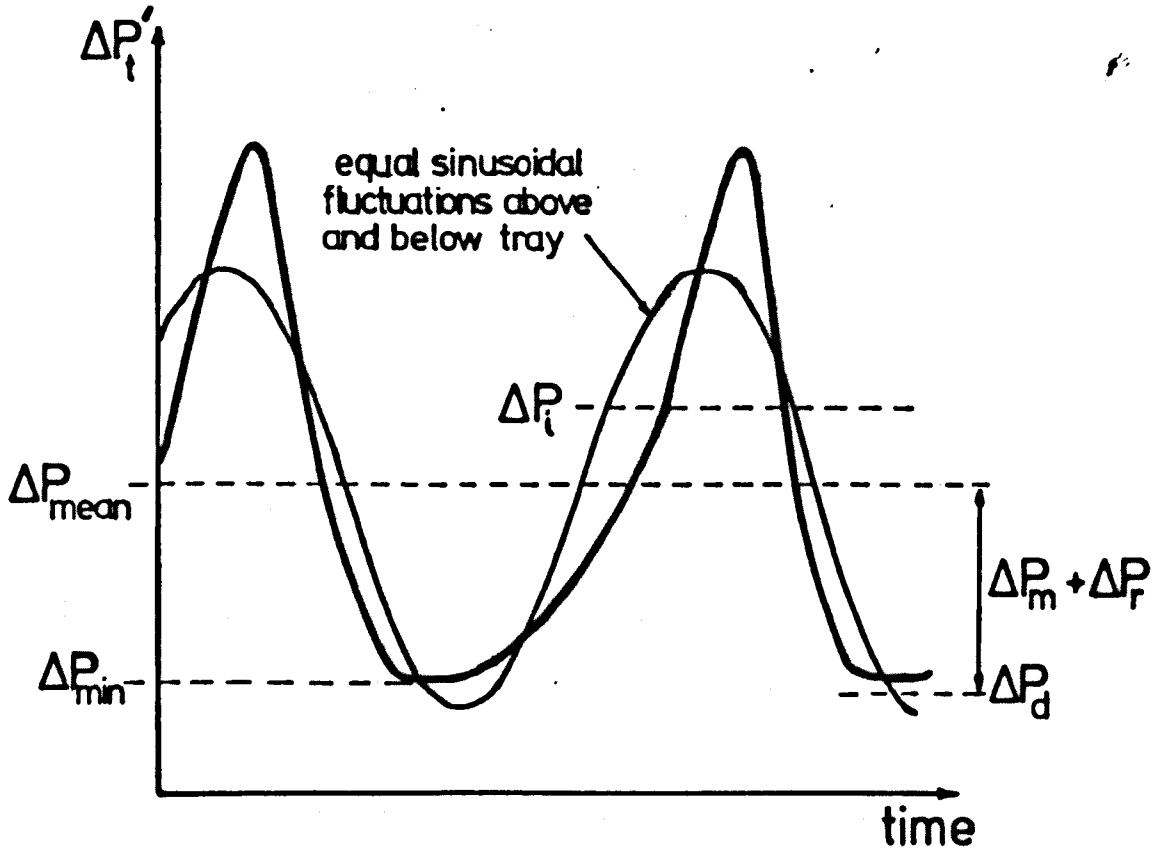

Fig. 8.3. AMPLITUDE OF PRESSURE FLUCTUATION

gas velocities may result however more from the decrease in the difference ($\Delta P_i - \Delta P_{min}$) than from a decrease in event synchronisation due to mode A, ($\Delta P_i = \Delta P_{min}$).

The amplitude decrease associated with cessation mode C (dominance of 'bubble' events) can be seen to vary significantly for the different trays. This variation can be attributed mainly to the changes in the overall gas volumetric flowrate, as dicsussed in section 8.1.3.3. The much lower amplitudes measured on trays M and O as compared with those for tray L(g) exemplify this. The same effect is evident in the comparison of the plots for trays E and C and of those for trays L(g), I and H(g). The effect is not so apparent in the series of plots for trays I, J and K, with the decrease in amplitude with decreasing volumetric flowrate being much more general.

Another experimental finding was that the amplitude was independent of the capacitance of the chamber beneath the test-tray (see Figure 5.13). This finding is consistent with the concept of a critical initiation pressure drop which will effectively control the pulsation amplitude independently of the chamber capacitance. It might have been expected that the changes in chamber capacitance would have affected the extent of mode C cessation at the low gas velocities on trays B(g) and H(g). The lack of evidence for such an effect is due probably to the changes in capacitance being too small.

Tray liquid crossflow velocity was found to have a variable effect on the pulsation amplitude. The differing behaviour can be accounted for largely in terms of the affect of crossflow on event uniformity and synchronisation. For the conditions used on tray B(g) ($v = 5$ m/s), Figure 5.4 shows Mode C (dominance of 'bubble' events) cessation to have reduced the pulsation amplitude. Liquid crossflow will counteract this

reduction by limiting event growth and also by tending to 'overwhelm' small variations in event liquid flow. The crossflow will also tend to increase the rate of hole closure thus reducing the waiting period. These factors will tend to increase the degree of event synchronisation and therefore the pulsation amplitude.For the conditions used on tray L(g) the event behaviour is highly synchronous and uniform in the absence of liquid crossflow. Thus there is little scope for an increase in amplitude and this explains why crossflow had little affect on the amplitude for this tray. For tray H(g) the increase in pulsation at the higher crossflow velocities in quite marked. Again this can be explained in terms of the crossflow restricting event growth and thus discouraging double event growth. Plots (e) and (f) of Figure 6.10 show an increase in the proportion of single events in the presence of liquid crossflow.

It can be concluded that the proposed model of pulsation production, dominated by the critical initiation tray pressure drop for the pulsating jet event, accounts largely for the observed occurrence of the pulsations and explains most of the measured variations in pulsation amplitude with regard to both the tray geometry and the operating conditions. It is therefore possible to use this model to predict how the occurrence of the pressure pulsations is likely to be affected by the tray or column geometry or by the physical properties of the operating fluids.

8.1.5 Prediction of the Effects of Column and Tray Geometry and Fluid Physical Properties on the Occurrence of Pulsations.

The effect of changing tray geometry on the pulsations has been covered adequately by using a wide range of tray geometries in the experimental work. For hole diameters below 4.76 mm., liquid surface tension may tend to limit the occurrence of pulsations at the lower gas velocities.

The tray thickness is unlikely to be important, except for any small effect which it may have on the event initiation pressure drop.

The occurrence of the pulsations has been shown to be little affected by changes in the system (column) geometry, although the changes performed were relatively small. The cessation of pulsations at low gas velocities has been shown to depend upon the relationship between the gas volumetric flowrate and the column chamber capacitances.

The structure and geometry of the column are important if mechanical or acoustic resonance occurs at the pressure pulsation fundamental frequency, as this will lead to increased column damage.

The likely effects of liquid physical properties on the pulsations can be summarised as follows:

i) Gas density. Density is the only gas physical property likely to affect the pulsations. Mode "A" pulsation cessation depends upon gas density, the superficial hole gas 'F' factor ($= v.\rho^{0.5}$), being the relevant gas flow parameter. F_{max}, the maximum value of 'F' for pulsation production, depends upon the dry tray loss coefficient and the event initiation pressure drop, i.e.

$$\Delta P_i = \frac{1}{2} . K . (F_{max})^2 = \frac{1}{2} . K.\rho. (v_{max})^2 \qquad N/m^2 \qquad (8.3)$$

For the air-water system, ΔP_i had a value of approximately 200 N/m^2. If the same value can be applied to other systems with different gas densities, then typical values of the maximum gas velocity for pulsation production are indicated in Table 8.1, for various values of gas density and dry tray loss coefficient. It must be remembered that these maximum velocities correspond to operation at relatively low tray liquid heads, and for heads above say 10 mm of water the maximum velocity will be below the value indicated.

TABLE 8.1 EFFECT OF GAS DENSITY AND DRY TRAY LOSS COEFFICIENT ON THE MAXIMUM GAS VELOCITY FOR PULSATION PRODUCTION.

Gas density Kg/m^3	Dry tray loss coefficient, K			
	1.5	2.0	2.5	4.0
	v_{max}, m/s (ΔP_i = 200 N/m^2)			
39.6	2.6	2.25	2.0	1.6
4.6	7.6	6.6	5.9	4.7
1.25	14.6	12.65	11.3	8.9
1.0	16.3	14.1	12.65	10.0
0.12	47.1	40.8	36.5	28.9

ii) and iii) Liquid density and liquid viscosity. The quantity of liquid on the tray has been expressed in terms of the tray liquid head (= $H_f . \rho_\ell . g$), which effectively accounts for variations in liquid density. In this work most pulsations have been observed to occur at liquid heads of below 20 mm of water (≈ 200 N/m^2, as ρ_{water} = 1000 kg/m^3). This is equivalent to a head of about 13 mm of pure nitric acid (density 1500 kg/m^3) or of about 25 mm of acetone (density 792 kg/m^3). The large majority of liquids used in industrial sieve-tray columns have densities within this range.

Liquid viscosity is also likely to affect the maximum head for pulsation occurrence as it will influence the degree of liquid disorder or turbulence on the tray. Although it may be possible to use a form of Reynolds Number as a turbulence criterion for predicting the maximum liquid head for pulsation occurrence, there are problems in defining a characteristic liquid velocity. However, it may be possible to assume

that the maximum head for pulsation occurrence is inversely proportional to liquid viscosity, i.e.

$$\frac{H \cdot \rho_\ell \cdot g}{\mu} < 2 \times 10^5 \ s^{-1} \text{ for pulsation occurrence.}$$

However, the propensity for bubble formation at high tray liquid heads will make this relationship invalid for viscosities much greater than that for water ($\simeq 10^{-3}$ kg/m.s).

Increasing viscosity may reduce the event liquid lateral spread, thus reducing the possibility of event interference on trays with small hole pitch. Viscosity may also influence the force required to induce the initiation of the pulsating jet.

iv) Liquid surface tension. Decreasing surface tension will reduce slightly the propensity for bubble formation and therefore encourage pulsation production, particularly at low gas velocities and for trays with small hole diameter and low free area. Decreasing surface tension may reduce the event initiation pressure drop, thus reducing the maximum hole gas 'F' factor for pulsation occurrence.

It is important to note that the majority of fluid systems of interest will have a value of surface tension below that for the air-water system ($\simeq 72.8 \times 10^{-3}$ N/m).

It can be concluded that although liquid physical properties are likely to affect the production of regular pressure pulsations, they are normally unlikely to affect any major increase in the area of operation over which the pressure pulsations occur, as found for the air-water system and as defined in terms of the tray liquid head and the superficial hole gas 'F' factor. Thus, the problem of damaging vibrations can be considered as being largely confined to operation at relatively low values of the

tray liquid head (below about 200 N/m^2) and the hole gas 'F' factor (below about 16 $kg^{0.5}/m^{0.5}$ s).

8.2 CORRELATION AND PREDICTION OF THE PRESSURE PULSATION FREQUENCY.

Knowledge of the pulsation frequency is necessary in order to avoid the occurrence of any system mechanical or acoustic resonance and consequent damage. Also, the hole event frequency affects other factors, not necessarily related to the production of pulsations, such as the rate of liquid entrainment and the degree of gas-liquid mixing and mass transfer on the tray.

The dominant type of event controlling the production of the pressure pulsations has been shown to be the pulsating jet. The pressure pulsation frequency will therefore correspond mainly to the pulsating jet frequency. Studies of gas-liquid interaction on single hole trays have been concerned almost entirely with 'bubble' events, during which the gas flow is restricted by bubble formation throughout the entire event period. Models of such events are therefore inapplicable to the prediction of the pulsation frequency. Waddington (2) and Brown (54) developed equations to predict hole event frequency on multi-hole trays; however, these were again based upon bubble events, and have been shown to be inadequate.

As previously mentioned, an attempt at modelling the pulsating jet event has been carried out by Muller (62) and this is considered in more detail in the next section.

Firstly, however, it should be noted that accurate frequency prediction of events occurring in industrial columns will be limited in that the precise tray operating conditions, in particular the tray liquid head, will be extremely difficult to specify exactly. Furthermore, as the conditions will change both with the position of the tray in the column and with the variations in the fluid loadings occurring during start-up, shut-

down, and normal running, then, if pulsations are likely to occur, their frequency is likely to cover a fairly broad range. Hence, the only way to avoid resonance damage is to ensure that the column mechanical and acoustic fundamental frequencies are well outside the pulsation frequency range. It is therefore perhaps more important, for this application, to be able to predict how the range of pulsation frequency will be affected by the liquid physical properties than it is to be able to predict the variation in frequency, within that range, with changes in operating conditions.

8.2.1 The Pulsating Jet Model of Muller (62).

Muller studied the pulsating jet event on a single hole tray below which was a well defined chamber volume supplied with a constant flow gas supply through a sonic nozzle. The chamber above the tray was at a constant reference pressure. A semi-empirical model was developed in order to interpret the experimental data and to give some insight into the mechanism of jetting.

Muller interpreted the pulsating jet event as occurring in two stages. During the first stage, gas-liquid momentum transfer with liquid entrainment occurs, and in the second stage the liquid flows back toward the hole, independently of the gas flow. An electrical analogue with 'lumped'parameters was developed to describe the system behaviour. Due to poor understanding of the fluid dynamics governing the liquid motion several of the lumped parameters were the product of highly empirical estimates, in particular those controlling the event frequency, which can be summarised as follows.

The factors determining the first stage of the event were the inertial mass of liquid acted on per event, (L_2), a friction factor determining the magnitude of the gas-liquid momentum transfer, (R), the average

gas volumetric flowrate, $(v.a_h)$, and the period over which momentum transfer was deemed to occur, (T_2).

L_2 was taken to equal the 'acoustic'(inertial) mass of the liquid occupying a cylinder with cross-sectional area equal to the hole area, and height equal to the liquid depth, and expressed as:

$$L_2 = 0.95 \cdot \rho_\ell \cdot H \cdot /a_h \qquad kg/m^4$$

R was based on the expression:

$$H.\rho_\ell.g + \Delta P_r = v.\ a_h.\ R.\quad x(\text{constant})$$

Assuming the pressure loss on the L.H.S. to be proportional to v^2, the final expression developed for R was:

$$R = 634 \cdot v \cdot H / a_h \qquad N.s/m^5$$

This value of R was maintained for the period T_2 and then had a zero value for the remainder of the event first stage and all of the second stage.

T_2 was a purely empirical, variable, time. Its value was adjusted in each computer solution of the analogue until the predicted frequency equalled the expected experimental value. In doing this Muller found that the required value of T_2 increased approximately in proportion to the liquid depth and decreased approximately as the square of the gas velocity.

The period of the second stage (liquid fall-back) was governed by two parameters, L_2 and C_2, the latter representing the 'elasticity' of the liquid bulk, causing it to flow back into the area of the hole. The period of the second stage corresponded to the natural frequency:

$$f_o = 1/2.\pi.\sqrt{L_2.C_2}$$

(In the text this was given as $1/2.\pi.(L_2.C_2)$).

C_2 was given a constant value of 1.76×10^{-9} m^5/N, this giving the best empirical fit,but there was no indication of how it might depend upon fluid properties. This value was claimed to give a natural frequency of 15.5 Hz. for a 6.35 mm diameter hole at a depth of 2 cm., this corresponding approximately to the minimum pulsating jet frequency observed at that depth. (A repeat calculation showed this to require $C_2 = 1.76 \times 10^{-10}$ m^5/N). It is of note that the plot of Mullers empirical and predicted frequencies indicates $f_o \propto 1/\sqrt{H.d^2}$, whereas his expressions for f_o and L_2 give $f_o \propto \sqrt{d^2/H}$.

In the model, the event frequency is higher than the 'natural' frequency because the period of the first stage is reduced by the short impulse of momentum transfer. Increasing R or decreasing T_2 increases the event frequency.

Once the lumped parameters had been adjusted for a given run, the model predicted quite accurately the pulsation frequency, the mean hole pressure drop and the pressure pulsation amplitude beneath the tray. However, the frequency prediction is a direct consequence of empirical fitting. The frequency is essentially controlled by the nature of the liquid motion on the tray and Mullers model gives little insight into this, or as to how it will be affected by the fluid physical properties or the close proximity of neighbouring holes.

It is important to note that Muller used relatively high gas velocities (> 15 m/s) and that the events studied corresponded to operation with $\Delta P_{min} > \Delta P_i$. As shown earlier, such events would have a negligible 'waiting period', and would not be synchronised when occurring on multi-hole trays. Such events occurring on a multi-hole tray

would therefore not be subject to any tray pressure drop fluctuations, (such as are present in the single hole system). Because of this there would quite possibly be different behaviour of a multi-hole tray and Mullers single hole tray for the same operating conditions. This criticism of single hole systems is even more applicable to 'bubble' events (particularly 'double bubble' and 'delayed release' events). These have been shown to be highly dependent upon fluctuations in chamber pressure. It is suggested that, when a single hole tray is used to study hole events which will not be synchronised on a multi-hole tray, then the tray pressure drop should be maintained constant. With the chamber above the tray at atmospheric pressure, the pressure beneath the tray may be maintained fairly constant by using a very large chamber, or a vented gas flow through a constant resistance. For better chamber pressure control, gas flow (approximately ten times the hole flow rate) could be vented through a fluidic pressure control valve constituting a jet pump and a vortex amplifier, similar to those described by Tippetts et al. (64).

It can be concluded that Muller's description of the pulsating jet event agrees well with that proposed in this work. However, Muller's analysis does not attempt to describe the fluid dynamics controlling the event frequency, and is of limited use in predicting frequency.

Muller indicates that the rate at which the liquid flows back toward the hole is proportional to the square root of the liquid head and independent of the gas flow, that the time for gas-liquid momentum transfer increases with decreasing gas velocity and increasing liquid depth, and that the magnitude of the transfer increases both with tray liquid depth and gas velocity.

8.2.2 Factors Controlling the Pressure Pulsation Frequency.

The prediction of the pulsation frequency based upon analysis of the controlling fluid dynamics is clearly beyond the scope of this work, both because of the required depth of such an analysis and because of the lack of detailed knowledge of the controlling fluid flow mechanism. It is possible however, that some insight into the effect of the fluid physical properties and the operating conditions on the pulsation frequency may be gained from a preliminary analysis of the pulsating jet event and from inspection of the empirical frequency data.

8.2.2.1 Factors controlling the frequency of the pulsating jet event.

Although the pulsating jet has been identified as the major event controlling the pulsation frequency, it must be remembered that other types of event occurring simultaneously on the tray will also influence the frequency.

The hole event (or pulsation) frequency is considered in terms of the event duration, t_t, (= 1000/f ms). Figure 8.4 shows the main stages of the pulsating jet event and also indicates the corresponding tray pressure drop fluctuation.

The event is divided into two main stages, (similar to those of Muller (62)).:

$$t_t = 1000/f = t_{max} + t_f \quad \text{ms} \qquad (8.4)$$

where:

t_{max} = time to reach maximum liquid radial spread.

t_f = time for the liquid to fall-back to the hole and for the initiation pressure drop to be reached. This time includes the waiting period, t_w, (absent in Muller's event).

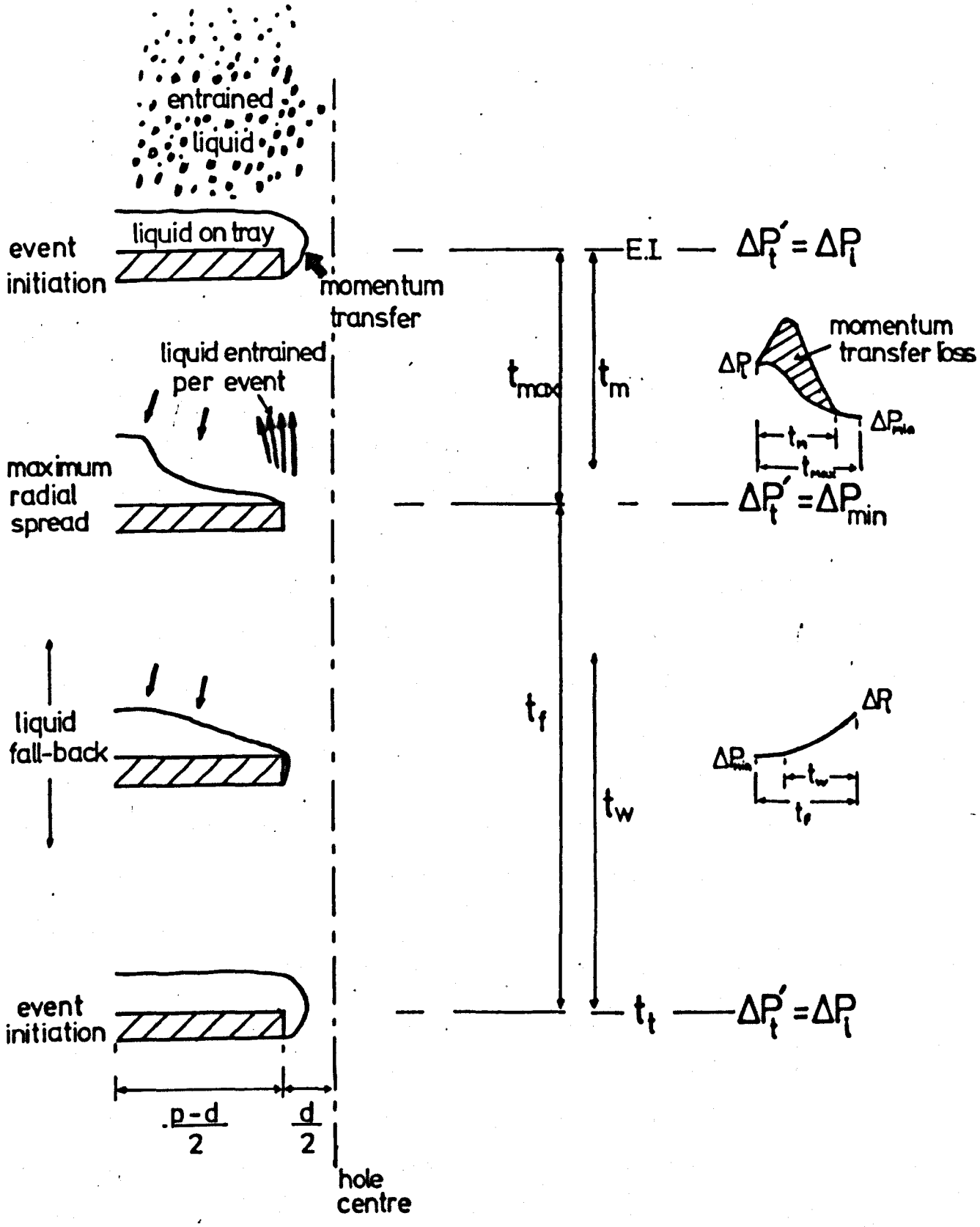

Fig. 8.4. PULSATING JET MECHANISM AND CORRESPONDING TRAY PRESSURE DROP FLUCTUATION

Contained within the first stage (t_{max}) is the period t_m during which the gas-liquid momentum transfer occurs (Muller's T_2). Muller (62) assumed that the total tray loss coefficient had a constant high value during momentum transfer. Figure 7.8 clearly shows this assumption to be inaccurate, the loss coefficient in fact rising to a transient peak value and then falling to a minimum.

In Chapter 7 the variation in loss coefficient was used to identify the maximum spread time (minimum loss coefficient). These values are shown in Table 8.2. Also shown are values for t_m based upon the point at which the loss coefficient no longer exhibits a rapid decline, and the fallback time, t_f. Times are also given for other operating conditions, based upon the pressure drops given in Table 7.2. These values are likely to be less accurate than those based upon the loss coefficient in that they do not account for gas flow fluctuations and gas inertial losses. However, the end of the rapid pressure drop decline should indicate fairly well the cessation of momentum transfer, thus t_m is given in preference to t_{max}. Table 8.2 also gives values of t_{max} and maximum radial spread distance as obtained from the film analysis (Table 6.4).

As already noted there is good agreement of the maximum spread times obtained from the film analysis with those from the flow/pressure analysis. For tray L(g) operating at v = 5 m/s., the values for t_m are less than the observed values of t_{max}, indicating most of the momentum transfer to have ceased before maximum radial spread is reached. The same indication is evident for tray H(g) at this gas velocity.

The time for momentum transfer, t_m, is seen to increase with increasing tray liquid head. This agrees with Muller's finding that T_2 increased with increasing head, but there is little evidence for his claim

TABLE 8.2 STAGE DURATIONS FOR PULSATING JET EVENT.

Tray	H(g)	H(g)	H(g)	L(g)	L(g)	L(g)	L(g)	L(g)	L(g)	L(g)
v(m/s)	5	7	9	5	5	7	7	7	7	9
h ($mm.H_2O$)	5.25	5.0	5.25	5.5	12.0	2.75	5.25	8.5	10.75	5.75
t_t=1000/f (ms)	71.4	51.0	40.0	64.9	55.6	52.1	51.0	49.0	47.2	42.0
Stage times (ms) from flow analysis (Chapter 7)										
t_{max}	28.5	20.0	17.5				25.0			22.5
t_m	(21.0)	(20.0)	(17.5)	20.0	27.5	15.0	(20.0)	25.0	27.5	(20.0)
t_f	43.0	30.0	22.5	45.0	27.5	37.5	25.0	25.0	20.0	20.0
Results from cine-film analysis (Table 6.4)										
t_{max}	26.3	21.5	17.4	33.8	34.1		25.5			22.0
s_m (mm)	7.7	5.5	4.2	7.3	6.4		5.2			4.3
Times from equation (8.5).										
t_t	69.2	51.4	41.0	66.0	55.8	54.2	50.6	47.8	46.6	41.5
16+h	21.25	21.0	21.25	21.5	28.0	18.75	21.75	24.5	26.75	21.75

All times in milliseconds.

that T_2 decreased as the square of the gas velocity increased. Muller claimed that the magnitude of the momentum transfer increased with increases in both the head and the gas velocity. The maximum spread distances are a good indication of the momentum transferred per event (larger impulses displacing more liquid). Although there is indication that momentum transfer increases with increasing head, there is a strong indication that it decreases with increasing gas velocity, consistent with the increase in event frequency and small decline in residual pressure drop. Some decrease in the liquid spread may occur at the higher gas velocities due to a greater proportion of the momentum being transferred to entrained liquid. (It should be noted that Muller maintained a constant depth of clear water on his single hole tray, irrespective of entrained liquid, whereas in this work entrained liquid constituted part of the measured tray liquid head. One effect of this is that the residual pressure drop of Muller will include losses due to maintaining the entrained liquid).

In Figure 8.4, a period was indicated during fall-back during which little hole restriction occurred and there was only a small rise in pressure drop. Such a period is evident for most of the pressure drops listed in Table 7.2. However, it is normally difficult to determine when this period ends and the more rapid rise in pressure drop associated with the waiting period begins. It should be noted that some of the times for fall-back given in Table 8.2 include the short time ($t_{max}-t_m$). The fall-back times shown clearly decrease with increasing tray liquid head, in agreement with the finding of Muller (62). Muller also indicated that fall-back was independent of the gas velocity, whereas there is clear indication in Table 8.2 that the fall-back time decreases

with increasing gas velocity. This decrease can be attributed partly to the reduction in the event radial liquid spread. The main reason however is likely to be the increase in the minimum pressure drop reducing the waiting period; this factor would be absent in Muller's system for which $\Delta P_{min} > \Delta P_i$.

Factors affecting the waiting period.

A good indication of the way in which the waiting period is affected by the various system parameters can be obtained from the flow analysis developed in Appendix X.

The relationship,

$$\frac{d\,\Delta P_t'}{dt} = \frac{2.c^2.\rho}{Q_e}\left(G - \left(\frac{\Delta P_t'}{S_1}\right)^{0.5} d'^{2.1}\right) \quad N/m^2 s \qquad (X.4)$$

was integrated numerically assuming a linear rate of hole closure;

$$d' = d - S_2.t \qquad (X.6)$$

The times obtained for the pressure drop to rise from the lower limit of ΔP_{min} (dry tray pressure drop) to the initiation pressure drop, ΔP_i, for various values of the controlling parameters, are listed in Tables 8.3 to 8.7.

For a tray liquid head of about 5 mm of water, Figure 7.8 indicates a hole closure rate in the range 0.11 to 0.18 m/s, the rate tending to increase with time. Despite the simplifying assumption of linear hole closure the theoretical times show good agreement with those predicted from the experimental results. The theoretical times corresponding approximately to the fall-back times given in Table 8.2 are underlined, (although some of these assume $\Delta P_i = 200\ N/m^2$ for tray L(g)).

Consideration of the theoretical times leads to the following main conclusions:

TABLE 8.3 EFFECT OF GAS VELOCITY AND RATE OF HOLE CLOSURE ON THE WAITING PERIOD - ΔP_i = 200 N/m^2; Q_e = 0.255 m^3.

Tray	v m/s	ΔP_{min} (N/m^2)	S_2, rate of hole closure (m/s)			
			0.1	0.1414	0.2	0.4
			t_w, waiting period (ms.)			
B(g)	5	23.4	30.3	22.4	16.8	9.8
B(g)	7	47.8	22.3	16.6	12.5	7.4
B(g)	9	79.0	15.7	11.8	9.0	5.4
B(g)	11	118.0	10.0	7.6	5.9	3.7
H(g)	5	33.1	40.5	30.4	23.1	13.9
H(g)	7	64.9	28.0	21.2	16.2	10.0
H(g)	9	107.3	17.7	13.6	10.6	6.8
H(g)	11	160.3	8.4	6.7	5.4	3.6
L(g)	5	28.6	61.9	44.6	32.3	17.4
L(g)	7	56.0	43.8	31.6	22.9	12.4
L(g)	9	92.6	28.4	20.6	15.0	8.3
L(g)	11	138.4	14.8	10.9	8.1	4.7

TABLE 8.4 EFFECT OF TRAY GEOMETRY ON WAITING PERIOD - ΔP_i = 200 N/m^2; v = 7 m/s; S_2 = 0.1414 m/s; Q_e = 0.255 m^3.

Tray	B(g)	C	E	G	H(g)	L(g)	O
t_w (ms)	16.6	21.8	21.9	21.3	21.2	31.6	31.4
ΔP_{min} (N/m^2)	47.8	45.0	61.2	64.3	64.9	56.0	67.7

TABLE 8.5 EFFECT OF CHAMBER VOLUME ON WAITING PERIOD.

- TRAY L(g) : ΔP_i = 170 N/m^2; v = 9 m/s ; S_2 = 0.1414 m/s.

- TRAY H(g) : ΔP_i = 200 N/m^2; v = 5 m/s ; S_2 = 0.1414 m/s.

Tray	ΔP_{min} (N/m^2)	Q_e equivalent chamber volume (m^3)					
		0.1	0.15	0.2	0.25	0.3	0.35
		t_w, waiting period (ms)					
L(g)	92.6	15.6	16.0	16.3	16.6	16.9	17.2
H(g)	33.1	26.6	27.9	29.1	30.3	31.4	32.4

TABLE 8.6 EFFECT OF INITIATION PRESSURE DROP ON WAITING PERIOD

- TRAY L(g); v = 7 m/s; S_2 = 0.2 m/s ; Q_e = 0.255 m^3

ΔP_{min} = 56 N/m^2.

ΔP_i (N/m^2)	170	200	220
t_w (ms)	20.3	22.9	24.4

TABLE 8.7 EFFECT OF GAS DENSITY ON WAITING PERIOD

- TRAY L(g) : ΔP_i = 170 N/m^2; Q_e = 0.255 m^3; S_2 = 0.2 m/s.

v(m/s)	ρ(Kg/m^3)	$F = v.\rho^{0.5}$	ΔP_{min}(N/m^2)	t_w(ms.)
22.59	0.12	7.83	56.0	23.8
7.0	1.25	7.83	56.0	20.3
3.649	4.6	7.83	56.0	19.4
1.244	39.6	7.83	56.0	18.7
7.0	0.5	4.95	22.4	34.6
7.0	3.0	12.12	134.5	5.1
7.0	4.5	14.85	201.8	-

i) The superficial hole gas velocity has a major effect on the waiting period, this being primarily due to the effect of the velocity on the minimum pressure drop.

ii) The rate of hole closure is the other major factor affecting the waiting period. This rate will be influenced mainly by the quantity of liquid on the tray. The fall-back analysis of Muller (62) indicated rate $\alpha\sqrt{\text{liquid depth}}$. (It should be noted, however, that the rate is not necessarily proportional to $\sqrt{\rho_\ell}$). This makes the closure rate 0.4 m/s equivalent to a liquid head of between 30 and 40 mm of water.

iii) The waiting period decreases slightly with increasing gas volumetric flowrate.

iv) Increasing the hole diameter increases the waiting period. This can be attributed to the area of a large hole being reduced by a lesser proportion than that of a small hole for the same reduction in diameter. This factor tends to be offset by the greater gas volumetric flowrate and the lower tray loss coefficient associated with the larger holes.

v) The waiting period increases slightly with decreasing chamber volume, the effect being more marked at lower gas volumetric flowrates.

vi) At a constant 'F' factor, decreasing the gas density slightly increases the waiting period, this being equivalent to increasing the chamber volume. At constant gas velocity, the gas density has a major affect on the waiting period, due to the density affecting the minimum tray pressure drop.

vii) Increasing ΔP_i increases the waiting period, but by a lesser amount than an equivalent change in the value of ΔP_{min}.

From the numerical solution it is possible to calculate the hole gas velocity at event initiation, based upon the values of d' and G_1' at

that point. This velocity is found to be fairly constant for a given tray, increasing only slightly with increasing superficial hole gas velocity. There is some variation with tray geometry but for the conditions considered this 'initiation' gas velocity lies mostly in the range 11.5 to 13.5 m/s. This is consistent with the finding that the time for momentum transfer, t_m, is largely independent of the superficial hole gas velocity. At higher gas velocities, when there is no waiting period (or event synchronisation), the time for momentum transfer may depend upon the gas velocity. The pulsating jet event of Muller (62) had no waiting period and he claimed that the value of t_m decreased with increasing gas velocity.

Further indication of the relative importance of the factors controlling the event frequency can be obtained from inspection of the experimental frequency data.

8.2.2.2 Correlation of the experimental frequency data.

Extensive pulsation frequency results were presented in Chapter 5. Expressing the frequency in terms of the event duration, t_t, much of the data is well represented by the purely numerical relationship:

$$\frac{1000}{f} = t_t = \left(0.152 - 0.24\,\frac{(\sqrt{h}-\sqrt{2})}{\sqrt{p}}\right).\sqrt{\frac{p-d}{p}}\,.\,\frac{10^4}{(n\,d^2)^{0.25}}\left(\frac{\sqrt{d}}{v} - 0.15\right) + 16 + h \qquad (8.5)$$

for $19.05<p<66.0$ mm; $4.76<d<15.87$ mm; $38<n<403$; $4<v<15$ m/s;

$2<h<25$ mm of water.

It is stressed that this is a purely numerical empirical fit of the data and has no foundation in the physical processes involved. However, it is useful in that it indicates the relative importance of the system variables investigated with respect to the pulsation frequency.

The event durations predicted by equation 8.5 are given in Table 8.2 and show a very good fit with the measured durations. Other predicted values are plotted on Figures 5.7, 5.8 and 5.10, and again a good fit with the measured pulsation frequencies is evident.

It is of particular note that the period (16+h), as shown by Table 8.2, is very similar to the value of t_m, the period for momentum transfer. This indicates that the remaining period in equation (8.5) is equivalent to the time required for the liquid motion to restrict the gas flow sufficiently to induce event initiation (i.e. $t_f + t_{max} - t_m$). The terms of the equation support this idea. The equation identifies the square root of the tray liquid head as the controlling liquid head parameter, as was indicated by Muller in his fall-back analysis. The influence of p and (p-d) can be taken to represent the effect of event interference or restriction. The term $1/(n\ d^2)^{0.25}$ can possibly be interpreted as representing the influence of the chamber capacitance/volumetric flowrate effect on the pressure drop build-up during the waiting period. The results showed the frequency to be largely unaffected by changes in the volumetric flowrate resulting solely from a change in the hole diameter. The equation accounts for this by the inclusion of the $\sqrt{d}/v$ term. It was shown in the previous section that the lack of dependence of frequency upon diameter can be attributed to the smaller relative area reduction of a given hole closure on a large hole as compared with a small hole.

In equation (8.5) the period associated with flow restriction becomes zero when $v = 0.15/\sqrt{d}$ or when $h = \left(\frac{15.2\sqrt{p}}{24} + \sqrt{2}\right)^2$. These are artificial limits produced by the empirical fitting. The single hole pulsating jet frequencies of Muller (37) (see Figure 3.3) clearly

show the velocity limit to be in error, (particularly for the smaller hole diameters), with the frequency continuing to rise with increasing gas velocity up to a value of at least 30 m/s. It is of interest to note, however, that at this gas velocity Muller's frequencies correspond to the limiting period 16 + h, as indicated by Table 8.8. Some agreement can

TABLE 8.8 COMPARISON OF THE MAXIMUM PULSATING JET FREQUENCY OF MULLER (37), (v = 30 m/s), WITH THE PERIOD 16 + h.

	h - Tray liquid head, (mm of water)			
	10	15	20	30
$1000/f_{max}$ (ms)	27.0	30.0	35.1	43.5
16 + h	26.0	31.0	36.0	46.0

be expected in that Muller used an air-water system. However, it should be noted that Muller's results indicate a further possible rise in frequency for an increase in velocity above 30 m/s.

Equation (8.5) does not include the effect of tray liquid crossflow velocity on the frequency. The measured increase in frequency with increasing crossflow velocity can be attributed to the crossflow increasing the rate of hole closure and thus reducing the waiting period. The tendency of crossflow to reduce the occurrence of bubble events may also affect the frequency.

8.2.3 Summary of the Prediction of Pressure Pulsation Frequency.

The analysis indicates that the pulsating jet event is made up of two main stages. The first stage is associated with gas-liquid momentum transfer. The second stage is associated with the restriction of the gas

flow through the tray holes by the liquid on the tray which causes the tray pressure drop to rise to the critical value required for event initiation.

The duration of the first stage, t_m, is largely independent of the superficial hole gas velocity but increases in proportion to the tray liquid head. This lack of dependence upon velocity probably results from the instantaneous hole gas velocity at event initiation being largely independent of the superficial hole gas velocity.

The second stage consists of the time required for the liquid to stop flowing away from the hole and to start restricting the gas flow, plus the time required for the pressure drop to build up to the initiation pressure drop (the waiting period). The initial period of this stage decreases with increasing gas velocity and is also affected by the hole pitch, its duration being considerably reduced when event interference occurs. The duration of the waiting period can be predicted fairly well by the simplified gas flow analysis developed in Appendix X assuming a linear rate of hole closure. This analysis identified the minimum tray pressure drop and the rate of hole closure as the major parameters controlling the duration of the waiting period, the former factor being determined mainly by the gas velocity and the gas density. It is likely that the rate of hole closure increases as the square root of the depth of liquid on the tray.

Most of the experimental pulsation frequency measurements are represented fairly well by the purely empirical relationship given in equation 8.5. The terms in this equation can, however, be related quite well to the two-stage description of the pulsating jet. A period (16+h) ms can be associated with the first stage, and the remaining terms with the second stage. Unfortunately equation 8.5 cannot be applied to systems operating with fluids other than air and water since the

constants in the equation are dimensional and may all be influenced by the fluid physical properties.

The effects of the column dimensions and the gas density on the frequency will be mainly due to their influence on the waiting period, and equation X.4 can be used to obtain a good indication of the size of these effects.

The main difficulty in frequency prediction is determining the influence of the liquid physical properties on, in particular, the time for momentum transfer, the rate of liquid fall-back and the event initiation pressure drop. Consideration of these factors indicate that, for a given tray liquid head, the pulsation frequency is likely to be increased by decrease in the liquid density, surface tension or viscosity. In the absence of any experimental data regarding the effects of fluid physical properties on either the pressure pulsation frequency or the pulsating jet frequency, further prediction of these effects is extremely difficult.

8.3 SUMMARY.

Synchronisation of the gas-liquid interaction on a sieve-tray is controlled primarily by the pulsating jet event, the initiation of which occurs at a critical tray pressure drop, ΔP_i. Three main factors oppose synchronisation:

i) When the dry tray pressure drop is greater than or equal to ΔP_i, synchronisation cannot occur;

ii) Non-uniformity of the hole events, which is mainly induced by liquid disorder or turbulence on the tray;

iii) The occurrence of a large proportion of 'bubble' type hole events.

The proposed model of synchronisation accounts largely for the observed range of occurrence of the pulsations and explains most of the measured variations in pulsation amplitude with regard to both the tray geometry and the operating conditions.

The maximum superficial hole gas velocity at which synchronisation can occur, v_{max}, depends upon the initiation pressure drop, the gas density and the dry tray loss coefficient, (see equation 8.3):

$$v_{max} = (2 \cdot \Delta P_i / K \cdot \rho)^{0.5}$$

For the air-water system studied $\Delta P_i \approx 200$ N/m^2, giving v_{max} = 11 to 14 m/s for the various trays used. The measured maximum velocity is normally less than the predicted value for tray liquid heads above about 10 mm of water.

For air and water, few pulsations were produced at liquid heads above 20 mm of water (200 N/m^2), and this maximum head is likely to apply for fluids of different density. Pulsations may occur at slightly higher heads for liquids of higher viscosity due to a reduction in liquid disorder or turbulence. Reducing surface tension is likely to reduce the occurrence of bubble events and may also decrease the value of ΔP_i, thus reducing v_{max}. Few fluid systems have a surface tension higher than that for water and air, and most liquids used in industrial absorption or distillation systems have a density within $\pm$ 50% of the value for water. Thus, fluid properties are normally unlikely to affect any major increase in the area of operation over which the pressure pulsations occur as found for the air-water system and as defined in terms of the tray liquid head and the superficial hole gas 'F' factor.

The pressure pulsation frequency corresponds to that of the pulsating jet event which can be considered as a two stage process. During the first stage gas-liquid momentum transfer occurs and during the second the liquid restricts gas flow through the tray and the pressure drop builds up to the value required for event initiation. The period of pressure buildup is fairly well described by the simplified flow analysis developed in Appendix X, assuming a linear rate of hole closure, (rate being proportional to the

square root of the tray liquid depth). This analysis accounts for the effects of gas density and column geometry on the pulsation frequency.

The duration of the first stage is largely independent of the superficial hole gas velocity but increases in proportion to the tray liquid head. The actual hole gas velocity at event initiation is fairly constant (11 to 13 m/s).

Most of the experimental pulsation frequency measurements are represented fairly well by the purely empirical relationship given in equation 8.5. The terms in this equation can be related quite well to the two stage description of the pulsating jet event.

In the absence of any empirical data it is difficult to quantify possible effects of the liquid physical properties on the pulsation frequency.

Chapter 9.

CONCLUSIONS AND SUGGESTIONS FOR FURTHER WORK.

9.1 CONCLUSIONS.

Damaging vibrations can occur in sieve-tray columns as a result of regular column pressure pulsations. An experimental study of such pulsations has been carried out using a large model sieve-tray column and air and water as process fluids. Regular pulsations of the gas pressure beneath the test-tray were produced by each of the fifteen tray geometries investigated, which included five hole diameters between 4.76 and 15.87 mm. They occurred over a specific range of operating conditions as determined by the superficial hole gas velocity and the tray liquid head. Most of the pulsations were produced at gas velocities below 12 m/s and tray liquid heads below 20 mm of water. The pulsation fundamental frequency varied between 12 Hz. and 40 Hz., with an r.m.s. amplitude of up to 60 N/m^2.

Superficial hole gas velocity and tray liquid head were the major flow parameters affecting pulsation frequency. In all cases the frequency increased almost linearly with increasing gas velocity. The effect of tray liquid head depended upon the hole pitch or separation. Frequency increased with increasing liquid head for trays with a hole edge-to-edge separation below about 22 mm. For separations above 22 mm. frequency was little affected or decreased slightly with increasing liquid head.

Pulsation frequency was little affected by changes in the hole diameter. Frequency was increased by up to 3 Hz. on increasing the number of holes in the tray from 38 to 108 or from 108 to 403.

Increasing the tray liquid crossflow velocity up to 190 mm/s could increase the frequency of the pressure pulsations by up to 4 Hz. and the amplitude by up to 25 N/m^2. The extent of the effect depended critically upon the tray geometry.

Reduction of the chamber capacitance beneath the test-tray increased the pulsation frequency slightly up to 1 Hz. Changing the capacitance had no appreciable effect on the pulsation amplitude.

Changes in the tray vibrational characteristics had no effect on the amplitude or frequency of the pressure pulsations. However the tray was found to be excited by both the fundamental and the harmonics exhibited in the pressure pulsation frequency spectrum. The highest levels of tray vibration occurred when a harmonic approached the tray fundamental frequency. Although the tray fundamental frequency was not lowered sufficiently to correspond to the fundamental frequency of the pressure pulsations, it is to be expected that when the correspondence occurs very high levels of tray vibration will result.

The gas-liquid interaction on the test-tray was studied using high speed cine-photography and electrical conductivity probes.

The gas-liquid interaction on the tray can be treated in terms of periodic hole events. During the production of regular pulsations there is normally a majority (up to 98%) of hole events whose duration is equivalent to the pulsation frequency and which are synchronised with the column pressure pulsations, event initiation occurring on average between 5 ms and 10 ms prior to the peak of the pressure pulse beneath the test-tray. For many operating conditions a minority of events also occurred which had a duration equivalent to about half the pulsation frequency. For operation outside the area of pulsation production there was little or no synchronisation of the hole events.

Quantitative measurements of the hole event durations, degree of synchronisation and growth rate and size were obtained from the film analysis. These measurements were consistent with the measured variations in the pressure pulsations. High amplitude pulsations were favoured by a high degree of hole event synchronisation, a large proportion of single events and a small variation in the hole event duration.

For operation at a relatively low tray liquid head, and in the absence of tray liquid crossflow, electrical conductivity probes provided an

accurate indication of hole events. For tray liquid heads above 12 mm of water or in the presence of high tray liquid crossflow, the probe signal became erratic and unreliable.

Various types of hole events were identified from the film analysis. The nature of the hole events depended mainly upon the superficial hole gas velocity and the tray liquid head, as indicated in Figure 6.15. Tray geometry had a secondary influence, except at low values of hole separation (below about 20 mm) where interference between events and growth restriction occurred.

During the production of regular pressure pulsations the hole events were mostly characterised by a period of gas flow restriction during which complete hole closure and subsequent bubble formation might occur, followed by a period of less restricted surging gas flow. The main types of event occurring were the pulsating jet and the imperfect bubble.

The fluctuations in the test-tray total pressure drop, overall gas volumetric flowrate and total loss coefficient, during a pressure pulsation cycle, were calculated from column dynamic (time varying) and static pressure measurements. Analysis of these calculations showed conclusively that the proposed descriptions of the pulsating jet and imperfect bubble events and the measurements of their liquid motion, as obtained from the film analysis, were in very good agreement with the measured pressure pulsations. For highly synchronised events occurring at low tray liquid heads (α 5 mm of water) the minimum tray loss coefficient approached that for a dry tray, this value occurring at a time corresponding to the point of maximum radial liquid spread, as determined from the film analysis.

Synchronisation of the gas-liquid interaction on the sieve-tray was controlled primarily by the pulsating jet event, for which initiation occurred at a critical value of tray pressure drop, ΔP_i.

Synchronisation could not occur when the dry tray pressure drop was greater than or equal to the initiation pressure drop. Synchronisation was opposed and eventually stopped by non-uniformity of the hole events, mainly resulting from liquid disorder or turbulence on the tray, and by the occurrence of a large proportion of 'bubble' type hole events.

The maximum superficial hole gas velocity at which synchronisation could occur, v_{max}, depends upon the initiation pressure drop, the gas density and the dry tray loss coefficient, according to the relationship:

$$v_{max} = (2 \cdot \Delta P_i / K \cdot \rho)^{0.5}$$

For the air-water system studied $\Delta P_i \simeq 200$ N/m^2, giving $v_{max} = 11$ to 14 m/s for the various trays used. Maximum velocity should be less than the predicted value for tray liquid heads above 10 mm of water.

The pressure pulsation frequency corresponded to that of the pulsating jet event which can be considered as a two-stage process. During the first stage the gas-liquid momentum transfer occurred. During the second stage the liquid restricted the gas flow through the tray and the pressure drop built up to the value required for event initiation. The period of pressure build-up could be predicted quite well by a simple flow analysis for the system assuming a linear rate of hole closure.

An empirical correlation (equation 8.5) was obtained which shows a good fit with most of the experimental pulsation frequency measurements. Although the equation was a purely numerical empirical fit of the data and had no foundation in the physical processes involved, its form related well to the proposed description of the two-stage pulsating jet event.

The correlation and the flow analysis enable the prediction of the effect on the pulsation frequency of changes in the operating conditions, the tray and column geometry and the gas density. In the absence of any data it is difficult to quantify possible effects of the liquid physical properties on the frequency.

Likely effects of the liquid physical properties on the occurrence of the pulsations have been discussed. It is important to note that most liquids used in industrial sieve-tray columns have a density comparable to that of water (1000 kg/m^3 ± 50%) and that the large majority of these fluid systems have a value of surface tension below that for the air-water system (≃ 72.8×10^{-3} N/m). It was concluded that although liquid physical properties are likely to affect the production of pulsations, they are normally unlikely to affect any major increases in the area of operation over which the pressure pulsations occur as found for the air-water system and as defined in terms of the tray liquid head and the superficial hole gas 'F' factor. Thus, the problem of damaging vibrations can be considered as being largely confined to operation at relatively low values of tray liquid head (below about 20 mm of water or 200 N/m^2) and hole gas 'F' factor (below about 16 $kg^{0.5}/m^{0.5}$ s).

9.2 SUGGESTIONS FOR FURTHER WORK.

The fluid physical properties have been identified as probably affecting the production of the regular pressure pulsations. Although such effects are likely to be relatively small their investigation would enable a more accurate prediction of the operating conditions over which pulsations will occur for the varied fluid system used in indistrial distillation and absorption columns. Knowledge of the affect of physical properties on the event initiation pressure drop should enable accurate prediction of the maximum hole gas 'F' factor for pulsation occurrence. Other factors, of slightly lesser importance, are the effect of liquid surface tension on the occurrence of 'bubble' type events and the effects of liquid viscosity and liquid density on the maximum tray liquid head at which pulsations occur. Knowledge of the effect of physical properties on the pulsation frequency would not only enable better avoidance of

potentially damaging column resonances, but also provide valuable information about the general behaviour of the pulsating jet.

A detailed theoretical and experimental study of the fluid dynamics of the pulsating jet event is important, not only because of its direct association with the production of pressure pulsations, but also because of its relevance to sieve-tray operation in the spray regime. Of particular interest are: the precise mode of event initiation; the detailed mechanism of momentum transfer; the quantity of liquid entrained and its projection velocity; the motion of the liquid on the tray following momentum transfer, including the extent of the liquid lateral spread and the subsequent fall-back of the liquid toward the hole. (Important in such a study may be the wetting properties of the tray, which have been found to affect the event frequency, and also perhaps the tray thickness.) It is of interest to note that when the event liquid lateral spread distance is comparable to the hole edge-to-edge separation and some event interference occurs, vapour-liquid mixing on the tray may be enhanced.

Cine-photography from beneath a glass sieve-tray could be used in a more detailed study of the mechanisms of gas-liquid interaction on the tray. The technique is particularly useful for observing liquid weeping. If a large glass section was used then local variations in tray operation, including areas of hole blockage or the local effects of tray 'swashing', should be readily identifiable. In conjunction with the use of a dye, this technique could provide useful information about the mechanism of liquid flow across the tray in the various operating regimes.

It is likely that some interference or interaction between event synchronisation on successive trays in the column may occur. The associated pressure pulsations should result in the events being of the same frequency but 180^{o} out of phase on successive trays. This requires, of

course, that the operating conditions, in particular the tray liquid head and gas velocity, are the same on each tray. Although such coupling may increase the degree of event synchronisation, the pressure pulsation amplitude will be limited by the event initiation pressure drop and the dry tray pressure drop. Thus the level of tray or column vibration is unlikely to be increased unless significant inter-tray mechanical coupling exists, in which case the column internals may be induced to vibrate as a whole.

Damaging vibrations have also been reported to occur in valve tray columns. Some study of pressure pulsation production by valve-trays would therefore be useful. It is suggested that in such a study differential pressure transducers be used to quantify the pressure pulsations directly in terms of the fluctuations in the tray pressure drop.

There is some scope for further study of sieve-tray pressure drops. The pressure losses associated with the gas-liquid mixture on the tray, in particular that loss termed the 'residual pressure drop' could be further clarified and associated more closely with the gas-liquid dynamics on the tray. In studying the residual pressure drop it is necessary to distinguish between the tray liquid head measured by tray mounted pressure tappings (as usually used on a multi-hole tray) and the liquid head based upon the clear liquid depth maintained by a weir device (as usually used on a single hole tray).

If a single hole tray is used to study sieve-tray hydrodynamics it must be remembered that, if the gas-liquid regime is unlikely to be synchronised on a multi-hole tray, then care must be taken to ensure that no fluctuations of the single hole tray pressure drop occur. Furthermore account should be taken of any interference which may occur on a multi-hole tray between the gas-liquid interaction occurring at neighbouring holes.

Appendix I.

SIEVE-TRAY DESIGN AND DIMENSIONS

Introduction.

This appendix gives details of the design and dimensions of the sieve-trays and gives the procedure used for changing the test-tray. Also given are the dimensions of the glass tray inserts and details of the glass drilling procedure. The location of the tray mounted pressure tappings are also specified.

I.1 TRAY DESIGN AND DIMENSIONS.

The trays were made from 3.175 mm. (0.125 inch) thick steel plate, with sharp edged drilled holes. Figure I.1 shows the basic tray design and dimensions.

Fifteen different test-tray hole geometries were used, as detailed in Table I.1.

Variations in the number of holes and the hole pitch were achieved by blocking up selected holes using adhesive vinyl tape. Care was taken to ensure that the tape did not interfere with active holes, the minimum tape-hole separation being about 3 mm.

For all the trays the holes were on 60 degree equilateral triangular pitch, and the percentage hole free area, ϕ, shown in Table I.1, for each tray, is given by:

$$\phi = \frac{100.\pi.}{2\sqrt{3}} \left(\frac{d^2}{p^2}\right) \quad \% \qquad \ldots\ldots\ldots \qquad (I.1)$$

The trays were made from mild steel, apart from trays F and I which were made from stainless steel type 310.

I.2 POSITION OF THE PERFORATED AREA OF THE TRAYS.

This section defines the position of the tray holes, and gives details of which holes were blocked off in order to alter the tray geometry. Individual hole locations are given for each tray in terms of hole 'columns' and hole 'rows', as defined in Figure I.2.

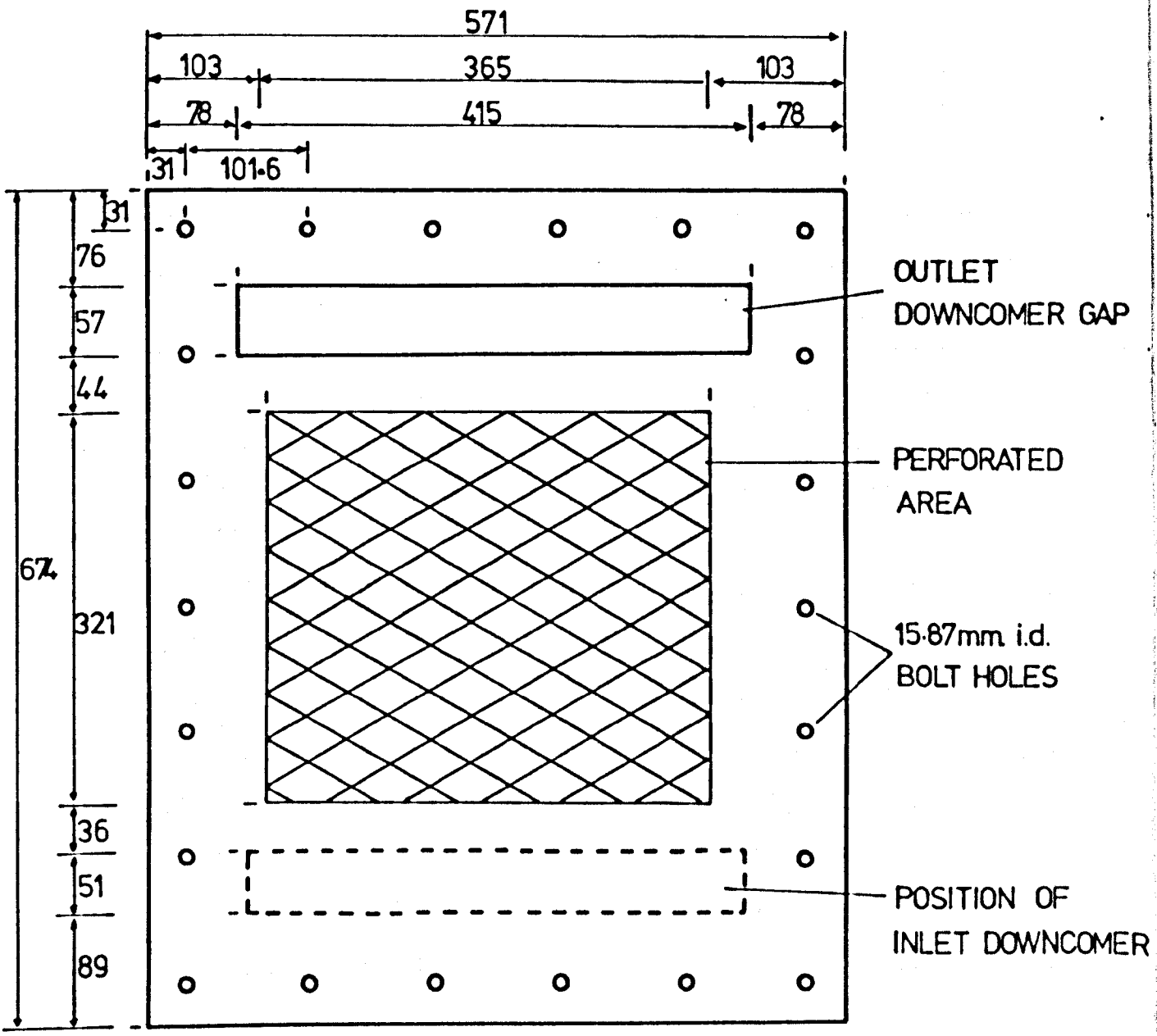

all dimensions in millimeters

Fig. I.1. SIEVE-TRAY DESIGN AND DIMENSIONS

TABLE I.1 GEOMETRY OF THE TEST-TRAYS.

Tray	Hole Diameter d,mm.(ins.)	Hole Pitch p.mm.(ins.)	Number of holes n	Hole Free Area		Modified Tray
				Perf. Area, ϕ, %	Hole Area cm^2.	
A	4.76 (3/16)	19.05 (3/4)	403	5.67	71.79	A
B	6.35 (1/4)	19.05 (3/4)	391	10.07	123.8	B
B(g)	6.6 (0.26)	19.05 (3/4)	391	10.89	171.0	B
C	9.53 (3/8)	19.05 (3/4)	403	22.7	287.2	C
D	9.53 (3/8)	19.05 (3/4)	256	22.7	182.4	C
E	9.53 (3/8)	19.05 (3/4)	108	22.7	76.96	C
F	9.53 (3/8)	27.8 (70/64)	108	10.66	76.96	F
G	9.53 (3/8)	33.0 (1.3)	108	7.57	76.96	C
H(g)	9.53 (3/8)	38.1 (1½)	108	5.67	76.96	C
I	12.3 (31/64)	38.1 (1½)	104	9.45	123.6	I
J	12.3 (31/64)	38.1 (1½)	68	9.45	80.84	I
K	12.3 (31/64)	38.1 (1½)	38	9.45	45.18	I
L(g)	15.87 (5/8)	38.1 (1½)	108	15.74	213.8	L
M	15.87 (5/8)	38.1 (1½)	38	15.74	75.21	L
N	12.3 (31/64)	66.0 (2.6)	38	3.14	45.18	I
O(g)	15.87 (5/8)	66.0 (2.6)	38	5.24	75.21	L

(g), signifies the use of a glass insert.

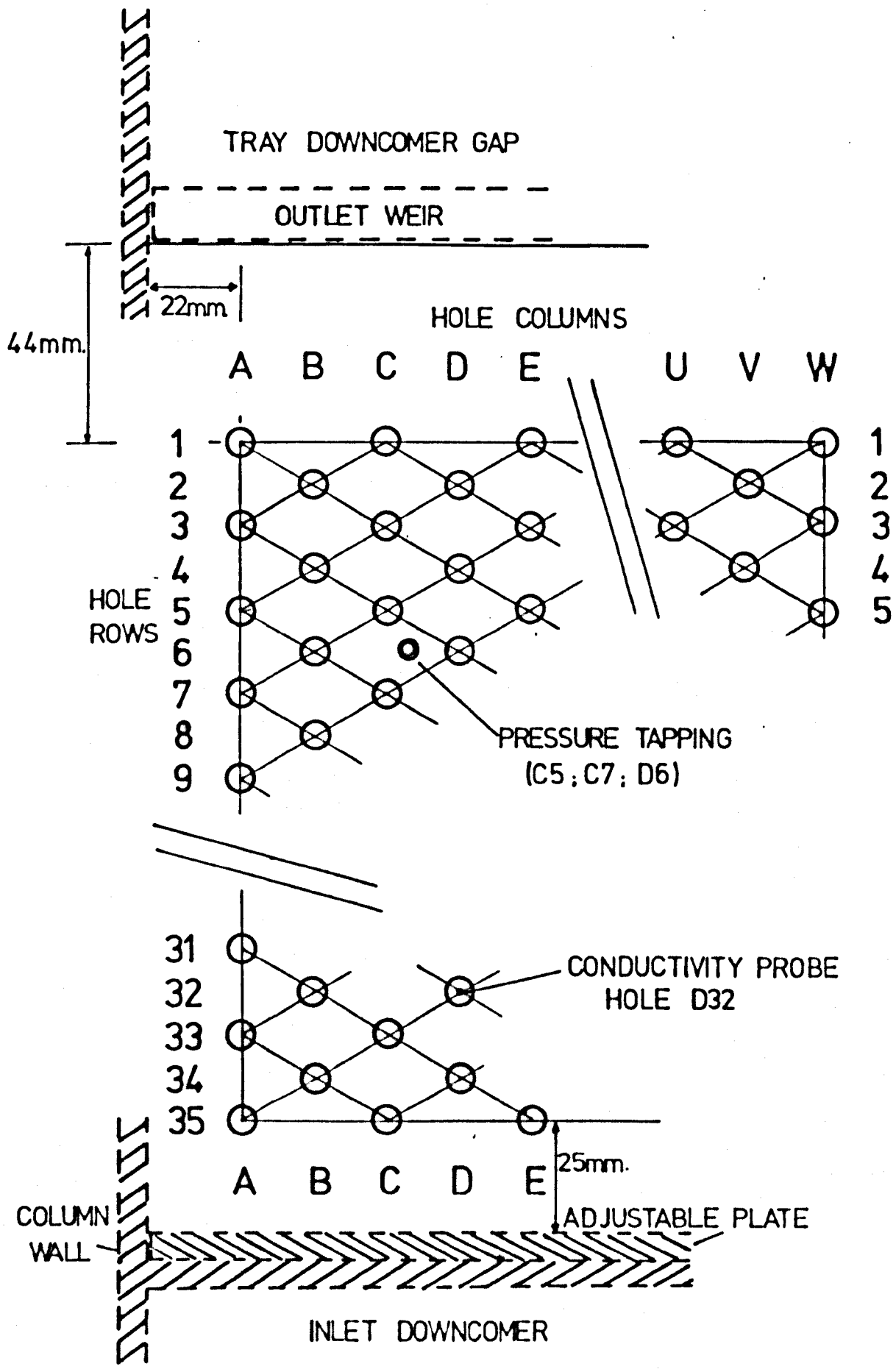

Fig.I.2. KEY TO SIEVE-TRAY HOLE LOCATIONS.

TRAY A. d = 4.76 mm.

All of the hole positions shown on Figure I.2 were used; i.e., columns A to W and rows 1 to 35. The total number of holes was 403, on 19.05 mm. pitch.

TRAY B. d = 6.35 mm.

All of the hole positions were used apart from row 35, which was blocked off by tape, leaving 391 holes, on 19.05 mm. pitch.

TRAY C. d = 9.53 mm.

All of the hole positions were used. The total number of holes was 403, on 19.05 mm. pitch.

TRAY D. d = 9.53 mm.

Holes around the outside of tray C were blocked off, to leave 256 holes, on 19.05 mm. pitch, as defined below.

Column	Rows	Column	Rows
B	10 to 26	M	1 to 35
E	9 to 27	N	2 to 34
F	8 to 28	O	1 to 35
G	7 to 29	P	2 to 34
H	6 to 30	Q	3 to 33
I	5 to 31	R	4 to 32
J	4 to 32	S	5 to 31
K	3 to 33	T	6 to 30
L	2 to 34	U	7 to 27

TRAY E. d = 9.53 mm.

Holes around the outside of tray C were blocked off, to leave 108 holes, on 19.05 mm. pitch, as defined below.

Column	Rows	Column	Rows
G	13 to 25	N	10 to 28
H	12 to 26	O	11 to 27
I	11 to 27	P	12 to 26
J	10 to 28	Q	13 to 25
K	11 to 29	R	14 to 22
L	10 to 30	S	15 to 21
M	11 to 29		

TRAY F. d = 9.53 mm.

This tray was formed by blocking off selected holes on a tray which had hole patterns on equilateral pitches of 24.1 mm. and 27.8 mm. superimposed on each other. Blocking off the holes left 108 holes on 27.8 mm. pitch. The hole positions are given below, with hole (A,1) being as defined in Figure I.2.

Column	Rows	Column	Rows
C	7 to 17	J	4 to 20
D	6 to 18	K	3 to 21
E	5 to 19	L	4 to 20
F	4 to 20	M	5 to 19
G	3 to 21	N	6 to 18
H	4 to 20	O	7 to 17
I	3 to 21		

TRAY G. d = 9.53 mm.

Columns A and W, and double rows of holes, were blocked off on tray C to leave 108 holes on 33.0 mm. pitch, as defined below.

Columns	Rows
A	13,19,25
B to V	4,7,10,13,16,19,22,25,28,31

TRAY H. d = 9.53 mm.

Alternate columns and diagonal lines of holes were blocked off on tray C to leave 108 holes on 38.1 mm. pitch as defined below.

Column	Rows	Column	Rows
A	3,7,11,15,19,23,27,31,35	M	3 to 35
C	1,5,9,13,17,21,25,29,33	O	1 to 33
E	3 to 35 (as above)	Q	3 to 35
G	1 to 33 (as above)	S	1 to 33
I	3 to 35	U	3 to 35
K	1 to 33	W	1 to 33

TRAY I. d = 12.3 mm.

On this tray the hole pattern was rotated through 90° with respect to Figure I.2; the hole columns were horizontal and the hole rows vertical, the top row being 31 mm. from the outlet weir. The tray contained 104 holes on 38.1 mm. pitch, as defined below.

Column	Rows	Column	Rows
A	2,4,6,8,10,12,14,16,18	G	2 to 18
B	1,3,5,7,9,11,13,15,19	H	1 to 19
C	2 to 18 (as above)	I	2 to 18
D	1 to 19 (as above)	J	1 to 19
E	2 to 18	K	2 to 18
F	1 to 19		

TRAY J. d = 12.3 mm.

Holes around the outside of tray I were blocked off to leave 68 holes on 38.1 mm. pitch.

Column	Rows	Column	Rows
B	3 to 17	G	4 to 16
C	4 to 16	H	3 to 17
D	3 to 17	I	4 to 16
E	4 to 16	J	3 to 17
F	3 to 17		

TRAY K. d = 12.3 mm.

Holes around the outside of tray I were blocked off to leave 38 holes on 38.1 mm. pitch, as defined below.

Column	Rows	Column	Rows
B	7 to 13	F	5 to 15
C	6 to 14	G	6 to 14
D	5 to 15	H	7 to 13
E	4 to 16	I	10

TRAY L. d = 15.87 mm.

This tray contained 108 holes on 38.1 mm. pitch with the same hole pattern as tray H.

TRAY M. d = 15.87 mm.

Holes around the outside of tray L were blocked off to leave 38 holes on 38.1 mm. pitch, as defined below.

Column	Rows	Column	Rows
C	17	K	5,9,13,17,21,25,29
E	11,15,19,23	M	7,11,15,19,23,27
G	9,13,17,21,25	O	9,13,17,21,25
I	7,11,15,19,23,27	Q	11,15,19,23

TRAY N. d = 12.3 mm.

Double rows of holes were blocked off on tray I, to leave 38 holes on 66.0 mm. pitch. For the columns in tray I the following rows were left; 1, 4, 7, 10, 13, 16, 19.

TRAY O. d = 15.87 mm.

Double rows of holes were blocked off on tray L, to leave 38 holes on 66.0 mm. pitch. For the columns in tray L the following rows were left; 1, 7, 13, 19, 25, 31 (for columns I and M, row 34 was also used).

I.3 LOCATION OF THE TRAY MOUNTED PRESSURE TAPPINGS.

Each tray had nine pressure tappings, as described in section 4.4. Their positions are specified below, for each tray, in terms of the three closest neighbouring holes; as exemplified in Figure I.2. Tappings which are specified in terms of only two holes were located directly between these holes.

TRAY	LOCATIONS		
A	(D6; D8)	(F16; F18)	(D26; D28)
	(L6; L8)	(L16; L18)	(L26; L28)
	(T6; T8)	(R16; R18)	(T26; T28)
B	(F8; F10)	(F18; F20)	(F28; F30)
	(L8; L10)	(L18; L20)	(L28; L30)
	(R8; R10)	(R18; R20)	(R28; R30)
C,D,E,G,H	(D6;D8;E7)	(E17;F16;F18)	(D26;D28;E27)
	(L6;L8;M7)	(K17;L16;L18)	(L26;L28;M27)
	(S7;T6;T8)	(R16;R18;S17)	(S27;T26;T28)
F	(E5; E7)	(E11; E13)	(E17; E19)
	(H6; I7)	(H12; I13)	(H18; I19)
	(L6; M7)	(L12; M13)	(L18; M19)
I,J,K,N	(C4;C6;D5)	(C10;D9;D11)	(C14;C16;D15)
	(F5; F7)	(F9; F11)	(F13; F15)
	(H5;I4;I6)	(H9;H11;I10)	(H15;I14;I16)
L,M,O	(E7;E11;G9)	(E19;G17;G21)	(E27;E31;G29)
	(M7; M11)	(K17;K21;M19)	(M27; M31)
	(U7;U11;S9)	(S17;S21;U19)	(S29;U27;U31)

I.4 PROCEDURE FOR CHANGING THE TEST-TRAY.

The outlet weir was slackened and reduced to zero height and the 22 flange bolts removed. The bracket fastening the column to the laboratory ceiling beam was loosened to allow vertical movement of the top two column sections. The tray pressure tappings, accelerometer and conductivity probes were disconnected and removed. Then, three persons lifted up the top two column sections whilst a fourth person slid out the old test-tray and slid in the replacement tray. The column was then bolted and secured, the tray pressure tappings, accelerometer and conductivity probes were replaced and reconnected, and the outlet weir was reset and sealed. The test-tray was then levelled using a spirit level.

I.5 DETAILS OF THE GLASS TRAY INSERTS AND DRILLING PROCEDURE.

Three different glass tray inserts were used, with hole diameters of 6.6 mm, 9.53 mm and 15.87 mm. Figure I3 gives their design and dimensions.

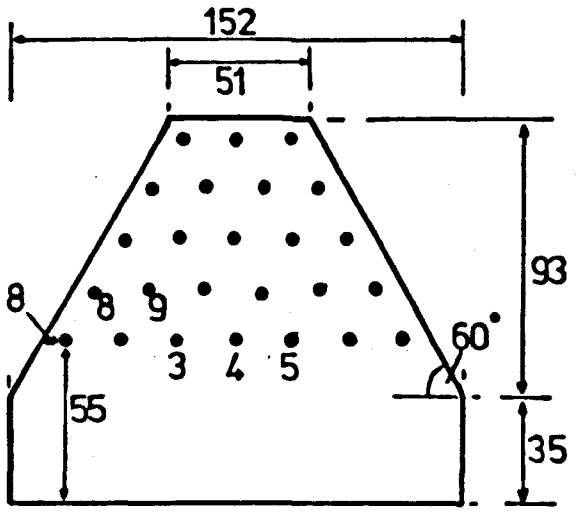

(a) insert for tray B(g)
25×6·6mm. dia. holes
on 19·05mm pitch.

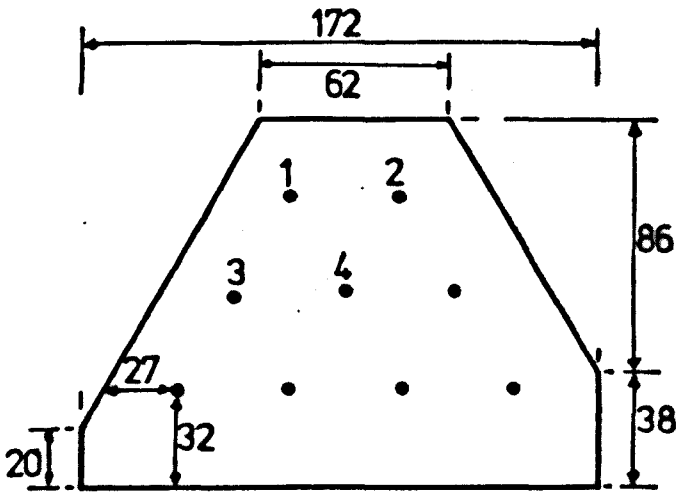

(b) insert for tray H(g)
9×9·53mm. dia. holes
on 38·1mm. pitch.

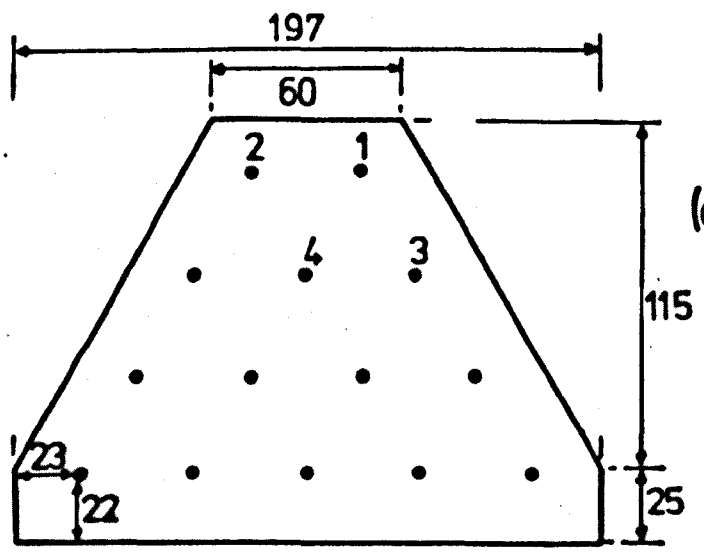

(c) insert for tray L(g)
14×15·87mm. dia. holes
on 38·1mm. pitch.

all dimensions in millimeters.

Fig. I.3. DETAILS OF GLASS TRAY INSERTS

The inserts were made from 3 mm. thick glass plate and the holes were drilled. To obtain holes with square edges, with no chipping, the following drilling procedure was used.

A multilayer 'sandwich' was constructed from a 6 mm. thick glass base plate (0.20 m by 0.18 m), three blank tray inserts and a perspex template, with a thin layer of injector wax between each plate. The 'sandwich' was built up as follows.

Some molten injector wax (M.Pt. ≈ 100° C) was put on the heated base plate and the first blank placed on top and pressed down until there was a thin layer of wax between the two pieces of glass with no trapped air bubbles. The procedure was then repeated with the second blank on the first, and then the second on the third. Finally, the perspex template, which was a replica of the desired insert, as shown in Figure I3, was placed on top. Heating the plates kept the wax molten long enough to permit sliding of the plates in order to line up the edges of the three blanks and the template.

The sandwich was allowed to cool and set, and then the holes were carefully drilled, by the glass-blower, using a glass-drill.

To separate the plates they were placed in an oven and slowly heated until the wax melted, permitting the plates to be carefully slid apart. Xylene was used as a solvent to clean the wax from the drilled inserts. It was found that at least one of the glass inserts had square edges holes without chipping.

Appendix II.

AIR FLOW ORIFICE-PLATE CALIBRATION

This appendix describes the calibration of the orifice-plate used for air flow rate measurement. It also contains details of the flowrate below which the orifice discharge coefficient changes, and of the centrifugal fan used for air supply.

II.1 ORIFICE-PLATE CALIBRATION.

The orifice-plate was calibrated using a rotating vane type anemometer (E. Schlicknecht ing., Furness Controls Ltd.). The anemometer gave direct air flow velocity reading to an accuracy of 0.03 m/s (0.1 ft/s). The anemometer velocity scale had been checked using a hot wire anemometer and been found to be accurate.

The orifice tube was disconnected from the column and the outlet pipe adaptor removed (see Figure 4.6). For seven air flow rates the orifice pressure drop was measured, to an accuracy of 0.58 mm (0.02 ins.) of water, using an inclined gauge manometer. At each flow rate air velocity measurements were made at the open end of the orifice tube using the vane anemometer. In accordance with British Standard 848 pt. 1, velocity measurements were taken on two perpendicular diameters at distances of 0.032D, 0.135D, 0.321D, 0.679D, 0.865D and 0.968D from the tube edge. It was not possible to position the anemometer as accurately as the above figures demand, but the accuracy obtained was considered sufficient for the purpose of this calibration.

The true gas velocity was found by averaging the velocity in each position, and the volume flowrate was calculated by multiplying this velocity by the tube internal cross-sectional area (as measured by i.d. calipers).

Table II.1 gives the results obtained and Figure II.1 shows a plot of the orifice pressure drop against the calculated volumetric flowrate. The theoretical orifice curve, as calculated below, is also shown on Figure II.1, and there is seen to be excellent agreement between the two plots.

II.2 THEORETICAL ORIFICE-PLATE PRESSURE DROP/FLOWRATE CORRELATION.

From British Standard 848 pt. 1, page 24, we have:

$$G = \frac{862}{60} \cdot \ell \cdot C_s \cdot \left(\frac{\Delta P_o}{\rho g}\right)^{0.5} \quad FT^3/s \qquad \ldots\ldots (II\text{-}1)$$

where:

G	=	Volume flowrate at upstream side tapping,	FT^3/s.
ℓ	=	diameter of orifice-plate ,	FT.
C_s	=	Orifice coefficient.	
ΔP_o	=	Differential pressure across the orifice,	ins. of water.
ρg	=	Gas density	lb/FT^3.
D	=	Orifice tube diameter	FT.

From the graph of C_s against ℓ/D, in B.S.848, we obtain $C_s = 0.65$.

Substituting in equation (II-1), we obtain:

$$G = 4.7 \sqrt{\Delta P_o} \quad FT^3/s$$

or $$G = 0.0264 \cdot \sqrt{\Delta P} \quad m^3/s \qquad \ldots\ldots (II\text{-}2)$$

where ΔP is the orifice-plate pressure drop measured in units of mm. of water.

Equation (II-2) is plotted in Figure II.1.

II.3 VARIATION OF ORIFICE COEFFICIENT, C_s, AT LOW REYNOLDS NUMBER.

In Spiers (61), page 108, it is shown that the orifice coefficient, C_s, changes significantly when the gas flow Reynolds Number, Re, (based on the orifice-plate diameter), falls below 20,000.

For our system we have:

$$Re = 8.19 \times 10^5 . \ G$$

Therefore the minimum flowrate, G_{min}, which can be used with the assumed value of the orifice coefficient is:

$$G_{min} = 0.024 \ m^3/s.$$

This is equivalent to a theoretical orifice pressure drop of approximately 1 mm. of water, as indicated on Figure II.1.

II.4 CENTRIFUGAL FAN SPECIFICATIONS.

The fan used was a Keith Blackman 3.1 H.P. 'TORNADO' centrifugal fan. It was powered by a 3-phase, 6.5 amp., 5 H.P. electric motor turning at 2850 revolutions per second. The fan delivered 0.33 m^3/s (700 FT^3/min.) at 455 mm. (18 in.) of water total pressure.

TABLE II.1 RESULTS OF ORIFICE-PLATE CALIBRATION.

Orifice pressure drop inches of water (mm. of water)	Anemometer velocity readings FT/s.						Average Velocity	Volume Flow
	0.032D	0.135D	0.321D	0.679D	0.865D	0.968D	FT/s	FT^3/s (m^3/s)
0.18 (4.6)	6.7	6.6	5.9	5.8	6.3	6.1	6.18	2.04(0.0577)
	6.4	6.4	6.1	5.7	6.0	6.2		
0.29 (7.4)	8.2	8.0	7.3	6.9	7.8	7.8	7.62	2.51(0.0712)
	8.1	8.0	7.3	6.9	7.5	7.6		
0.69 (17.5)	13.8	12.9	10.8	10.5	11.7	12.2	11.75	3.87(0.1095)
	12.4	12.0	10.8	10.4	11.4	12.0		
1.19 (30.2)	17.0	16.0	14.4	13.7	15.8	16.3	15.36	5.07(0.143)
	16.8	16.0	14.0	13.5	15.0	15.8		
2.38 (60.5)	24.5	23.0	20.5	19.0	22.5	23.8	22.0	7.25(0.205)
	24.0	23.0	20.0	19.0	21.5	23.5		
3.55 (90.1)	30.0	28.0	24.5	22.5	27.0	28.5	26.5	8.75(0.248)
	29.5	27.5	24.5	22.5	25.8	28.0		
4.74 (120.2)	34.5	32.0	27.5	25.5	31.0	33.0	30.3	10.0(0.283)
	33.5	31.0	27.5	26.0	29.0	32.5		

Orifice tube end cross-sectional area = 0.33 FT^2 (0.0307 m^2).

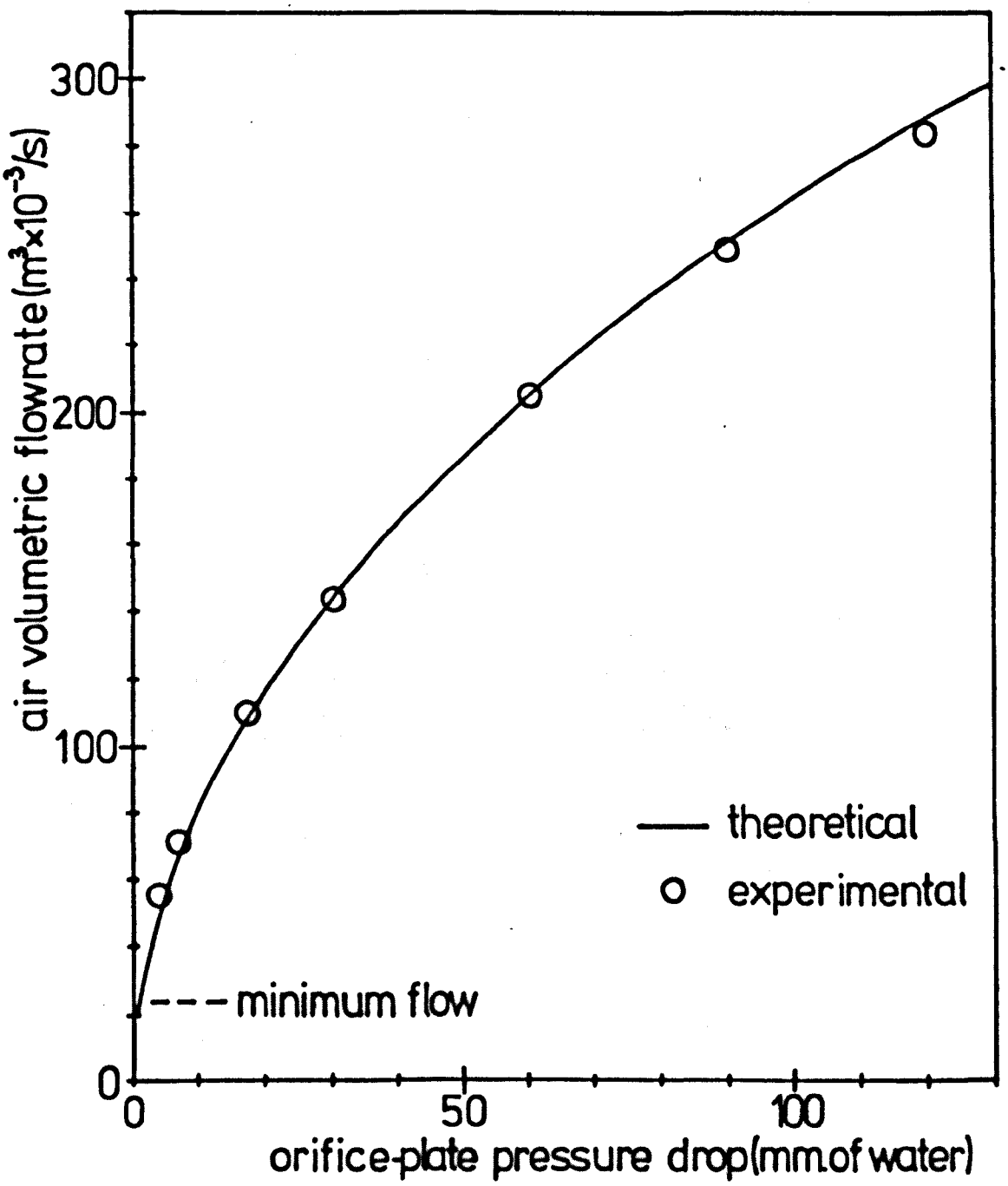

Fig. II.1. ORIFICE-PLATE CALIBRATION CURVE.

Appendix III.

CALIBRATION OF THE WATER FLOW RATE MEASUREMENT ROTAMETER AND FLOW INDICATOR.

III.1 CALIBRATION PROCEDURE.

The rotameter (Tube 262597/1702/R, Rotameter M.C. Ltd.) and the Drayton flow indicator were calibrated using the following procedure.

The period of time required for a given volume water to flow through the measuring device into a large tank was measured using a stop-watch, for several constant water flow rates. The flow rate as indicated on the measuring device was then compared with the calculated water flow rate.

Results for each device are given in Tables III.1 and III.2, respectively.

Table III.1 Rotameter Calibration.

Rotameter Reading galls/hr.	Time taken to fill volume		Calculated flow rate galls/hr.
	3 galls. sec.	6 galls. sec.	
50	218	436	49.6
100	109	218	99.3
150	70	144	150
200	55	108	200
250	42	87	249
300	37	72	300
350	31	62	349
400	27	53	405
450	24	47	458
500	20	42	508

Table III.2 Flow-indicator Calibration.

Flow indicator reading galls/hr.	Time to fill volume		Calculated flow rate galls/hr.
	1.5 gall.sec.	3 gall. sec.	
10	562	1127	9.6
20	278	551	19.5
30	175	351	30.8
40	132	260	41.3
50	105	211	51.3

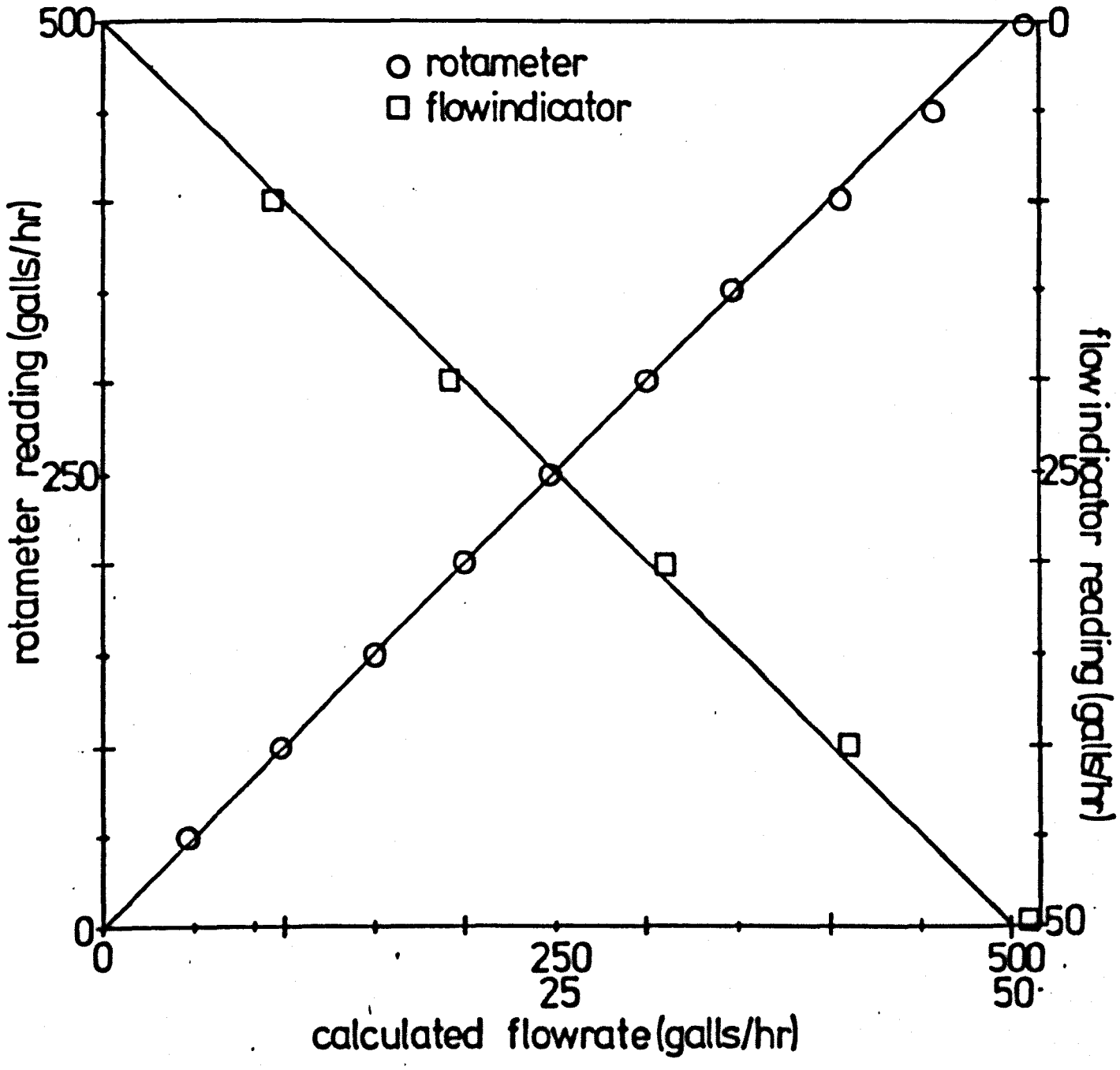

Fig. III.1 WATER FLOWRATE CALIBRATION

The results are plotted on Figure III.1, and there is seen to be good agreement between the calculated and the indicated flow rates. The marked graduations were therefore taken as accurate.

Some difference between the flow rates may have resulted from the difficulty in maintaining a completely constant water flow rate, especially at the higher flows, with frequent small flow adjustments being necessary.

Appendix IV.

CALIBRATION OF PRESSURE TRANSDUCERS AND ACCELEROMETERS.

IV.1 PRESSURE TRANSDUCER CALIBRATION.

The transducers had calibration curves supplied with them; these showed a linear sensitivity ($\pm$ < 0.5%) of 2,240 pC./at. (picoCoulombs/ atmosphere) over the range 0 to 10 at., where 1 at. = 98,066.5 N/m^2.

This is equivalent to a sensitivity of 0.224 pC per mm. of water. The amplifier gains were set to give an output voltage of 10 mV for an input charge of 0.224 pC., i.e. 10 mV per mm. of water pressure impulse. This was checked experimentally for various magnitudes of pressure impulse. Figure IV.1 shows details of the apparatus used.

With valve 1 and valve 2 open, the transducer detected atmospheric pressure. Valve 2 was then closed and the balloon inflated until the desired pressure impulse, b, was indicated on the inclined manometer gauge, (accurate to 0.22 mm. of water). Valve 1 was then closed, sealing the system, and valve 2 opened quickly, thus giving a known pressure impulse, b, to the pressure transducer. The resulting impulse charge from transducer was amplified and transformed to a voltage, V, by the charge amplifier,

The voltage was displayed and measured on the storage cathode ray oscilloscope. The procedure was repeated for several values of pressure impulse.

Typical results are given in Table IV.1. They show the transducer calibration to be correct. The calibration was carried out several times during the experimental programme.

Table IV.1 Transducer Calibration Results.

Manometer reading, b, mm. of water.	C.R.O. displacement V, volts	Sensitivity mV/mm. of water
250	2.5	10
180	1.8	10
120	1.2	10
60	0.6	10
30	0.3	10
10	0.1	10

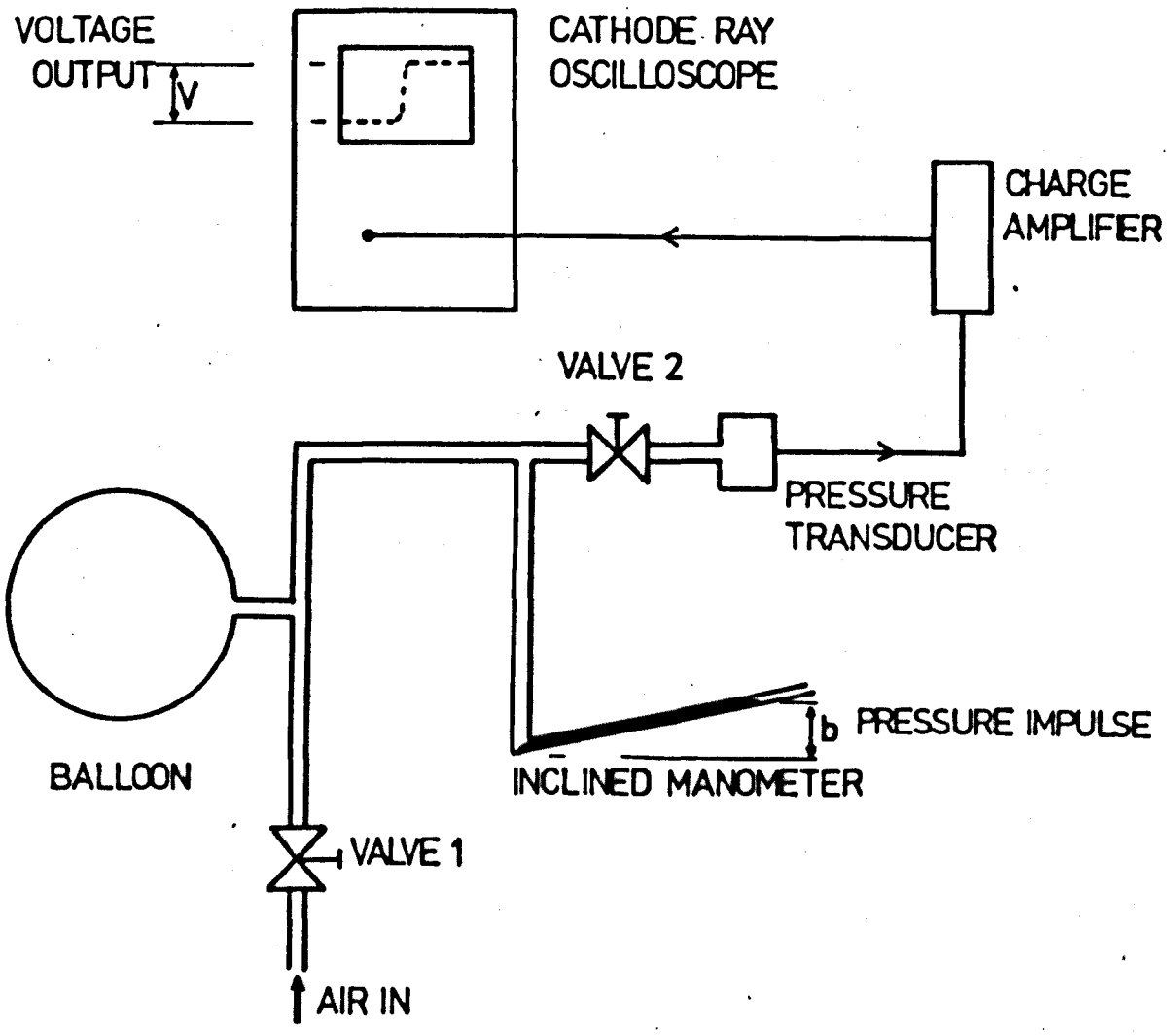

Fig. IV.1. PRESSURE TRANSDUCER CALIBRATION APPARATUS

IV.2 ACCELEROMETER CALIBRATION.

The two Bruel and Kjaer accelerometers (type 4334) were calibrated at 50 mV/g. Hence, a 50 mV signal fed to the Bruel and Kjaer preamplifier (type 2625) was equivalent to an acceleration of 10 m/s^2 on the accelerometer. With a standard 50 mV, 50 Hz, input signal, the preamplifier gain was adjusted until an output voltage of 150 mV was obtained. This meant that for this gain, with the preamplifier selector switch at a velocity setting of "10 Hz, 0.3 m/s", an output of 150 mV would correspond to an accelerometer velocity of 0.3 m/s.

Appendix V.

EXPERIMENTAL CHECK OF SOME OF THE RESULTS OBTAINED BY WADDINGTON (2).

Waddington obtained results using three active sieve trays. Experiments were carried out to check some of these results using a single active tray (test-tray B), measurements being made of the total tray static pressure drop and the dynamic pressure in the chamber beneath the test-tray.

V.1 TOTAL TRAY STATIC PRESSURE DROP MEASUREMENTS.

A check was carried out of the pressure drops reported in Figure 6.2.1 of ref.(2) for weir heights of 25.4 mm. and 76.2 mm. The total tray pressure drop was measured as described in Section 4.4.

The results are shown in Figure V.1. The results obtained at 76.2 mm. weir height show good agreement, although there is some indication that Waddington underestimated the air flow rate. The results obtained at the 25.4 mm. weir height show wide disagreement. The pressure drop is relatively easy to measure accurately, and it is therefore likely that the disagreement is due to Waddington misreporting or overestimating the water flow rate, his results corresponding to a flow rate of approximately one quarter of that reported.

V.2. DYNAMIC PRESSURE MEASUREMENTS.

A check was carried out of the dynamic pressure predominant frequency components reported in figure 6.8.2 of ref.(2) for weir heights of 25.4 mm and 76.2 mm.

The gas dynamic pressure was measured in the chamber beneath the test-tray using pressure transducer 1 positioned as shown in Figure 4.8. Signal analysis was carried out using the Bruel and Kjier frequency analyser, as described in Section 4.8.2.

The results are shown in Figure V.2. Those obtained for the 25.4 mm. weir height show good agreement, although there is evidence that Waddington underestimated the airflow rate by about 10%. For a weir height

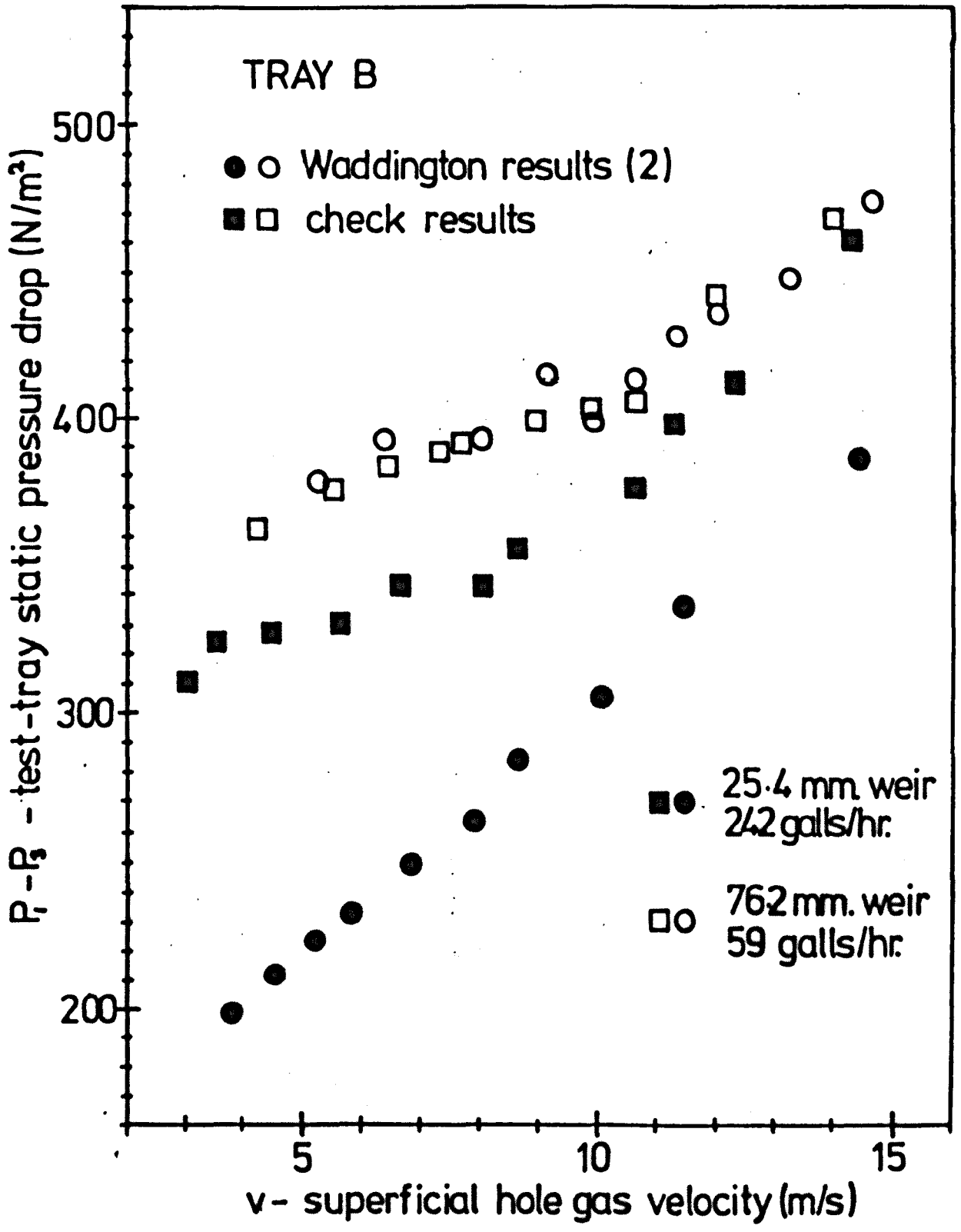

Fig. V.1. CHECK ON WADDINGTON PRESSURE DROP RESULTS (2)

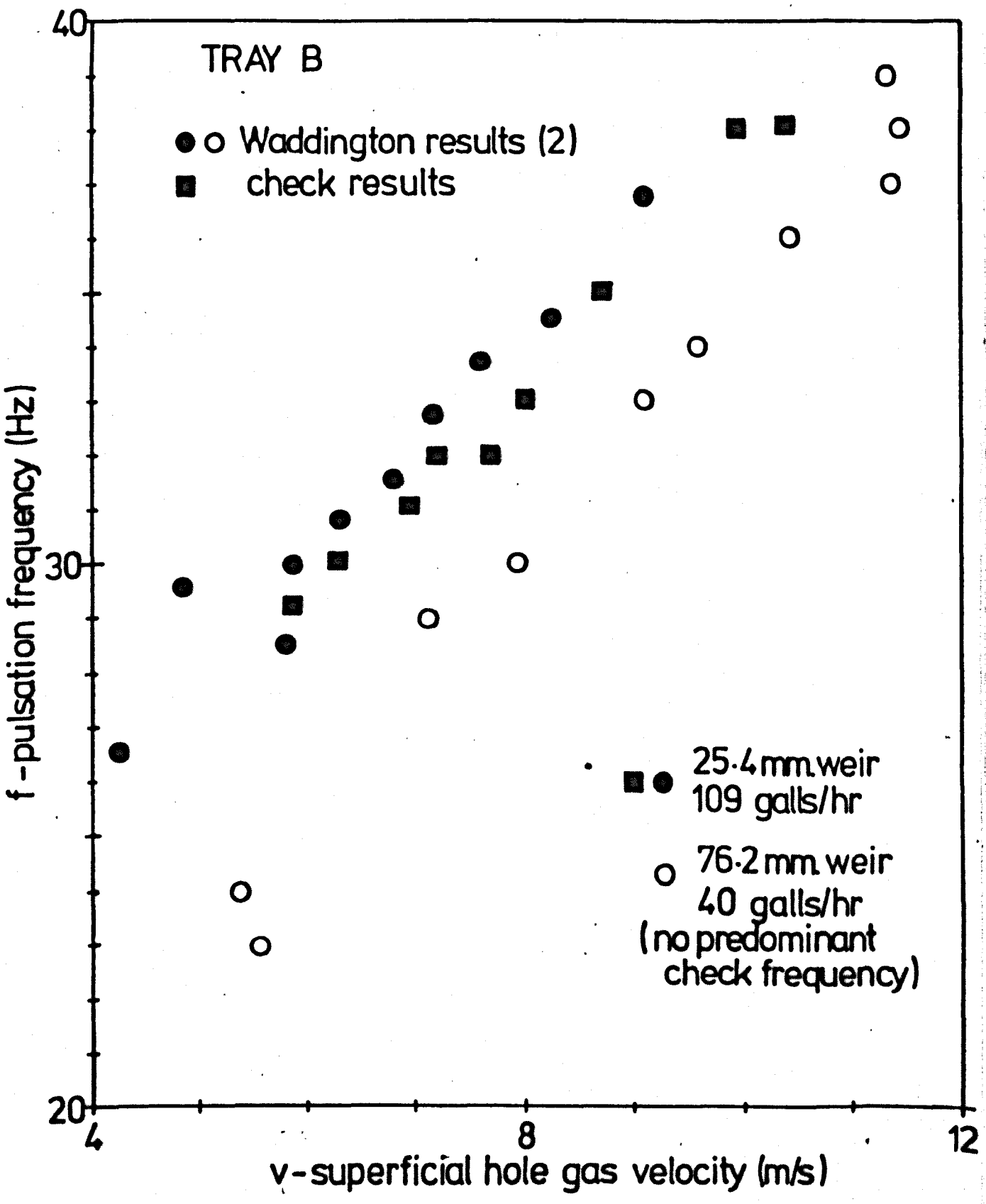

Fig. V.2. CHECK ON WADDINGTON PULSATION FREQUENCY RESULTS (2)

of 76.2 mm. no predominant frequency component was detected for operation at air flow rates above the seal point ($V \approx 6.0$ m/s). Plot (a) of Figure 5.4 indicates that no pulsations are produced at tray liquid heads greater than 20.0 mm. of water. It is possible that liquid leakage past the outlet weir on one of the trays used by Waddington, lowered the tray liquid head on that tray sufficiently to result in the production of the reported pulsations.

V.3. CONCLUSIONS.

i) Good agreement was found with the pulsations reported by Waddington at a weir height of 25.4 mm.

ii) The pulsations reported by Waddington at a weir height of 76.2 mm; could not be reproduced using a single active sieve-tray. It is possible that the reported pulsations could have resulted from liquid leakage on one of the trays.

iii) There is an indication that Waddington underestimated the air flow rate by about 10%.

Appendix VI.

CALCULATION OF TRAY LIQUID HEAD.

VI.1 CALCULATION OF THE TRAY LIQUID HEAD.

In Section 3.1.3 it was shown that the tray liquid head can be calculated from the measured static pressure drop across the gas-liquid mixture on the tray, P_2-P_3, by considering the gas momentum head, ΔM.

We have

$$P_2 - P_3 = H.\ \rho\ell.\ g - \Delta M \quad N/m^2 \quad \ldots \quad (3.10)$$

where, $$\Delta M = \bar{u}^2\ .\rho\ .\ (1/a - 1) \quad N/m^2 \quad \ldots \quad (3.11)$$

Introducing the hole blockage factor, θ, of Cervenka and Kolar, (52), we obtain;

$$\Delta M = u^2\ .\rho\ .\ (1/a.\theta - 1) \quad N/m^2 \quad \ldots \quad (VI\text{-}1)$$

where $$\theta = 1 - (2.35\ \sigma/d)/(P_1-P_2) \quad N/m^2 \quad \ldots \quad (3.9)$$

The value of θ was calculated for each tray from equation (3.9), using the measured values of (P_1-P_2). Figure VI.1 shows a typical plot of θ against superficial hole gas velocity. θ was then used to calculate the gas momentum head using equation (VI-1). Figure VI.2 shows a typical plot of ΔM against superficial hole gas velocity.

(P_1-P_2) varied slightly with the changing tray liquid head, and an average value was obtained for each superficial hole gas velocity.

Figure VI.1 shows θ to be little affected by changes in the hole pitch or the number of holes. The difference in gas momentum head between the two trays seen in Figure VI.2 results from the difference in tray free area.

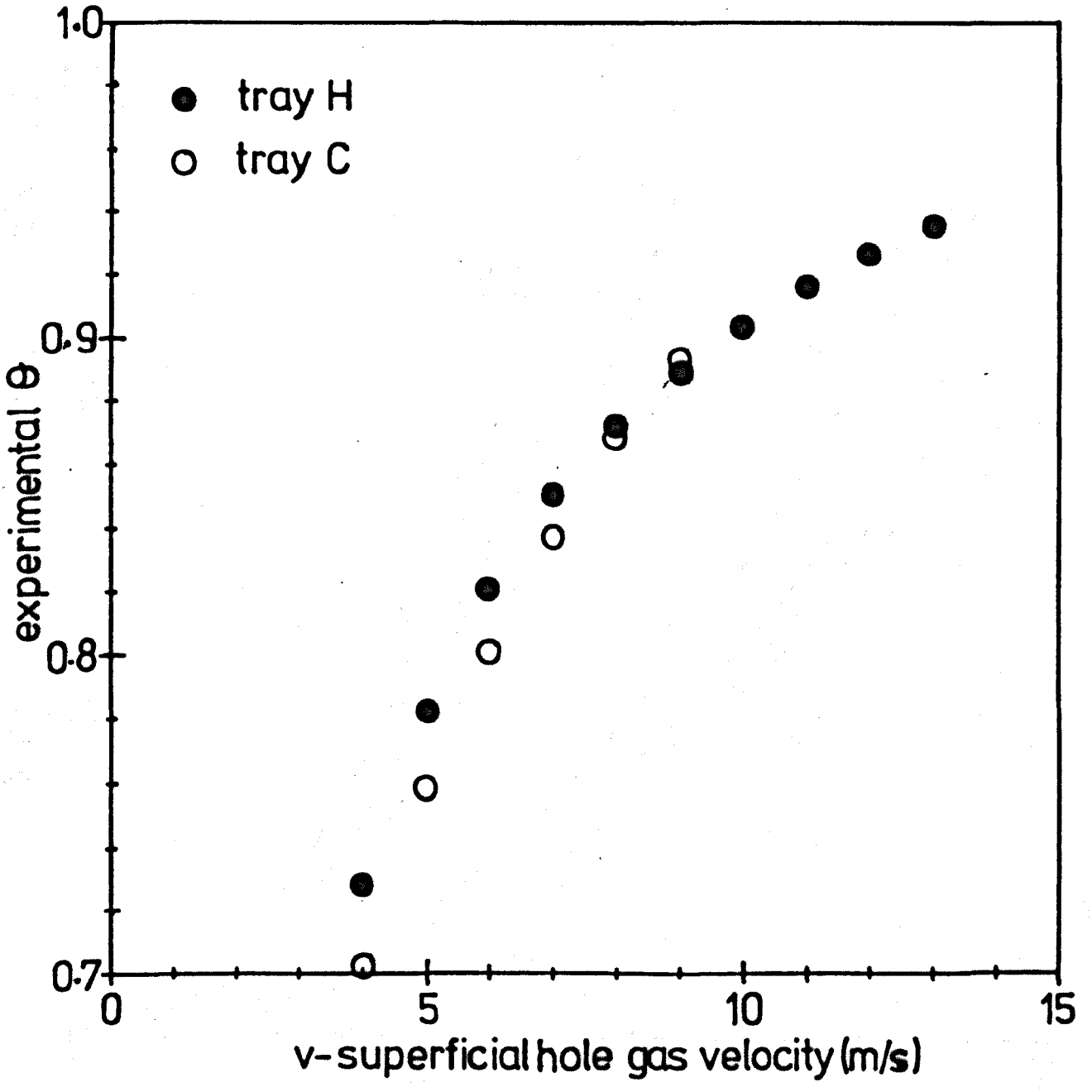

Fig. VI.1 EXPERIMENTAL θ AGAINST GAS VELOCITY

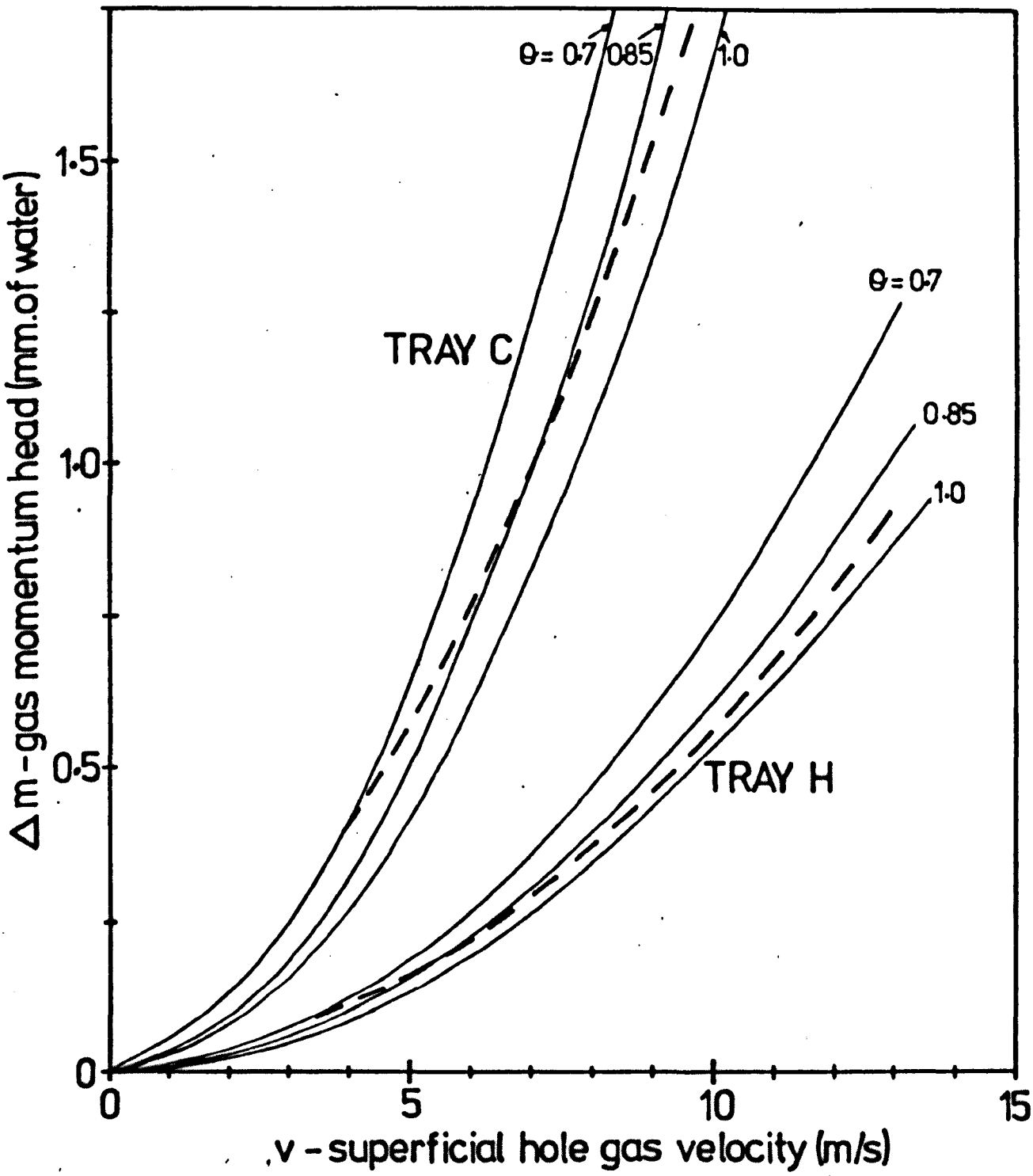

Fig. VI.2. GAS MOMENTUM HEAD AGAINST GAS VELOCITY

Appendix VII.

DEFINITION OF TERMS USED IN VISUAL DESCRIPTION OF GAS-LIQUID REGIMES.

The gas-liquid regime on the test-tray and the weep rate were visually classified and recorded using the qualitative terms which follow.

GAS-LIQUID REGIME - The terms are given in order of increasing tray liquid head.

F.S.	-	Fine Spray;
S	-	Spray;
B.S.	-	Bubble-Spray;
B	-	Bubble;
Fr.B.	-	Froth-Bubble;
Fr.	-	Froth;
T.Fr.	-	Turbulent Froth;
Sw.	-	Swashing (gas-liquid bulk oscillations).

WEEP RATE.

O.W.	-	Occasional weeping;
M.W.	-	Moderate weeping;
H.W.	-	Heavy weeping;
W.R.	-	Weeping-Raining;
R.	-	Raining;
H.R.	-	Heavy Raining.

S.P. was used to signify Seal Point.

Parantheses were used to indicate intermediate regimes or weep rates.

A regime term preceded by a fraction was used to indicate the approximate proportion of the tray over which gas-liquid interaction was occurring (very low tray liquid heads).

The 'Bubble' term used does not correspond to the 'bubble regime' described in Chapter 2, but to a regime in which, as the tray-liquid

head was increased for constant gas flow rate, the spray density increased significantly near to the tray and 'bubbles' could apparently be seen forming. Further increase in tray liquid head resulted in the gradual disappearance of the spray droplets, with the 'bubbles' becoming more predominant. Further increase in tray liquid head resulted in 'Froth' formation.

Appendix VIII.

INVESTIGATION OF THE EFFECT OF THE TRAY MECHANICAL VIBRATION CHARACTERISTICS ON THE COLUMN PRESSURE PULSATIONS.

It is possible that the mechanical vibrational characteristics of the test-tray have an effect on the production of the gas pulsations, particularly if the tray vibration fundamental frequency is close to the gas pulsation frequency.

Waddington (2) showed that the production of column gas pulsations was not affected by small changes in the tray mechanical vibration response. To investigate the possibility further the vibration characteristics of test-tray B were altered. Two methods of alteration were used. Firstly, the test-tray was stiffened using two diagonal metal struts to link it to the top tray. Secondly, the tray was loosened by cutting slots along its sides.

VIII.1 TEST-TRAY STIFFENED USING METAL STRUTS.

The test-tray was stiffened by fastening it to the top tray using two diagonal metal struts. The arrangement used is shown in Figure VIII.1. The struts were 63 cm. long and were made from 5 mm. by 25 mm. steel strip. They had a 25 mm. flange at each end, drilled with an 8 mm. diameter hole through which the struts were bolted to the trays. Frequency analyses were carried out, using the Bruel and Kjaer frequency analyser and level recorder, of the dynamic pressure below the test-tray and of the test-tray vibration acceleration level, and tray static pressure drops were also measured. The measurements were taken with a weir height of 76.2 mm. for a range of gas flow rates and at two values of tray liquid head. One value of liquid head was 2 mm. of water, corresponding to operation in the spray regime, and the other was about 11 mm. of water, corresponding to operation in the froth regime.

VIII.1.1 Results.

The results are given in Table VIII.1. The letters 'S' and 'U' signify tests carried out with the tray stiffened and unstiffened respectively. The number in parantheses is the frequency component

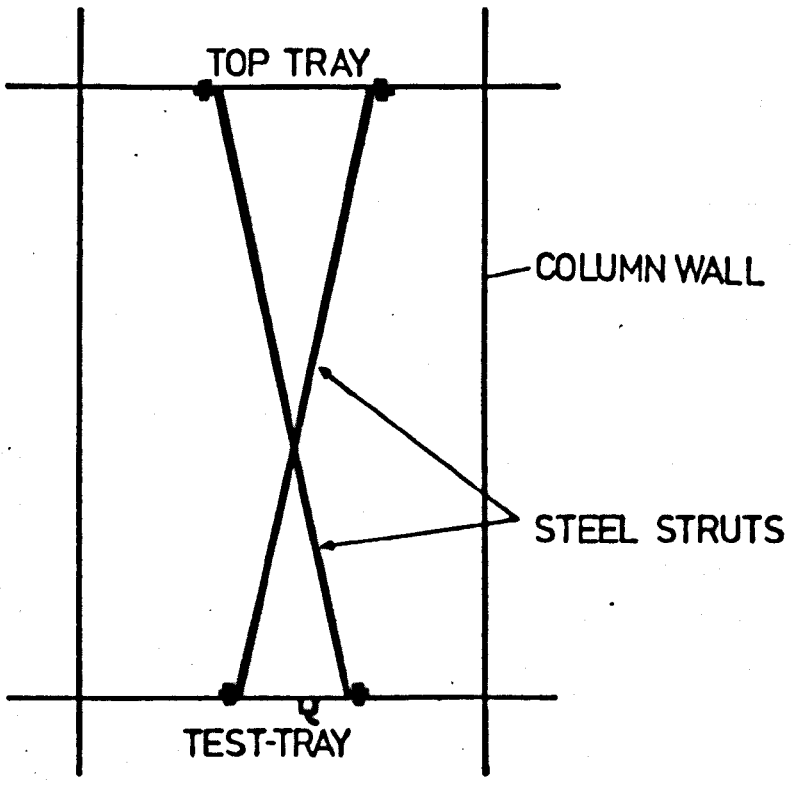

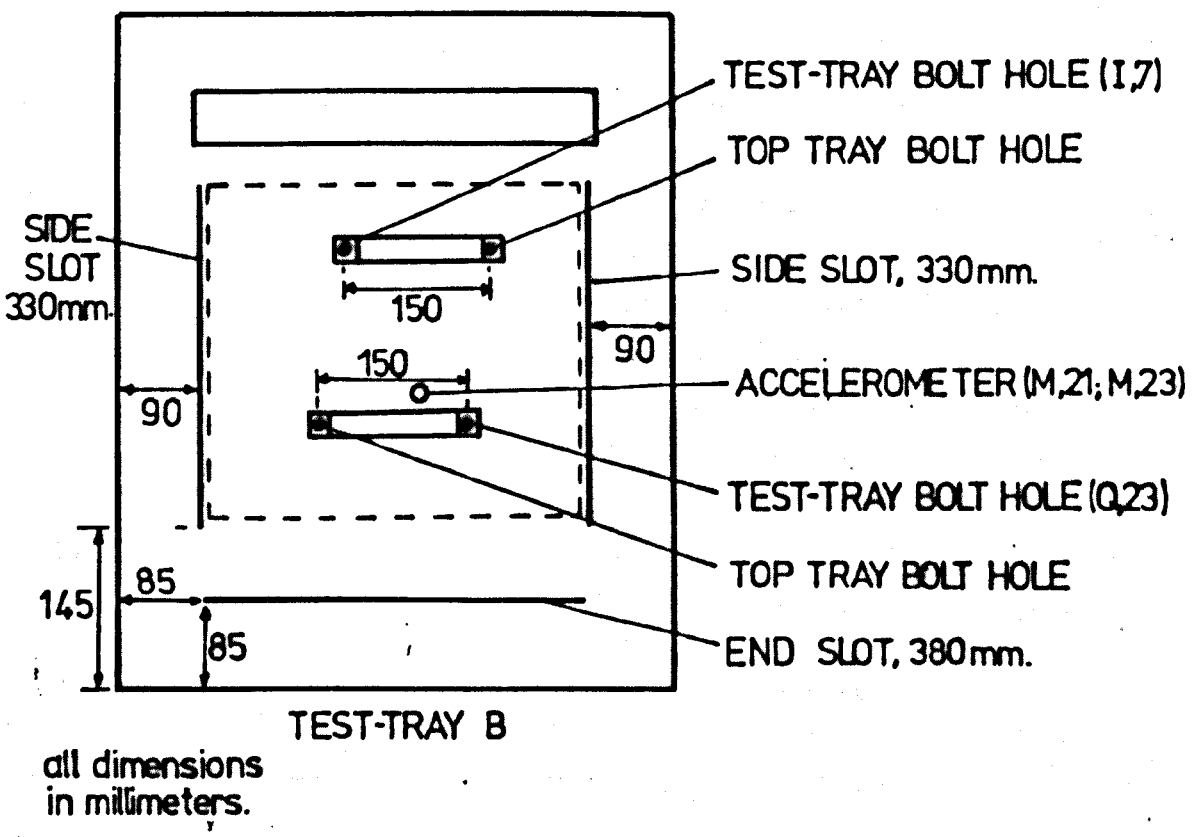

Fig. VIII.1. POSITIONS OF TRAY STRUTS, SLOTS AND ACCELEROMETER

Table VIII.1. Results of Tray Stiffening Experiment.

Gas Vel. v m/s	Pressure Analyses Main Frequencies Hz (N/m^2)				Tray Analysis Main Frequencies Hz (m/s^2)			
SPRAY REGIME ; tray liquid head 2.0 mm.of water								
U 9.15	31(43)	62(15)	93(3)	124(5)	31(1.9)	62(1.3)	93(3.7)	124(3.3)
S 9.15	31(44)	62(14)	93(4)	124(4)	31(1.6)	62(0.53)	93(1.7)	124(0.6)
U 9.9	32(31)	64(12)	96(4)	128(4)	32(1.5)	64(1.2)	96(3.3)	128(1.8)
S 9.9	32(35)	64(15)	96(8)	128(4)	32(1.1)	64(0.5)	96(1.3)	128(1.2)
U 10.8	34(31)	68(12)	102(7)	136(4)	34(1.5)	68(1.3)	102(7.0)	136(1.7)
S 10.8	34(28)	68(12)	102(7)	136(2)	35(0.8)	68(0.3)	102(0.4)	136(2.1)
U 11.7	36(27)	72(8)	108(5)	144(3)	36(1.3)	72(0.9)	108(6.7)	
S 11.7	36(28)	72(10)	108(5)	144(3)	36(0.95)	72(0.4)	108(0.37)	144(0.53)
FROTH REGIME ; tray liquid head ≈ 11.0 mm. of water.								
U 4.4	26(39)				26(0.67)	105(2.4)		
S 4.3	26(38)				26(0.33)	102(0.33)	180(0.53)	
U 4.7	27.5(35)				27.5(0.59)	108(1.06)		
S 4.7	27.5(32)				27.5(0.47)	95(0.17)	155(0.33)	
U 6.0	28(27)				28(0.53)	110(0.94)		
S 6.0	29(20)				29(0.37)	95(0.23)	155(0.8)	
U 6.7	30(12)				30(0.7)	108(1.06)		
S 6.7	30(14)				30(0.43)	94(0.3)	155(0.94)	
U 7.5	31.5(11)				31.5(0.37)	110(0.94)		
S 7.5	32(8)				32(0.21)	94(0.13)	155(0.94)	
U 8.2	32.5(6)				32.5(0.24)	110(0.85)		
S 8.2	33(6)				33(0.21)	93(0.15)	155(0.6)	

amplitude, expressed in units of N/m^2 for the pressure signal and m/s^2 for the vibration signal.

It can be seen that stiffening the test-tray changed its vibrational response but had no effect on the gas pulsations in the chamber below.

For operation in the froth regime stiffening the tray raised its fundamental vibration frequency from about 110 hz to about 155 Hz. For such operation the tray vibrated at both this fundamental frequency and the fundamental gas pulsation frequency. Stiffening the tray reduced its overall level of vibration, especially at the lower frequencies.

For operation in the spray regime the dynamic pressure frequency spectrum is seen to contain a well defined harmonic series. As was mentioned in Section 5.3.1 these harmonics probably result from the shape of the pressure pulses. Figure VIII.2 shows a typical dynamic pressure signal, and also the test-tray and column wall vibration signals. The tray is seen to respond to all of the pressure harmonics and, as expected, when a harmonic approaches the tray fundamental frequency the vibration level is much increased. Stiffening the tray raised its fundamental frequency to a value which corresponded to a higher pressure pulsation harmonic frequency, corresponding to lower amplitude, thus decreasing the overall tray vibration level.

The tray vibration signal shown in Figure VIII.2 was for conditions at which the second harmonic of the pressure pulsation frequency spectrum corresponded to the tray fundamental frequency.

Clearly much higher tray vibration levels would be expected to occur if the tray fundamental frequency corresponded to the pressure pulsation fundamental or first harmonic. To investigate this, slots were cut in the tray to lower its fundamental frequency.

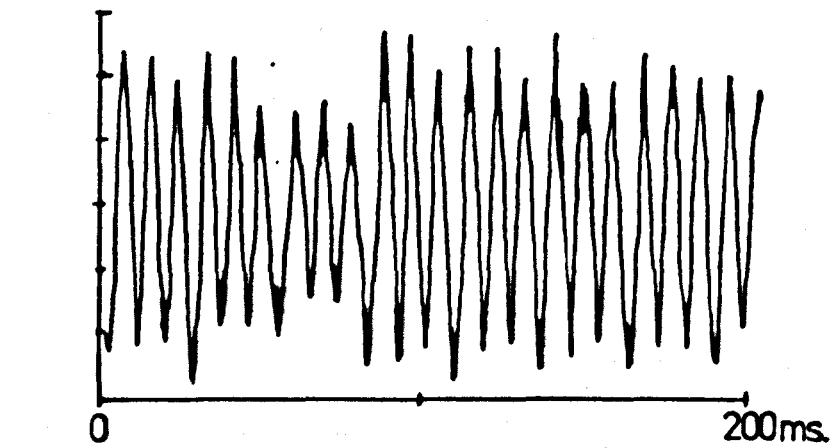

TRAY VIBRATION

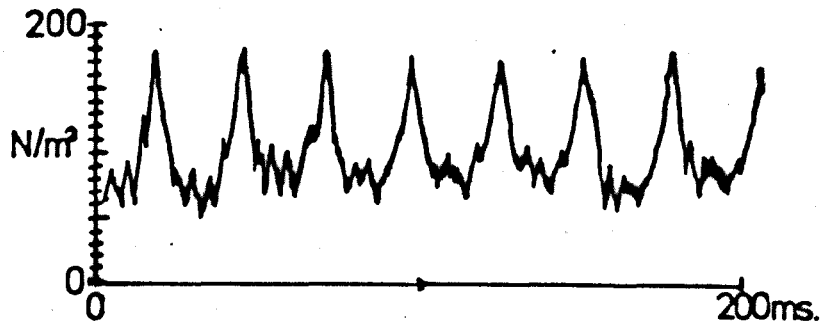

PRESSURE PULSATIONS
BENEATH TEST-TRAY

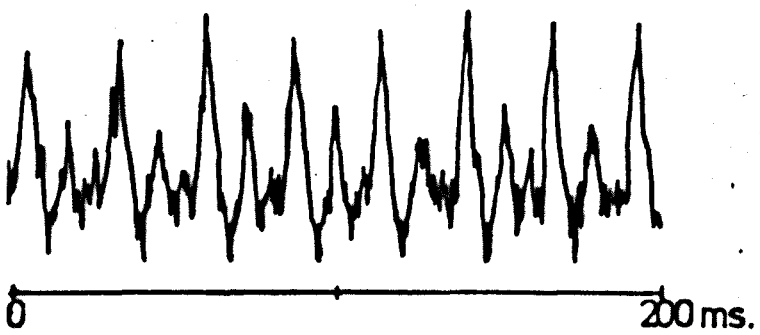

COLUMN WALL
VIBRATION

TEST-TRAY B (unstiffened)
v = 10.0 m/s
h = 4.5 mm of water
f = 35 Hz.
A = 31 N/m²

Fig. VIII.2. EXAMPLES OF COLUMN WALL AND TRAY VIBRATION

VIII.2 TEST-TRAY LOOSENED BY CUTTING SLOTS IN IT.

Firstly, two 150 mm. long slots were cut, one down each side of the test-tray. Secondly, these slots were extended to a length of 330 mm, and a third slot, 380 mm. long was cut along the edge of the tray. The location of the slots and of the accelerometer are shown in Figure VIII.1 (The stiffening struts were removed).

The fundamental frequency of the dry tray (when installed in the column) was determined by analysing its vibrational response to mechanical excitation using the S.D.C. real time analyser. To determine the tray fundamental frequency under liquid loading the tray vibration was analysed at high liquid loadings, corresponding to operation outside the region of pulsation production.

With a weir height of 76.2 mm, and at various values of gas flow rate and tray liquid head, the tray static pressure drops were measured, and frequency analyses performed of the dynamic pressure above and below the test-tray and the test-tray vibrational velocity. The tray velocity was measured using a preamplifier setting of 10 Hz (0.3 m/s).

VIII.2.1 Results.

The results are presented in Tables VIII.2 and VIII.3. The vibration velocity is expressed in units of m/s., and an indication is given of the prevailing gas-liquid regime, (Section 5.2.1 (vi)).

Cutting slots in the tray failed to bring its fundamental frequency down to a value corresponding to the gas pulsation fundamental frequency. The two slots reduced the fundamental frequency from about 10 Hz to about 90 Hz for the dry tray, and to about 87 Hz under liquid loading. The three slots reduced it to about 60 Hz dry and to 52 Hz under liquid loading.

Table VIII.2 Results for Two Slots Cut in Test-Tray B.

Dry tray fundamental frequency = 90.5 Hz.

Run No.	v m/s	h mm of water	Main Frequencies Hz	Pressure Amplitudes Below tray N/m^2	Pressure Amplitudes Above tray N/m^2	Tray Vibration level m/s	Gas-liquid regime
1	8.0	1.5	27.0,54.0,81.0	13,3,0.6	12, 6, 3	1.8,0.5, 0.4	¦ BS
2	8.0	1.5	29.4,58.6,88.2	30,10,2	29,24,10	5,3,13	FS
			Slight decrease in pulsation frequency tuned tray at 87.6 Hz, 18 m/s				
3	8.0	3.25	28.2,56.4,84.6	35,7,1.5	29,12,5	4,1.6, 3.7	FS
4	8.0	4.5	29.4,58.6,88.0	30,4,0.5	29,11,2	4.2,1.5, 4.0	(F)S
5	8.0	6.25	30.2,60.4,90.6	27,3,-	26,10,1	3.8,0.8, 1.8	B(S)
6	16.0	6.0	- 87.0	-	-	0.8	
7	16.0	16.0	- 86.5	-	-	1.0	

Table VIII.3. Results for Three Slots cut in Test-Tray B.

Run No.	v m/s	h mm. of water	Main frequencies Hz	Pressure Amplitudes Below tray N/m^2	Pressure Amplitudes Above tray N/m^2	Tray vibration level m/s	Gas-liquid regime
1	8.0	1.5	27.4,55.0	11,1.5,	8,- ,	1.8,4.0,	¦ BS
2	8.0	1.5	30.2,60.6,91.0	38,15,4.5	33,20,10	16,17,0.9	FS
3	8.0	2.75	28.4,56.8	14,1.8,	11,2.5,	1.8,4.0	FS
4	8.0	5.25	29.8,59.6,89.4	32,6,1	28,12,4	12,7,-	(F)S
5	8.0	6.25	30.4,60.6,91.0	35,7,1	30,12,1.5	13,6.5,-	
6	8.0	7.75	31.0,62.2,93.4	30,6,1	27,10,1	10,3.5 -	B(S)
7	8.0	9.75	32.0,63.8,	12,1.5,	8,1.5,	3.5,0.7,	(Fr)B(S)
8	16.0	5.0	,52.2,	-	-	,4.5,	
9	16.0	11.0	,52.0,	-	-	,1.5,	
10	6.0	6.0	24.6,49.4,	30,3.5,	NOT	5.6,2.0,	(B)S,OW
11	6.0	7.0	25.6,51.4	23,1.0,	RECORDED	3.7,2.4	
12	6.0	7.75	26.4,52.8,	13,0.5,	↓	3.0,2.0,	
13	6.0	9.0	27.6,55.2,	15,1.0,		2.0,1.7,	
14	6.0	9.75	28.2,56.4,	18,1.3,		2.7,2.5,	B,(Fr),(MW)
15	6.0	11.0	29.0,58.0,	20,2.0,		4.5,1.5,	Fr(B),MW
16	6.0	13.0	29.8,59.6,	14,1.4,		5.0,1.0	Fr,MW
17	6.9	11.75	30.6,61.2,	19,1.3,		5.0,1.3,	Fr,(MW)
18	7.7	10.75	31.6,63.2,	12,1.3,		3.7,0.7,	Fr,(B),(OW)
19	8.5	7.75	32.2,64.4,	18,2.0,		3.4,0.6,	

Comparison of the amplitude and frequency of the pressure pulsations given in Tables VIII.2 and 3, with those reported in Chapter 5, Figures 5.4(a) and 5.7, shows the changes in the tray vibration characteristics to have had no apparent effect on the gas pulsations.

As was found when the tray was stiffened, the tray was excited at the components of the pressure pulsation frequency spectrum, with increased levels of vibration occurring when a pressure pulsation harmonic approached the tray fundamental frequency. Runs 2 and 4 in table VIII.2, and runs 10, 11 and 12 in table VIII.3 demonstrate this 'resonance' effect.

It is seen that pulsation frequency harmonics were evident in both the spray and the froth regimes, although those in the froth regime were of lower amplitude.

VIII.3. CONCLUSIONS.

Changes in the mechanical vibration characteristics of the test-tray have no effect on the production of gas pulsations.

The tray is excited by both the fundamental and the harmonics of the pressure pulsation frequency spectrum, with the highest levels of tray vibration occurring when a harmonic approaches the tray fundamental frequency.

It is to be expected that when the tray fundamental frequency is low enough to correspond with the fundamental pressure pulsation frequency, high levels of tray vibration will occur.

Appendix IX.

INVESTIGATION OF THE SYSTEM NOISE AND ACOUSTIC RESPONSE OF THE EXPERIMENTAL RIG.

It was indicated in Section 5.3.1 that some relatively high frequency pressure variation is generated within the experimental rig. This 'noise', which can be detected on the pressure traces shown in Figure 5.2, was investigated by measuring the dynamic pressure within the experimental system when there was gas flow but no liquid flow.

The system acoustic properties were investigated by measuring the dynamic pressure response to discrete frequency excitation from a loud-speaker.

An attempt was made to introduce a column acoustic resonance at the pressure pulsation fundamental frequency. This was done by attaching a long side tube to the chamber beneath the test-tray. A movable plunger within the tube allowed the effective tube length to be varied.

IX.1 SYSTEM NOISE.

Real time frequency analysis of the dynamic pressure within the experimental system was carried out for various air flowrates in the absence of water flow. Specific frequencies were detected which were found to be mainly independent of the air flow rate and test-tray geometry Table IX.1 gives the main frequencies detected at various locations within the system for a superficial hole gas velocity of 5.3 m/s through test-tray L. A 25 mm. thick layer of foam rubber was placed on the test-tray to simulate the gas-liquid mixture.

Table IX.1. shows the system noise to be of a relatively high frequency with respect to the regular pressure pulsations, and to be of quite low amplitude.

The measurements taken in the orifice tube when the column was disconnected show most of the noise to be generated by the centrifugal fan/orifice tube system and not by acoustical resonance within the column.

TABLE IX.1 MAIN FREQUENCIES OF EXPERIMENTAL SYSTEM NOISE.

Location of pressure transducer	Main frequencies Hz (N/m^2) (and amplitude)
Bottom Chamber	182(21),202(9), 226(17), 790(2)
Chamber below test-tray	182(10), 224(12), 790(3)
Chamber below test-tray with 7.62 m. side tube	104(3), 152(4), 182(8), 200(6), 226(14), 268(2.7), 792(2)
Chamber above test-tray	146(4), 184(3.5), 226(3), 262(2), 790(1)
Orifice tube with column disconnected	148(10), 184(24), 206(9), 228(5), 790(1)

Static pressure drops	Bottom tray (B) and drop catcher	- 200 N/m^2
	Test-tray (L) and foam rubber	- 181 N/m^2
	Top-tray (A)	- 250 N/m^2

IX.2 SYSTEM ACOUSTIC RESPONSES TO EXCITATION BY A LOUDSPEAKER.

A variable frequency signal generator, a constant gain amplifier and a loudspeaker were used to excite the column. The loudspeaker was attached to a 0.14 m. diameter hole cut centrally in the side of the chamber beneath the test-tray, opposite the downcomer.

The dynamic pressure response to excitation at discrete frequencies in the range 16 to 1000 Hz was determined using the S.D.C. real time analyser in the peak memory mode. Analyses were performed for various locations of the pressure transducer and both with and without fluid flow.

No appreciable resonance was found to occur for frequencies below about 150 Hz. For all conditions most resonance occurred in the frequency range 175 Hz to 210 Hz, with a further, much lower, resonance in the range 780 Hz to 800 Hz, depending on conditions. These frequencies agree closely with those found to be present in the system 'noise', generated in the absence of external excitation.

The acoustic resonant frequencies in the column were calculated, treating it as a series of rectangular boxes. This gave the lowest expected mode of resonance to be at 217 Hz.

IX.3 USE OF A SIDE-TUBE TO CHANGE COLUMN ACOUSTICS.

It has been shown that there is no appreciable system noise or resonance in the frequency range corresponding to that of the regular pressure pulsations induced by the gas-liquid interaction on the tray (12 Hz to 40 Hz). In an attempt to introduce a resonance in the column in this frequency range a side tube was attached to the chamber beneath the test-tray. It was arranged perpendicular to the column wall and was fixed to a 0.15 m. diameter hole cut on the same side of the column as the gas inlet.

The tube was made from up to three 3.0 m. lengths of 0.15 m. internal diameter p.v.c. An airtight disc, which fitted inside the pipe,

was attached to a 3.5 m. length of metal rod to form a movable plunger which was used to vary the effective length of the tube.

Using different lengths of tube, the dynamic pressure beneath the test-tray was analysed both with and without external excitation for various operating conditions, as described in Section IX.1 and IX.2.

No low frequency resonance was detected. Some results are given in Table IX.1 and these show the introduction of a 7.62 m. tube to have very little effect on the system behaviour, with no frequencies present below 100 Hz.

A standing half-wave in a 7.62 m. tube would have a frequency of about 22 Hz, for a 8.95 m. tube, this would be about 19 Hz. In runs 6 and 8 of experiment 3, Section 5.4, an 8.95 m. length of tube was used to increase the chamber volume, but there was no apparent resonance effect on the amplitude or frequencies of the measured pressure pulsations.

It can be concluded that the use of the side tube failed to introduce a suitable low frequency column resonance. An attempt to influence the gas pulsation by introducing a signal of similar frequency, using the loudspeaker, also failed to produce any noticeable effect.

IX.4 CONCLUSIONS.

It can be concluded that the dynamic pressure variation generated in the experimental system in the absence of gas-liquid interaction on the sieve-tray is of a relatively high frequency (> 150 Hz) compared to the regular pressure pulsations (12 Hz to 40 Hz). This system noise is generated mainly by the centrifugal fan and orifice tube.

Furthermore, there are no significant system acoustic resonance frequencies below 150 Hz. An attempt to introduce low frequency resonance by attaching a tube to the column was unsuccessful, and the tube had no effect on the regular pressure pulsations.

Appendix X.

SIMPLIFIED ANALYSIS OF SYSTEM GAS FLOW.

Introduction.

The flow system, as shown in Figure 7.1, is complex. However, some simplifications can be carried out to produce a rather approximate but useful description of the system, applicable particularly to the build-up in pressure drop across the tray as the resistance of the tray holes increases.

X.1 SIMPLIFYING ASSUMPTIONS.

(i) Any effects due to gas inertia are ignored. As indicated by equation 7.4, pressure losses due to inertial changes are relatively small, even at the higher rates of flow change.

(ii) The total tray pressure drop results from equal pressure fluctuations above and below the test-tray, that above being the inverse of that below. As shown by Figures 7.2 and 7.3, this is a fairly good approximation. This approximation will be less valid when the pressure fluctuation above the tray is required to fall below atmospheric pressure, this only being possible due to gas inertia effects. However, this requirement will only occur for high amplitude fluctuations at low gas volumetric flowrates.

(iii) The test-tray is considered to lie between two equal chambers of effective volume Q_e m^3, fed by a constant gas flowrate of G m^3/s. This is fairly accurate in that the flow system upstream and downstream of the test-tray are very similar, and the contained resistances relatively small. Figures 7.2 and 7.3 show little change in pulsation amplitude across the bottom tray. Some reduction in Q_e with increasing gas volumetric flowrate can be expected to result from the increasing influence of the top and bottom tray flow resistances.

X.2 SIMPLIFIED ANALYSIS.

From Chapters 2 and 7 we have:

$$\frac{d P_1}{dt} = C (G_o - G_1) \qquad (7.2)$$

and

$$C = c^2 . \rho . /Q \qquad (2.2)$$

With the simplifying assumptions, these equations give the direct relationship:

$$\frac{d \Delta P_t'}{dt} = \frac{2 . c^2 . \rho}{Q_e} (G - G_1') \quad N/m^2 . s \qquad (X.1)$$

This relationship enables an estimate for Q_e to be made by comparing Figures 7.4 and 7.5. Such a comparison shows Q_e to have a value in the range 0.23 to 0.33 m^3; decreasing, as expected, with increasing G. This range compares favourably with the combined volume of the two chambers below (= those above) the test-tray of 0.255 m^3.

X.3 APPLICATION OF SIMPLIFIED ANALYSIS TO THE INCREASE IN TRAY PRESSURE DROP DURING THE 'WAITING PERIOD' PRIOR TO EVENT INITIATION.

In section 7.3 it was shown that the increase in tray pressure drop prior to event initiation could be well represented by assuming it to result from a gradual decrease in a time-dependent equivalent hole diameter, d'. Using this concept, and ignoring gas inertia effects, equations 7.6, 7.7 and 7.10 give the relationship:

$$\Delta P_t' = \frac{1}{2} . \rho . C_T . (p^2/t)^{0.2} . \frac{16}{n^2 . \pi^2} . \frac{G_l'^2}{d'^{4.2}} \quad N/m^2 \qquad (X.2)$$

Where: C_T is the coefficient in equation (7.10), e.g. C_T = 0.935 for tray L(g).

Introducing a factor S_1 and rewriting, equation (X.2) becomes:

$$G_1' = \frac{\Delta P_t'^{0.5}}{S_1} \cdot d'^{2.1} \quad m^3/s \qquad (X.3)$$

Combining equations (X.1) and (X.3) gives:

$$\frac{d\,\Delta P_t'}{dt} = \frac{2 \cdot c^2 \cdot \rho}{Q_e} \left(G - \left(\frac{\Delta P_t'}{S_1} \right)^{0.5} \cdot d'^{2.1} \right) \quad N/m^2.s \qquad (X.4)$$

From equation (X.4) it can be shown easily that when $d' = d$, $\Delta P_t'$ will fall until it reaches a value given by:

$$\Delta P_t' = \Delta P_{min} = \frac{1}{2} \cdot K \cdot \rho \cdot v^2 \quad N/m^2 \qquad (X.5)$$

Having reached this minimum value, any decrease in d' will cause the total tray pressure drop to increase.

For a given variation in d', solution of equation (X.4) will yield the time required for the tray pressure drop to rise from its minimum value to the event initiation pressure drop. Unfortunately, equation (X.4) cannot be solved analytically. Numerical integration of equation (X.4) was therefore necessary. This was carried out using the 'Basic' computer programme listed in section X.4, with a step time of 0.00005 s. d' was assumed to decrease at a constant linear rate s_2 m/s; i.e.

$$d' = d - s_2 t \quad m. \qquad (X.6)$$

Solutions were obtained for four different values of s_2, and various values of tray geometry, gas velocity, gas density, initiation pressure drop and equivalent chamber volume. The results are listed in Tables 8.3, 8.4, 8.5, 8.6 and 8.7.

X.4 NUMERICAL SOLUTION OF EQUATION (X.4)

```
2     PRINT "PRESSURE DROP BUILD UP"
4     PRINT
6     PRINT
8     PRINT
25    PRINT "SUP. HOLE GAS VELOCITY,M/S ";
26    INPUT V1
29    PRINT "HOLE DIAMETER,M ";
30    INPUT D1
33    PRINT "INITIATION PRESSURE DROP,N/M2 ";
34    INPUT E1
37    PRINT "NUMBER OF HOLES ";
38    INPUT N1
41    PRINT "DRY TRAY LOSS COEF ";
42    INPUT K1
45    PRINT "CHAMBER VOLUME,M3 ";
46    INPUT Q1
49    PRINT "GAS DENSITY,KG/M3";
50    INPUT R1
53    PRINT "RATE OF HOLE CLOSURE,M/S ";
54    INPUT S2
57    PRINT "STEP TIME,S ";
58    INPUT T2
70    LET G1=(N1*3.1416*V1*D1^2)/4
80    LET S1=8*R1*K1*D1^0.2/(3.1416*N1)^2
90    LET S3=110224*R1*2/Q1
94    LET T1=0
96    LET P1=S1*G1^2/D1^4.2
98    LET P3=P1
100   LET T1=T1+T2
110   LET D2=D1-(S2*T1)
120   LET G2=((P1/S1)^0.5)*D2^2.1
130   LET P1=(G1-G2)*T2*S3+P1
140   IF P1>E1 GOTO 200
150   GOTO 100
200   PRINT "BUILD UP TIME,S  = ";T1
205   PRINT "MINIMUM PRESSURE DROP ,N/M2 = ";P3
210   PRINT "FINAL PRESSURE DROP,N/M2 = ";P1
215   PRINT "MEAN GAS FLOW ,M3 = ";G1
220   PRINT "FINAL GAS FLOW, M3 = ";G2
300   GOTO 4
500   END
```

REFERENCES

1. I.C.I., Agricultural Division, Teesside,'Confidential Records'.

2. Waddington, W., 1973, M.Eng. Thesis, University of Sheffield.

3. Waddington, W., Erskine, J.B., 1973, International Symposium: 'Vibration Problems in Industry', Keswick, paper 211.

4. Waddington, W., I.C.I. Agricultural Division, Teesside,report E.D.N. 4083.

5. Waddington, W., Kohler, H.K., Brown, D.J., 1974, Trans. I.Chem.E., 52, 381.

6. Ho, G.E., Muller, R.L., Prince, R.G.H., 1969, International Symposium: 'Distillation'. Brighton, (I.Chem.E.), 2.10.

7. Prince, R.G.H., Chan, B.K.C., 1965, Trans.I.Chem.E., 43, 49.

8. Biddulph, M.W., Stephens, J.S., 1974, A.I.Chem.E., 20, 60.

9. Phipps, M.A., 1976, I.C.I. Agricultural Division, Teesside, personal communication.

10. Scully, J.C., 1971 'The Theory of Stress Corrosion Cracking'. N.A.T.O. Scientific Affairs Division, Brussels.

11. West, J.M., Dept. of Metallurgy, University of Sheffield, personal communication.

12. Davidson, L., Amick, E.H. Jr., 1956, A.I.Chem.E., 2, 337.

13. Hughes, R.R., Handlos, A.E., Evans, A.D., Maycock, R.L., 1955, Chem.Engng. Prog., 51, 557.

14. Cervenka, J., Kolar, V., 1973, Coll. Czec. Chem. Comm., 38,3750.

15. Wallis, G.B., 1969, 'One Dimensional Two-Phase Flow', McGraw-Hill.

16. Rennie, J., Evans, F., 1962, Brit. Chem.Engng., 7, 498.

17. Fane, A.G., Lindsey, J.K., Sawistowski, H., 1973, Indian Chem. Eng., XV, 37.

18. Calderbank, P.H., Rennie, J., 1962, Trans. I. Chem. E., 40, 191.

19. Calderbank, P.H., Burgess, J.B., 1975, Chem.Eng.Sci., 30, 1107.

20. Ashley, M.J., Haselden, G.G., 1972, Trans.I.Chem.E., 50, 119.

21. McAllister, R.A., Plank, C.A., 1958, A.I.Chem.E., 4, 282.

22. Barker, P.E., Self, M.F., 1962, Chem.Eng.Sci., 17, 541.

23. Hinze, J.E., 1965, Symposium on Two-Phase Flow, University of Exeter, F101.

24. Biddulph, M.W., 1975, A.I.Chem.E., 21,41.

25. Pinczewski, W.V., Fell, C.J.D., 1975, A.I.Chem.E., 21, 1019.

26. Pinczewski, W.V., Fell, C.J.D., 1974, Trans. I.Chem.E., 52,294.

27. Fane, A.G., Sawistowski, H., 1969, International Symposium: 'Distillation', Brighton, (I.Chem.E.), 1.8.

28. Pinczewski, W.V., Fell, C.J.D., 1972, Trans.I.Chem.E., 50, 102.

29. Lindsey, J.K., 1972, Ph.D. Thesis, Imperial College of Science and Technology.

30. Porter, K.E., Wong, P.F.Y., 1969, International Symposium: 'Distillation', Brighton (I.Chem.E.), 2.22.

31. Burgess, R.G., Robinson, K., 1969, International Symposium: 'Distillation', Brighton (I.Chem.E.), 2.34.

32. Payne, G.J., Prince, R.G.H., 1977, Trans. I.Chem.E., 55, 266.

33. Jeronimo, M.A., Sawistowski, H., 1977, I.Chem.E., 4th Annual Research Meeting, Swansea.

34. Eduljee, H.E., 1972, The Chemical Engineer, March, 123.

35. Valentin, F.H.H., 1967, Spon's Chem.Eng.Series, 'Absorption in Gas-Liquid Dispersions - Some Aspects of Bubble Technology.'

36. Hayes, W.B., Hardy, B.W., Holland, C.D., 1959, A.I.Chem.E., 5, 319.

37. Muller, R.L., Prince, R.G.H., 1972, Chem.Eng.Sci., 27, 1583.

38. Payne, G.J., Prince, R.G.H., 1975, Trans. I.Chem.E., 53, 209.

39. Banerjee, T.S., Roy, N.K., Rao, M.N., 1969, Indian J. of Tech., 7, 301.

40. Pinczewski, W.V., Loon, R.E., Fell, C.J.D., 1973, Trans. I.Chem.E., 51, 374.

41. Yeo, H.K., 1975, M.Sc. Thesis, University of New South Wales.

42. McCann, D.J., Prince, R.G.H., 1969, Chem.Eng.Sci., 24, 801.

43. McCann, D.J., Prince, R.G.H., 1971, Chem.Eng.Sci., 26, 1505.

44. Davis, B.T., Porter, K.E., 1965, Symposium on Two-Phase Flow, University of Exeter, F.301.

45. Brambilla, A., Nardini, G., Nencetti, G.F., Zanelli, S., 1969, International Symposium: 'Distillation'. Brighton, (I.Chem.E.), 2.63.

46. Hunt, C.A., Hanson, D.N., Wilke, C.R., 1955, A.I.Chem.E., 1, 441.

47. Kolodzie, P.A., Van Winkle, M., 1957, A.I.Chem.E., 3, 305.

48. McAllister, R.A., McGinnes, P.H., Plank, C.A., 1958, Chem.Eng. Sci., 9, 25.

49. Durgaprasada, C.H., Rao, C.V., 1972, Indian J. of Tech., 10, 1.

50. Cervanka, J., Kolar, V., 1973, Coll. Czec. Chem. Comm., 38, 2891.

51. Davy, C.A.E., Haselden, G.G., 1975, A.I.Chem.E., 6, 1218.

52. Kolar, V., Cervenka, J., 1974, Coll. Czec. Chem. Comm., 39, 2723.

53. Kupferberg, A., Jameson, G.J., 1969, Trans. I. Chem.E., 47, 241.

54. Brown, R.S., 1958, Ph.D. Thesis, University of California.

55. Kupferberg, A., Jameson, G.J., 1970, Trans. I. Chem.E., 48, 140.

56. Chan, B.K.C., Prince, R.G.H., 1966, A.I.Chem.E., 12, 232.

57. Davidson, J.F., Garland, C.S., 1975, Chem.Eng. Sci., 30, 177.

58. Cermak, J., 1973, Coll. Czec. Chem. Comm., 38, 3373.

59. Titomanlio, G., Rizzo, G., Acierno, D., 1976, Chem.Eng.Sci., 31,404.

60. LaNauze, R.D., Harris, I.J., 1974, Trans. I.Chem.E., 52, 337.

61. Spiers, H.M., 1955, Technical Data on Fuel, 5th Edition, British National Committee, World Power Conference.

62. Muller, R.L., 1970, Ph.D. Thesis, University of Queensland.

63. Kirshner, J.M., Silas, K., 1975, 'Design Theory of Fluidic Components', Academic Press Inc.

64. Tippetts, J.R., Rimmer, E., Higginson, J., McGuigan, J.A., 1977, paper presented at A.S.M.E., W.A.M., Atlanta, Georgia.